HSV-1 INFECTION IN HUMAN INDUCED PLURIPOTENT STEM CELL-DERIVED NEURONS: CELLULAR MODELS FOR QUIESCENCE AND DRUG DISCOVERY

by

Lora Lee McClain

B.S. in Biology, University of Pittsburgh, Johnstown, 2003

Submitted to the Graduate Faculty of

the Department of Human Genetics in

the Graduate School of Public Health in partial fulfillment

of the requirements for the degree of

Doctor of Philosophy

University of Pittsburgh

2016

UNIVERSITY OF PITTSBURGH

GRADUATE SCHOOL OF PUBLIC HEALTH

This dissertation was presented

by

Lora Lee McClain

It was defended on

March 2, 2016

and approved by

Candace Kammerer, Ph.D., Associate Professor
Department of Human Genetics, Graduate School of Public Health, University of Pittsburgh

Paul Kinchington, Ph.D., Professor
Departments of Ophthalmology, Molecular Genetics, and Biochemistry
School of Medicine, University of Pittsburgh

Zsolt Urban, Ph.D., Associate Professor
Department of Human Genetics, Graduate School of Public Health, University of Pittsburgh

Dissertation Advisor: Vishwajit L. Nimgaonkar, M.D., Ph.D., Professor
Departments of Psychiatry and Human Genetics
School of Medicine, Graduate School of Public Health, University of Pittsburgh

Vishwajit L. Nimgaonkar, M.D., Ph.D.

HSV-1 INFECTION IN HUMAN INDUCED PLURIPOTENT STEM CELL-DERIVED NEURONS: CELLULAR MODELS FOR QUIESCENCE AND DRUG DISCOVERY

Lora Lee McClain, Ph.D.

University of Pittsburgh, 2016

ABSTRACT

Background: Herpes simplex virus, type 1 (HSV-1) establishes latency in human sensory ganglia following primary infection through mucosal tissues. Once latent, the virus persists for the host's lifetime, with periodic reactivations that cause lytic lesions. First-line medications like acyclovir (ACV) abort lytic reactivations, but drug resistance has been reported and second line drugs may cause serious side effects. These facts, together with inefficacy of antivirals against latency, compel new drug screens; human neural tissues that model aspects of latency are arguably well-suited for such screens.

Studies:

Study 1. Human induced pluripotent stem cell-derived neurons (iPSC-neurons) were used to model HSV-1 infection employing an HSV-1 construct that incorporates dual fluorescent reporter genes from different kinetic expression groups. Lytic infection was demonstrated initially. 'Quiescent' infection was next established using protocols from animal models of latent infection. The quiescent infection fulfilled most criteria for latency, including viral gene expression and heterochromatization patterns.

Studies 2 and 3: The antiviral activity of two series of compounds was investigated using monkey epithelial cells and iPSC-neurons. Anti-lytic activity that reduced viral copy number

and protein levels was induced by four compounds, of which two compounds also inhibited reactivation of HSV-1 from quiescence/latency. Four compounds were also efficacious against varicella zoster virus and/or human cytomegalovirus infections.

Study 4: Moderate throughput platforms for antiviral drug screens based on iPSC-neurons were designed, with readouts based on high content analysis and flow cytometry.

Conclusions: Lytic and latent HSV-1 infection was modeled in human iPSC-neurons, with features similar to animal models. Compounds with novel effects against HSV-1 infections were identified using the iPSC-neuron model. Platforms for moderate throughput drug screens are feasible using human iPSC-neuron models.

Public Health Significance: Herpesviruses are highly prevalent, with rates exceeding 95% in some populations. Recurrent HSV-1 eye infections are the leading cause of infectious corneal blindness in the USA. HSV-1 encephalitis that is particularly devastating to neonates can be fatal. Associations between HSV-1 seropositivity and cognitive impairment have been reported even without encephalitis. There are no effective HSV-1 vaccines and there are growing concerns about antiviral drug efficacy. In view of the enormous burden, there is a compelling need for novel drug screens.

TABLE OF CONTENTS

LIST OF TABLES

LIST OF FIGURES

PREFACE

I would like to thank research participants and all my colleagues from the Program for Genetics and Psychoses: Mikhil Bamne, Ph.D.; Hoyee Cheng, B.S.; Kodavali Chowdari, Ph.D.; Sue Clifton, M.S.; Cathy Cortese; Leonardo D'Aiuto, Ph.D.; Peter Dimitrion; Ayantika Ghosh, Ph.D.; Rebecca Lipski, M.S.; Hader Mansour, M.D., Ph.D.; Vishwajit Nimgaonkar, M.D., Ph.D.; Konsale Prasad, M.D.; Annie Watson, M.S.; Joel Wood, B.S.; and Yun Zhi. I am especially grateful for Hoyee Cheng, who has been exceptional in helping me manage the lab and provided outstanding supporting technical help during my graduate studies. I would also like to acknowledge Dr. Leonardo D'Aiuto for cell culture training and laboratory techniques, for his advice in experimental design and interpretation, and for the critical reading of this dissertation. I have known most of these exceptional individuals for more than 10 years and delight in their enthusiasm and dedication to our work; it was my honor to work with them.

From the department of Human Genetics, I would like to thank all my professors, and I am especially grateful to my committee members Candace Kammerer, Ph.D., and Zsolt Urban, Ph.D. for your guidance, support, and help with experimental designs. I would also like to especially acknowledge Michael Barmada, Ph.D., Ilyas Kamboh, Ph.D., and David Finegold, M.D. for your passionate teaching of human genetics, critical thinking, and professionalism. Thank you for helping me to achieve my dream to study and graduate from this department. I would also like to acknowledge Samantha Rosenthal, B.S., who was my study partner from the

start, and always my friend; I am especially appreciative of our scientific conversations and also for our coffee and study breaks.

From the Departments of Ophthalmology and Molecular Genetics & Biochemistry: Paul Kinchington, Ph.D., my committee member whose inexhaustible knowledge in virology generated ideas and solutions that were instrumental in the designs of this project, and Michael Yee, B.S., my first virology laboratory teacher. Mark Schurdak, Ph.D. from the Drug Discovery Institute of the University of Pittsburgh, and Paolo Piazza, Ph.D. from the Department of Infectious Diseases and Microbiology, I would also like to especially acknowledge your guidance, support, and help with data analysis. Dr. David Bloom, Ph.D. from the University of Florida provided valuable interpretation of data and help with future studies. I would like to acknowledge our funding source, the Stanley Medical Research Institute and Dr. Robert Yolken, M.D., Ph.D., from the Stanley Division of Neurovirology, Department of Pediatrics, Johns Hopkins University School of Medicine for support and guidance of our efforts presented here. I would also like to acknowledge all my other coauthors for making this work possible.

Finally, I would like to acknowledge my mentor, Dr. Vishwajit Nimgaonkar. I was grateful to work with you for six years before applying to the Ph.D. program and even more fortunate to stay in your lab during my time as a graduate student. I hope to exude the same passion as you in my future endeavors, while maintaining your enthusiasm, patience, and professionalism.

I dedicate these years and this work to my parents, Carol and Roy Crise, who have always supported my life's aspirations, to my husband Craig McClain and my father-in-law Robert McClain, who awarded me with unwavering support, and finally to my daughter Leah Clare McClain: never give up and keep reaching higher.

Attributions

The work presented here is a result of collaborative efforts by many individuals. I would like to attribute their work.

The initial iPSC characterization, initial testing of the HSV-1 infection models, neural stem cell method, supervision of lab work, troubleshooting, and data analysis were performed by Dr. Leonardo D'Aiuto at Western Psychiatric Institute and Clinic, University of Pittsburgh, Pennsylvania.

The 3-dimensional FISH method outlined in the "Persistent Infection by HSV-1 is Associated with Changes in Functional Architecture of iPSC-Derived Neurons and Brain Activation Patterns Underlying Working Memory Performance" manuscript was conducted by Dr. Luigi Viggiano at Western Psychiatric Institute and Clinic, University of Pittsburgh, Pennsylvania.

The RT-qPCR for Chapter 3 was performed and analyzed by Dr. Kodavali Chowdari at Western Psychiatric Institute and Clinic, University of Pittsburgh, Pennsylvania.

Dr. Jadranka Milosevic analyzed the microarray data in Chapter 3 at the University of Pittsburgh, Pennsylvania.

The flow cytometry and analyses for Chapters 3 and 4 were performed in collaboration with Dr. Paolo Piazza at the Graduate School of Public Health, University of Pittsburgh, Pennsylvania and Benjamin Treat in the laboratory of Dr. Paul Kinchington at the University of Pittsburgh, Pennsylvania, respectively.

Dr. Konsale Prasad and colleagues performed and analyzed the MRI work for Chapter 3 at the University of Pittsburgh, Pennsylvania.

The targeted proteomics work for Chapter 3 and analyses was performed by Dr. Matthew McDonald and Dr. Robert Sweet at the University of Pittsburgh, Pennsylvania.

The electrophysiological studies were performed by Yun Zhi, Madeleine Wilcox, and Dr. Jon Johnson at the University of Pittsburgh, Pennsylvania.

The antiviral testing of novel compounds on HCMV infections for Chapter 4 was performed by Dr. Ravit Boger and colleagues at the Johns Hopkins School of Medicine in Baltimore, MD.

Dr. James McNulty and colleagues synthesized the molecules used for antiviral testing in Chapter 4 at his laboratory at McMaster University, Ontario Canada.

The laboratories of Dr. Paul Kinchington and Dr. Fred Homa provided the viruses used in this thesis.

Dr. Mark Schurdak performed the image acquisition and analyses for the 96- and 384-well cell culture plates that were imaged at the Drug Discovery Institute of the University of Pittsburgh, Pennsylvania.

iPSC cell lines were made and characterized at the University of Pittsburgh and Rutgers University RUCDR.

The quantitative polymerase chain reaction work was performed in the Genomics Research Core at the University of Pittsburgh, Pennsylvania.

The details of my contributions to the work in this thesis are described in detail in Appendix E.

1.0 INTRODUCTION

1.1 PUBLIC HEALTH SIGNIFICANCE

Herpesvirus infections are highly prevalent in human populations globally. The prevalence of seroconversion by age 15 is 40% worldwide; furthermore, seropositivity increases with age and is estimated at greater than 70% in older US adults (Whitley, 1996; Smith et al., 2002). HSV-1 primary infection often presents as herpetic gingivostomatitis (Mohan et al., 2013). In addition to recurrent facial lesions, HSV-1 infection can infect other areas of the body, such as the eyes or brain, leading to ocular keratitis (Farooq & Shukla, 2012), and rarely, encephalitis, respectively (Whitley, 2006). Moreover, data from the United States National Health and Nutrition Examination Surveys (NHANES) indicates HSV-1 is an emerging genital infection with an increasing incidence (Xu et al., 2006); additionally, individuals with genital herpes have a two- to four-fold increased risk to acquire the human immunodeficiency virus (HIV; Holmberg et al., 1988; Wald & Link, 2002; Freeman et al., 2006; Anuradha et al., 2008; Patel et al., 2012). A wealth of evidence points to associations of HSV-1 seropositivity and cognitive decline in individuals without prior history of encephalitis, diagnosed with schizophrenia, their first-degree relatives, and unrelated controls of different ethnicities (Prasad et al., 2012; Fruchter et al., 2015). The burden of disease is much greater for immunocompromised patients.

1.1.1 Herpes Keratitis

Herpes keratitis (HK) is an infection of the eye caused by HSV-1 and it is the leading cause of infectious corneal blindness in developed countries (Dawson & Togni, 1976; reviewed in Farooq & Shukla, 2012). Its global incidence is approximately 1.5 million cases per year (Farooq & Shukla, 2012) and 40,000 new cases of visual impairment or blindness are reported per year (Flagg & Weinstock, 2011; Farooq & Shukla, 2012). Visual impairment and blindness are due to corneal opacification, a result of tissue scarring caused by recurring viral insults that trigger host immune damage (Halford et al., 2004) ACV is the preferred treatment for HK, taken orally or topically. Rates of viral reactivation can be reduced when treating HK with prophylactic, long-term antivirals (Herpetic Eye Disease Study Group, 1998). Following primary HSV-1 infection at the oromucosal surface, latency is established in the nerves of the trigeminal ganglia where the virus can reactivate and enter the ophthalmic nerves and infect the cornea (Hill et al., 2014). Alternatively, there is controversial evidence that corneal cells may serve as a site of latency, beside the trigeminal ganglia and dorsal root ganglia (Zheng, 2002; Polcicova et al., 2005).

1.1.2 Herpes Simplex Encephalitis

Herpes simplex encephalitis (HSE) is a devastating lytic HSV-1 infection of the brain. HSV-1 is the most common agent to cause acute, sporadic encephalitis worldwide (Whitley, 2006) with a prevalence rate in the United States of approximately 1 in 300,000 individuals (Whitley, 2006). HSE infection, with or without proper treatment of intravenous acyclovir, results in mortality rates of approximately 30% and 70%, respectively (Whitley, 2006).

Individuals that survive infection will carry life-long, devastating neurological sequelae, including, but not limited to: neurological deficits, seizures, and neuropsychological dysfunctions (McGrath et al., 1997). During HSE infection, the virus is undetectable in the peripheral blood using current testing methods; therefore, HSE is tested clinically in cerebrospinal fluid (CSF) sample using polymerase chain reaction (PCR) to amplify viral nucleic acid fragments (Debiasi & Tyler, 2004)

There is mounting evidence of a Mendelian predisposition to develop HSE. As a vital part of the innate immune system, the toll-like receptor (TLR) family mediates interferon and cytokine production after the detection of pathogen-associated molecular patterns (PAMPs) on antigens (Doyle et al., 2002). TLR3 recognizes double-stranded RNA, an intermediate nucleic acid present in most viral infections, including HSV-1 infection (Jacobs & Langland, 1996). Inborn errors of TLR3 and other molecules of the TLR3 signaling pathway can result in a predisposition to develop childhood HSE upon primary infection and an overall increased susceptibility to HSV-1 infection in some children (Lafaille et al., 2012; Zhang et al., 2013; Lim et al., 2014).

Missense mutations in TLR3 were identified in two unrelated patients who developed HSE, the mutations were not detected among control individuals (Zhang et al., 2007). However, these mutations show incomplete penetrance as relatives of the two cases were HSV-1 seropositive, but were never diagnosed with HSE (Zhang et al., 2007). Similarly, exonic mutations in other genes of the TLR3 signaling pathway also confer increased risk of HSE development including UNC93B1 (Casrouge et al., 2006), TRIF (Sancho-Shimizu et al., 2011), and TRAF3 (Pérez de Diego et al., 2010) These studies suggest that either the HSV-1 primary infection is inadequately controlled in CNS-resident non-haemopoietic cells during the primary

infection (Zhang et al., 2013), or viral reactivation is inadequately controlled (Zhang et al., 2007). Both possibilities confer risk due to diminished interferon production.

1.1.3 Neonatal Herpes Simplex

Herpes simplex can infect neonates at birth by vertical transmission of the virus to the neonate from the mother. The incidence of neonatal HSV disease ranges from 1:1,500 (Kimberlin, 2004) to 1:3,200 in the United States (Brown et al., 2003). The most common form of neonatal exposure is by contact with the virally infected birth canal, especially in mothers who have seroconverted in their 3rd trimester (Brown et al., 1997). Patterns of neonatal herpes fall into three categories. The most severe pattern is viral infection of the internal organs; this is usually fatal. Among survivors, the greatest morbidity is associated with CNS infection that manifests as seizures, lethargy, failure to thrive, or encephalitis. Lesions that occur only on the neonatal external skin surfaces have the best prognosis, but if left untreated, the infection may lead to more serious infections to the internal organs and/or CNS. Similar to post-neonatal HSE infection, the death rate in the first 12 months of life is 85% for disseminated disease and 50% for CNS infection (Whitley et al., 1980). However, the advent of high-dose antiviral therapy has reduced the 24-month mortality rate to 31% for disseminated disease and 6% for CNS infection, among survivors, no neurological sequelae occurred in 83% and 31%, respectively (Kimberlin et al., 2001).

1.1.4 Herpes Simplex Virus and Cognitive Dysfunction

The cognitive dysfunction observed in survivors of herpesvirus encephalitis resembles the cognitive dysfunction in those with schizophrenia (SZ), but is milder (Kapur et al., 1994; Hokkanen & Launes, 2000). Furthermore, HSV-1 has been detected in the post mortem brains of SZ patients (Kudelova et al., 1988) and Alzheimer's disease patients, who also manifest cognitive decline (Wozniak et al., 2009). There is a growing body of evidence indicating a robust association of HSV-1 seropositivity with cognitive dysfunction, even among individuals without a prior history of encephalitis or dementia (Dickerson et al., 2003; Dickerson et al., 2008; Shirts et al., 2008; Schretlen et al., 2010; Yolken et al., 2011; Thomas et al., 2013; D'Aiuto et al., 2015; Fruchter, et al., 2015). HSV-1 seropositivity in SZ patients is associated with a greater reduction in the gray matter volume in distinct brain regions, compared with seronegative patients (Prasad et al., 2007; Prasad et al., 2011; D'Aiuto et al., 2014), with cognitive deficits including difficulty with memory, such as challenges to learn new verbal and visual stimuli; executive functioning, such as reasoning; and difficulties performing day-to-day tasks (Aleman et al., 1999; Weickert et al., 2000). A double-blind, placebo-controlled study revealed improved cognition in SZ patients who received the antiviral valacyclovir as an adjunct to their antipsychotic medication for 18 weeks (Prasad et al., 2012). Cognitive decline over time has been noted also among African-Americans (Watson et al., 2012), or Caucasian individuals who are not diagnosed with psychoses such as SZ (Dickerson et al., 2008; Watson, 2012).

These associations suggest that HSV-1 latency may not be as benign as once thought. Given the high prevalence of HSV-1 in the general population, increased risk of cognitive decline from infection resulting in neuronal cell death warrants further investigation, as well as new treatment options (Becker, 1995).

1.2 HERPESVIRIDAE

The *Herpesviradae* family comprises eight viral species that infect *Homo sapiens*. These viruses have linear, double-stranded DNA genomes, an icosahedral capsid, a proteinaceous tegument layer, and a lipid envelope (Chisholm & Lopez, 2011). Additionally, they can establish latency in a variety of cell types following primary infection. Herpesviruses are divided into three subfamilies.

Human *alphaherpesvirinae* viruses include herpes simplex virus, type 1 (HSV-1), type 2 (HSV-2), and varicella zoster virus (VZV). An individual contracts HSV by close, physical contact with another HSV-positive individual who is shedding the virus. HSV-1 and -2 display lytic viral infection as grouped vesicles on mucosal membranes and establish latency in sensory neurons of cranial nerves, such as trigeminal ganglia (HSV-1; Warren et al., 1978) or sacral ganglia (HSV-2); however these sites of latency are not exclusive to either type of virus. Primary HSV-1 infection usually occurs during childhood or adolescence and most commonly infects oromucosal surfaces, whereas primary HSV-2 infection generally is delayed until the onset of sexual activity and most commonly occurs at genital mucosal surfaces.

Primary VZV infection is commonly known as chickenpox and may reactivate later in life, when it is called called zoster (shingles), usually following a decline in age-related immunity; symptoms include skin lesions that resolve within 12-14 days and neuralgia that may resolve within 4-6 weeks, but may last longer. However, some individuals may experience neuralgia lasting longer than 6 weeks, as well as other complications like myelitis, meningoencephalitis, or vasculopathy (Nagel & Gilden, 2014). VZV maintains a latent state in sensory neurons of the dorsal root or nerve ganglia along the entire neuraxis (Gilden et al., 2009). Reactivation is commonly restricted to specific neurons of viral activity that innervate that

particular dermatome in immunocompetent individuals (Gnann et al., 2002), Antiviral treatment is required for individuals who experience ophthalmic zoster, due to tissue scarring and a potential for permanent visual impairment. Following the US approval of the live attenuated varicella vaccine in 1995, the mortality of VZV infection has plummeted to less than 20 per year (Horien & Grose, 2012). The vaccine is based on the Oka strain, which has reduced reactivation compared with the wild-type VZV and thus may also reduce incidence of zoster (Hardy et al., 1991; Hambleton et al., 2008; Vere et al., 2013). Individuals who are seropositive for VZV and are between the ages of 60 – 80 years may benefit from a booster vaccination by the zoster vaccine, reducing shingles risk by 51% (Gilden, et al., 2009). The US prevalence for VZV, estimated in the National Health and Nutrition Examination Survey (NHANES) study (n=16,050), is 93% for children aged 6-19 years and 98% for adults aged 20-49 years (Reynolds et al., 2010).

Human *betaherpesvirinae* viruses include human cytomegalovirus (HCMV), human herpesvirus type 6 (HHV-6), and type 7 (HHV-7). HCMV infects a broad range of human tissues and likely establishes latency in macrophages and lymphocytes. Primary HCMV infection are asymptomatic in the majority of individuals, but can lead to serious disease in the immunocompromised population, with fever, pneumonia, seizures, hepatitis, and visual impairment. Congenital HCMV infection can result from seroconversion of the mother during pregnancy and is devastating to neonates; HCMV is a significant infectious cause of infantile intellectual disability and hearing loss (Damato & Winnen, 2002). HCMV infection is estimated to be present in over 95% of the global adult population (Cannon et al., 2010).

HHV-6 variant B (HHV-6B) and HHV-7 cause roseola infantum, typically presenting with fever, rash, and febrile convulsions (Ward, 2005). HHV-6 variant A (HHV-6A), HHV-6B,

and HHV-7 each have an estimated prevalence of greater than 90% in developed countries by 6 years of age (Hall et al., 1994; Huang et al., 1997; Agut, et al., 2015). HHV-6 has a wide cell tropism *in vivo*, and replicates in the brain, salivary glands, tonsils, kidneys, liver, endothelial cells, and macrophages; HHV-7 is a T-lymphotropic virus (Ponti et al., 2008). Like other herpesviruses, HHV6 maintains a latent state and is capable of reactivation; unlike other herpesviruses, HHV-6 can integrate into subtelomeric regions of host cell chromosomes with a prevalence of about 1% in developed nations (Agut et al., 2015). While there is little difference between the HHV-6 variants in genomic sequence (<4%), there are differences in their patterns of infection. Variant 6A is not readily found in saliva, unlike 6B, which is more likely to be detected in leukocytes and saliva; and 6B may not result in development of a rash, unlike variant 6A (Ward, 2005).

Human *gammaherpesvirinae* viruses include Epstein-Barr virus (EBV) and Kaposi's sarcoma-associated herpesvirus (KSHV). EBV infects epithelial cells and then B-lymphocytes, where the latter is the site of latency as the virus can persist following memory B-cell maturation (Vere et al., 2013). Primary EBV is asymptomatic in the majority of infected individuals, but some individuals can experience infectious mononucleosis. EBV can reactivate from B-lymphocytes, manifesting as an epithelial cell infection (Hadinoto et al., 2009). EBV infection is also associated with many cancers, including Burkitt's lymphoma, a neoplastic proliferation of B-lymphocytes and nasopharyngeal carcinoma (Lo et al., 2012). Approximately 200,000 new cases of EBV-associated cancers are reported each year, worldwide (Parkin, 2006; Fukayama, 2010). EBV is prevalent in up to 90% of the global adult population (Hislop, 2015).

KSHV is likely the causative agent of Kaposi sarcoma (KS), an endothelial cell tumor of blood and lymphatic vessels. KS presents as isolated lesions on the limbs, lymph nodes, mucosa,

and/or internal organs. KSHV is necessary but not sufficient for the presence of Kaposi sarcoma; the immunocompromised are at elevated risk. Progression to cancer is most prominent in HIV/AIDS patients and organ transplant recipients. Like other herpesviruses, KSHV supports cycles of latency and lytic infection, and viral transcripts are found in B-lymphocytes, macrophages, keratinocytes, endothelial and epithelial cells *in vivo* (Boshoff & Weiss, 1998). KSHV prevalence is unlike the other ubiquitous herpesviruses; in developed countries, it is disproportionally prevalent in HIV-infected men and range from 30% to 65% (Martin, 2011). It is most frequently found in Middle Eastern and African individuals, where the prevalence in the general population is between 15% and 60% (Martin, 2011).

The viruses that belong to the *Herpesviradae* family are highly prevalent in the human population and represent a significant public health importance. A common feature of herpesviruses is their ability to establish and maintain persistence in the host in the face of immunity. They can remain in this state for the entire life-span of the host. However, specific stimuli can result in viral reactivation and produce recurrent diseases.

1.3 HSV-1 LYTIC CYCLE

The HSV-1 virion consists of a 152 kilobase, linear, double stranded DNA genome housed in an icosahedral capsid. Surrounding the viral capsid is a proteinaceous tegument consisting of viral encoded proteins, and the tegument is enclosed by an envelope. The envelope is derived from the host cell embedded with viral glycoproteins.

The HSV-1 genome is characterized by a guanosine:cytosine content ratio of approximately 68% (J. C. Brown, 2007) and contains two unique DNA sequences (U_L and U_S),

which are flanked by two inverted repeats (TR_L and IR_L; IR_S and TR_S; FIGURE 1). The viral genome contains approximately 74 open reading frames of which three are present in two copies (Dolan et al., 1998); the majority of these transcripts do not undergo splicing (Wagner, 1985).

Figure 1. Representation of the HSV-1 genome.

The HSV-1 lytic lifecycle begins with attachment and entry into permissive host cells. Viral glycoproteins embedded in the viral envelope bind to various surface receptors—these include: heparan sulfate chains on cell surface proteoglycans (Shukla et al., 1999), herpesvirus entry mediator (HVEM; Montgomery et al., 1996), or nectin1 (Cocchi et al., 1998; Geraghty et al., 1998); entry may occur via endocytosis by fusion of the plasma membrane (Nicola et al., 2003). There are 12 viral envelope proteins containing glycan chains, and are classified as viral glycoproteins; of which four have been shown to be essential for viral attachment and fusion with the host membrane (Turner et al., 1998; Cocchi et al., 2004). After the viral envelope fuses with the host cell plasma membrane, the tegument proteins (Radtke et al., 2010; G. Smith, 2012) and the nucleocapsid are released into the host cell cytoplasm. The nucleocapsid, containing the viral DNA, transits to the host cell nucleus via processes mediated by the dynein (Sodeik et al., 1997) and dynactin motor protein complexes (Döhner et al., 2002). Next, the viral nucleocapsid docks to the host nuclear pore complex on the outer nuclear membrane, rapidly releasing DNA into the host cell nucleus (Ojala et al., 2000; Sae-Ueng et al., 2014), where a portion of incoming genomes circularize (Jackson & DeLuca, 2003), or adopt a branched structure (Martinez et al., 1996) and serve as the template for DNA replication (Lemaster & Roizman, 1980; Batterson et al., 1983; Fenwick & Everett, 1990; Zhang & McKnight, 1993; Strang & Stow, 2005).

During productive infection, host RNA polymerase II transcribes viral genes in a temporal manner, beginning with the five IE genes, designated as Infected Cell Polypeptides (ICP) 0, ICP4, ICP22, ICP27, and ICP47 (Honess & Roizman, 1974, 1975). Transcription of IE genes occurs independently of *de novo* viral protein synthesis (Weir, 2001). The IE gene transcription is initiated by a multiprotein transcription factor complex comprised of viral tegument protein VP16 (Pellett et al., 1985) and host proteins HCF1 (Kristie & Roizman, 1987) and Oct1 (O'Hare, 1993). VP16 associates with Oct1 (Kristie & Roizman, 1987) and binds to a common core sequence that is shared among IE gene promoters, known as the TAATGARAT regulatory element (Stern et al., 1989). The IE proteins are required for the transcription of early (E) proteins, which are involved in the production and regulation of viral DNA synthesis (Honess & Roizman, 1974). Following DNA synthesis, late (L) genes are expressed, which in general, encode proteins that contribute to virus structure and assembly.

While HSV-1 requires the use of host cell transcription machinery, it also encodes six proteins that comprise the DNA replisome (a two subunit DNA polymerase (DNA pol; UL30 and UL42), a single stranded DNA binding enzyme (ICP8), and a three subunit helicase-primase complex (UL5, UL52, and UL8; Muylaert et al., 2011)). Viral gene UL9 encodes the origin binding protein that binds and unwinds viral DNA at one or more of the three origin sites (Aslani et al., 2002). The helicase-primase complex travels in the 5' to 3' direction at the replication fork and the DNA pol presumably carries out leading and lagging strand synthesis while ICP8 binds the single-stranded DNA during polymerization. UL30 is the catalytic subunit of HSV DNA pol and is necessary for production of progeny virions (Dorsky & Crumpacker, 1988). Viral DNA has been hypothesized to replicate by several mechanisms, including theta replication (Roizman, 1979), rolling circle mechanism (FIGURE 2; Skaliter et al., 1996) , and trombone mechanism of

replication (Bermek et al., 2015) at one or more of the three origin sites. Additionally, viral DNA also exists as a complex, branched structure during replication (Martinez et al., 1996) and evidence suggests recombination of viral DNA may lead to this branched structure (Wilkinson & Weller, 2003; Weller & Sawitzke, 2014). DNA replication results in concatemeric units that are later cleaved into single genomes during encapsidation (Weller & Coen, 2012). The genes required to construct the viral capsid are translated by host ribosomes and transported back into the host nucleus where assembly of the nucleocapsid occurs. Following capsid maturation, the terminase packages an HSV-1 genome into the viral capsid (Bauer et al., 2013).

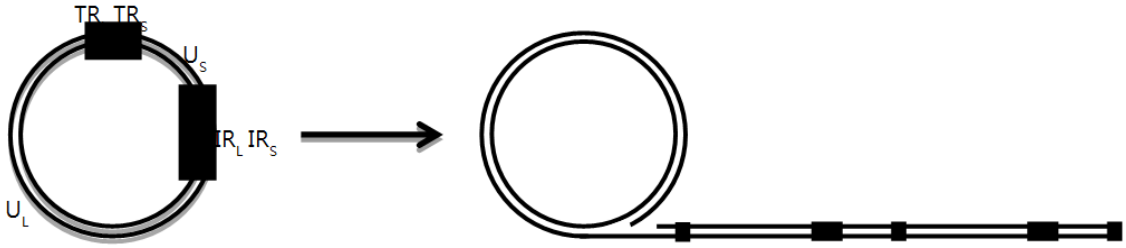

Figure 2. Representation of the rolling circle DNA replication model for HSV-1.

Once the viral DNA is encapsidated, the resulting nucleocapsid begins egress from the cell. The nucleocapsid is too large to transverse nuclear pore complexes, thus a different route is taken. During primary envelopment, the nucleocapsid buds through the inner nuclear membrane into the perinuclear space, along with selected tegument proteins VP16, vhs, pUL11, UL37, and pUS3 kinase (Baines et al., 1995; Reynolds et al., 2002; Naldinho-Souto et al., 2006; Read & Patterson, 2007). The viral particle proceeds to de-envelopment by fusion with the outer nuclear membrane (Lycke et al., 1988; Reynolds et al., 2002). In the cytoplasm, a secondary envelopment of the viral particle occurs at the *trans*-Golgi network (TGN), where viral particles associate with tegument proteins and bud into the TGN membranes, thus acquiring its envelope

(Wisner & Johnson, 2004; Turcotte et al., 2005; Sugimoto et al., 2008). The viral particles continue egress utilizing kinesin protein motor proteins (Diefenbach et al., 2002) to the host cell membrane and can fuse with resulting exocytosis (Johnson & Baines, 2011) or spread cell-to cell by tight junctions to adjacent cells (Johnson, et al., 2001). Lytic cycles are typically lethal for the host cells.

1.4 HSV-1 LATENCY

A hallmark of herpesviruses is their ability to persist for the entire lifetime of their hosts in a latent, but reactivatable form. For HSV-1, a reservoir of latent viral genomes is typically established and maintained in the nuclei of sensory neurons of the peripheral nervous system (PNS) following the primary infection. HSV-1 DNA does not integrate into the host genome, but exists in the nucleus as a circular, heterochromatic episome (Bloom et al., 2010), probably in specific nuclear compartments that allow for heterochromatin formation (Catez et al., 2012). In a mouse model of latency, approximately 5-20% of neurons harbor latent viral genomes, where viral DNA copy number is estimated at 1 to 100 per neuron (Mehta et al., 1995; Yang et al., 2000). A small fraction of neurons harbor more than 1,000 copies of viral genomes per cell (Sawtell, 1997).

After the virus infects peripheral epithelial cells, it enters the axon termini of the nerves in the infected tissues, and viral components are retrogradely transported to the sensory neurons of the trigeminal ganglia or dorsal root ganglia (Baringer & Swoveland, 1973; Smith, 2012). HSV-1 latency is established in the nuclei of these PNS neurons. The entry site of the virus determines the ability to establish latency: if HSV-1 directly enters the neuronal soma instead of

the neuronal termini, a productive infection is favored (Hafezi et al., 2012). Establishment of latency when the virus enters the axon termini may be due to the progressive loss of VP16 during the retrograde transport of the virus to the soma. As a consequence, IE gene transcription could be delayed due to insufficient quantities of VP16, resulting in viral latency. However, productive infection can be induced by superinfection with other viruses, suggesting that the viral genome reaches the nucleus and is poised for replication (Hafezi et al., 2012).

Hallmarks of HSV-1 latency include i) heterochromatinization of the viral genome, with the exception of the region encompassing latency-associated transcripts (LAT) sequence; ii) lack of infectious virion production; and iii) transcriptional repression of the viral genes with the exception of LAT, and its splicing products (Spivack & Fraser, 1987; Stevens et al., 1987).

Viral lytic genes are silenced during latency; however, low levels of lytic transcripts can be detected in addition to latency associated transcripts (LAT) in latently infected neurons (Kramer & Coen, 1995; Kramer et al., 1998; Feldman et al., 2002). In fact, single cell analysis revealed expression of one or more lytic genes in greater than one-third of latently infected neurons, albeit at low copy numbers (Ma et al., 2014). This observation supports the model of reactivation described by Kim and colleagues as ‘animation’: a continuous attempt of the virus to reactivate despite the repressive action of the host (Kim et al., 2012). The animation model describes a biphasic viral gene program, in contrast to the lytic HSV-1 infection (which postulates a temporal gene transcription program). Phase I of the animation model describes a reactivation stimulus that produces a temporary, albeit extensive de-repression of lytic transcripts that is independent of the VP16-inducing complex. During this phase, HSV-1 lacks the ability to produce infectious viral particles (Kim et al., 2012). Indeed, if conditions during Phase I are favorable for lytic infection, the virus proceeds to a lytic infection. However, if viral products

are not able to accumulate to a sufficient supply, the virus retreats back to a latent state; a minority of Phase I events proceed to Phase II, where an ordered cascade of viral genes are transcribed, DNA is replicated, and infectious viral particles are produced (Kim et al., 2012).

LAT is an 8.3 kb capped and polyadenylated noncoding viral RNA, which is spliced into more stable 2.0 kb fragments in the nucleus (Stevens, et al., 1987; Zwaagstra et al., 1990; Farrell et al., 1991). LAT transcripts can be detected in approximately one-third of latently infected mouse neurons (Mehta, et al., 1995), but its exact mechanism on viral latency is unknown. LAT transcripts are expressed during the late stages of lytic infections in murine models of infection (Spivack et al., 1988; Rodahl & Stevens, 1992; Chen et al., 1995). LAT has multiple effects in the establishment or maintenance of latency (Javier et al., 1988; Steiner et al., 1989; Block et al., 1990; Kramer et al., 2011). LAT has been shown to function as a primary microRNA (miRNA) precursor that encodes several viral miRNAs (Umbach et al., 2008; Umbach et al., 2009). Some of these LAT-derived miRNAs (miRNA-H2 and –H6) are antisense to HSV-1 immediate early genes, and can down-regulate IE lytic genes ICP0 and ICP4, thus suggesting a regulatory role of LAT in latency (Umbach, et al., 2008). Recent observations lead to the suggestion that LAT may enhance the formation of repressive H3K27me3 on lytic promoters during latency (Cliffe et al., 2009). The presumptive role of LAT in the epigenetic regulation of HSV-1 latency raises the possibility that chromatin modifications are mediated in part by specific miRNAs transcribed from the LAT region. Additionally, LAT may increase neuronal survival by blocking apoptosis. Infections using a LAT-null strain results in a reduced establishment of latency and greater neuronal morality (Thompson & Sawtell, 2001). Likewise, reactivation is also reduced, which may be due to the decreased number of surviving neurons (Hill, et al., 1990; Perng et al., 2000; Sawtell & Thompson, 1992; Thompson & Sawtell, 1997, 2001).

HSV-1 Chromatin in Lytic and Latent Infection.

HSV-1 chromatin composition varies during lytic and latent infections. Histone proteins are not bound to viral DNA within infectious virions (Cohen et al., 1980; Pignatti & Cassai, 1980; Oh & Fraser, 2008). During lytic infection, viral DNA binds cellular histones upon host nuclear entry (Cereghini & Yaniv, 1984). However, the histone occupancy is low, and viral chromatin does not display a regular chromatin pattern (Conn & Schang, 2013). Similar to host chromatin, histone modifications of viral chromatin, such as acetylation or methylation, are dynamic. As early as one hour post infection, HSV-1 DNA is associated with histones bearing marks of active transcription (H3K9ac); however, methylated H3K9 is associated with viral DNA as lytic infection proceeds (Kent et al., 2004; Silva et al., 2008), suggesting that nucleosomes are not absent from viral DNA during lytic infections, but are unevenly dispersed along the viral genome.

During latency, HSV-1 DNA is maintained as a non-integrated, heterochromatic episome highly enriched in repressive marks H3K9me3 and H3K27me3 (Bloom et al., 2010; Cliffe, et al., 2009). Lytic genes are transcriptionally repressed and exhibit classical features typical of heterochromatin (Rock & Fraser, 1983; Efstathiou et al., 1986; Deshmane & Fraser, 1989; Knipe & Cliffe, 2008). Furthermore, association of viral genome with heterochromatic proteins HP1 (Canzio et al., 2011) and Bmi1 (a member of the polycomb repressor complex) has been documented (Kwiatkowski et al., 2009). LAT is enriched in epigenetic marks typical of transcriptionally active regions in latent infections, such as dimethyl H3K4 and acetyl H3K9, H3K14 (Bloom, et al., 2010). In animal studies, HSV-1 silencing occurs by heterochromatin-like formation without DNA methylation (Dressler et al., 1987; Kubat et al., 2004; Quina et al., 2006), which is typical in invertebrates, but not in mammals (Deaton & Bird, 2011). The

upstream epigenetic mechanism(s) leading to the heterochromatization of the viral genome are largely unknown.

Reactivation from Latency.

While the exact cause(s) of viral reactivation is unknown, several external stimuli have been associated with viral reactivation, such as tiredness and emotional stress (Lorette et al., 2006; Stock et al., 2001), UV light (Spruance, 1985; Spruance et al., 1995), and menstruation (Spruance et al., 1995). Upon reactivation, viral progeny are anterogradely transported back and infect the cells proximal to the primary infection, giving rise to recurrent infection.

The ability of HSV-1 to maintain in a latent, but reactivatable state is fundamental to its ability to persist in human populations. The latent form of HSV-1 is composed of heterochromatic, circular viral DNA. In this state, the host immune response does not seem to have the capability to detect the virus. Identification of novel antiviral drugs may be expedited by using cell types that are the most relevant for HSV-1 infections: human neurons. Currently, the use of induced pluripotent stem cells to differentiate neurons provide a useful model to screen for high throughput drug screening using human neuronal cells.

1.5 ANIMAL AND HUMAN MODELS

1.5.1 Animal Models

Although HSV-1 can infect a variety of mammalian species, humans are the natural host and reservoir of infection. Still, much valuable information has been obtained from mouse and

rabbit models of lytic and latent HSV-1 infection. Variations among the animal models are dependent on the viral strain, the animal, and its gender (Webre et al., 2012). For example, the viral strains 17*syn*$^{+}$ or McKrae are considered frequent 'reactivators', compared with strain KOS (Sawtell et al., 1998), so they are commonly used to infect animals for reactivation studies. Though animal models have yielded valuable information in the past, they cannot recapitulate many features of human infections, such as the cognitive deficits; furthermore, HSV-1 evolved mechanisms of latency in human neurons. Thus, a human model of HSV-1 infection would be a valuable complement to the herpes virologist's toolkit. In the following section, popular animal models of HSV-1 infection, as well as *in vitro* cell models, including induced pluripotent stem cell-derived neurons are reviewed.

Murine models

Due to their small size, the relatively low cost to house, and modest levels of care, murine models are the most frequently investigated animal models of HSV-1 infection. Infections are introduced through the cornea (Dyson et al., 1987), the nose (Tan et al., 2014), the skin (Salinas-Jasmin et al., 2015), the ear (Smith et al., 2001), the oral mucosa (Dyson et al., 1987; Kastrukoff et al., 2012), or the footpad (McKendall, 1980). Inoculation on the oral mucosa, which represents the mode of inoculation most resembling the natural course of disease in humans, results in a burst of viral activity at the site of entry (Kastrukoff et al., 2012). In animals that survive HSV-1 infection, latency is established in the trigeminal ganglia or the brainstem (Kastrukoff et al., 1982; Barnett et al., 1995; Labetoulle et al., 2000; Decman et al., 2005; Kastrukoff et al., 2010), which can occur within 24 hours post-infection (Steiner et al., 1990). Studies focusing on immune response, primary infection, or vaccine efficacy are well suited for

murine models. Despite the aforementioned advantages, rodents have small eyes, making slit lamp examination of corneal HSV-1 infections difficult. Furthermore, assessing viral activity can be difficult as mice produce less tear fluid and have smaller CNS tissue mass or corneas compared with rabbits.

In addition to the anatomical disadvantages, HSV-1 infection differs in mouse from human hosts. For example, the rate of spontaneous shedding of HSV-1 in the mouse is relatively low to non-existent compared with humans and the development of recurrent lesions during spontaneous reactivation has not been described (Webre, et al., 2012). In addition, herpes simplex encephalitis (HSE) produces diffused lytic foci in the mouse brain, but in the human brain, distinct pockets of lytic activity are observed (Meyding-Lamadé et al., 2003; Barker et al., 2014). Furthermore, there are 4 amino acid substitutions in the coding sequence of mouse Oct-1 (which interacts with viral protein VP16 and facilitates viral immediate early gene transcription) compared to human Oct-1. The difference in the amino acid sequence causes a lower binding affinity of murine Oct-1 to VP16 than the human homolog (Cleary et al., 1993). Moreover, mouse cells that are infected with HSV-1 undergo RIP-3-mediated necroptosis as a means to eliminate virally-infected cells (Wang et al., 2014; Huang et al., 2015); but RIP3 is not activated in infected human cells, hindering downstream necroptotic actions (Guo et al., 2015), further highlighting the differences in mouse and human.

HSV-1 reactivation in the mouse can be induced by several methods. After the initial infection, surviving mice are assumed to house latent HSV-1 in the trigeminal ganglia or the CNS (Burgos et al., 2002; Thompson & Sawtell, 1997, 2001). Experimental methods of *in vivo* viral reactivation include heat stress by submerging the animal in a 42°C waterbath (Sawtell & Thompson, 1992; Higaki et al., 2009), administering epinephrine (Willey et al., 1984) or sodium

butyrate (NaB; Neumann et al., 2007; Neumann et al., 2007), and ultraviolet radiation following immunosuppression (Shimeld et al., 1990). Murine latent HSV-1 infections can also be reactivated by excising, sectioning and culturing the trigeminal ganglia or superior cervical ganglia (Gussow et al., 2006; Kobayashi et al., 2012). Removal of the tissue is sufficient to consistently produce reactivation of the latent HSV-1 in the excised neurons (Schang et al., 2002).

Reactivation can also be induced by exposing explanted latent TGs to heat stress (Halford et al., 1996), sodium butyrate (NaB; Danaher et al., 2005), trichostatin A (TSA; Danaher, et al., 2005), phosphatidylinositol 3-kinase inhibitor (PI3Ki; Camarena et al., 2010; Kobayashi et al., 2012), or withdrawal of nerve growth factor (NGF) from the cell culture medium (Wilcox & Johnson, 1987; Kobayashi, et al., 2012).

Rabbit models

A key advantage of the rabbit model is the relatively large size of the eye, thus facilitating post-infection examination of corneal lesions. Similar to human infection (Kaufman et al., 2005; Kumar et al., 2009; Choudhary et al., 2015), latently infected rabbits shed viral particles in their tears (Nesburn et al., 1998; Perng et al., 2015) and saliva (Hill et al., 2012). Rabbits provide more cells, tears, saliva, and neuronal tissue than the mouse, but incur more costs to house and care and lack the diverse genetic strains that is present in mouse models. Additionally, latently infected rabbits experience spontaneous reactivation (Bloom et al., 1994), however not all latently infected humans experience reactivation (Al-Dujaili et al., 2011).

Application of HSV-1 virions to scarified corneas is a common mode of inoculation in the rabbit model. Following infection, surviving animals contain latent HSV-1 in the trigeminal

ganglia (Nesburn et al., 1972). Though spontaneous reactivation occurs in latently infected rabbits (Nesburn et al., 1972), experimental methods can also be used to induce reactivation, such as administration of epinephrine (Kwon et al., 1981; Hill et al., 1985; Rivera et al., 1988; Danaher et al., 2005; Bloom et al., 2010; Creech & Neumann, 2010), sodium butyrate (Neumann et al., 2007), nicotine patch (Myles et al., 2004), latanoprost (Gordon et al., 2003), cyclophosphamide/ dexamethasone (Gordon et al., 2003; Haruta et al., 1989), or by inducing mechanical (Nesburn et al., 1977) or electrical (Green et al., 1981) stimulation. Similar to the murine model of reactivation, latent HSV-1 infections can be reactivated by excising the trigeminal ganglia and culturing the cells *in vitro* (Trousdale et al., 1991).

Comparisons between the mouse and rabbit models have disclosed key host related differences in infection outcomes. For example, experiments utilizing LAT-deletion viral mutants produced opposing effects between the species where the mouse displayed a reduction in H3K27me3 on IE viral promoters and robust viral activity (Cliffe et al., 2009), but the rabbit model showed decreased lytic gene production and reactivation (Giordani et al., 2008). Perng and colleagues also described variations of viral activity in the mouse and rabbit when studying LAT-mutant viruses (Perng et al., 2001).

Non-human primate models

Modeling HSV-1 infection in non-human primates is less popular, because of the high maintenance cost. Furthermore, primates, such as owl monkeys (*Aotus trivirgatus)* or marmosets (*Callithrix jacchus*), have a high fatality rate from HSV-1 encephalitis (Deisboeck et al., 2003). These models are better suited for Herpes Simian B virus (B virus) infection. B virus naturally infects non-human primates, and it is pathologically and genetically similar to HSV-1 infection

in humans. B virus infection of humans results in severe encephalitis of the central nervous system and is frequently fatal, therefore, working with this virus exposes staff to considerable risks and require biosafety level 4 facilities. Because of such protective measures, cases of zoonotic transmission to humans are rare (Nsabimana et al., 2008).

1.5.2 Cellular Models

In vitro models of HSV-1 infection circumvent the costs and the ethical concerns associated with animal models, but, critically, simple *in vitro* cell models do not account for the influence of the immune system. Productive infection can occur in most cell types, including African green monkey kidney epithelial (Vero) cells, murine neuron-like cells (PC-12; Hogk et al., 2013), human fibroblasts, human neuron-like cells (SH-SY5Y), human neurons generated from aborted fetuses, or derived from human embryonic stem cells (Dukhovny et al., 2012) or from human induced pluripotent stem cells (D'Aiuto et al., 2012).

PC-12 cells

The PC-12 cell line is derived from a pheochromocytoma in the adrenal gland of a male *Rattus novegicus* (Greene & Tischler, 1976). When cultured in the presence of nerve growth factor (NGF), PC-12 cells form neuron-like cells (Greene & Tischler, 1976; Tischler et al., 1983). Exposure of HSV-1 infected PC-12 cells to NGF induces a state similar to viral latency that is reactivatable once NGF is removed from the cell culture (Block et al., 1994). NGF is critical to block productive viral infection. After an initial peak in viral activity, HSV-1 quiescence is established in infected PC-12 cells cultured in the presence of NGF. A robust HSV-1 reactivation is induced following NGF withdrawal (Block, et al., 1994). The NGF

withdrawal model for reactivation was initially described by Wilcox and colleagues who utilized primary neuronal cultures (Wilcox & Johnson, 1988). However, a significant LAT production has not been observed in quiescent PC-12 model (Block, et al., 1994). Another PC-12 model utilized acyclovir to induce a quiescent/latent state, followed by the induction of reactivation by heat stress (43°C for 3 hours), histone deacetylase inhibitors sodium butyrate or trichostatin A (Danaher et al., 2005). Several investigators have used the PC-12 model of HSV-1 infection to study aspects of viral lifecycle (Danaher et al., 2013), 3-dimensional cell culture systems (Hogk et al., 2013), and HSV-1 DNA damage repair (Millhouse, et al., 2012).

Non-neuronal human cell systems.

Non-neuronal cell types used in HSV-1 quiescence models include human fibroblasts and erythroblasts. These quiescence models mimic some, but not all aspects of an *in vivo* latent infection.

Human fibroblasts repress HSV-1 activity at 42°C when infected with ultra-low multiplicities of infection (MOI=0.003). In these culture conditions, viral reactivation can be induced by superinfection with other herpesviruses (Russell & Preston, 1986) or an adenovirus vector which supplies ICP0 (a protein which effectively promotes reactivation) at 37°C (Zhu et al., 1990). Alternatively, HSV-1 quiescence can be induced in fibroblasts in the presence of (E)-5-(2-bromovinyl)-2'-deoxyuridine combined with human interferon alpha (5BVdU+IFNα); superinfection with HCMV leads to HSV-1 reactivation (Wigdahl et al., 1982). This approach has also been successfully used in cultured rat fetal neurons (Wigdahl et al., 1984).

Alternatively, HSV-1 quiescence can be established by infecting fibroblasts that are cultured at 41°C with a relatively low concentration of fetal bovine serum (0.2%). The quiescent

infection is maintained at 41°C for six days; after this period of time, reactivation can be induced by infection at 37°C with adenovirus vector that supplies ICP0 (McMahon & Walsh, 2008).

Human erythroblasts enter a quiescent state following an infection with a mutant HSV-1 virus that does not express immediate early (IE) genes (d109; Samaniego et al., 1998). The IE genes are essential for the downstream production of early and late genes, and as a result, infection with a virus deficient for these critical proteins induces a quiescent state characterized by heterochromatization of viral DNA (Ferenczy & DeLuca, 2009) and marked reduction in viral mRNA production (Harkness et al., 2014).

SH-SY5Y neuroblastoma epithelial cells

SH-SY5Y is a human cell line is derived from a neuroblastoma. The cell line contains a trisomy of chromosome 1q (Ross et al., 1983). Following exposure to retinoic acid, these cells display some features of human neurons (Biedler et al., 1978), including the dopamine transporters, dopamine receptors (Colapinto et al., 2006), and other proteins commonly expressed in neurons, like synaptophysin, beta III tubulin, and tyrosine hydroxylase (enzyme catalyzing L-tyrosine to L-DOPA, the dopamine precursor; Higashi et al., 2015). Given their origin and ability to produce components of dopamine neurons, SH-SY5Y cells are commonly used in neurodegeneration research (Xie et al., 2010). This cell model has also been sparsely used in HSV-1 research to analyze i) aspects of lytic HSV-1 infection in regards to LAT expression (Kang et al., 2003); ii) nucleosome deposition on the viral genome (Oh & Fraser, 2008); and iii) feasibility for the use of HSV-1 vector system to deliver therapeutic genes (Xu et al., 2014). A model of HSV-2 latency was established in SH-SY5Y cells using ACV treatment,

which was reported to be sustained for 14 days; viral reactivation was induced by the use of heat stress (43°C) for 1.5 hours and forskolin (Sun et al., 2010).

Primary neuronal cultures

As the most relevant cell type that supports HSV-1 latency, primary human neurons have been used, albeit infrequently (Bastian et al., 1972; Baringer & Swoveland, 1973; Wigdahl et al., 1984; Li et al., 2011). Post-mortem human brain tissues from the trigeminal ganglia can be explanted and infectious virion production occurs within 3 weeks post-autopsy from individuals who harbor latent viral genomes (Bastian et al., 1972; Baringer & Swoveland, 1973). A human primary neuron model of HSV-1 latency was initially described by Wigdahl and colleagues (Wigdahl et al., 1984). Human fetal neurons were plated and incubated with mitotic inhibitors to eliminate contaminating non-neuronal cell types. HSV-1 was added to the primary neurons and viral replication and cytopathic effect was observed 24 to 48 hours after infection. To induce a quiescent infection in the human primary neurons, cells were pretreated with HSV-1 replication inhibitors 5BVdU+IFNα, followed by infection the next day. The combination of 5BVdU+IFNα inhibited viral gene expression and established a latent-like state for 7 days. After this 7-day period, viral inhibitors were removed, and latency was maintained for a further nine days until a fraction of neurons sporadically reactivated (Wigdahl et al., 1984).

Human induced pluripotent stem cell-derived neurons

Induced pluripotent stem cells (iPSC) are derived from somatic cells, i.e., fibroblast (Takahashi & Yamanaka, 2006; Fusaki, et al., 2009), keratinocytes (Aasen et al., 2008; Petit et al., 2012), adipose tissue (Sugii et al., 2010) and other cell types. Originally described in 2006

by Takahashi and Yamanaka, mouse fibroblasts are induced into a pluripotent state by the expression of four factors, Oct3/4, Sox2, c-Myc, and Klf4 (Takahashi & Yamanaka, 2006). These proteins function in the early embryo to maintain a pluripotent state for some cells (Nichols et al., 1998; Avilion et al., 2003; Cartwright et al., 2005; Li et al., 2005). Remarkably, iPSCs show similar morphology and protein expression as pluripotent embryonic stem cells (ESC; Takahashi & Yamanaka, 2006). In addition, these cells have the ability to self-renew and to further differentiate into the three germ layers of the human body (endoderm, mesoderm, and ectoderm; Takahashi & Yamanaka, 2006).

Differentiating human iPSCs into neurons is based on the pattern of gene expression in the developing embryo. By the 4th week of life, the neural plate has folded over itself and fused, creating the neural tube, which will form the central nervous system. Thus, neurons are derived from the ectodermal germ layer. Multipotent neural stem cells (NSC) develop from the ESCs, which are further differentiated into neuronal cells. By exposing iPSCs to the growth factors N2 (ThermoFisher, catalog 17502048) and rhFGFβ (R & D Systems, catalog 233-FB-025), NSCs can be derived, and then differentiated into neurons over the course of 4-12 weeks (D'Aiuto et al., 2014). *In vivo*, neurons follow a step-wise path that begins with neural progenitor cells and can continue to mature neurons (von Bohlen Und Halbach, 2007). At each stage of neurogenesis, cells produce an array of proteins that wax and wane over time. By utilizing antibodies that recognize these neural antigens, the stages of *in vitro* neurogenesis can be analyzed in the neuronal differentiation of iPSCs. Human iPSC-derived neurons begin as multipotent neural stem cells that express neuroectoderm markers Musashi, Nestin, and Sox1. After exposing the NSCs to culture medium supplemented with B27 and BDNF (factors that promote neuronal growth) for 4 weeks, the cells display a neuron morphology and express TUJ1

(neuron-specific class III beta-tubulin that is expressed in neuronal precursors, early post-mitotic, and mature neurons; Yang et al., 2004), MAP2 (microtubule associated protein in dendrites of mature neurons; Harada et al., 2002), VGLUT (vesicular glutamate transporter mediates packing glutamate into synaptic vesicles; Herman, et al., 2014), and NR1 (a subunit of the NMDA, or glutamate, receptor; Furukawa et al., 2005). In addition, neurons respond to the neurotransmitter glutamate and agonists of the NMDA receptor (AMPA and NMDA) in whole-cell patch-clamp experiment (D'Aiuto et al., 2014).

HSV-1 infection models utilize human iPSC-neurons derived from human fibroblasts (Lafaille et al., 2012; D'Aiuto et al., 2015; McClain et al., 2015; McNulty et al., 2016). HSV-1 quiescence is induced adopting the method described by Wigdahl and colleagues (Wigdahl et al., 1982). Briefly, iPSC-neurons are pretreated with antiviral compounds 5BVDU+IFNα for 24 hours. The cells are then infected and maintained for 7 days in the presence of 5BVDU+IFNα. The virus can be reactivated by histone deacetylase inhibitor sodium butyrate for 5 days (D'Aiuto, et al., 2015; McClain, et al., 2015; McNulty, et al., 2016).

Alternatively, neurons can be directly differentiated from fibroblasts (Vierbuchen et al., 2010). This direct conversion bypasses the need for NSC generation. The “i-N cells” have not yet been employed to model HSV-1 infections.

These models have been of tremendous importance to the understanding of HSV-1 biology and the development of antiviral drugs. Despite their undeniable importance in developing antiviral therapies, finding novel drugs exhibiting higher efficacy compared to the current therapies may be achieved by using disease-relevant human cell types. The advent of iPSC technologies provides for the first time an opportunity to generate human neurons to a scale compatible with drug screening platforms.

1.6 ANTIHERPETIC DRUGS AND DRUG RESISTANCE

No effective vaccines for HSV-1 infections are currently available (Kuo et al., 2014), therefore we are forced to rely on drugs for treatment. Acyclovir (ACV) and its derivatives are the most effective drugs available for acute infection with HSV-1 and are therefore considered the first-line treatment. ACV is a guanosine analogue lacking a 3' hydroxyl that is necessary for the reaction with the phosphate group during DNA synthesis. Thus, the absence of the 3' hydroxyl group results in the inability of adjacent nucleosides to bind into the growing DNA strands during replication. ACV is also a potent inhibitor of viral DNA polymerase. ACV is activated to ACV-triphosphate where the first phosphorylation is carried out by the viral kinase, thymidine kinase (tk). This initial reaction ensures that ACV inhibits DNA replication in virally infected cells. Subsequent phosphorylations occur via host kinases. Once incorporated into the growing viral DNA templates, replication stalls and dismantles, ultimately shutting down viral production. ACV is a potent antiviral for acute infections, but cannot eliminate the HSV-1 latent reservoir (Field & Thackray, 2000).

ACV has modest bioavailability when taken orally, estimated at 6% to 10% (Biron, 2006). To improve bioavailability, modifications were made to the parent chemical structure, leading to the generation of Valacyclovir (VACV, the L-valine ester of ACV), which increased oral bioavailability to 55% (Biron, 2006). Severe HSV-1 infections such as encephalitis require high-dose intravenous ACV, but the majority of other infections such as common cold sores require oral or topical VACV dosing only. ACV and VACV are also effective against other herpesviruses, but with decreasing efficacy. In decreasing order of highest therapeutic index, they are HSV-1, HSV-2, and VZV. VACV or ACV are commonly prescribed for infections caused by these viruses. ACV has some antiviral activity for other human herpesviruses, such as

EBV, HHV-6, HCMV, or HHV-8, although to a much lesser extent (De Clercq et al., 2001). ACV and VACV are well tolerated, though uncommon adverse effects include neurotoxicity (Asahi et al., 2009) and nephrotoxicity (Izzedine et al., 2005).

Viral resistance to ACV is rare, with estimates of less than 1% in immunocompetent individuals. Resistance manifests as sustained viral shedding or progressive disease in the presence of the drug. In the case of immunocompetent individuals with herpes keratitis, the prevalence of ACV-resistant virus is higher (~6.4%; Duan et al., 2008). Drug resistance is more common among patients who are immunocompromised (prevalence is 4% to 10%; Piret & Boivin, 2014). DNA sequences of clinical isolates revealed that 95% of resistant cases harbor viruses with mutations in the gene encoding viral tk (van Velzen et al., 2012), resulting in infections displaying a reduced pathogenicity, a reduced establishment of latency, and an impaired potential to reactivate lytic infection (Coen, 1994; Besecker et al., 2007). Alternative first-line drugs are the guanosine analog, Penciclovir (PCV) and its prodrug, Famciclovir (FCV). PCV has a mechanism of action similar to ACV, as well as the likelihood of PCV-resistant viruses through selection of tk mutants.

Other second-line drugs have been developed to inhibit the infection of ACV-resistant viral strains, e.g., Foscarnet and Cidofovir, but they cause varying degrees of host toxicity. Foscarnet (FOS) reversibly inhibits viral DNA polymerase of several herpesviruses. FOS interferes with pyrophosphate cleavage from the incoming nucleosides, which are blocked from binding to the growing DNA strand. Because DNA replication requires pyrophosphate cleavage to proceed, viral replication is inhibited. FOS does not require viral tk phosphorylation and is useful for tk-mutant viruses that are resistant to first-line antivirals; however, mutations in viral

DNA polymerase at pyrophosphate binding sites may confer resistance. FOS is administered intravenously and side effects may occur in the kidney and CNS.

Cidofovir (CDV) is an antiviral that is active against several DNA viruses. CDV is an acyclic nucleoside phosphonate and does not require involvement by viral tk. Host kinases complete the phosphorylations and then CDV can be incorporated into the growing viral DNA strand with a consequent block of DNA replication. CDV has a very low bioavailability (5%; Cundy et al., 1996) and must be administered intravenously. However, nephrotoxicity (Safrin et al., 1997), neutropenia, and hypospermia have been associated with CDV treatment. It is also considered a carcinogen and teratogen.

Brincidofovir is a prodrug of CDV, in which a lipid side-chain is conjugated to the parent CDV molecule, improving cellular uptake and bioavailability (Painter et al., 2012). Brincidofovir is less toxic than CDV, and side effects are mostly limited to gastrointestinal-related symptoms. It also has broader spectrum of antiviral effects, against HSV, VZV, HCMV, and other DNA viruses. It is presently being investigated in clinical trials. Considering that FOS and CDV do not require activation by phosphorylation of a viral tk, they may also incorporate into the growing host DNA strands during replication, leading to cellular toxicity and the aforementioned system-wide toxic profiles.

Ganciclovir (GCV, a guanosine analog) and its prodrug valganciclovir (VGCV) represent the current standard therapy for HCMV and has comparable efficacy against HSV-1 as ACV (Frank et al., 1984). Due to poor oral bioavailability of GCV (5%), VGCV was developed to increase drug oral bioavailability (60%; Pescovitz et al., 2000). Their mechanism of action is similar to ACV, and can also inhibit cellular DNA polymerases (Kimberlin & Whitley, 2007). Due to this, GCV and VGCV are associated with considerable adverse reactions on many organ

systems including kidney, bone marrow, gastrointestinal tract, CNS, and other side effects; GCV is also considered a potential human carcinogen (Laboratories, 2016). Second-line drugs, such as FOS and CDV, are available to treat resistant strains and HCMV-retinitis. HCMV resistance is estimated in the immunocompromised population at 13% to >25% (Jabs et al., 1998; Limaye, 2002).

In addition, other nucleoside analogs show promise against HSV-1 and other herpesviruses. Valomaciclovir, a guanine nucleoside analog confers antiviral effects against HSV-1, HSV-2, EBV, and VZV, with the latter two viruses showing the greatest sensitivity (Lowe et al., 1995). N-methanocarbathymidine (N-MCT), a thymidine analog has encouraging effects in HSV, EBV, and KSHV infections (De Clercq, 2013). Valomaciclovir and N-MCT have a mechanism of action similar to ACV in requiring viral tk phosphorylation, and therefore run the risk of viral resistance *via* tk mutations.

New antiviral compounds against HSV-1 and HSV-2 in clinical trials target the viral helicase/primase complex. They include Pritelivir or Amenamevir. The HSV helicase/primase complex is a heterotrimer that includes viral products UL5, UL52, and UL8. This complex functions during DNA replication to create a replication fork and to prime the leading and lagging strands for polymerization (Chattopadhyay et al., 2006). Hence, helicase/primase inhibitors (HPI) interfere with the complex to bind to the DNA, reducing DNA unwinding, priming, and ultimately viral DNA replication. These new compounds produce a potent anti-HSV-1 or HSV-2 response. HPIs operate in a tk-independent manner and can serve as alternatives to ACV-resistant viruses (Field et al., 2013). However, DNA mutations in any of the proteins in the viral helicase/primase complex derived from selection pressure can confer HPI-resistance (Biswas et al., 2007).

Other new drugs in development for HCMV are Maribavir, an inhibitor of viral protein kinase and Letermovir, a terminase inhibitor that have both shown effective antiviral results. Maribavir exerts antiviral effects by inhibiting DNA packaging and nuclear egress of encapsidated HCMV DNA (Biron et al., 2002). Maribavir has also been used to treat GCV-resistant HCMV infection (Biron et al., 2002) and also inhibits EBV infection *in vitro* (Williams et al., 2003). Clinical trials revealed neurological adverse reactions in healthy individuals, where taste disturbances (80%) was the most common and appears to be dose-dependent (Lalezari et al., 2002). Letermovir is a potent inhibitor of viral HCMV terminase (a viral protein complex that cleaves single genomes from post-replicated viral DNA and facilitates genome packaging into the viral capsid prior to egress; Bogner, 1998, 2002). Letermovir is specific to HCMV-infected cells and remains active against GCV-resistant viral strains (Marschall et al., 2012). Unlike GCV, toxicity studies of recipients of solid organ transplants or hematopoietic stem cell transplants were generally well tolerated and reduced HCMV infection (Chemaly et al., 2014; Stoelben et al., 2014).

In summary, antiviral compounds have greatly reduced the morbidity and mortality associated with HSV-1 disease, including keratitis and encephalitis and improved the quality of life for infected individuals. Additionally, antivirals like ACV or VACV are safe and efficacious for the majority of the population. However, antivirals like GCV or CDV have serious side effects with limited antiviral effectiveness, and no drug exists to eliminate the latent virus. Modifications to parent molecules may decrease toxicity and increase efficacy, but viral resistance will remain or increase, especially among immunocompromised individuals. A new generation of chemotherapeutics is needed that has different mechanisms of action, with high potency, low toxicity, and high oral bioavailability.

2.0 AIMS & RATIONALE

Aim 1. <u>Characterize and evaluate a quiescent HSV-1 infection model in human iPSC-derived neurons</u>. Most of our knowledge of HSV-1 biology comes from animal or cellular models. Yet, HSV-1 causes human specific infections and humans are the only natural reservoir for HSV-1 latency. Hence, a human neuronal cell model of HSV-1 infections could usefully complement currently available animal and cell models. Since it is difficult to obtain living human neurons that harbor latent viral genomes for scientific research, an alternate route to generate relevant models was investigated. Here, we have generated and optimized a human cellular model of HSV-1 infection using human induced pluripotent stem cell-derived neurons (iPSC-neurons). The model was used to investigate aspects of lytic infection, quiescent infection, chromatin accessibility of selected viral genes, and patterns of host gene expression. Future applications of modeling HSV-1 infections in human iPSC-neurons include testing compounds for novel antiviral effects. This section will also cover the general method sections and two peer-reviewed manuscripts that detail i) a method to generate neural stem cells and their differentiation into iPSC-neurons, and ii) evaluating lytic and latent HSV-1 models in human iPSC-neurons.

<u>Aim 1a.</u> Characterize a human iPSC-based cellular model of HSV-1 lytic and latent infections. We acutely infected iPSC-neurons for a 24-hour time period. To induce a

quiescent infection in iPSC-neurons, an antiviral cocktail of (E)-5-(2-Bromovinyl)-2′-deoxyuridine along with human interferon alpha was applied to infected cells for a period of 7 days. The level of viral repression was gauged by withdrawal of the antiviral compounds. We used a histone deacetylase (HDAC) inhibitor to reactivate quiescent infections. Viral copy number, viral gene expression, and the production of infectious virions were quantified. Patterns of viral genome occupation in the host nuclei were evaluated. Additionally, neuronal gene expression changes were assessed in the aforementioned models of HSV-1 infection.

<u>Aim 1b.</u> Evaluate the chromatin accessibility state of selected viral gene promoters in HSV-1 acutely and quiescently infected iPSC-neurons. To further evaluate models of lytic and latent HSV-1 infections, we used acutely and quiescently infected iPSC-neurons to assess whether certain viral loci are competent for transcription. We have used quantitative PCR to amplify viral gene promoters after exposing viral DNA to micrococcal nuclease (MCN). In addition, we also investigated the co-localization of proteins that are associated with transcriptional repression and with viral DNA by combining immunocytochemistry (using an anti-heterochromatin protein-1 mouse monoclonal antibody) with fluorescent *in situ* hybridization (FISH, using a probe that is complementary to viral genomes).

HYPOTHESIS: Protocols to establish HSV-1 latency in murine models can be adapted to human iPSC-neurons.

Aim 2. <u>Antiviral screening and groundwork for high-content drug screening.</u> Viral resistance to current antivirals occurs more frequently in immunosuppressed individuals. Moreover, the use of antiviral acyclovir may harmful to renal failure patients. Therefore, obtaining novel antivirals with different mechanisms of action are warranted. To enable moderate throughput screening for antiviral compounds to treat HSV-1 infections, a robust and cost-effective cellular platform was evaluated. Initial cell-based drug screening platforms require: (i) generation of large numbers of neurons in a multi-well culture systems and (ii) meaningful readouts to assess drug efficacy. This section will also cover two peer-reviewed manuscripts that detail our initial efforts to screen small compound libraries in HSV-1 infected human iPSC-neurons for antiviral effects i) using molecules that were previously reported to have lysosomotropic activities and ii) using novel, naturally occurring alkaloids derived from the Amaryllidaceae plant family. Following these studies, we sought to optimize methods to allow for future moderate throughput agnostic compound antiviral screening campaign.

Aim 2a. Generation of culture plates containing human iPSC-neurons distributed in monolayer fashion. We evaluated seeding densities of human iPSC-neurons on 96- or 384-well culture plates conducive to acutely and quiescently infected HSV-1 cultures.

Aim 2b. Automated analysis of the viral state in infected cells. High content microscopy analysis methods were used to compare the feasibility of using an HSV-1 viral construct that expresses fluorescent reporter genes during lytic infections or using the KOS wild-type virus detected with immunocytochemistry using an anti-ICP4 monoclonal antibody.

HYPOTHESIS: Human iPSC-neuronal cultures and HSV-1 infection conditions can be adapted to high-content screening in 384-well plates.

3.0 AIM 1. CHARACTERIZE AND EVALUATE A QUIESCENT HSV-1 INFECTION MODEL IN HUMAN IPSC-DERIVED NEURONS

Aim 1. Characterize and evaluate a quiescent HSV-1 infection model in human iPSC-derived neurons. Most of our knowledge of HSV-1 biology comes from animal or cellular models. Yet, HSV-1 causes human specific infections and humans are the only natural reservoir for HSV-1 latency. Hence, a human neuronal cell model of HSV-1 infections could usefully complement currently available animal and cell models. Since it is not feasible to obtain living human neurons that harbor latent viral genomes for scientific research, an alternate route to generate relevant models were investigated that were based on human fetal neuron models (Wigdahl, 1984). Here, we generated and optimized a human cellular model of HSV-1 infection using human induced pluripotent stem cell-derived neurons (iPSC-neurons). The model was used to investigate aspects of lytic infection, quiescent infection, chromatin accessibility of selected viral genes, and patterns of host gene expression. Future applications of modeling HSV-1 infections in human iPSC-neurons include testing compounds for novel antiviral effects.

This section will also cover the general method sections and two peer-reviewed manuscripts that detail i) a method to generate neural stem cells and their differentiation into iPSC-neurons, and ii) evaluating lytic and latent HSV-1 models in human iPSC-neurons.

Aim 1a. Characterize human iPSC-based cellular model of HSV-1 lytic and latent infections.

Aim 1b. Evaluate the chromatin accessibility state of viral gene promoters in HSV-1 acutely and quiescently infected iPSC-neurons.

3.1 GENERAL METHODS SECTION

The following section will describe the general methods, as well as the methods utilized to investigate Aim 1.

3.1.1 Cell Propagation

African green monkey kidney fibroblast cells (Vero) were grown in "Vero medium" (Eagle's Minimum Essential Medium (EMEM; Lonza, catalog 12611F), supplemented with 10% fetal bovine serum (FBS; HyClone, GE Healthcare Life Sciences, catalog SH3054103), and 5% antibiotic/antimycotic (HyClone, GE Healthcare Life Sciences, catalog SV3007901). Cells were grown in an incubator under standard conditions (5% CO_2, 37°C, and 100% humidity) and the cell culture medium was changed every 2-3 days.

CV-28 cells are Vero cells that have been transformed to express the wild-type viral gene UL28. These cells were used to propagate Dr. Homa's HSV-1 virus that contains a 1,881 bp deletion in viral gene UL28, an essential gene for viral assembly (Tengelsen et al., 1993).

3.1.2 Viral Propagation

Human herpesvirus type 1 is considered a Biosafety Level 2 (BSL-2) pathogen. The virus was handled in accordance to standard and special practices, safety equipment, and facilities for BSL-2 pathogens.

Infection. Vero cells (80% confluent) were infected at an MOI of 3 in a T-75 flask. The quantity of virus for cell infection was calculated utilizing the following formula (Blaho et al., 2005):

(MOI= 3) x (cell count) x (1/HSV-1 titer in pfu/µl) = amount of HSV-1 stock to add (µl)

The virus was adsorbed on the Vero cells for 2 hours at 37°C. Following the infection, the inoculum was removed and cells were washed with phosphate buffered saline (PBS). Fresh Vero medium was added to the flask (13 ml) and cells were incubated for 2-3 days, until the appearance of cytopathic effect (CPE). The cells and supernatant were transferred into 15 ml conical tubes following detachment with a cell scraper. Cells were centrifuged at 1000 rpm for 5 minutes. The supernatant medium was removed, leaving behind 1.5 ml and the cell pellet was resuspended using a vortex for 1-2 min. The tube was then placed into liquid nitrogen bath to freeze. The tube was then transferred into a 37°C water bath to thaw the cell lysates. The freezing/thawing method was repeated for a total of 3 times. During the freezing/thawing cycles, the cells were lysed to release intracellular virus into the supernatant. After the last thaw, the tube was centrifuged at 3000 rpm for 5 minutes and the top medium containing cell-free viral particles was transferred into sterile 1.5 Eppendorf tubes. The viral titer was determined by plaque assay on Vero cells as follows.

3.1.3 HSV-1 Quantitative Titrations

Three 6-well plates with 2.5 x 10^5 Vero cells per well were prepared the day before the titration procedure. Ten microliters of freshly prepared viral stock supernatant was added to 10 ml of Vero medium (dilution = 10^{-3}). The viral suspension was mixed by gentle inversion (Tube 1). One hundred microliters of viral suspension from Tube 1 was transferred in another tube containing 10 ml of Vero medium (Tube 2; dilution = 10^{-5}). Viral suspension was further diluted to 10^{-6}, 10^{-7}, 10^{-8}. One milliliter of each dilution was used to infect the aforementioned Vero cells. Infections were performed in triplicate. The virus was adsorbed on the cells for 2 hours at room temperature on a Belly Dancer shaker. After the infection, medium was removed and overlaid with 3 ml of Vero medium containing 1% carboxymethyl cellulose (CMC; Fisher, catalog 150560). The cells were cultured in standard culture conditions until viral plaques appeared (36-48 hours after infection). When infecting with the viral construct carrying EGFP and RFP reporter genes, plaques are counted under the fluorescent microscope. For HSV-1 KOS strain that does not contain fluorescent reporter genes, the cells were cultured until viral plaques appeared (3-5 days after infection). The CMC medium was removed and wells were gently washed with PBS. Crystal violet was added to each well to quantify plaques. The wells with the dilution that contained between 30 and 300 plaques were counted and utilized as viral titer using the following formula:

(number of plaques) x (dilution) = PFU/ml

NOTE 1: Preparation of 3% CMC. In a clean glass bottle, 3 grams of CMC was added to 100 ml PBS. The mixture was placed on a heated (40°C) stirplate (Sybron Barnstead

Thermolyne Nuova II Stirrer, catalog SP18425) and stirred for 2-3 h or until dissolved. The 3% CMC solution was autoclaved and diluted with Vero medium to 1% prior to use on cell cultures.

NOTE 2: Preparation of crystal violet. Five milliliters of formaldehyde (37% stock solution) was mixed with 0.5 g Gentian Violet, 0.9 g NaCl, 52.6 ml 95% ethanol, and 42.4 ml distilled water. The preparation was stirred overnight with a stir bar on a Nuova II stir plate.

3.1.4 HSV-1 Infections

HSV-1 infections proceeded similarly, unless otherwise stated.

1. The viral construct used in the majority of the experiments in this work was based on an HSV-1 construct that incorporated green and red fluorescent reporter genes under the control of the promoters for ICP0 and glycoprotein C, respectively (FIGURE 3; courtesy of Dr. Paul Kinchington, Ph.D., University of Pittsburgh; Ramachandran et al., 2008). The EGFP expression designates the virus has entered a lytic infection as it is driven by a viral immediate early gene promoter. The RFP is driven by a viral late gene promoter, signifying the virus is committed to viral replication. During a lytic infection on either Vero (MOI=1) or iPSC-neurons (MOI=0.3), EGFP can first be observed after 24 hours after infection, while RFP expression can be observed after 48 hours after infection (FIGURE 4).

Figure 3. HSV-1 structure of the viral construct.

2. A viral construct with a 1,881 bp deletion in the UL28 gene and a GFP reporter gene tagged to VP26 was used for viral infections on Vero and iPSC-neurons (Tengelsen, et al., 1993; courtesy of Dr. Fred Homa, Ph.D., University of Pittsburgh). UL28 is a viral protein that plays an essential role in cleaving and packaging viral DNA. Thus, the deletion in this viral construct results in progeny virions that lack the viral genome and the construct is replication defective (Tengelsen, 1993; Yu & Weller, 1998). The resulting progeny virions are unable to produce secondary infections (Tengelsen, 1993). During a lytic infection on Vero cells (MOI=1), EGFP was detected after 24 hours (FIGURE 5).

3. KOS is a wild-type HSV-1 strain that was obtained from a lesion on a human oral mucosa (ATCC VR-1493). This virus does not contain fluorescent reporter genes.

Lytic Infection. Acute infections in Vero cells and iPSC-neurons were performed at MOI=1 and 0.3, respectively. A lower MOI was chosen for the iPSC-neurons due to increasing cytotoxicity at higher MOIs (data not shown). The virus adsorbed on the cells for 2 hours at 37°C with gentle swirling every 30 minutes. Following the infection, the inocula were removed, cells were washed with PBS, and then cultured with the corresponding culture medium. The cells were analyzed 48 hours post infection by flow cytometry or high content imaging.

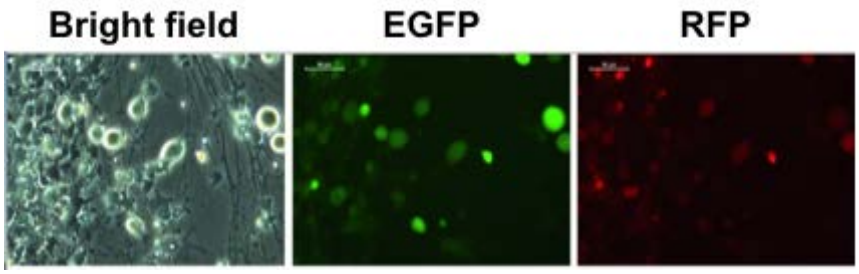

Figure 4. EGFP and RFP expression in acutely infected human iPSC-neurons.

The virus expressed EGFP and RFP under the control of viral promoters ICP0 and glycoprotein C, respectively (48 hours post infection; MOI=0.3; Courtesy of Dr. Paul Kinchington, Ph.D., University of Pittsburgh). Scale bar is 50 μM.

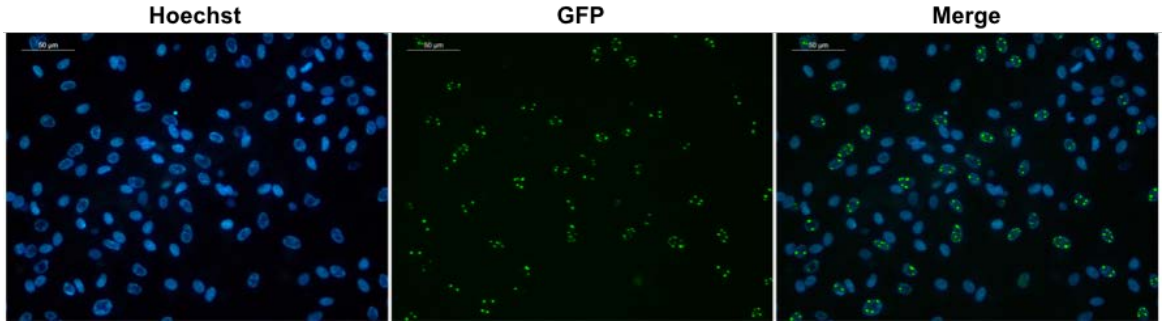

Figure 5. EGFP expression in acutely infected Vero cells.

The viral construct was based on a replication defective HSV-1 that incorporated a green fluorescent reporter gene tagged to VP26, a capsid protein (24 hours post infection; MOI=1; Courtesy of Dr. Fred Homa, Ph.D., University of Pittsburgh). Scale bar is 50 μM.

Quiescent infections. Unless otherwise stated, quiescent infection proceeded as follows: Human iPSC-neurons were pretreated with (E)-5-(2-Bromovinyl)-2′-deoxyuridine along with human interferon alpha (5BVdU+IFNα, 30 μM and 125 u/ml, respectively) for 24 hours and then infected with HSV-1 (virus containing reporter genes for EGFP and RFP, and HSV-1 strain KOS) at indicated MOIs for 2 hours in medium containing 5BVdU+IFNα. The inocula were

removed, cells were washed in PBS, culture medium containing 5BVdU+IFNα was added, and cells were cultured for 7 days. Half volume of culture medium was replaced with fresh medium every other day. After this period of time, the cell culture medium was removed and cells were washed with PBS. Next, viral reactivation was induced by culturing cells with culture medium containing sodium butyrate (NaB; 5 mM; a histone deacetylase inhibitor) for 5 days (FIGURE 16). The number of fluorescent cells was analyzed by flow cytometry. Note: The replication defective virus was not able to sustain a quiescent infection; the neurons displayed significant cytopathic effect the day after the infection (data not shown). Thus, this virus was not used to model quiescent HSV-1 infections further.

3.1.5 Cell Preparation for Flow Cytometry

Cell supernatants were collected into sterile 1.5 Eppendorf conical tubes and kept at -70°C until required for plaque reduction assay. To create a single-cell suspension, cells were dissociated by treatment with accutase for 2 minutes (for iPSC-neurons) or 10 minutes (for Vero cells) at 37°C. Proteolytic enzymes were diluted by adding Dulbecco's Modified Eagle Medium:F12, 1:1 mixture (DMEM/F12; Lonza, catalog 12-719F). Cells were collected and centrifuged at 1,200 rpm for 5 minutes. Cells from each sample were resuspended in PBS and transferred into a 96-well V-bottom plate (Corning™ Costar™, catalog 3894). Cells were pelleted by centrifugation at 2,500 rpm for 5 minutes. Supernatant was removed and cells were incubated with PBS containing LIVE/DEAD® Fixable Viability Aqua dye (ThermoFisher Scientific, catalog L34957) for 20 minutes per the manufacturer's instructions to measure cell viability. The cell suspension was diluted 3-fold with PBS and then centrifuged at 2,500 rpm for 5 minutes. Following centrifugation, the supernatant was discarded and the cells were

resuspended in 240 µl of fixative solution (3:1 PBS:10% Formalin). Cells were centrifuged as described above and kept in the dark by wrapping with aluminum foil to avoid fluorescence quenching.

3.1.6 Immunocytochemistry (ICC)

DAY 1. Cells were fixed in 4% paraformaldehyde (PFA) at room temperature for 20 minutes. Three washes of PBS were performed for 5 minutes each. Cells were incubated for one hour in 10% goat serum containing 0.02% Triton X-100 to permeabilize cell membranes. Cells were washed three times for 5 minutes in PBS. The primary antibody diluted in goat serum (per manufacturer's recommendation) was added to each well and incubated overnight at 4°C.

DAY 2. The primary antibodies were removed and three washes of PBS were performed for 5 minutes each. Fluorescent secondary antibodies were diluted in goat serum at indicated dilutions (Table 1) and added to cells for one hour at room temperature in the dark. Three washes of PBS were performed for 5 minutes each. Hoechst 33342 (ThermoFisher Scientific, catalog H3570; 1 to 1,000 dilution) was added for 2 minutes to counterstain the nuclei. Cells were washed two times with PBS to remove residual Hoechst solution, mounted with VECTASHIELD mounting medium (Vector Laboratories, catalog H1200), and sealed with clear nail polish.

Table 1. Primary antibodies.

Antibody	Manufacturer	Catalog Number	Dilution
Calbindin	Abcam	ab11426	1:200
Cart	Abcam	ab76503	1:100
Fez2	Abcam	ab67410	1:200
HP1	Millipore	05-689	1:200
HS3ST2	Novus Biologicals	NBP1-89374	1:50
ICP0	Abcam	ab6513	1:1000
ICP4	Abcam	ab6514	1:1000
MAP2	Millipore	MAB3418	1:200
Musashi	Abcam	ab21628	1:200
Nestin	R & D	MAB1259	1:1000
NR1	Abcam	ab68144	1:400
Pax6	Abcam	ab5790	1:200
S-100-β	Abcam	ab41548	1:200
Sox1	Abcam	ab87775	1:200
VGLUT1	Synaptic Systems	135303	1:200
β Tubulin III (Clone Tuj-1)	R & D	NL1195V	1:50

3.1.7 Viral Copy Number Measurement by Quantitative PCR (qPCR).

Cells were harvested into 1.5 ml Eppendorf tubes and DNA was extracted using DNeasy Blood & Tissue Kit (Qiagen, catalog 69504) following manufacturer's instruction. The DNA was quantified using Quant-iT™ PicoGreen® dsDNA Assay Kit (ThermoFisher, catalog P11496) and qPCR reactions were carried out by using 5 ng/reaction. The EGFP locus within the HSV-1 viral construct genome was amplified in the qPCR reaction using custom-designed oligonucleotide primers.

qPCR conditions. In each assay for the standard curve and the unknown samples, the following reagents were added for the qPCR master mix in a 384-well plate (MicroAmp®

Optical 384-Well Reaction Plate with Barcode, ThermoFisher Scientific, catalog 4309849): 2X TaqMan® master mix (ThermoFisher Scientific, catalog 4370048), 1X probe master mix (Pereira et al, 2013), and 5 ng of DNA in a total reaction volume of 10 µl. The probe master mix includes a final concentration of 18 µM EGFP forward primer (5'-ccacatgaagcagcacgactt-3'), 18 µM EGFP reverse primer (5'-ggtgcgctcctggacgta-3'), and 5 µM probe (5'-6FAM- ttcaagtccgccatgcccgaa-TAMRA-3'). Samples were loaded on AB Prism 7900HT for the following conditions: 95°C for 3 min followed by 45 cycles of 95°C for 15 sec and 55°C for 30 sec, and finished with 72°C for 30 sec.

Standard Curve. pEGFP-N1 plasmid (Clontech) DNA was quantified by Quant-iT™ PicoGreen® dsDNA Assay Kit (ThermoFisher, catalog P11496) per manufacturer's instruction and the resulting concentration was entered into the University of Rhode Island Genomics and Sequencing Center calculator to estimate copy number (http://cels.uri.edu/gsc/cndna.html). The quantity of DNA (in nanograms) and the length of the plasmid (4,733 base pairs) is entered and approximate copy number is calculated. Copy number of the diluted plasmid DNA samples ranged from 298 billion to 29.8 copies. The resulting CT values for each condition were plotted in a scatterplot graph and the regression line was fitted to the data. The standard curve was used to calculate copy number of the test samples (FIGURE 6).

copy number	CT
298,000,000	13.7542
5,960,000	17.9586
2,980,000	20.1051
596,000	22.0699
298,000	23.8097
59,600	25.7778
29,800	27.1934
2,980	31.1223
596	32.8376
298	34.8282
29.8	36.0944

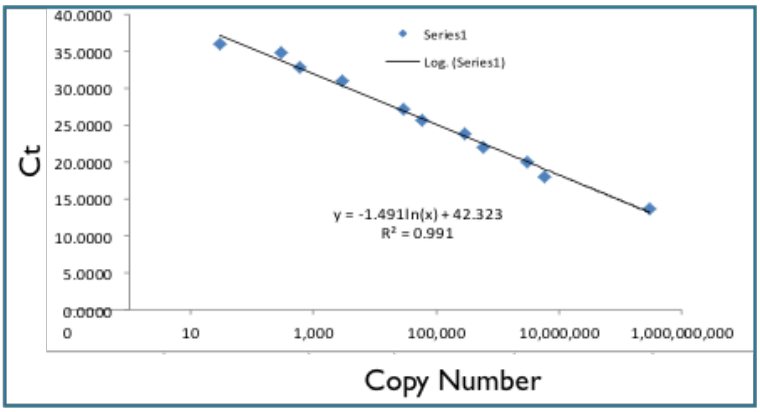

Figure 6. Standard curve generated using pEGFP-N1 plasmid.

Test Samples. Cells were mechanically harvested, and total DNA was extracted using DNeasy Blood & Tissue Kit following manufacturer's instruction. The DNA was quantified by Quant-iT™ PicoGreen® dsDNA Assay Kit per manufacturer's instruction. The final amount of DNA added to the qPCR reaction was approximately 5 nanograms. In the qPCR reaction, technical triplicates were measured for each biological triplicate. The viral copy number of each test condition was calculated using the standard curve.

3.1.8 Fluorescent *in situ* Hybridization

3.1.8.1 HSV-1 Probe Generation

HSV-1 genomic DNA (10-20 ng) was amplified using GenomiPhi (GE Healthcare, catalog 25-6600-30) according to manufacturer's instruction. The resulting product was checked on a 1% agarose gel for the presence of high molecular weight DNA product. One microgram of the GenomiPhi-amplified DNA was labeled with fluorescent dUTP via nick translation kit (Abbott Molecular, catalog 07J00-001) following manufacturer's instruction and placed in a thermal cycler at 15°C for 12 hours, and then 65°C for 10 minutes. The nick-translated product

was ethanol-precipitated along with 10 µg Cot-1 DNA® (ThermoFisher, catalog 15279011) and 40 µg sheared salmon sperm DNA. The supernatant was removed, the pellet washed with 200 µl of 70% ethanol, and air-dried in a dark environment at room temperature.

DNA was dissolved in 3 µl of sterile water. The probe was then mixed with 9 µl of Vysis LSI/WCP hybridization buffer and stored at -20°C in the dark until ready for use (up to 1 year).

3.1.8.2 Two-Dimensional (2D) Fluorescent *in situ* Hybridization (FISH)

Cell Fixation. Cells infected on matrigel-coated microscope slides or chamber slides (Nunc™ Lab-Tek™ Chambered Coverglass, Thermo Scientific™, catalog 155380) were washed three times with PBS and fixed in 4% paraformaldehyde (Fisher Scientific, catalog 15710-S) for 10 minutes. Slides were washed three times for 3 minutes each with 0.01% Triton™ X-100 (Sigma Aldrich, catalog X100-5ML) and then washed in 0.5% Triton X-100 for 10 minutes. Slides were washed three times for 10 minutes each in PBS. Slides were incubated in 50% formamide/2X SSC solution for at least one hour, preferably overnight. Slides could be kept in this solution at 4°C for long-term storage up to 3-4 months.

Probe Denaturation and Hybridization. Slides were removed from the 50% formamide/2X SSC solution and drained on a paper towel to remove excess fluid. The probe (250 ng) was pipetted onto the target area of the slide in a drop-wise fashion. This area was covered with a coverslip. Slides were protected from light during this and all subsequent steps. Bubbles were removed by guiding them to the edge of the coverslip by pressing a clean p1000 pipette tip along the top coverslip. Excess fluid was removed from the edge of the coverslip with a Kimwipe and the coverslip was completely sealed around its perimeter using Elmer's rubber cement. The slides were placed on a Vysis Hybrite at 75°C for 2 minutes to denature cellular

and probe DNA and then left overnight at 37°C for hybridization. To prevent slides from drying out, paper towels soaked in water lined the Vysis Hybrite internal compartments.

Slide Washing and Detection. All steps were performed under light protection. Following hybridization, the rubber cement on the coverslips was carefully peeled away and the coverslip was slowly guided to the edge of the slide and removed. The slides were placed in a Coplin jar filled with 2X SSC. To remove cross-hybridization signals, the slides were washed in SSC three times for 5 minutes each in 2X SSC at 37°C, followed by three washes, 5 minutes each, in 0.1X SSC at 60°C. Nuclei were counterstained with Hoechst 33342 (1 to 1,000 dilution) for 2 minutes, and mounted on microscope slides in VectaShield mounting medium (Vector Laboratories, catalog H-1000) and sealed with clear nail polish. Slides were analyzed with a fluorescent microscopy and stored at 4° C in a covered slide box.

3.1.9 Three-Dimensional (3D) FISH

Cell Fixation. Procedure was conducted at room temperature unless otherwise specified. Cells were fixed in 4% paraformaldehyde for 10 minutes and then washed three times with 0.5% Triton X-100 for 3 minutes each to increase cell membrane permeability. Three rounds of PBS washing were performed for 30 seconds each. Glycerol (20%) was added to the cells for 60 minutes. Cells were snap-frozen by dipping the slides into liquid nitrogen for 30 seconds and then thawed to room temperature on a clean paper towel. The cells were frozen/thawed for a total of 5 times and then cells were washed in PBS for three rounds for 10 minutes each. Cells were incubated twice in 2X SSC for 3 minutes each and then incubated in 50% formamide/2X SSC for one hour.

Probe Penetration Treatment with Pepsin Solution. Slides were incubated in 2X SSC for 2 minutes and then PBS for 3 minutes. A pepsin solution (0.005% pepsin in 0.01 N HCl) was applied to the cells for 6 minutes at 37°C to aid in probe penetration *via* controlled protein degradation. Cells were rinsed twice in PBS/50mM $MgCl_2$ for 5 minutes each to inactivate the pepsin solution. Cells were post-fixed in 1% paraformaldehyde for 10 minutes and then washed in PBS once for 5 minutes. Slides were incubated twice in 2X SSC for 5 minutes each and then exposed for at least 1 hour in 50% formamide/2X SSC.

Probe Denaturation and Hybridization and *Slide Washing and Detection* were performed identical to the master FISH protocol.

3.1.10 FISH in Suspension

The procedure of FISH on cells in suspension was identical to the 2D FISH protocol. The only difference was that between all washing steps, cells were pelleted in a microcentrifuge at 1,000 rpm for 2 minutes. This speed reduced damage to the structures of the cells and significantly reduced sample loss. After centrifuging, top medium was carefully removed with a p1000 pipette and cell pellet was gently resuspended by flicking the tube. To perform the probe hybridization, cells were placed into a 0.2 µl PCR tube with 10 µl probe and a thermal cycler was used in place of the Vysis Hybrite under identical temperature and time conditions. All subsequent steps were performed under light protection. After the final washing step, cells were exposed to Hoechst 33342 (1 to 1,000 dilution) for 2 minutes and then two rounds of PBS washes to remove residual Hoechst solution. After the final PBS addition, cells were centrifuged and the PBS removed. The cell pellet was resuspended in one drop of VectaShield mounting medium, and transferred onto a Superfrost™ microscope slide (Fisher Scientific, catalog 12-550-

123). Cells were covered with a coverslip and sealed with clear nail polish. Alternatively, cells were prepared for flow cytometry as previously described for quantification (see methods section 3.1.5).

3.1.11 Co-ICC/FISH

The 2D FISH protocol was completed on cells affixed to microscope slides. However, Hoechst staining and the subsequent two PBS washings were omitted. Following the final washing step of 0.1 X SSC at 60°C, cells were exposed to 0.02% Triton X-100 in goat serum for one hour to permeabilize cell membranes and block non-specific antibody binding. Slides were washed once in PBS for 5 minutes. Primary antibody diluted in 10% goat serum (per the manufacturer's recommendation) was added to each well and incubated overnight at 4°C in a dark environment. The "Day 2" procedure outlined in ICC protocol is followed identically under light protection (see methods section 3.1.6).

3.1.12 Reverse Transcriptase Quantitative Polymerase Chain Reaction

The alterations of viral gene expression at the RNA level were analyzed by reverse transcriptase quantitative polymerase chain reaction (RT-qPCR). Decreased transcription of viral genes were indicative of viral inhibition, or viral life cycle gene class inhibition. As reported (McNulty et. al., 2016), cells were collected into a 1.5 ml Eppendorf tube and RNA was extracted using Qiagen RNeasy Mini kit (Qiagen, catalog 74104) following the manufacturer's protocol. RNA quality was checked by loading 1 µl on a 1% agarose gel. A high quality RNA sample showed two sharp bands corresponding to the 28S and 18S rRNAs. Any bands located

above the 28S rRNA band indicated genomic DNA contamination and smeared product at or below the 18S rRNA indicated degraded RNA. Total RNA was converted to cDNA using random hexamer primers provided by the Qiagen RT kit (Qiagen, catalog 205311) following manufacturer's protocol. The resulting product was diluted to 0.5X with 20 µl PCR-grade water. The following reagents were mixed in a 384-well plate (MicroAmp® Optical 384-Well Reaction Plate with Barcode, ThermoFisher Scientific, catalog 4309849): 2X Taqman master mix, 20X probe mix, and 1 µl of the diluted cDNA for a total reaction volume of 10 µl. Forward, reverse, and internal probe oligos specific to viral genes were custom designed. The probe mix contained a final concentration of 18 µM forward, 18 µM reverse primer, and 5 µM internal probe. Probe sequences are as follows:

ICP4_Forward: 5'–CGA CAC GGA TCC ACG ACC C–3'
ICP4_Reverse: 5'–GAT CCC CCT CCC GCG CTT CGT CCG–3'
ICP4_probe: 5'–VIC–ACC GCC AGA GAC AGA CCG TCA GA–MGB-NFQ–3'

HSV DNA Pol_ Forward: 5'–AGA GGG ACA TCC AGG ACT TTG T–3'
HSV DNA Pol_ Reverse: 5'–CAG GCG CTT GTT GGT GTA C–3'
HSV DNA Pol_probe: 5'–6FAM–ACC GCC GAA CTG AGC A–MGB-NFQ–3'

LAT_Forward: 5'–GAC AGC AAA AAT CCC CTG AG–3'
LAT_Reverse: 5'–ACG AGG GAA AAC AAT AAG GG–3'
LAT_probe: 5'–6FAM–CGA CAC GGA TTG GCT GGT GT–MGB-NFQ–3'

Endogenous control gene probes were specific to beta-actin (ACTB) and spanned exons 2 and 3 (Applied Biosystems, catalog 4310881E). Samples were loaded on Applied Biosystems Prism 7900HT for the following conditions: 95°C for 12 min followed by 40 cycles of 95°C for 15 sec and 55°C for 60 sec. Resulting cycle threshold (Ct) values were converted to fold-change

utilizing the following equation (Schmittgen & Livak, 2008): $2^{-\Delta\Delta C_T}$ = (C_T [gene of interest] – C_T [endogenous control]) sample A – (C_T [gene of interest] – (C_T [endogenous control] sample B. Sample B was considered the untreated group.

3.1.13 CHART-PCR

To investigate whether specific viral genes are competent for transcription, their accessibility to micrococcal nuclease (MCN) was analyzed by **Ch**romatin **A**ccessibility **R**eal **T**ime-(CHART) qPCR (Rao et al., 2001) with modifications.

3.1.13.1 MCN Digestion and DNA Extraction

*Cells and viruses***.** Human induced pluripotent stem cell (iPSC)-derived neurons (iPSC-neurons) were cultured as previously described (D'Aiuto et al., 2012). Approximately 1.8 x 10^7 iPSC-neurons were harvested from each condition. The HSV-1 strain was genetically modified to express enhanced green fluorescent protein (EGFP) and monomeric red fluorescent protein (RFP) under the control of viral promoters ICP0 and gC, respectively (Ramachandran et al., 2008).

Viral infection. To test lytic HSV-1 infection, cell-free virus was adsorbed onto iPSC-neurons at an MOI = 0.3 for 2 hours. The inoculum was removed, cells were washed with PBS, and the medium was exchanged. The cells are harvested at 8 hours post infection (hpi) to eliminate the risk of confounding secondary or tertiary infections. For the quiescent infection, iPSC-neurons were pretreated with 5BVdU + IFNα (30 μM and 125 u/ml, respectively) for 24 hours. HSV-1 was adsorbed onto the cells for 2 hours in the presence of 5BVdU+IFNα at an MOI=0.3, the inoculum was removed, the cells were washed with PBS, and fresh neurobasal

medium containing 5BVdU + IFNα was added. Half of the volume of medium was exchanged every other day for a total of 7 days and cells were harvested. iPSC-neurons that were not infected were also processed for CHART-PCR.

MCN digestion and DNA extraction. The cells for each condition (uninfected, infected, or quiescently infected) were gathered into separate 15 ml conical tubes by gentle pipetting with a Gilson® PIPETMAN (p1000) and centrifuged at 1,500 rpm for 5 minutes. The supernatant was carefully removed and 4 ml of ice-cold EZ Lysis Buffer was added to lyse the cells while leaving the nuclei intact (Nuclei EZ Prep Nuclei Isolation Kit, Sigma Aldrich, catalog NUC-101). Samples were vortexed and left on ice for 5 minutes. The tubes were centrifuged at 1,750 rpm for 5 minutes at 4°C. The pellet containing the nuclei was placed on ice after the supernatant was removed and discarded.

The following steps were critical for the experiment. Because the nuclei could aggressively clump at this step, we optimized it by rapidly working on one sample at a time. In each tube (one condition), 250 µl of MCN digestion buffer (10 mM Tris (pH 8), 1 mM $CaCl_2$ in autoclaved water) was added, triturated, and quickly distributed evenly into 5 Eppendorf tubes. These 5 tubes were kept on ice until all conditions were processed. One tube per condition was kept on ice and not exposed to the MCN. The other 4 tubes per condition received 0.5 units, 1.0 units, 3.0 units, or 5.0 units of MCN (Sigma Aldrich, catalog N3755-200UN). The tubes were gently tapped and placed into 39°C for 20 minutes. The nuclease activity was stopped by adding 5 mM EGTA (final concentration; pH 8) per tube. MCN digestion buffer (133 µl) and 17 µl of 10% SDS were added per sample. An equal volume of phenol was added and tubes were mixed by inversion. Samples were centrifuged at 14,000 rpm for 10 minutes. The top layer was carefully removed and placed into a new Eppendorf tube. One-tenth volume of 3M sodium

acetate was added and mixed. Two volumes of ethanol (100%) was added and samples were mixed by inversion and placed into -70°C for 30 minutes. The samples were centrifuged at 14,000 rpm for 30 minutes and the supernatant was carefully poured off. The DNA pellet was washed twice with ethanol (70%) and allowed to air-dry. Twenty microliters of PCR-grade water was added per tube, except the undigested samples, where 40 µl was added. Following DNA extraction, each sample was quantified using Quant-iT™ PicoGreen® dsDNA Assay Kit (ThermoFisher, catalog P11496) per manufacturer's instruction.

3.1.13.2 CHART-PCR

qPCR Conditions. The qPCR was carried out in 384-well plates (ThermoFisher Scientific, catalog 4309849). For each reaction, 5 ng of DNA was added to a 10 µl master mix composed of 2X TaqMan master mix (ThermoFisher Scientific, catalog 4370048), and 1X probe master mix (18 µM forward primer, 18 µM reverse primer, and 5 µM internal oligo).

Samples were analyzed as technical triplicates and loaded on AB Prism 7900HT for the following conditions: EGFP: 95°C for 3 min followed by 45 cycles of 95°C for 15 sec and 55°C for 30 sec, and finished with 72°C for 30 sec; host genes *GAPDH* and *RHO*: 95°C for 3 min followed by 45 cycles of 95°C for 15 sec and 60°C for 30 sec, and finished with 72°C for 30 sec; and viral genes ICP4, ICP27, gC, and LAT: 95°C for 12 min followed by 45 cycles of 95°C for 15 sec and 55°C for 1 minute.

Primers. Primers were optimized for thermal cycling conditions and the identity of the PCR product was verified by Sanger sequencing. The promoter region of each gene was targeted for CHART-PCR (Table 2; Dr. David Bloom, Ph.D. provided the sequences for the LAT promoter). The amplified region of EGFP was downstream of the ICP0 promoter region.

Table 2. Primer sequences for the promoter regions of control host loci and viral loci.

	Forward Primer	Reverse Primer	Internal oligo
ICP4p	5'-GACGTAGCACGGTAGGTCAC-3'	5'-CTTTTTCCCACCCAAGCAT-3'	5'-6FAM-CCGTCGACGCGGAACTAGCG-TAMRA-3'
ICP27p	5'-CGGCCTGACAGAGCTGTATT-3'	5'-CCGAGAGGATGATGGAACAG-3'	5'-6FAM-AAGGGGCTGTCGGGCGTC-TAMRA-3'
gCp	5'-TGTGTGATGATTTCGCCATAA-3'	5'-ATGGGGGTGTGAGTTCGAT-3'	5'-6FAM-CACTACCGAGGGCGCTTGGT-TAMRA-3'
LATp	5'-CAATAACAACCCCAACGGAAAGC-3'	5'-TCCACTTCCCGTCCTTCCAT-3'	5'-6FAM-TCCCCTCGGTTGTTCC-TAMRA-3'
GAPDHp	5'-AGACCTTGGGCTGGGACT-3'	5'-GAACAGGAGGAGCAGAGAGC-3'	5'-6FAM-AAATTGAGCCCGCAGCCTCC-TAMRA-3'
RHOp	5'-TGACCTCAGGCTTCCTCCTA-3'	5'-ATCAGCATCTGGGAGATTGG-3'	5'-6FAM-ATTAGGCCCTCAGTTTCTGCAGCG-TAMRA-3'

3.1.14 Other Assays for Viral Titers in the Latency Model

RNA FISH (Prieto et al., 2007) and PCR *in situ* (Bagasra, 2007) assays were attempted. We reasoned that an RNA FISH probe specific for the viral latency associated transcript (LAT) would provide a method to quantify latently infected cells, especially if it could be paired with flow cytometry. Similarly, PCR *in situ* that amplified a viral gene may provide a method to detect the viral genome in latently infected neurons. However, in the results were variable and the assays were abandoned because they were not reproducible.

3.2 LARGE-SCALE GENERATION OF HUMAN IPSC-DERIVED NEURAL STEM CELLS/EARLY NEURAL PROGENITOR CELLS AND THEIR NEURONAL DIFFERENTIATION

Leonardo D'Aiuto[1,y], Yun Zhi[1,2,y], Dhanjit Kumar Das[1,3], Madeleine R Wilcox[4], Jon W Johnson[4], Lora McClain[1,5], Matthew L MacDonald[1], Roberto Di Maio[6,7], Mark E Schurdak[8], Paolo Piazza[9], Luigi Viggiano[10], Robert Sweet[11], Paul R Kinchington[12,13], Ayantika G Bhattacharjee[1], Robert Yolken[14], and Vishwajit L Nimgaonkar[1,5,*]

[1]Department of Psychiatry; Western Psychiatric Institute and Clinic; University of Pittsburgh School of Medicine; Pittsburgh, PA USA;
[2]Department of Pharmacology and Pharmaceutical Sciences; School of Medicine; Tsinghua University; Beijing, China;
[3]Genetic Research Center; National Institute for Research in Reproductive Health; Mumbai, India;
[4]Department of Neuroscience and Center for Neuroscience; University of Pittsburgh; Pittsburgh, PA USA;
[5]Department of Human Genetics; Graduate School of Public Health; University of Pittsburgh; Pittsburgh, PA USA;
[6]Pittsburgh Institute for Neurodegenerative Diseases and Department of Neurology; University of Pittsburgh; Pittsburgh, PA USA;
[7]Ri.MED Foundation; Palermo, Italy;
[8]Drug Discovery Institute; University of Pittsburgh; Pittsburgh, PA USA;
[9]Department of Infectious Diseases and Microbiology; University of Pittsburgh; Pittsburgh, PA USA;
[10]Department of Biology; University of Bari "Aldo Moro"; Bari, Italy;
[11]Mental Illness Research, Education, and Clinical Center; VA Pittsburgh Healthcare System; Pittsburgh, PA USA;
[12]Department of Ophthalmology; University of Pittsburgh School of Medicine; Pittsburgh, PA USA;
[13]Department of Molecular Genetics & Biochemistry; University of Pittsburgh; Pittsburgh, PA USA;
[14]Stanley Division of Neurovirology; Department of Pediatrics; Johns Hopkins University School of Medicine; Baltimore, MD USA.

D'Aiuto L, Zhi Y, Kumar Das D, Wilcox MR, Johnson JW, McClain L, MacDonald ML, Di Maio R, Schurdak ME, Piazza P, Viggiano L, Sweet R, Kinchington PR, Bhattacharjee AG, Yolken R, Nimgaonkar VL. Large-scale generation of human iPSC-derived neural stem cells/early neural progenitor cells and their neuronal differentiation. *Organogenesis*.2014;10 (4):365–377.

3.2.1 Abstract

Induced pluripotent stem cell (iPSC)-based technologies offer an unprecedented opportunity to perform high- throughput screening of novel drugs for neurological and neurodegenerative diseases. Such screenings require a robust and scalable method for generating large numbers of mature, differentiated neuronal cells. Currently available methods based on differentiation of embryoid bodies (EBs) or directed differentiation of adherent culture systems are either expensive or are not scalable. We developed a protocol for large-scale generation of neuronal stem cells (NSCs)/early neural progenitor cells (eNPCs) and their differentiation into neurons. Our scalable protocol allows robust and cost-effective generation of NSCs/eNPCs from iPSCs. Following culture in neurobasal medium supplemented with B27 and BDNF, NSCs/ eNPCs differentiate predominantly into vesicular glutamate transporter 1 (VGLUT1) positive neurons. Targeted mass spectrometry analysis demonstrates that iPSC-derived neurons express ligand-gated channels and other synaptic proteins and whole-cell patch-clamp experiments indicate that these channels are functional. The robust and cost-effective differentiation protocol described here for large-scale generation of NSCs/eNPCs and their differentiation into neurons paves the way for automated high-throughput screening of drugs for neurological and neurodegenerative diseases.

3.2.2 Introduction

Research in neuropsychiatry and neurodevelopmental disorders has been hampered by difficulty in obtaining neuronal cells from affected individuals that can be cultured and amplified in vitro. Human embryonic stem (hES) cells and human iPSCs (Takahashi & Yamanaka, 2013)

have revolutionized such research, as they can be differentiated into neurons *in vitro* from specific individuals (Beevers et al., 2013; D'Aiuto et al., 2012; Eigentler et al., 2013), potentially enabling personalized medicine by overriding the problems of allogenic recognition. Compelling evidence now indicates that iPSC-based models can be used to model selected aspects of neurological and neurodegenerative disorders (Brennand et al., 2011; Liu et al., 2012; Kaye & Finkbeiner, 2013). Besides their potential to provide important molecular insights into pathogenic mechanisms, iPSC-based cellular platforms can also be used for drug discovery in specific differentiated cell types (Boissart et al., 2013). Such platforms require replicable, efficient, and cost effective protocols to generate uniform cultures of neurons in sufficient numbers to enable screening of potentially thousands of different compounds. For high-throughput screening, NSCs or NPCs from hES cells or iPSCs are currently transferred into multi-well culture plates for neuronal differentiation (Zhao et al., 2012; Charbord et al., 2013; Efthymiou et al., 2014). Different strategies are employed to derive the NSCs or NPCs, such as generation of EB followed by differentiation into neural rosettes (Dhara & Stice, 2008; Muratore et al., 2014; Velasco et al., 2014). EBs are 3-dimensional spherical aggregates that recapitulate several aspects of early embryogenesis. EBs generated from hES cells and human iPSCs efficiently differentiate into neural rosettes when cultured in specific selective culture media with growth factor supplements (Kurosawa, 2007), but EBs can have variable differentiation outcomes based on factors such as their initial size (Bauwens et al., 2008). To enable more homogenous differentiation, microwell arrays have been specifically developed to allow the formation of EBs with uniform size (StemCell Technologies, Inc. Inc.).

The drawbacks related to EBs motivated differentiation protocols based on adherent culture systems that eliminate the EB generation step. Another advantage of adherent culture

systems is that more uniform exposure to morphogens and growth/differentiation factors is achieved (Dhara & Stice, 2008). Neural rosettes (which represent a distinct class of NSCs; Elkabetz & Studer, 2008) generated in these adherent culture systems are isolated mechanically, then transferred and cultured into low attachment plates, where they form spherical cell aggregates called neurospheres that can be propagated as 3-dimensional structures (Cho, et al., 2008), or expanded as monolayer cultures of NSCs/ NPCs (Zhao et al., 2012) However, neurospheres are not ideal for large-scale production of neurons in multi-well plates for high-throughput screening because of technical difficulties in loading uniform numbers of spheres with uniform size into individual wells. Thus, monolayer cultures of NSCs/NPCs would be advantageous. Several protocols to derive NSCs/NPCs efficiently from hES cells or iPSCs currently utilize Noggin to induce neuronal differentiation (Baharvand et al., 2007; Kirkeby et al., 2012), but the need for Noggin significantly increases the cost of the differentiation process.

We have recently developed a method for efficient differentiation of human iPSCs into neurons (D'Aiuto, et al., 2012) that does not involve generation of EBs. Using an adherent culture system that does not require Noggin, we generate NSCs/eNPCs in a scalable manner. This process takes about 4 weeks and approximately 4 additional weeks are required for differentiation mainly into VGLUT1 positive neurons. Here, we describe a detailed step-by-step protocol that allows efficient, robust, cost effective and large-scale generation of neurons. This differentiation protocol has been successfully applied to 6 different iPSC lines.

3.2.3 Results

3.2.3.1 Outline of differentiation protocol and nomenclature

The steps of large-scale generation of NSCs/eNPCs from iPSCs and their differentiation into neurons are schematically described in FIGURE 7. Human iPSC cultures are exposed for 5 d to Neural Precursor (NP) Selection medium, and successively for 7 d in NP expansion medium. Following this phase, differentiating iPSC cultures are characterized by the presence of cellular aggregates that include emerging neural rosettes. These cells express NSCs markers, such as NESTIN (Elkabetz & Studer, 2008), SOX1 (Venere et al., 2012), and MUSASHI (Kim et al., 2012; FIGURE 8). The expression of PAX6 (Elkabetz & Studer, 2008) is limited to the areas forming neural rosettes (FIGURE 8). This observation is in line with data by Suter et al. (Suter et al., 2009) showing that PAX6 expression follows the expression of SOX1. The cellular aggregates progressively develop into increasing numbers of neural rosettes.

To facilitate further differentiation into NSCs/eNPCs, cellular aggregates are manually fragmented and cultured in ultra-low attachment plates where they round up, forming spherical cellular aggregates (FIGURES 7 and 9). Microscopic and immunocytochemical analyses of the spherical cellular aggregates show features of neurospheres similar to those generated by culturing human sub-ventricular zone from postmortem brains (Gonzalez-Perez, 2012; FIGURES 9a, 9b and 49). Because it is unclear whether these spherical cellular aggregates possess all the characteristics of neurospheres, they are termed neurosphere-like structures (NLSs) in this report. Note that most of the NLSs contain multiple neural rosettes. The NLSs are further purified by transferring them into matrigel-coated plates (FIGURE 7). When the NLSs are thus flattened, it is possible to clearly observe the neural rosettes (FIGURE 9) that are subsequently dissected and transferred into new ultra-low attachment plates where they round up

overnight to form new purified NLSs (FIGURE 7). Purified NLSs can then be expanded as monolayer cultures of NSCs/eNPCs (FIGURE 10) and further differentiated into neurons (FIGURES 11 and 12).

3.2.3.2 Characterization of iPSC-derived NSCs/eNPCs and neurons

Western blotting analysis of NSCs/eNPCs showed a relatively low expression level of NeuroD1, indicating the absence of, or the presence of only a minor fraction of late NPCs (Gao et al., 2009) (FIGURE 10a). Hence, NPCs were denoted as "early" (eNPCs). Expression of NCS markers MUSASHI, PAX6, NESTIN, and SOX1 is depicted in FIGURE 10b. Analysis of PAX6 expression in NSCs/ eNPCs by high-content imaging in individual wells of a 96-well plate showed that greater than 99% of the cells have PAX6 FITC levels above background (FIGURE 10c).

Following culture in neurobasal medium supplemented with B27 and BDNF for 4 weeks (see Reagents setup), more than 90% of differentiating cells were TUJ1 positive (FIGURE 11). Immunocytochemical analysis showed that in our culture conditions, neuronal cells are also prevalently VGLUT1 positive (FIGURE 11). Expression of the NR1 subunit of NMDA receptors was detected in a substantial fraction of neurons (FIGURE 11). A small fraction of neurons were GAD1 positive (D'Aiuto et al., 2012). No dopaminergic neurons were observed following immunocytochemistry. A subpopulation of neurons stained for CALBINDIN (FIGURE 12), a cytosolic calcium-binding protein with increased expression in layer 3 of pyramidal cells in the dorsolateral prefrontal cortex (DLPFC) compared with layer 5 pyramidal cells in the same region (Hayes & Lewis, 1992). In addition, expression of the neuropeptide CART, which is increased layer 3 versus layer 5 pyramidal cells (Dr. David Lewis, unpublished), was observed only in discrete areas of the neuronal cultures (FIGURE 12). Conversely, low-level staining was

observed for the layer markers FEZ2 and HS3ST2, which have higher expression in layer 5 pyramidal cells vs. layer 3 cells (Dr. David Lewis, unpublished; FIGURE 12). Taken together, these results indicate that neurons obtained with our differentiation procedure possess features of DLPFC layer 3 pyramidal neurons.

In whole-cell patch-clamp experiments, currents were recorded from ligand-gated channels after 2 months of neuronal differentiation of NSCs/eNPCs in neurobasal medium. Glutamate receptor-mediated currents were recorded at a holding potential of -85 mV in response to application of 100 µM glutamate + 100 µM glycine (6 of 10 cells; in responding cells peak current range was -88.5 to -771.1 pA, average -376.6 pA; FIGURE 13a), 100 µM AMPA (8 of 13 cells; in responding cells peak current range was -15.5 to -481.8 pA, average -186.6 pA; FIGURE 12 and 13b) and 100 µM *N*-methyl-D-aspartate (NMDA) + 100 µM glycine (4 of 7 cells; in responding cells peak current range was -80.0 to -320.0 pA, average -233.5 pA; FIGURE 13c). GABA receptor-mediated currents were recorded at a holding potential of 15 mV in response to application of 1 mM GABA (11 of 12 cells; in responding cells peak current range was 75.5 to 3958.8 pA, average 736.9 pA; FIGURE 13d).

We observed robust expression of numerous neuronal proteins, both pre- and post-synaptic in iPSC-derived neurons (FIGURES 14a and 14b). In general, synaptic protein expression was higher in human cortex tissue compared to iPSC-derived neurons per mg total protein (FIGURE 14c). This is unsurprising, as the cellular composition of human cortex and neuronal cultures generated from iPSCs is very different. It does indicate, however, that the iPSC-derived neurons express many neuron-specific genes.

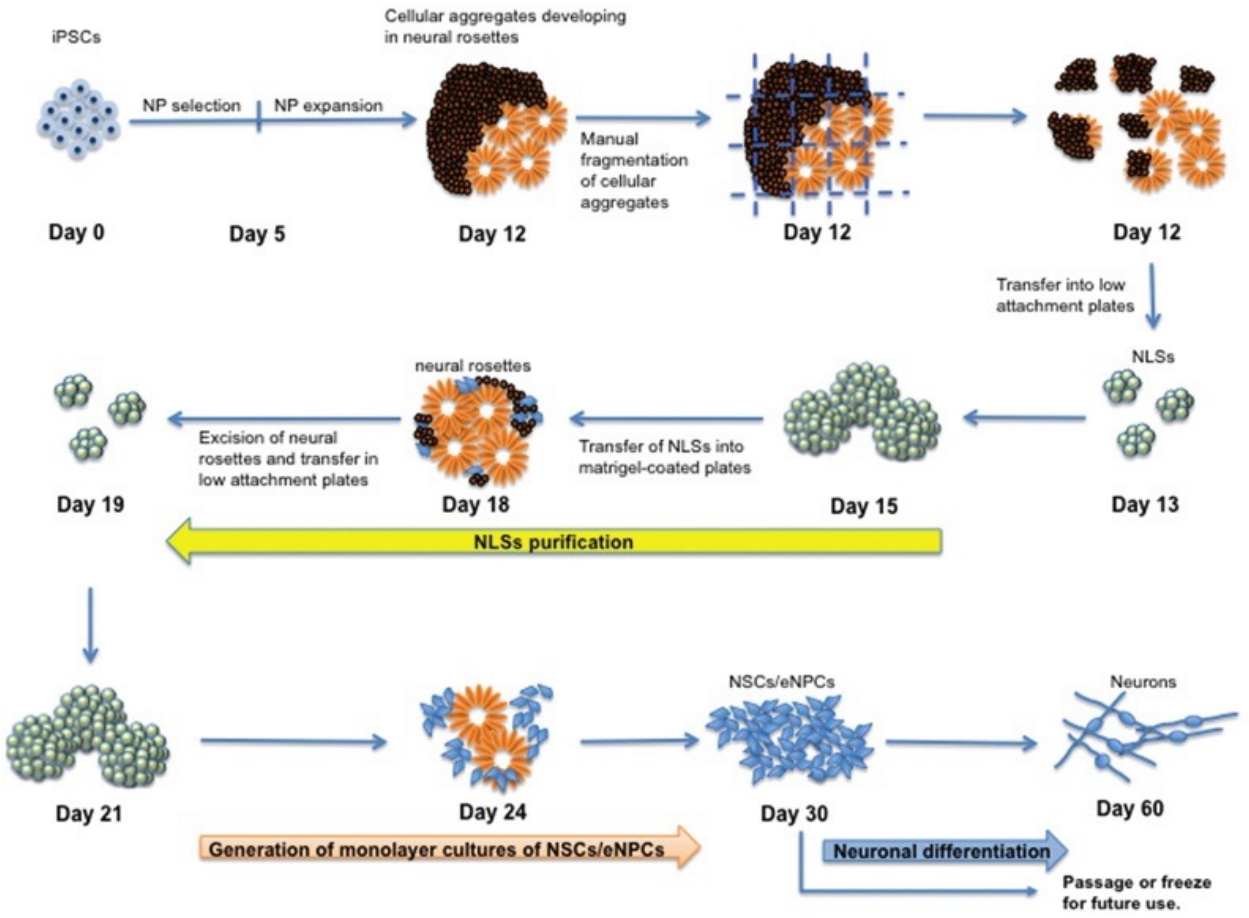

Figure 7. Schematic flow diagram to depict the stages of differentiation into neurons from induced pluripotent stem cells (iPSCs).

NSCs: neural stem cells; eNPCs: early neural progenitor cells; NLSs: neurosphere-like structures.

3.2.4 Discussion

The relatively simple culture media described in this protocol allows a large-scale generation of NSCs/eNPCs. Variability in the yield of NCSs migrating away from neural rosettes has been noticed among iPSC lines from different individuals. Furthermore, fibroblast-like cells are observed during the expansion of NSCs/eNPCs, but these cells are manually eliminated. One 6-well plate of confluent NSCs/eNPCs is sufficient to generate approximately 15 (384-well)

plates of highly enriched neuronal cultures (more than 90% of TUJ1 positive cells). High content analysis has shown a uniform distribution of NSCs/eNPCs over the different wells in 384-well plates. The relative proportions of astrocytes and oligodendrocytes have not been investigated because the goal of this study was to provide a generalizable method for large-scale generation of NSCs/eNPCs that can be further differentiate into neurons in microtiter well format for high throughput analyses. The cost to generate a neuronal culture in a 384-well plate (where NSCs/eNPCs have been cultured in neurobasal medium for 4 weeks) starting from iPSCs is approximately $190.

The protocol detailed here enables a scalable and cost-effective derivation of NSCs/eNPCs that can be further differentiated into VGLUT1 positive neurons displaying features of layer 3 pyramidal cells. Synaptic protein expression was, on average, less in iPSC-derived neurons compared to human cortex tissue. This finding is to be expected considering the numerous differences between cell culture and tissue. Further studies are needed to evaluate whether NSCs/eNPCs generated with this protocol can be differentiated into other neuronal cell types.

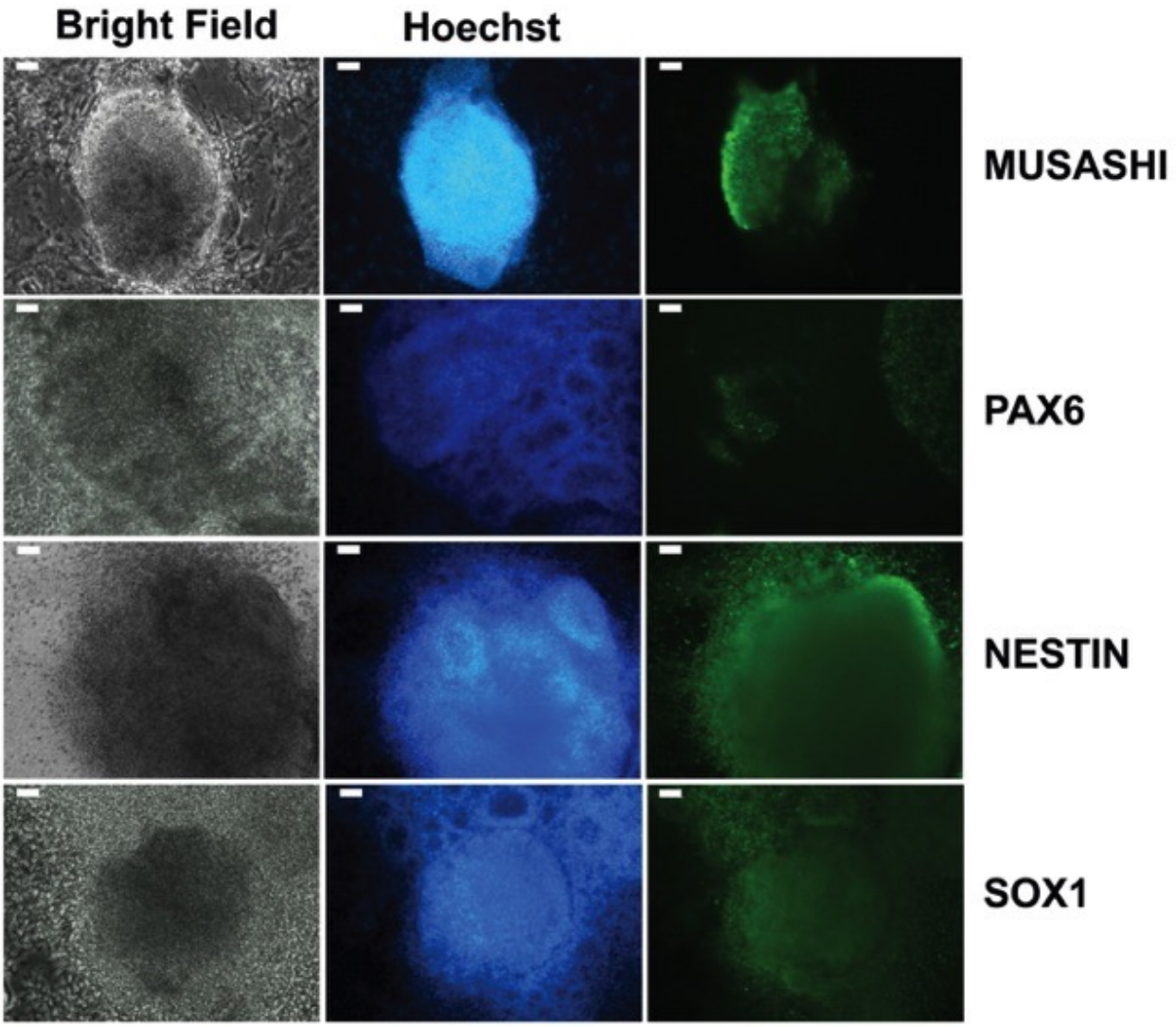

Figure 8. Expression of neural stem cell markers in cellular aggregates developing into neural rosettes observed in differentiating iPSCs cultured in NP expansion medium.

Forming neuronal rosettes are more clearly distinguishable in Hoechst staining where nuclei of each neural rosette are arranged radially around a central cavity. Scale bar is 50 μm.

3.2.5 Materials and Methods

3.2.5.1 Human iPSC cell lines

Lines HFF1-S, 73-56010-02, 73-56010-01, 71-500-9000, and 71-500-9001 were generated at NIMH funded Rutgers University Cell and DNA Repository (RUCDR) from skin fibroblasts. ATR1, another line was derived from T lymphocytes. Cells were reprogrammed with Sendai viral vectors expressing the transcription factors Sox2, c-Myc, Klf4, and Oct4. Following QC measures described earlier (D'Aiuto et al., 2012), iPSCs were maintained in 6-well plates with the supplemented mTeSR1™ medium (Stem Cell Technologies) changed daily, allowing for manual cleaning of differentiated cells. The protocol was approved by the University of Pittsburgh Institutional Review Board and written informed consent was obtained from all participants.

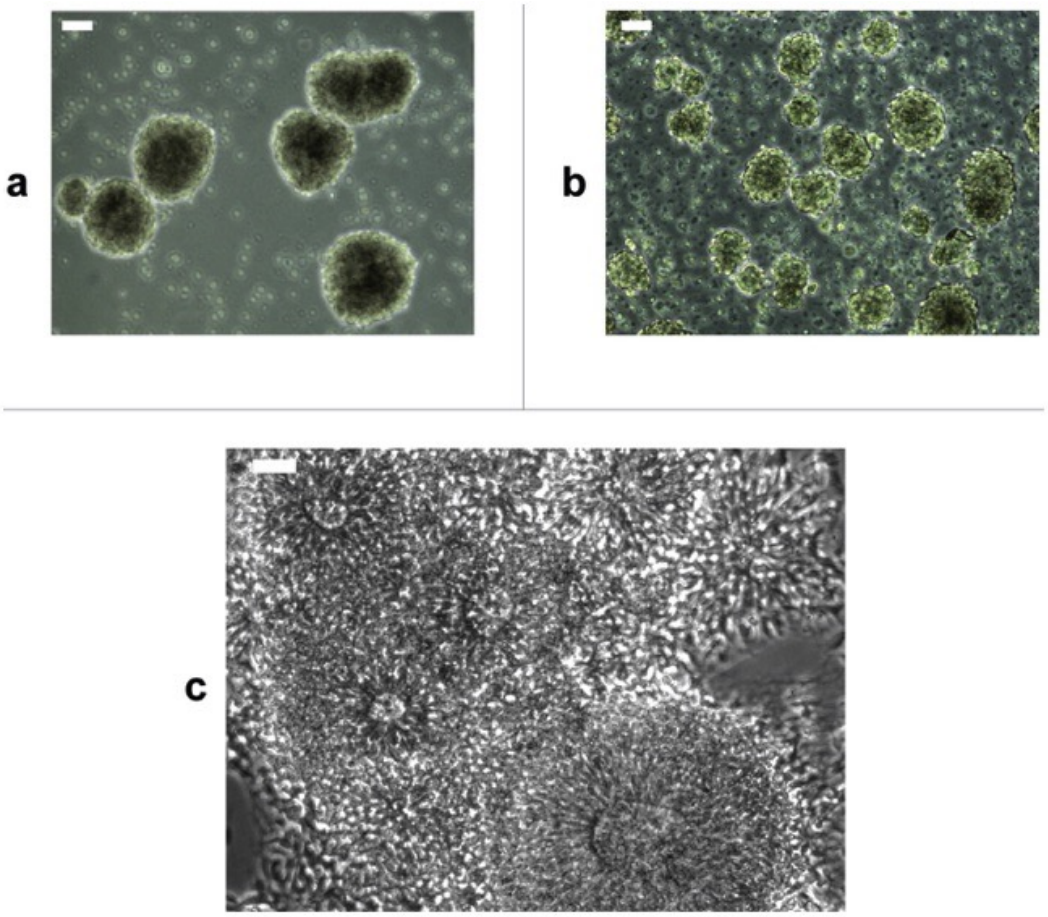

Figure 9. Generation of NLSs and neural rosettes.

(a) NLSs generated from cellular aggregates developing into neural rosettes. **(b)** NLSs generated from single cell suspension of cellular aggregates in Aggrewell plates. **(c)** Microphotograph of neural rosettes observed 12 hours after plating purified NLSs. Scale bar is 50 μm.

3.2.5.2 Reagent setup

NP selection medium. Dulbecco's minimum essential medium/F12 medium supplemented with 0.5% N2 (GIBCO), 1 mM L-glutamine, 1% nonessential amino acids, 50 U/ml penicillin G, 50 mg/ml streptomycin, and 0.1 mM 2-mercaptoethanol (Cho et al., 2008).

NP expansion medium. Dulbecco's minimum essential medium/F12 medium supplemented with 1% N2, 20 ng/ml rhFGFb (Invitrogen), 1 mM L- glutamine, 1% nonessential amino acids, 50 U/ml penicillin G, 50 mg/ml streptomycin, and 0.1 mM 2-mercaptoethanol (Cho et al., 2008).

Neurobasal medium. Neurobasal medium supplemented with 2% B27 (GIBCO), 10 ng/ml BDNF (PeproTech), 50 U/ml penicillin G, and 50 mg/ml streptomycin.

Matrigel aliquot preparation. Thaw a 5 ml container of matrigel qualified for use with mTeSR1™ medium (BD) on ice. Alternatively, matrigel can be thawed by placing it on ice and leaving it at 4°C overnight. Prepare aliquots by adding 500 ml matrigel into cryovials on ice. Store aliquots at -20°C for use.

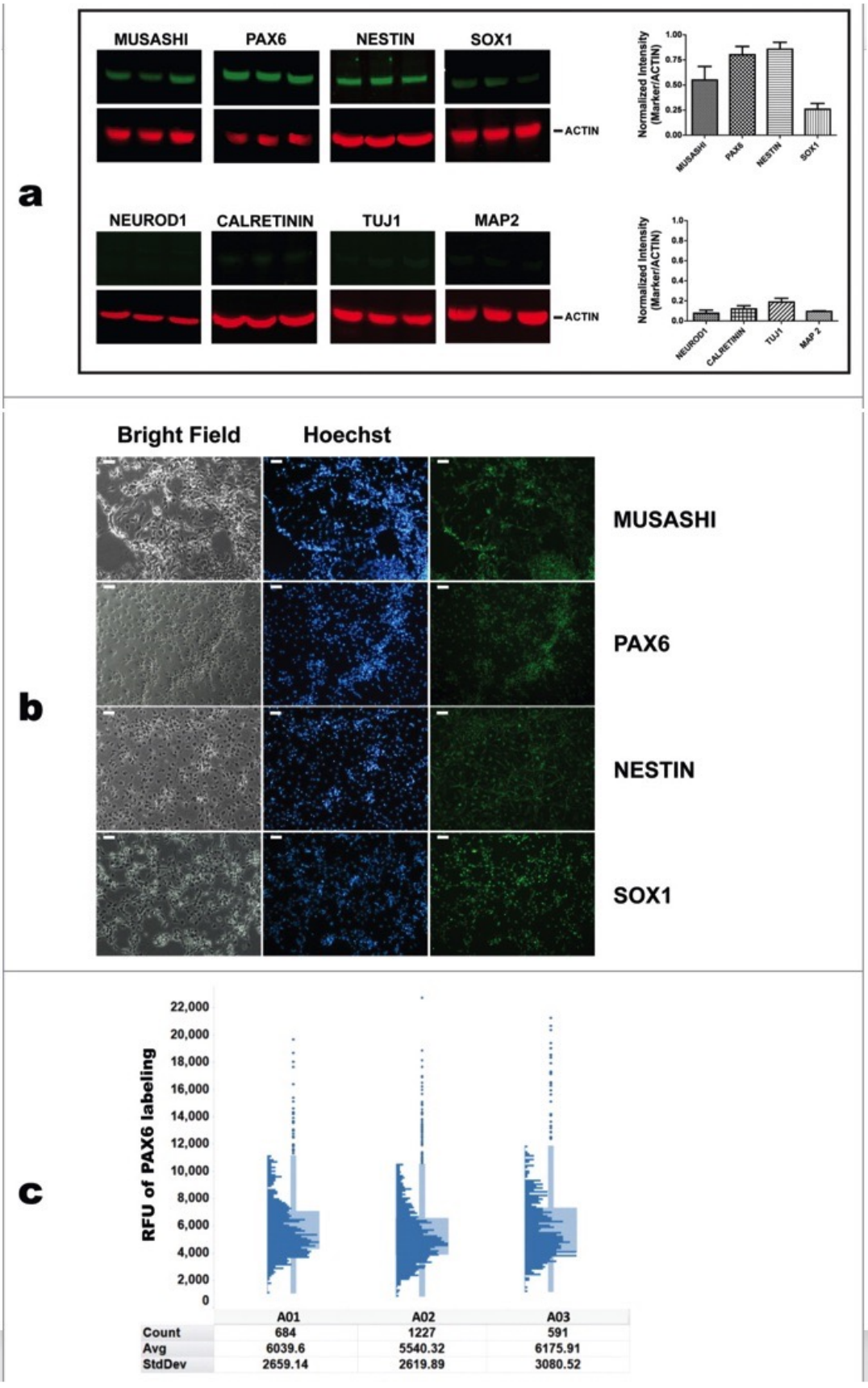
a
MUSASHI
PAX6
NESTIN
SOX1
ACTIN
Normalized Intensity (Marker/ACTIN)
NEUROD1
CALRETININ
TUJ1
MAP2
b
Bright Field
Hoechst
MUSASHI
PAX6
NESTIN
SOX1
c
RFU of PAX6 labeling
22,000
20,000
18,000
16,000
14,000
12,000
10,000
8,000
6,000
4,000
2,000
0
A01
A02
A03
Count 684 1227 591
Avg 6039.6 5540.32 6175.91
StdDev 2659.14 2619.89 3080.52

Figure 10. Characterization of iPSC- derived NSCs/eNPCs.

(a) Left: Immunoblots showing the expression of markers specific for NSCs (MUSA- SHI, PAX6, NESTIN and SOX1), late NPCs (NEUROD1) and neurons (CALRETININ, TUJ1, and MAP2) in iPSC-derived NSCs/eNPCs. Right: Normalized expression of NSC markers. The data represent an average of 3 independent experiments. (b) Immunocytochemical analysis of iPSC-derived NSCs/ eNPCs. Scale bar is 50 μm. (c) Quantification of PAX6 expression using High Content Analysis. RFU: relative fluorescence unit. A01-A03 denote biological replicates. The distribution of PAX6 labeling among NSCs/eNPCs is shown in the histograms. The histograms indicate RFU intensity in the vertical axis and number of cells at that intensity in the horizontal axis. The points outside the histograms indicate outliers. The tables below the histograms indicate the number of cells measured in the populations (Count), the average (Avg) and standard deviation (StdDev) of the overall PAX6 labeling in the population. Greater than 99% of the cells have PAX6 FITC levels above background. The average background level in the well is <400 gray levels. The minimum level in the cell is around 1,000 to 2,000. More than 99% of the cells show levels greater than 500.

3.2.5.3 Differentiation procedure

Generation and passaging of feeder-free iPSC cultures

We recommend using iPSCs at low passage number in order to reduce the probability of karyotypic abnormalities (Taapken et al., 2011). We transfer one iPSC colony from feeder-based culture into a 6-well matrigel-coated plate as follows.

i. **MATRIGEL PREPARATION**. Thaw a matrigel aliquot on ice. Pipette 50 ml PBS into a disposable falcon 50 ml tube. Add 1 ml of the PBS into the cryotube containing 500 µl matrigel. Mix quickly and transfer back to the 50 ml falcon tube. Mix matrigel/PBS mixture by pipetting up and down with a 10 ml pipette and dispense into plates. To coat one well of a 6-well plate, use 1 ml matrigel/PBS mixture. **NOTE:** Thawing the matrigel requires approximately 2 hours. Keep matrigel aliquot on ice at all times.

ii. **iPSC SEEDING**. Examine iPSC culture under a microscope to select undifferentiated colonies. Using a marking pen, draw a circle around undifferentiated iPSC colonies on the

bottom of the plate (differentiated iPSC are characterized by non-uniform cell morphology in any portion of the colonies). Replace the medium in which iPSCs are cultured with pre-warmed (37°C) mTeSR1™ medium. Cut selected colonies into pieces of uniform size using a bent 20-gauge needle; harvest the iPSC clumps with a 10 ml pipette, and transfer into new culture well coated with matrigel, prepared as described in step 1(i). Culture iPSCs in mTeSR1™ medium for 5–7 d in an incubator under standard conditions (5% CO2, 37°C, and 100% humidity). Change culture medium every day. Eliminate unwanted differentiated iPSCs from each well by scraping with a pipette tip. When the iPSC colonies become confluent (colony size approximately 1.5–2 mm), passage iPSC colonies 1:6 as described above.

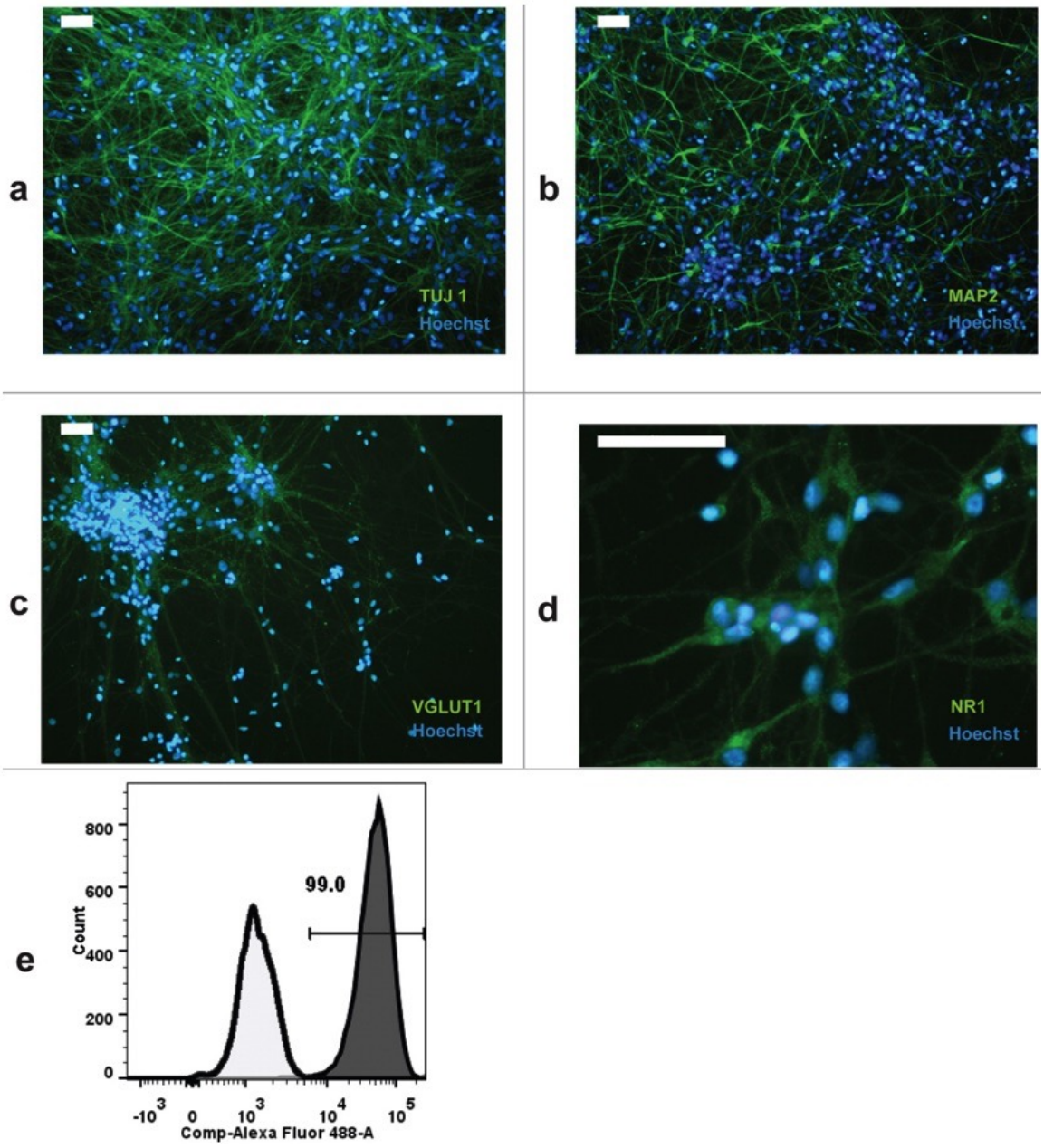

Figure 11. Immunostaining of iPSC-derived neurons.

TUJ1 (a), MAP2 (b), VGLUT1 (c), and NR1 subunit of the NMDA receptor (d). The percentage of TUJ1 positive neurons was analyzed by flow cytometry; cells were permeabilized with Cytofix/Cytoperm (Becton Dickinson) and dead cells were excluded from the analysis. Filled histogram shows the fraction of TUJ1 stained cells compared to secondary antibody staining (e). Scale bar is 50 μm in a-c, and 75 μm in d.

Derivation of NSCs/eNPCs from iPSCs. DURATION: 12 d

Wash iPSC colonies with 2 ml 1X PBS at room temperature twice. Add 2 ml of pre-warmed NP selection medium and incubate under standard conditions. Change medium every other day. At day 5, replace NP selection medium with NP expansion medium and culture for 7 d After 3-5 d in NP expansion medium, 50–70% of colonies show the presence of cellular aggregates expressing NSCs markers NESTIN (Elkabetz & Studer, 2008), SOX1(Venere et al., 2012), and MUSASHI (Kim et al., 2012; FIGURE 8). If there is paucity of neural structures after 7 d culture in NP expansion medium, continue to culture the cells for 5–7 more days.

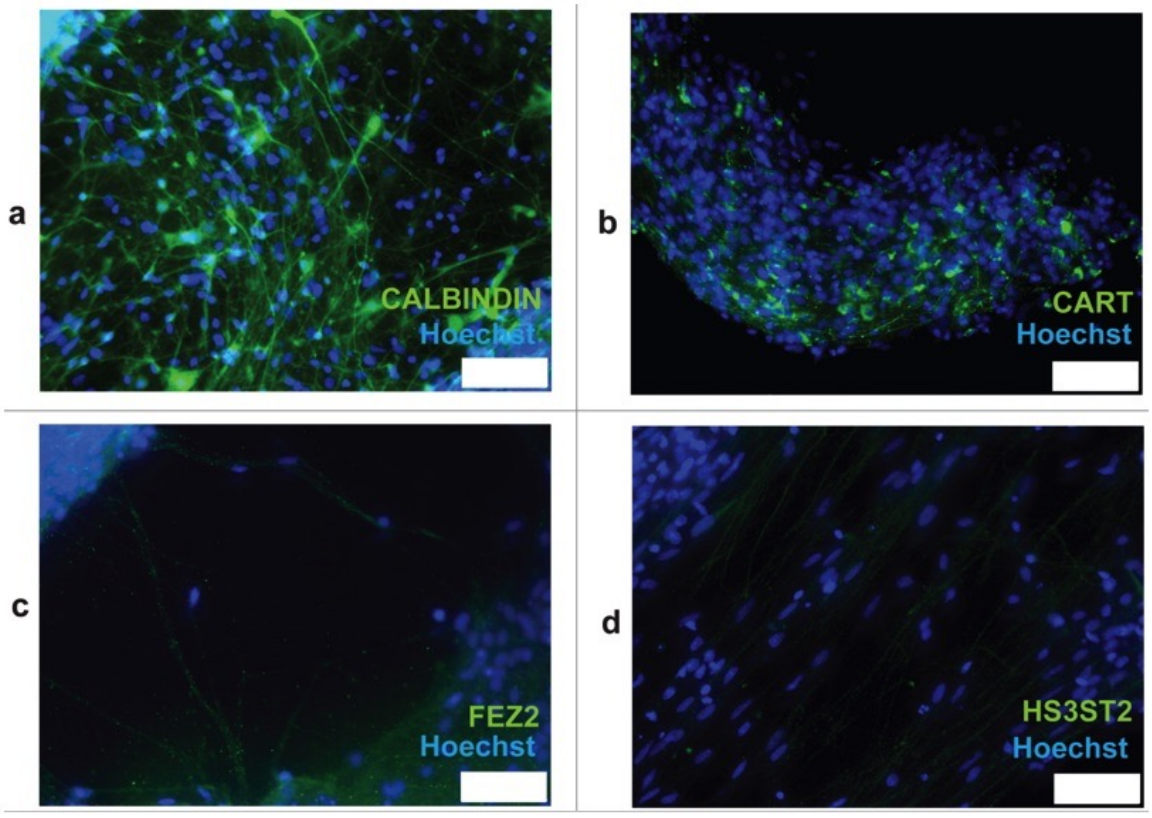

Figure 12. Immunostaining of iPSC-derived neurons.

CALBINDIN (a), CART (b), FEZ2 (c), and HS3ST2 (d). Scale bars are 75 µm.

Generation of NLSs. DURATION: 3–4 d

After 7 d in NP expansion medium, proceed to generate NLSs as follows.

i. Aspirate the medium, wash the cells twice with 1 ml DMEM/F12 and add 2 ml of pre-warmed NP expansion medium. With the plate under the microscope (use the 4X objective), use a bent 20-gauge needle to dissect cellular aggregates into pieces of approximately 40–50 μm diameter.

ii. Collect the NP expansion medium containing the dissected cell aggregates and transfer into an ultra-low attachment 6-well plate. Culture in standard incubator conditions overnight.

iii. On the following day, cell aggregates should round up into floating spherical cellular aggregates denoted NLSs (FIGURE 9a).

iv. Culture NLSs for 2–3 d in NP expansion medium. Change half the culture medium every day as follows. Collect NLSs in suspension from the plate and transfer into a 15 ml conical tube. Allow NLSs to settle to the bottom of the conical tube for 10 min. Replace half of the culture medium with fresh medium. Transfer the NLSs back to the 6-well ultra-low attachment plate. To distribute NLSs uniformly on low attachment plates, re-suspend NLSs by pipetting up and down 3–4 times with a 5 ml pipette. As the NLSs tend to sink to the bottom rapidly, transfer into 2 wells at a time, resuspending each time. Continue culturing until the NLSs reach a diameter of approximately 300 μm.

Alternative method for size-controlled formation of NLSs. DURATION: 4–5 d

Derivation of size-controlled NLSs is more expensive than the method described above. However, the percentage of NLSs differentiating into neural cells is higher with this method. To

generate size- controlled NLSs, dissect cellular aggregates and transfer them into a 15 ml conical tube. Pellet the cells by spinning down for 30 sec at 1,200 rpm. Discard the supernatant and add 2 ml of StemPro Accutase (Life Technologies). Incubate at 37°C for 10 min (dissociate cells thoroughly by pipetting with a P1000 Pipetman every 2– 3 min). Add 8 ml of DMEM/F12 and mix by inverting the tube 2– 3 times. Leave the conical tube for 10 min to enable the undissociated clumps to settle to the bottom of the tube. Transfer the single cell suspension into a new 15 ml conical tube and centrifuge for 5 min at 1,200 rpm. Discard the supernatant and re-suspend the cells in 5 ml of NP expansion medium. Count viable cells using the trypan blue method. Adjust the volume of cell suspension to a density of 2 x 10^6 cells/ml. Add 2 ml of NP expansion medium to each well of an Aggrewell plate (Stem cell Technologies, Vancouver BC). Centrifuge the plate for 5 min at 1,200 rpm and discard the medium. Transfer 1 ml of cell suspension into each well to be used and centrifuge the plate as described above. Incubate plate overnight under standard culture conditions. Following overnight incubation, the cells should form spherical cell aggregates of approximately 40– 50 µm (FIGURE 9b). After 24 hours, collect the NLSs by using a transfer pipette and transfer to an ultra-low attachment 6-well plate. Culture the NLSs as described above until they reach the desired size (approximately 200–250 µm). To efficiently dislodge NLSs from single micro-wells of the Aggrewell plate, apply mild positive pressure on different regions at the bottom of the well, using a transfer pipette bulb. After harvesting NLSs, ensure that all the NLSs have been collected by reviewing the donor plate under the microscope. Repeat the previous steps if necessary.

Purification of NLSs. DURATION: 6–7 d

Transfer the NLSs floating in the NP expansion medium into a 15 ml falcon tube and allow them to settle for 10 min. Aspirate the supernatant and re-suspend the NLSs into 12 ml of

NP expansion medium. Distribute the NLS suspension (2 ml/well) in a matrigel-coated 6-well plate. Incubate in standard conditions. Following overnight incubation, NLSs tend to adhere to the bottom of the culture plate and flatten. At this stage, neural rosettes can be observed (FIGURE 9c). Place the culture plate under an inverted microscope. Dissect and collect the neural rosettes following the same procedure described in steps 3(i) and 3(ii). Incubate in standard conditions. On the following day, neural rosettes should round up into NLS. Culture NLSs for 2–3 d until the NLSs reach a size of approximately 300 μm. Change half the culture medium every other day as described in step 3(iv).

Generation of monolayer cultures of NSCs/eNPCs. DURATION: 9d

Collect the NLSs into NP expansion medium and transfer into a matrigel-coated 6-well plate. Incubate in standard conditions. After a few hours, NLSs adhere to the surface of the culture plate and NSCs migrate away. At this stage, heterogeneous cultures will be generated, consisting of NSCs and eNPCs. Fibroblast-like cells may still be observed and should be removed under the inverted microscope by scraping them with a pipette tip.

Passaging NSCs/eNPCs

Aspirate NP expansion medium and rinse with DMEM/F12. For 6-well cultures, add 1 ml of StemPro Accutase per well and incubate for 3 min at 37°C. Add 2 ml of DMEM/F12 medium and gently detach cells by pipetting up and down with a p1000 tip. Transfer the cell suspension into a 15 ml conical tube. Centrifuge 5 min at 1,200 rpm. Discard the supernatant, re-suspend the cells with 12 ml of NP expansion medium, and culture in standard conditions in the appropriate plates coated with matrigel. On the next day, replace NP expansion medium with mTeSR1™ medium and culture until the cells are confluent (FIGURE 10b). When confluent, the cultures in 6-well plates should contain approximately 3 x 10^6 cells/well. From this stage onwards, NSCs/

eNPCs are cultured and passaged in mTeSR1™ medium. The NSCs/eNPCs can be stored at -135°C or in liquid nitrogen. We do not recommend expanding NSCs/NPCs for more than 12 passages to reduce the risk of chromosomal aberration (Nguyen, 2013). Freezing and thawing procedures of NSCs/ eNPCs are described in Supplementary Information.

Generating neuronal cultures in 96- and 384-well plates. DURATION: 4 weeks.

Dissociate NSCs/eNPCs with StemPro Accutase as described above. Count the cells and re-suspend them in an appropriate volume of mTeSR1™ medium. Distribute cells in 96-well plates at 10^4 cells/well or in 384-well plate at 2.5 x 10^3 cells/well. On the next day, change mTeSR1™ to neurobasal medium and culture for 4 weeks. Replace half of the culture medium with fresh medium every other day by using a multi-channel pipette. Under these conditions, highly enriched cultures of neurons are generated (FIGURE 11).

Immunocytochemistry and Microscopy

Immunocytochemistry was performed as previously described (D'Aiuto et al., 2008). Primary antibodies used were mouse anti-human NESTIN monoclonal antibody (R&D Systems, 1:200 dilution), rabbit polyclonal anti-SOX1 antibody (Abcam, 1:200 dilution), rabbit polyclonal anti-MUSASHI antibody (Abcam, 1:200 dilution), rabbit polyclonal anti-PAX6 antibody (Abcam, 1:200 dilution), mouse anti-ß TUBULIN III monoclonal antibody (clone Tuj-1, R&D System, 1:50 dilution), mouse monoclonal anti- MAP2 (Millipore, 1:200 dilution), rabbit polyclonal anti-VGLUT1 antibody (Synaptic Systems, 1:200 dilution), rabbit anti-NMDAR1 monoclonal antibody (Abcam, 1:400 dilution), rabbit polyclonal to CALBINDIN antibody (Abcam, 1:200 dilution), rabbit polyclonal to FEZ2 antibody (Abcam, 1:200 dilution), rabbit polyclonal to HS3ST2 antibody (Novus Biologicals, 1:50 dilution), mouse monoclonal to CART antibody (Abcam, 1:100 dilution). Alexa Fluor 488 goat anti-rabbit secondary antibody (Life

Technologies, 1:200 dilution) and Alexa Fluor 488 goat anti- mouse secondary antibody (Life Technologies, 1:200 dilution) were used for detection. Counterstaining was done with Hoechst 33342 (Life Technologies, 1:1000 dilution). Images were acquired using a Leica IL MD LED inverted fluorescence microscope.

Western blots

Cell lysates were prepared with 10 volumes of RIPA buffer (25 mM Tris–HCl pH 7.6, 150 mM NaCl, 1% NP-40, 1% sodium deoxycholate, and 0.1% SDS), denatured by heating at 95°C and then separated by electrophoresis on 4–12% gradient SDS-polyacrylamide gels, transferred onto Immobilon membranes (Millipore). Immunoblots were probed with monoclonal antibodies similar to those employed in immunocytochemistry analysis; other antibodies used were rabbit anti-CALRETININ monoclonal antibody (Abcam, 1:800 dilution), rabbit anti-NEUROD1 polyclonal antibody (Abcam, 1:200 dilution). The blots were probed with fluorescently labeled secondary antibodies (Li-Cor antibodies) to detect immunoreactivity. Fluorescent signal intensities were then quantified using an Odyssey Imaging scanner (Li-Cor).

Quantification of PAX6 expression using high content analysis

NSC/eNPCs were fixed with 4% paraformaldehyde and labeled with rabbit polyclonal anti- PAX6 antibody followed by Alexa Fluor 488 goat anti-rabbit secondary antibody, and with Hoechst 33342 to identify individual cellular nuclei. Cells were imaged on the ImageXpress Ultra (IXU) High Content imager with 20x objective using the 405 nm excitation/447 nm emission to visualize the Hoechst nuclear stain, and 488 nm excitation/514 nm emission filter to visualize the PAX6 Alexa Fluor 488 stain. Images were analyzed using the Multiwavelength Cell Scoring application within the MetaXpress software that runs the IXU, and the average intracellular intensity of the PAX6 stain was determined for each cell.

Electrophysiological recordings

iPSC-derived NSCs/eNPCs were plated onto matrigel-coated 18 mm coverslips and cultured for 8 weeks in neurobasal medium for neuronal differentiation. Neuronal cells were visualized on 18 mm coverslips with a Zeiss inverted microscope. The external recording solution contained 140 mM NaCl, 2.8 mM KCl, 1 mM $CaCl_2$, 0.01 mM EDTA (to eliminate contaminating Zn^{2+}, which inhibits some NMDA receptor subtypes), 10 mM HEPES, pH 7.2 ± 0.05 adjusted with NaOH, osmolality 290 ± 10 mmol/kg adjusted with sucrose, and agonists added at indicated concentrations. The pipette solution contained 130 mM K- gluconate, 10 mM NaCl, 1 mM $CaCl_2$, 1.1 mM EGTA, 10 mM HEPES, 2 mM ATP-Na_2, 2 mM $MgCl_2$, pH 7.2 ± 0.05 adjusted with KOH, osmolality 275 ± 10 mmol/kg.

Whole-cell recordings from iPSC-derived neurons were performed using pipettes pulled from borosilicate glass and fire-polished (5–8 MΩ). Membrane currents were recorded with an Axopatch 200B amplifier (Molecular Devices) in voltage-clamp mode, low-pass filtered at 5 kHz, and digitized at 10 kHz with a Digidata 1322a (Molecular Devices). Series resistance was compensated at 75–85%. For data presented here, recordings were rejected if holding current at -85 mV exceeded -600 pA (Molecular Devices). Rapid solution exchange was achieved using an in-house-fabricated fast perfusion system (Qian et al., 2002) connected to gravity-fed reservoirs. All experiments were performed at room temperature. Peak currents are measured relative to baseline current prior to agonist application using Clampfit 10.3 (Molecular Devices).

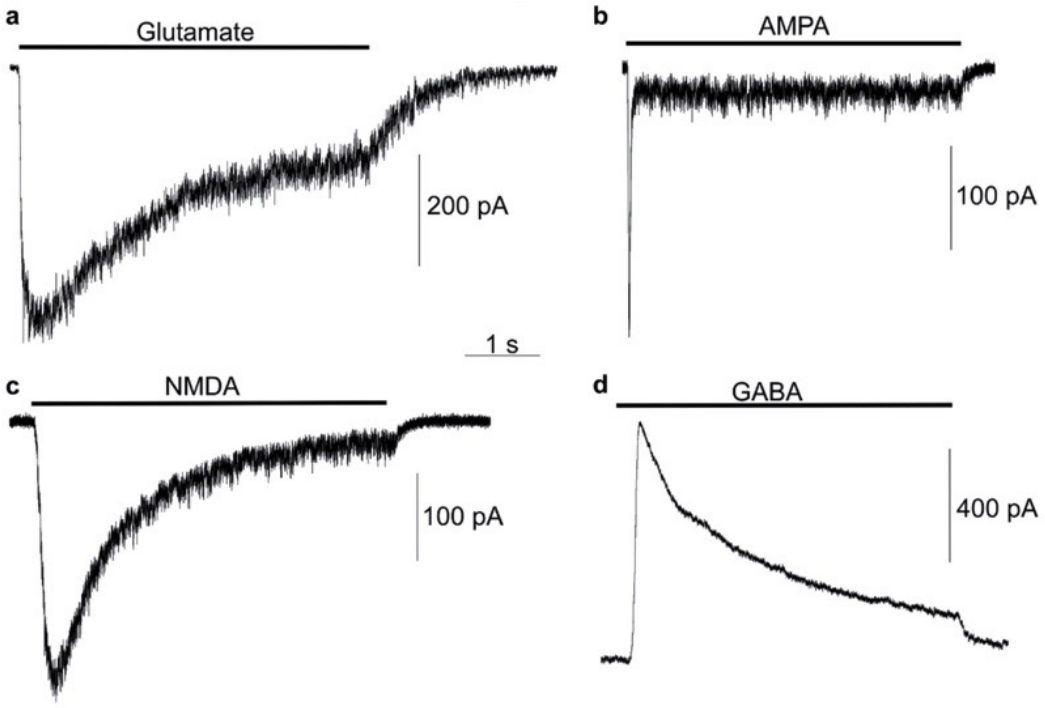

Figure 13. Electrophysiological recordings of iPSC-derived neurons.

Example traces of whole-cell voltage-clamp recordings from HFF1-S cells in response to application of the indicated agonists. Currents were recorded in a Mg+-free extracellular solution at a holding potential of -85 mV (a–c) or 15 mV (d) during approximately 5 s applications (indicated by horizontal bar above each trace) of 100 µM glutamate + 100 µM glycine (a, peak current -494.3 pA), 100 µM AMPA (b, peak current = -261.8 pA), 100 µM NMDA + 100 µM glycine (c, peak current = -324.4 pA), or 1 mM GABA (d, peak current = 851.8 pA).

Targeted Proteomics

Cell lysates were prepared as described above and total protein quantified by micro BCA (Pierce). Human postmortem cortex gray matter homogenates previously prepared from 3 normal subjects were obtained (Deo et al., 2013). Twenty micrograms of protein from iPSC-derived neurons or human cortex gray matter tissue homogenate were mixed with 20 µg of a stable isotope labeled neuronal proteome standard, separated by electrophoresis on a 4–12% gradient SDS-polyacrylamide gel, and subject to on-gel digestion as previously described (MacDonald et al., 2012). Liquid Chromatograph – Selected Reaction Monitoring analyses were conducted on a

TSQ Quantum triple stage quadrupole mass spectrometer (ThermoFisher Scientific) with an Ultimate 3000 HPLC (Dionex) and a PicoChip Column (New Objective). Two µl (»1 µg protein) sample was loaded onto the column at 1 µl/min for 12 min, and eluted at 300 nl/min over a 25 min gradient from 3–35% mobile phase B (Acetonitrile containing 0.1% formic acid). SRM transitions were timed using 1 min retention windows, depending on the number of SRMs to be assayed. Transitions were monitored, allowing for a cycle time of 1 sec, resulting in a dynamic dwell time never falling below 10 msec. The MS instrument parameters were as follows: capillary temperature 275°C, spray voltage 1100 V, and a collision gas of 1.4 mTorr (argon). The resolving power of the instrument was set to 0.7 Da (Full Width Half Maximum) for the first and third quadrupole. Data were acquired using a Chrom Filter peak width of 4.0 sec. Peak areas and area ratios were calculated within Skyline (Lista et al., 1988). Raw files were loaded into Skyline files containing target proteins/peptides/transitions. All individual SRM transitions and integration areas were manually inspected. Transitions for which the signal-to-noise ratio was below 3 were excluded from analysis. The ratios of the integrated areas for “light” endogenous peptides and “heavy” 13C6STD peptides were calculated to obtain peptide measures using multiple transitions per peptide. 165 peptides from 116 proteins were measured.

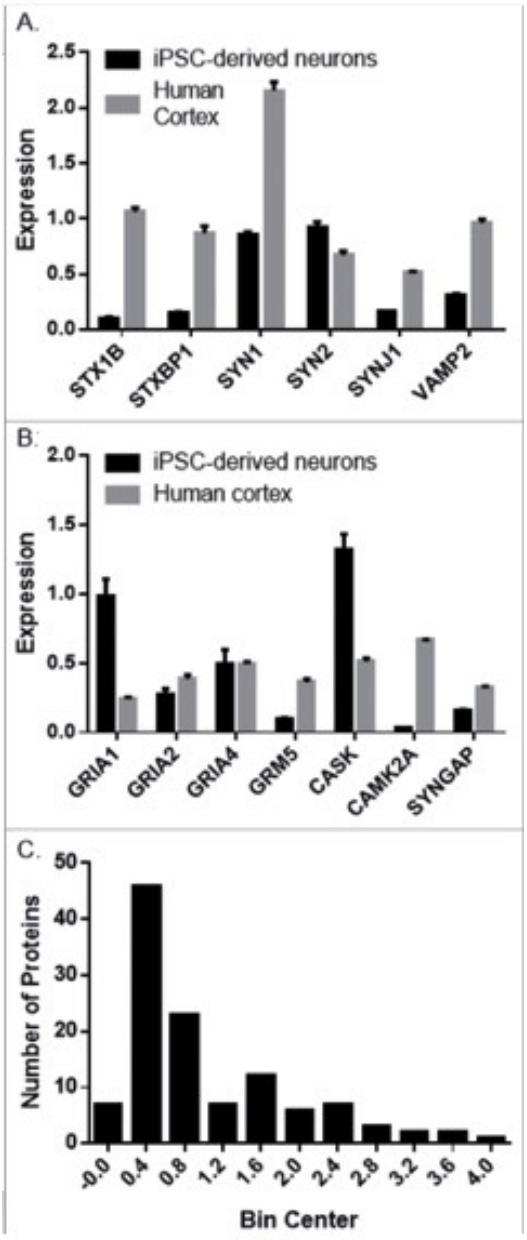

Figure 14. Targeted proteomic comparison of iPSC-derived neurons and human cortex gray matter.

Expression of representative presynaptic (A) and post-synaptic (B) proteins in iPSC-derived neurons (NSCs/eNPCs cultured in neurobasal medium for 6 weeks) and human cortex gray matter. (C). Distribution of the averaged difference between the 2 groups expressed as a ratio of iPSC-derived neurons: Cortex gray matter.

3.2.6 Acknowledgments

We thank our study participants and research staff. The content is solely the responsibility of the authors and does not necessarily represent the official views of the National Institute of Mental Health, the National Institutes of Health, the Department of Veterans Affairs, or the United States Government.

3.2.7 Funding

This project was funded from NIH grants MH63480 and MH045817, and MH071533, by Stanley Medical Research Foundation 07R-1712, and by the Ri.MED. We also thank China Scholarship Council for providing a fellowship to YZ and thank Indo-US Science & Technology Forum (IUSSTF) for providing a fellowship to DKD. The Biomedical Mass Spectrometry Center and UPCI Cancer Biomarker Facility are supported in part by award P30CA047904.

3.3 PERSISTENT INFECTION BY HSV-1 IS ASSOCIATED WITH CHANGES IN FUNCTIONAL ARCHITECTURE OF IPSC-DERIVED NEURONS AND BRAIN ACTIVATION PATTERNS UNDERLYING WORKING MEMORY PERFORMANCE

Leonardo D'Aiuto1,10, Konasale M. Prasad1,10, Catherine H. Upton1, Luigi Viggiano2, Jadranka Milosevic3, Giorgio Raimondi4, Lora McClain1, Kodavali Chowdari1, Jay Tischfield5, Michael Sheldon5, Jennifer C. Moore5, Robert H. Yolken6, Paul R. Kinchington7,8, and Vishwajit L. Nimgaonkar*,1,9

1Department of Psychiatry, WPIC, University of Pittsburgh, School of Medicine, Pittsburgh PA;
2Department of Biology, University of Bari "Aldo Moro", Bari, Italy;
3Division of Pulmonary, Allergy and Critical Care Medicine, University of Pittsburgh School of Medicine, Pittsburgh, PA;
4Department of Plastic and Reconstructive Surgery, Johns Hopkins University School of Medicine, Baltimore, MD;
5Department of Genetics and The Human Genome Institute of New Jersey, Rutgers, The State University of New Jersey, Piscataway, NJ;
6Stanley Division of Neurovirology, Department of Pediatrics, Johns Hopkins University School of Medicine, Baltimore, MD;
7Department of Ophthalmology, University of Pittsburgh School of Medicine, Pittsburgh, PA;
8Department of Molecular Genetics & Biochemistry, University of Pittsburgh, Pittsburgh, PA;
9Department of Human Genetics, Graduate School of Public Health, University of Pittsburgh, Pittsburgh, PA
10These authors contributed equally to the article.

D'Aiuto L, Prasad KM, Upton CH, Viggiano L, Milosevic J, Raimondi G, McClain L, Chowdari K, Tischfield J, Sheldon M, Moore JC, Yolken RH, Kinchington PR, Nimgaonkar VL.Persistent infection by HSV-1 is associated with changes in functional architecture of iPSC-derived neurons and brain activation patterns underlying working memory performance. Schizophr. Bull. 2015;41:123–132. doi: 10.1093/schbul/sbu032.

NOTE. Dr. Konsale Prasad's research group designed, performed, and analyzed the MRI studies that are not within the scope of this thesis.

3.3.1 Abstract

Background: Herpes simplex virus, type 1 (HSV-1) commonly produces lytic mucosal lesions. It invariably initiates latent infection in sensory ganglia enabling persistent, lifelong infection. Acute HSV-1 encephalitis is rare and definitive evidence of latent infection in the brain is lacking. However, exposure untraceable to encephalitis has been repeatedly associated with impaired working memory and executive functions, particularly among schizophrenia patients. *Methods*: Patterns of HSV-1 infection and gene expression changes were examined in human induced pluripotent stem cell (iPSC)-derived neurons. Separately, differences in blood oxygenation level-dependent (BOLD) responses to working memory challenges using letter n-back tests were investigated using functional magnetic resonance imaging (fMRI) among schizophrenia cases/ controls. *Results*: HSV-1 induced lytic changes in iPSC-derived glutamatergic neurons and neuroprogenitor cells. In neurons, HSV-1 also entered a quiescent state following co-incubation with antiviral drugs, with distinctive changes in gene expression related to functions such as glutamatergic signaling. In the fMRI studies, main effects of schizophrenia ($P = .001$) and HSV-1 exposure (1-back, $P = 1.76 \times 10{-}4$; 2-back, $P = 1.39 \times 10{-}5$) on BOLD responses were observed. We also noted increased BOLD responses in the frontoparietal, thalamus, and midbrain regions among HSV-1 exposed schizophrenia cases and controls, compared with unexposed persons. *Conclusions*: The lytic/quiescent cycles in iPSC-derived neurons indicate that persistent neuronal infection can occur, altering cellular function. The fMRI studies affirm the associations between non-encephalitic HSV-1 infection and

functional brain changes linked with working memory impairment. The fMRI and iPSC studies together provide putative mechanisms for the cognitive impairments linked to HSV-1 exposure.

3.3.2 Introduction

Herpes simplex virus, type 1 (HSV-1) causes human specific infections in the majority of US adults (http:// www.cdc.gov/nchs/nhanes.htm) and increasing numbers of neonates (Gupta et al., 2007; Flagg & Weinstock, 2011). Mucosal lesions such as cold sores occur after primary infection, and recurrent infections can induce blinding stromal keratitis. HSV-1 causes fulminant lytic infection in all human cells except sensory ganglia, where latent infection can be established in neurons that serve as reservoirs for lifelong recurrent infections. Persistent infection is thus marked by sporadic productive, lytic infections alternating with latency, when gene expression is largely silenced and only the untranslated latency-associated transcripts (LAT) are abundantly expressed (Steiner et al., 2007).

Periodic reactivation can cause HSV-1 encephalitis, with extensive cognitive impairment, and postencephalitic sequelae (Steiner et al., 2007). Its rarity (~0.04%) suggests that HSV-1 infection does not ordinarily affect the brain, but viral DNA has been detected in 35% of nonencephalitic postmortem brain tissues (Baringer & Pisani, 1994; Karatas et al., 2008), suggesting spread to the brain during persistent infection. Mild/moderate impairments in attention, working, and verbal memory untraceable to prior encephalitis or socioeconomic status (SES; Baringer et al., 1994) were reported repeatedly among HSV-1 exposed schizophrenia patients and even healthy individuals (Dickerson et al., 2003; Dickerson et al., 2004; Dickerson, et al., 2008; Shirts et al., 2008; Schretlen et al., 2010; Yolken et al., 2011; Prasad et al., 2012; Dickerson et al., 2012; Watson et al., 2013), with only one discrepant report (Aiello et al., 2008).

The estimated ORs for cognitive dysfunction among HSV-1–exposed young adults are 1.25–3.2 (Dickerson et al., 2008; Watson et al., 2013), indicating population attributable risks between 15.2%– 59.3%. Reduced prefrontal cortical gray matter volume was also reported among HSV-1–exposed schizophrenia patients (Prasad et al., 2007; Prasad et al., 2011), with progressive cognitive impairments and gray matter loss (Prasad et al., 2011). The cognitive impairments were alleviated with an antiviral agent in a randomized placebo-controlled trial (Prasad et al., 2012). These studies together affirm the majority of Bradford-Hill criteria, suggesting causal links (Prasad et al., 2012).

To generate testable mechanisms for the associations, we investigated cellular models using human induced pluripotent stem cells (iPSCs), because existing HSV-1 models utilize nonhuman tissues or transformed cell lines; such models may not recapitulate human specific infection (Giordani et al., 2008; Bloom et al., 2010; Nicoll et al., 2012). With functional magnetic resonance imaging (fMRI), we separately evaluated brain activation patterns while participants performed the n-back task, a well-established working memory task that identifies consistent patterns of brain activation differences among schizophrenia cases (Friedman & Goldman-Rakic, 1994; Carter et al., 1998).

3.3.3 Methods

3.3.3.1 iPSC-Based Studies

iPSCs. iPSCs were generated from human skin biopsies. Line 5404 from a schizophrenia patient was used for all experiments. Line HFF1-S, from neonatal foreskin of an anonymous donor was used for confirmatory studies. Neural progenitor cells (NPCs) and glutamatergic

neurons (D'Aiuto et al., 2012) were derived from iPSCs (D'Aiuto et al., 2012) (FIGURES 50 and 51 and supplementary information described in Appendix B).

HSV-1 Infection. We used a genetically engineered HSV-1 construct incorporating enhanced green fluorescent protein (EGFP) and monomeric red fluorescent protein (RFP) as reporter genes whose expression is driven by the viral promoters ICP0 and glycoprotein C, respectively (Ramachandran et al., 2008). EGFP expression in infected cells indicates that HSV-1 has entered lytic cycles, while RFP expression indicates commitment to viral DNA replication. Cells were incubated with HSV-1 for 2 h at specified multiplicity of infection (MOI). To inhibit viral replication, cells were pre-incubated with antivirals used in animal models: acyclovir (50 μM), or (E)-5-(2-bromovinyl)-2′-deoxyuridine (5BVdU, 30 μM) along with interferon-alpha (IFN-α, 125 U/ml; Carter et al., 1998). The proportion of cells expressing EGFP and RFP was determined by flow cytometry (FC). Images were acquired using a Leica IL MD LED inverted fluorescence microscope and a Leica DM5500B fluorescence microscope.

Viral Gene Expression. RNA was extracted using Qiagen kits. Complementary DNA was synthesized using total RNA with SuperScript III recommended protocol (Invitrogen) and quantitative PCR (qPCR) performed using the target and reference (beta actin) Taqman probes with Applied Biosystems-recommended protocols (ABI). All experiments were conducted in triplicate and the comparative Ct method used for quantification (Talkowski et al., 2010).

Three-Dimensional Fluorescence In Situ Hybridization. Three-dimensional fluorescence in situ hybridization (3D-FISH) was performed using the HSV-1 genome as a probe (Cremer et al., 2007). To visualize viral DNA in host cellular nuclei, iPSC-derived neurons were infected after 60 days of differentiation in neurobasal medium on matrigel-coated chamber slides. Neurons were infected with HSV-1 in the presence or absence of 5BVdU+IFN-α at MOI 0.3. On

average, 50 nuclei from each cellular preparation were scanned. Digital images were generated using Leica LAS AF, 3D Visualization Module. Hybridization signals were subjected to uniform thresholding to demarcate the signals.

Oligonucleotide Microarray Analyses. Cy3-labeled cRNA was used for hybridization to Agilent Human GE 8x60K V2 Gene Expression microarrays (Agilent Technologies), the microarrays scanned using the Agilent Microarray Scanner and data analyzed with Agilent Feature Extraction software (A 9.1.3; D'Aiuto et al., 2012). Differentially expressed genes were determined using unpaired t tests and Benjamini-Hochberg correction with $P \leq .05$ and the fold change of 2 as thresholds. The data were deposited in NCBI's Gene Expression Omnibus database (http://www. ncbi.nlm.nih.gov/geo/query/acc.cgi?acc=GSE46043).

fMRI Studies

Clinical Evaluations. Participants (schizophrenia = 19, controls = 23) completed the Structured Clinical Interview for DSM-IV (First et al., 1995) followed by consensus diagnoses (Prasad et al., 2007). SES was evaluated using the Hollingshead Index (Hollingshead, 1975). Exclusion criteria included substance abuse in the past month or dependence in the last 6 months, history of medical/neurological disorders, mental retardation (DSM-IV), illness duration over 8 years or participation in prior HSV-1 studies. The controls were screened for absence of psychosis and substance abuse (Prasad et al., 2007). After complete description of the study, written informed consent was obtained.

HSV-1 Exposure. IgG antibodies to HSV-1 were assayed using solid-phase enzyme immunoassays (Prasad et al., 2012).

MRI Studies. Structural MRI was acquired on a Siemens 3T Tim Trio whole-body scanner using the MPRAGE sequence to co-register fMRI data, overlay the blood oxygenation

level-dependent (BOLD) responses and identify regions-of-interest. Scanning parameters were: echo time (TE) = 3.52 ms, repetition time (TR) = 2300 ms, flip angle = 9°, thickness = 0.8mm, and number of slices = 192 (Stolz et al., 2012). In the same session, subjects performed a letter n-back task and whole-brain BOLD responses were collected using gradient-echo echo-planar imaging (EPI). Scanning parameters for the fMRI were: TE = 31ms, TR = 2000 ms, 36 axial/oblique slices of 4-mm thickness, field of view = 240 mm, flip angle = 80°, and matrix size = 64 × 64. The letter n-back task consisted of 6 blocks (2 blocks each of 0-back, 1-back, and 2-back) of English upper case letters as stimuli. Each stimulus was presented for 500ms. The interstimulus interval (ISI) was jittered randomly between 1.5 and 5.5 s with an average ISI of 3.5 s. Each block was followed by 20 s rest. The first block presented was always 0-back to acclimatize the subjects in the scanner, followed by a randomized order of presentation. Stimuli were presented using E-prime through back projection on a white screen. Subjects responded through a fiber-optic button system by pressing the assigned button every time they saw X on the screen for the 0-back, if they saw the same letter preceding the one presented earlier for the 1-back and if they saw a letter shown 2 letters before the one they were seeing for the 2-back. The responses were collected for both accuracy and response time.

Image Processing. fMRI data were analyzed using SPM8 (http://www.fil.ion.ucl.ac.uk/spm/software/spm8/). Images were realigned and normalized to a standard EPI template and smoothed with 8 × 8 × 8 Gaussian kernel. A full-factorial random effects model was implemented within SPM8 with age, sex, and SES as covariates. We preferred to compare groups across each task level since the behavioral data between-group showed significant differences across each task level rather than between levels of performance. A priori combined intensity and spatial extent threshold significance was determined by running 10,000

Monte Carlo simulations on AlphaSim (Maldjian et al., 2003) for the whole brain. The simulation showed that the BOLD differences within a cluster of 1385 contiguous voxels with a minimum voxel-wise difference of $P < .05$, would provide a $P < .05$ corrected for both the intensity and the spatial extent of the clusters. Task performance data were analyzed using generalized linear models for mean response time and the Mann-Whitney U tests for accuracy. Percent signal changes were extracted from the regional masks of Brodmann areas (BA) defined by the WFU PickAtlas (Ward, 2000) that contained the peak intensity voxel and were analyzed using ANOVA on SPSS 21.

3.3.4 Results

3.3.4.1 iPSC-Based Studies

HSV-1 Infection in NPCs and Neurons. At 24h postinfection (p.i.), FC analysis showed ~30% and ~15% of EGFP-positive (EGFP+) cells in infected NPCs and neurons respectively, indicating lytic infection (FIGURE 15). A ~2-fold reduction of EGFP+ cells was observed in NPCs and ~3-fold reduction in neurons when HSV1infected cells were co-incubated with acyclovir, compared with vehicle-treated controls. Separately, NPCs and neuronal cultures co-incubated with 5BVdU and IFNα showed a greater reduction in EGFP+ cells (percentage of EGFP+ cells were ~8% and ~2%, respectively), compared with untreated control cells or acyclovir-treated cells, suggesting that the antiviral agents suppressed viral gene expression.

Even in the presence of 5BVdU+IFN-α, the majority of infected NPCs detached from culture plates without a concomitant increase in the frequency of EGFP+ and RFP+ cells, suggesting that HSV-1 quiescent infection cannot be established consistently in NPCs (FIGURE 16, top panel).

In contrast, when neuronal cultures were infected at MOI of 0.3 with 5BVdU+IFN-α and maintained from day −1 to day +7 p.i., only 9% of cells expressed EGFP, suggesting that viral gene expression was suppressed in the majority of cells and lytic infection was present in a minority (FIGURE 16, middle panel). Infectious viral particles were undetectable in the supernatant for 7 days of infected neuronal cultures treated with inhibitors, based on subsequent Vero cell plaque assays (FIGURE 16, bottom panel, left). Culture supernatants from these neuronal cultures tested against new neuronal cultures (1/20 of the volumes of the culture supernatants were applied to neuronal cultures) failed to yield EGFP+ or EGFP+/RFP+ cells in all cultures up to 48 h p.i., consistent with the plaque assays (FIGURE 16, bottom panel, right). Though the green fluorescence in the initial neuronal cultures indicates activation of the ICP0 promoter, productive infection was thus fully suppressed and quiescent infection may be present (FIGURE 16, middle panel).

Withdrawal of 5BVdU+IFN-α was followed by ~3-fold increase of EGFP+ cells and ~5-fold increase of EGFP+/RFP+ cells (FIGURE 16, middle panel). Infectious viral particles were undetected in most cultures, although a relatively low level of infectious virus (~3 log(10) pfu/ml) was detected in 3 out of 9 cultures (data not shown). Culture supernatants were also tested for presence of virions by application to additional neuronal cultures. Only sporadic EGFP+ and EGFP+/RFP+ cells were observed when neuronal cultures were infected with up to 1/20 of the volume of the culture supernatants (FIGURE 16, bottom panel, right). Thus, withdrawal of 5BVdU and IFN-α reactivates lytic cycle genes, but productive infection is still substantially suppressed.

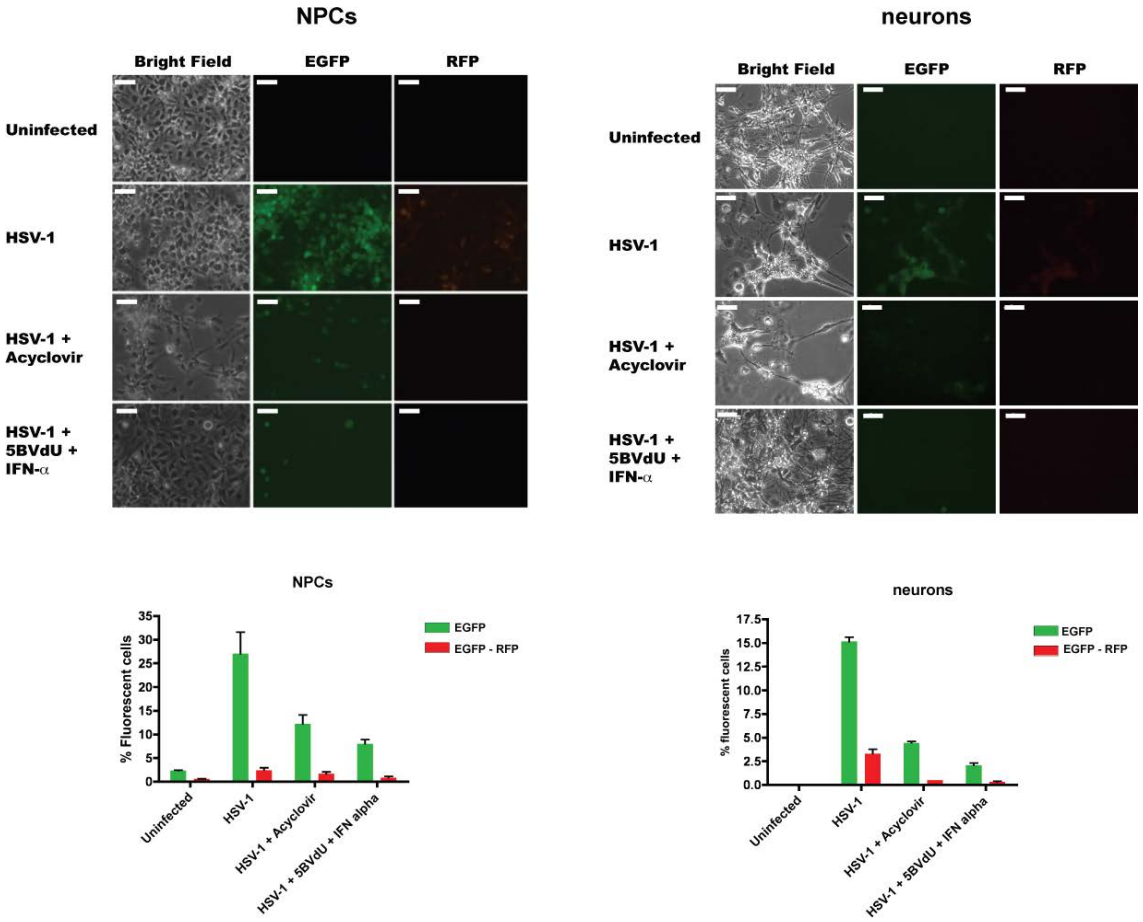

Figure 15. Comparative efficiency of antiviral drugs to reduce acute infection in induced pluripotent stem-derived neural progenitor cells (NPCs) and neurons.

Top panel: microphotographs of NPCs and neuronal cultures infected with herpes simplex virus, type 1 (HSV-1) (multiplicity of infection of 0.1 and 0.3, respectively) in the presence or absence of viral replication inhibitors acyclovir or 5-(E)-5-(2bromovinyl)-2-deoxyuridine along with interferon-α. Bottom panel: fluorescence-activated cell sorting analysis of uninfected and HSV-1 infected NPC and neuronal cultures. Scale bar is 50 μm.

Reactivation of Quiescent Infection with Sodium Butyrate. Neurons were cultured for 5 days with sodium butyrate (NaB) (5mM), a histone deacetylase inhibitor, after initial 7-day treatment with 5BVdU+IFN-α. FC showed ~2-fold increase of EGFP+ cells and ~6-fold increase of EGFP+/RFP+ cells, (FIGURE 16, middle panel). Productive infection was confirmed by applying NaB-treated culture supernatants to fresh neuronal cultures, yielding a high proportion

of EGFP+ and EGFP+/RFP+ cells (FIGURE 16, bottom panel, right). The viral titer of culture supernatant was ~4 log(10) pfu/ml (FIGURE 16, bottom panel, left). Thus, HSV-1 can be recovered from quiescently infected neurons with NaB.

Nuclear Localization of the HSV-1 Genome During Neuronal Infection. Lytic or quiescent infection was induced in iPSC-derived neurons as described and HSV-1 genomes visualized using 3D-FISH. In acutely infected cultures, numerous FISH signals corresponding to HSV-1 genomes were found in the central region of the nucleus, and the host chromatin showed displacement toward the nuclear periphery (FIGURE 52a). In neurons with quiescent infection, only a weak signal was detected at the nuclear periphery (FIGURE 52b).

Viral and Neuronal Gene Expression. Using qPCR assays, viral LAT, ICP4, and DNA polymerase genes were expressed at higher levels during lytic vs quiescent infection (fold-changes: LAT: 54, ICP4: 63, DNA polymerase: 51). Microarray analysis of host neuronal gene expression indicated that 10,087 genes were altered significantly during lytic infection ($P < .05$, corrected for multiple comparisons, mean fold changes <0.5 or >2), but during quiescent infection, only 1,525 genes changed significantly; the latter included glutamate receptor and voltage-gated ion channel genes (FIGURE 17). During lytic infection, Ingenuity Pathways Analysis (IPA) indicated enrichment of glutamate receptor signaling, mitochondrial dysfunction, axonal guidance signaling, chondroitin and dermatan sulfate degradation pathways; an overlapping set were altered in quiescently infected cells (FIGURE 17).

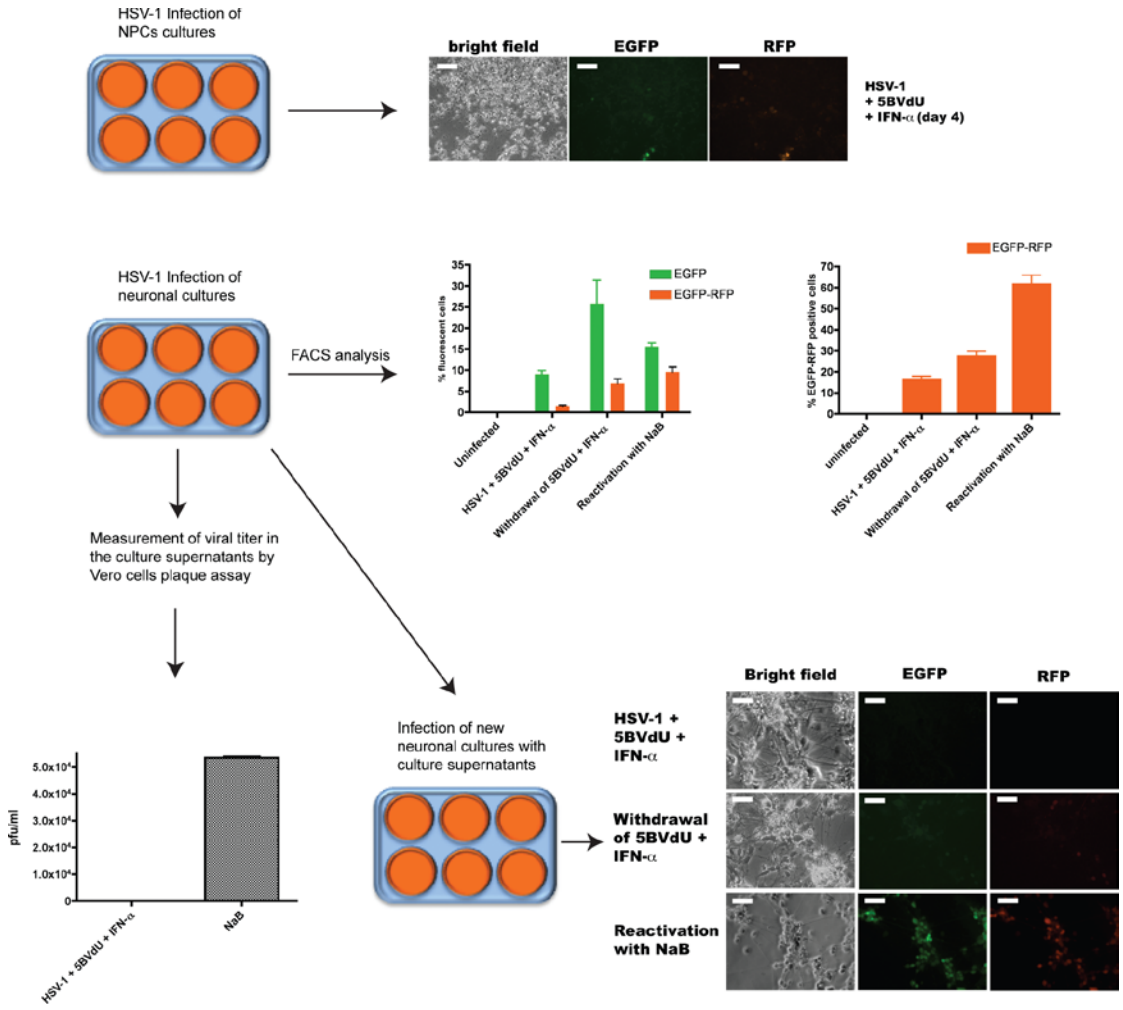

Figure 16. Quiescent infection established in neurons but not in neural progenitor cells (NPCs).

Top panel: microphotographs of induced pluripotent stem-derived NPCs infected with herpes simplex virus, type 1 (HSV-1) in the presence of 5-(E)-5-(2-bromovinyl)-2 deoxyuridine (5BVdU) and interferon (IFN)-α (5BVdU+IFN-α). Middle and bottom panels: neuronal cultures were incubated under the following conditions: (1) uninfected, (2) infected with HSV-1 and 5BVdU + IFN-α for 7 days ("HSV-1+5BVdU+IFN-α"), (3) infected with HSV-1 and cultured with 5BVdU+IFN-α for 7 days, then drugs were removed from culture medium, and infected cells were further cultured for 5 days in neurobasal medium alone ("withdrawal of 5BVdU+IFN-α"), (4) infected with HSV-1 and cultured with 5BVdU+IFN-α for 7 days, then drugs were removed from culture medium, and infected cells were further cultured for 5 days in neurobasal medium with sodium butyrate (NaB) ("reactivation with NaB"). The relative fraction of enhanced green fluorescent protein+/ red fluorescent protein+ cells in each condition is shown (middle panel, right). Viral titer in the supernatants from the culture plates was measured using Vero plaque assays (bottom panel, left). Microphotographs in the bottom panel, right, show the effects of adding supernatants from the original cultures to fresh neuronal cultures (label to left of each microphotograph indicates the culture condition from which the supernatant was derived). Scale bar is 50 μm.

fMRI Studies

Participants. HSV-1 exposure was significantly more prevalent among schizophrenia cases (HSV1+ = 13, HSV1− = 6) than healthy controls (HC; HSV1+ = 6, HSV1− = 17; $\chi 2$ = 7.53, df = 3, P = .006), but the mean age (schizophrenia, 27.44 ± 9.87 years; HC, 26.38 ± 6.78 years, t = 0.41, P = .4) and gender (schizophrenia, M/F 10/9; HC, M/F 8/15, $\chi 2$ = 1.35, df = 3, P = .25) distribution did not differ significantly across diagnostic groups or by serological status (all P > .4). Although the SES of schizophrenia patients (27.03 ± 8.76) was significantly lower than the HC (41.59 ± 9.01) ($\chi 2$ = 5.28, P < .001), it did not differ by HSV-1 status in the case/control groups.

Letter n-*Back Task*. The overall sensitivity of performance (d′) was 2.95, with no significant differences across diagnostic or serostatus groups. The response time of 0-back (schizophrenia, 676.94 ± 121.25 ms; HC, 627.38 ± 192.77 ms; Wald $\chi 2$ = 4.01, df = 1, P = .045) and 1-back (schizophrenia, 795.31 ± 181.15 ms; HC, 712.57 ± 275.82 ms; Wald $\chi 2$ = 5.94, df = 1, P = .015) showed diagnosis effect but not HSV-1 status or diagnosis-by-serostatus interaction effects. The 2-back task response time showed a trend for the main effect of diagnosis (schizophrenia, 895.29 ± 504.43 ms; HC, 825.64 ± 276.44 ms; Wald $\chi 2$ = 2.9, df = 1, P = .088) and HSV-1 status (HSV1+ = 986.74 ± 527.78 ms; HSV1− = 712.39 ± 438.30 ms, Wald $\chi 2$ = 3.45, df 1, P = 0.06) and diagnosis-by-HSV1 status interaction (Wald $\chi 2$ = 3.6, df = 1, P = .058). There were no significant main effects of diagnosis, HSV-1 status or diagnosisby-HSV1 status interaction on accuracy of performance. Besides, we did not observe either diagnosis or HSV1 status effect on mean response times or accuracy between each level of task across the groups. Therefore, the groups were contrasted at each level of task for BOLD response differences.

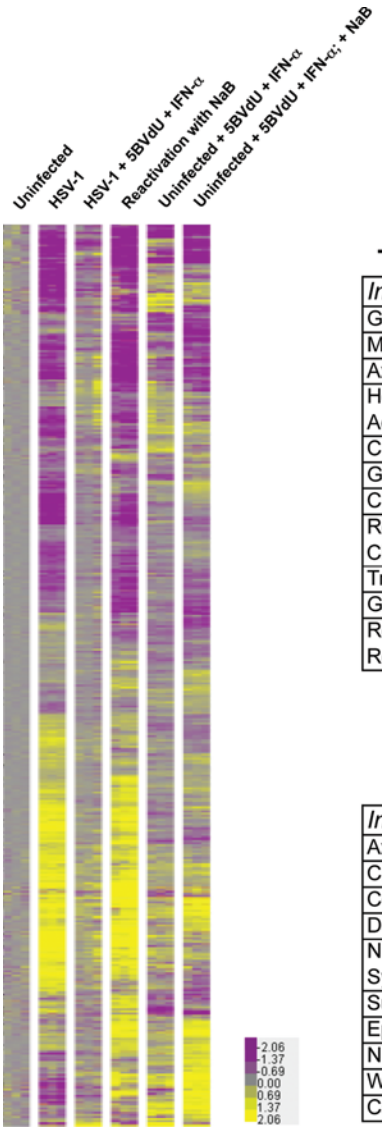

Top Functions affected as a result of HSV-1 lytic infection

Ingenuity Canonical Pathways	*-log(p-value)*	*Ratio*	*P-value*
Glutamate Receptor Signaling	3.64	0.541	2.28E-04
Mitochondrial Dysfunction	3.56	0.49	2.75E-04
Axonal Guidance Signaling	2.81	0.389	1.53E-03
Hepatic Fibrosis / Hepatic Stellate Cell Activation	2.73	0.464	1.88E-03
CREB Signaling in Neurons	2.72	0.422	1.89E-03
Granulocyte Adhesion and Diapedesis	2.31	0.446	4.93E-03
Chondroitin Sulfate Degradation (Metazoa)	2.24	0.75	5.73E-03
Role of Osteoblasts, Osteoclasts and Chondrocytes in Rheumatoid Arthritis	2.21	0.416	6.13E-03
Triacylglycerol Biosynthesis	2.16	0.576	6.85E-03
G Protein Signaling Mediated by Tubby	2.13	0.486	7.48E-03
Role of NFAT in Regulation of the Immune Response	2.08	0.398	8.38E-03

Top Functions affected in quiescent cultures

Ingenuity Canonical Pathways	*-log(p-value)*	*Ratio*	*P-value*
Axonal Guidance Signaling	3.283	0.101	5.21E-04
Chondroitin Sulfate Degradation (Metazoa)	3.182	0.417	6.58E-04
Complement System	3.058	0.242	8.74E-04
Dermatan Sulfate Degradation (Metazoa)	2.995	0.385	1.01E-03
Nitric Oxide Signaling in the Cardiovascular System	2.88	0.147	1.32E-03
Superpathway of Cholesterol Biosynthesis	2.837	0.259	1.46E-03
Ephrin Receptor Signaling	2.341	0.107	4.56E-03
NF-κB Signaling	2.309	0.118	4.90E-03
Wnt/β-catenin Signaling	2.163	0.118	6.87E-03
Caveolar-mediated Endocytosis Signaling	2.145	0.136	7.15E-03

Figure 17. Gene expression analysis in acutely and quiescently infected neurons.

The heat map represents statistically significant ($P \leq .05$), differentially expressed genes after one-way ANOVA analysis and Benjamini-Hochberg correction applied. Columns represent individual samples (each group n = 3); selected genes are represented in rows. Upregulated genes are shown in yellow, and downregulated genes are shown in purple. Right: Ingenuity Pathways Analysis of acutely and quiescently infected neuronal cultures.

BOLD Response Differences (FIGURE 18)

Main Effect of Task, Diagnostic Status, and HSV-1 Status. Task Main Effect The task main effect was noted in the prefrontal (BA 10, 45 and anterior cingulate gyrus,), posterior

parietal cortex (BA 40), occipital and insular cortices for the 1-back, and the prefrontal (BA 8 and 10), posterior parietal (BA 40), occipital and inferior temporal cortices for the 2-back, but not for the 0-back task where only the occipital cortex (BA 17 and 18) showed increased activations.

HSV-1 Main Effect A significant effect of HSV-1 exposure was noted in the prefrontal and subcortical regions for the 1-back (BA 8) and 2-back (BA 6, 8, left thalamus, substantia nigra, and red nucleus), but not for the 0-back.

Diagnosis Main Effect 0-back did not show diagnosis main effect. We observed diagnosis main effect for 1-back in the inferior parietal lobule (BA 40), and for the 2-back task in the superior temporal gyrus (STG, BA 42, 22), and the right cuneus, but not in the prefrontal regions at the combined intensity and spatial extent threshold used here.

Diagnosis-by-HSV-1 Interactions A significant interaction was noted in the left superior parietal lobule (BA 7, $F = 16.30$, $P = 3.02 \times 10{-}4$) for the 0-back, but not for the 1-back and 2-back tasks.

Associations with HSV-1 Status. The t tests to investigate directionality of effects showed increased BOLD responses for all contrasts comparing HSV-1–exposed subjects with those not exposed.

Table 3. fMRI Results with Contrasts.

Contrast	*x*	*y*	*z*	Region	Brodmann Area	Statistic	Corrected *P*
Main effect of task							
1 back	−30	22	4	Left inferior frontal gyrus, insula	45, 47, 13	40.16	3.59×10^{-7}
	2	56	2	Bilateral medial frontal, superior frontal, and anterior cingulate	10	37.12	7.34×10^{-7}
	40	−46	44	Right inferior parietal lobule and subgyral	40	19.85	9.10×10^{-5}
2-back	56	−4	−30	Right fusiform, inferior temporal, and middle temporal gyri	20, 21	33.53	1.79×10^{-6}
	−36	−52	56	Left inferior parietal lobule	40	42.51	2.10×10^{-7}
	48	14	38	Right middle frontal gyrus	8, 10, 46	83.06	1.57×10^{-10}
	−2	56	4	Left medial frontal gyrus	10, 11, 32	44.19	1.45×10^{-7}
Main effect of HSV1 serostatus							
1-back	−4	26	64	Left superior frontal gyrus	6	17.87	1.76×10^{-4}
2-back	−12	−22	−10	Left thalamus	—	26.45	1.39×10^{-5}
	−22	−2	68	Left superior and middle frontal gyrus	6	25.97	1.21×10^{-5}
Main effect of diagnosis							
1-back	−62	−36	34	Left inferior parietal lobule	40	13.92	.001
2-back	−62	−18	8	Left transverse temporal and superior temporal gyrus	22, 41, 42	25.02	1.83×10^{-5}
Pooled sample of SZ and HC ($HSV1^+ > HSV1^-$)							
1-back	−4	26	64	Left superior and medial frontal gyrus, anterior cingulate	6, 8, 32	**4.23**	8.79×10^{-5}
	−2	−26	8	Left thalamus	—	2.89	.003
2-back	−12	22	−10	Left thalamus, substantia nigra, and bilateral red nucleus	—	5.10	6.94×10^{-6}
	−22	−2	68	Left frontal lobe, superior frontal gyrus	6	5.14	6.06×10^{-6}
Within SZ subjects ($HSV1^+ > HSV1^-$)							
1-back	20	22	66	Right middle frontal gyrus and right superior frontal gyrus	6	4.61	2.90×10^{-5}
2-back	−2	−20	−12	Bilateral red nucleus, brainstem, and midbrain	—	4.17	1.02×10^{-4}
Within HC subjects ($HSV1^+ > HSV1^-$)							
1-back	−2	4	38	Bilateral cingulate gyrus	24, 32	3.24	.001
2-back	62	−58	12	Right superior temporal gyrus, right middle temporal gyrus	21,22,39	4.51	3.86×10^{-5}
	−20	−4	70	Left superior frontal gyrus	6, 9, 32	3.73	3.32×10^{-4}
	6	−10	4	Left medial dorsal, ventral lateral, and anterior nuclei of thalamus	—	3.73	3.64×10^{-4}
Between $HSV1^+$ SZ and $HSV1^+$ HC ($HSV1^+$ SZ > HC)							
1-back	4	−76	4	Right cuneus and lingual	17, 18, 23, 30	3.76	3.31×10^{-4}
2-back	26	−70	−10	Right fusiform gyrus and lingual gyrus	18, 19	4.24	8.55×10^{-5}
Between $HSV1^+$ SZ and $HSV1^+$ HC ($HSV1^+$ SZ < HC)							
2-back	−24	6	56	Left superior and middle frontal gyrus	6, 24, 32	3.26	.001
Between $HSV1^-$ SZ and $HSV1^-$ HC ($HSV1^-$ SZ > HC)							
1-back	4	−4	30	Bilateral limbic lobe, bilateral cingulate gyrus	24	4.07	1.36×10^{-4}
2-back	−60	−26	4	Left superior temporal gyrus, left middle temporal gyrus	21, 22, 41, 42	3.63	4.71×10^{-4}
	34	54	30	Right superior frontal gyrus, right middle frontal gyrus[a]	9, 10	3.69	3.97×10^{-4}
	8	−12	60	Right medial frontal gyrus	6	3.53	.001
	60	−58	10	Right superior temporal gyrus, right middle temporal gyrus	21, 22, 39	3.39	.001

Note: BA, Brodmann area; fMRI, functional magnetic resonance imaging; HC, healthy control; HSV1, herpes simplex virus, type 1;SZ, schizophrenia.

[a]BA 9 and 10 was significant when the cluster size was reduced to 1343 voxels that corresponded to corrected P < .06. All other regions were examined at cluster size of 1385 that corresponded to corrected P < .05.

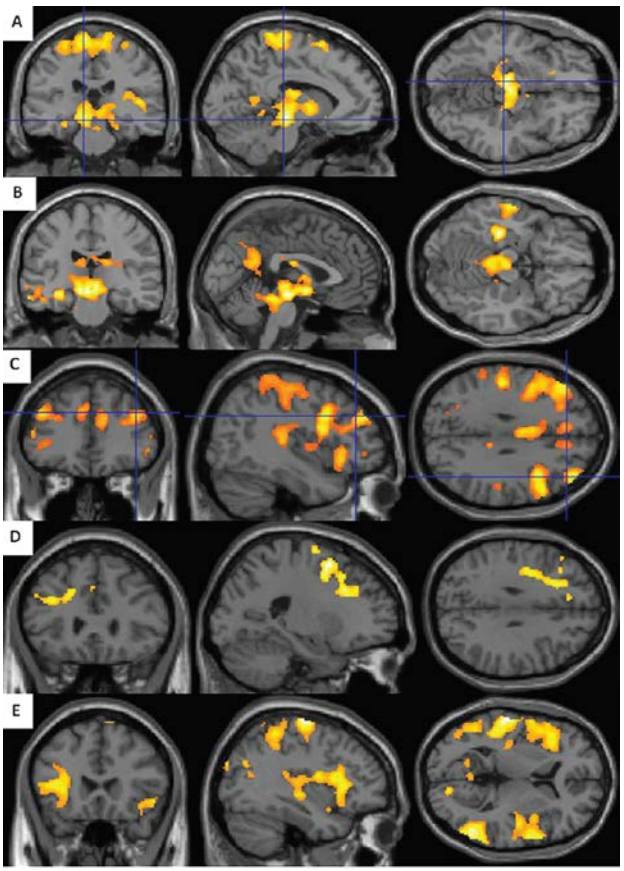

Figure 18. Blood oxygenation level dependent (BOLD) response differences in response to 2-back challenge.

(A) Combined schizophrenia and healthy control sample. Herpes simplex virus, type 1 (HSV1)+ show greater activation compared with HSV-1− subjects in the substantia nigra, the red nucleus, and thalamus. (B) HSV1+ schizophrenia subjects show increased activation in bilateral red nucleus and substantia nigra compared with HSV1− schizophrenia subjects. (C) Increased activation in the prefrontal and parietal regions among HSV1+ in controls compared with HSV1− controls. (D) HSV1+ schizophrenia subjects showed decreased BOLD responses in the anterior cingulate regions compared with HSV1+ HC. (E) HSV1− schizophrenia subjects showing increased BOLD responses in bilateral superior temporal gyri. Increased activation in the prefrontal Brodmann areas 9 and 46 showed a trend (corrected P = .06).

Combined Schizophrenia and HC Controlling for Diagnostic Status HSV-1 exposure was associated with increased BOLD responses in the prefrontal and subcortical regions for the 1-back (BA 6, 8, 32, thalamus) and 2-back (BA 6, thalamus, substantia nigra, and red nucleus) tasks, but not for the 0-back task where BOLD responses were increased mainly in the bilateral superior temporal gyri (BA 42, 22, and 40) (Table 3). BOLD responses for 1-back task was elevated nearly 2.5-fold in the thalamus ($t = 2.5$, $P = .016$) among HSV1+ compared with HSV1− subjects. For the 2-back task, HSV1+ subjects showed 3-fold increase in BOLD responses compared with HSV1− within the substantia nigra, thalamus, and red nucleus cluster ($t = 3.9$, $P = .0003$; Table 3).

BOLD Responses Within and Across Schizophrenia/HC Groups, Grouped by Serological Status. Within schizophrenia subjects, HSV-1 exposure was associated with increased BOLD responses in the BA 6, and the red nucleus, the substantia nigra, the left parahippocampal regions for 1-back and 2-back tasks, respectively (Table 3). In contrast, HSV-1–exposed HC showed increased BOLD responses in the anterior cingulate gyrus (BA 24 and 32), prefrontal (BA 6, 9), and temporal cortices compared with HSV1− HC. The BOLD responses were decreased in the anterior cingulate region (BA 24 and 32) and BA 6 among HSV1+ schizophrenia subjects compared with HSV1+ HCs for the 2-back task. schizophrenia-HC comparisons among HSV-1–negative individuals showed increased BOLD responses in schizophrenia subjects in the anterior cingulate (BA 24) for the 1-back and in BA 9, 10 and bilateral superior temporal gyri for the 2-back tasks.

3.3.5 Discussion

The iPSC-derived neurons recapitulate lytic HSV-1 infection and can be induced into a quiescent, persistent, reactivable infection. Like established animal models, quiescent infection is accompanied by reduced viral replication, retention of the viral genome in the nucleus, lack of infectious virions, expression of LATs (Kosz-Vnenchak et al., 1990; Matthews et al., 1993; Liu et al.2000; Kramer et al., 2003; De Clercq, 2005; Margolis et al., 2007; Giordani et al., 2008; Bloom et al., 2010; Nicoll et al., 2012) in neurons. Quiescent infection was not observed in NPCs. During lytic infection, microarray analyses showed extensive changes in cognition-related pathways, such as glutamate and cAMP response element-binding protein (CREB) signaling. Fewer changes occurred in quiescent infection, but they too included cognition-relevant glutamate receptor and ion channel genes. We therefore propose a model in which persistent infection occurs in brain neurons similar to that in sensory ganglia, and over time impairs neuronal function (suggested by altered gene expression) without producing florid encephalitis; the altered function may underlie observed cognitive deficits. The relatively high sensitivity of NPCs to HSV-1 infection also suggests that individuals infected in childhood can experience cognitive impairment secondary to altered NPC proliferation and differentiation (Regnell et al., 2012) suggesting the neurodevelopmental implications of HSV-1 exposure. This model needs to be tested and immunological/ glial responses explored; simultaneous *in vitro* and MRI studies in the same persons may also be worthwhile.

The fMRI results suggest increased processing time for working memory performance associated with schizophrenia and HSV-1 exposure. The 2-back mean response time showed a trend toward significance for the diagnosis, HSV-1 status, and diagnosis-by-HSV-1 exposure interaction, with nonsignificant differences in accuracy of performance. fMRI data mainly

showed increased BOLD responses among both schizophrenia and HSV-1–exposed individuals suggesting that an increased neurobiological effort in the prefrontal cortex (PFC), posterior parietal cortex, hippocampus/parahippocampus, thalamus, substantia nigra, and superior temporal lobes is needed to achieve accuracy of working memory performance comparable to unexposed participants. Notably, the HSV-1-exposed individuals showed BOLD responses in the midbrain regions and thalamus. The trigeminal nucleus that receives neuronal inputs from the trigeminal ganglion is situated close to the red nucleus and substantia nigra, and projects to the thalamus. Increased BOLD response in these regions raises the possibility of altered dopamine transmission among HSV-1–exposed subjects. The increased activation in the STG is notable since this region is markedly affected during HSV-1 encephalitis (Steiner et al., 2007). HSV-1–exposed HC showed activation differences in the classical working memory network that include prefrontal cortex and posterior parietal cortex, whereas HSV-1–exposed schizophrenia subjects recruited regions outside this network (substantia nigra where dopamine neurons are situated, red nucleus, thalamus, and superior temporal gyrus) to perform at the same level as HC. Besides, HSV-1-exposed schizophrenia subjects showed similar prefrontal activations compared to HSV-1 unexposed schizophrenia subjects while performing on par with them, possibly by recruiting other networks involving STG and subcortical structures.

Some shortcomings should be noted. Though functional (D'Aiuto et al., 2012), the iPS-derived neurons cannot completely recapitulate the milieu interior of the human brain. The fMRI studies did not show diagnosis effects at the PFC; possibly reflecting inadequate power since lowering the statistical threshold to $P < .06$ corrected for intensity and spatial extent shows diagnosis effect. Because HSV-1 virions are usually undetectable in serum (Steiner et al., 2007), HSV-1 exposure was indexed through serum antibody assays in the fMRI studies.

In conclusion, HSV-1 induces quiescent infection in human iPSC-derived neurons that resembles animal models of latent infection. The fMRI studies indicate increased hemodynamic responses during working memory challenge among HSV-1–exposed individuals without prior encephalitis. We propose specific testable cellular and other models for the published HSV-1–associated cognitive dysfunction.

3.3.6 Funding

MH 63480 (V.L.N.); MH72995 MH 93540 and the American Psychiatric Institute for Research and Education-Lilly Award (K.M.P.); EY08098 (P.R.K.); and Stanley Medical Research Institute (07R-1712 to V.L.N.).

3.3.7 Acknowledgments

We thank our study participants and research staff. Dr R.H.Y. is a member of the Stanley Medical Research Institute (SMRI) Board of Directors and Scientific Advisory Board. The terms of this arrangement are being managed by the Johns Hopkins University. The authors have declared that there are no conflicts of interest in relation to the subject of this study.

3.4 ADDITIONAL VIROLOGICAL ASSAYS

In order to further characterize our model of HSV-1 latency, additional experiments were performed for Aim 1a: (i) to assess the time course of change in viral DNA copy number in host cells and viral titers in the supernatant; (ii) to evaluate nuclear localization of viral genomes during lytic and quiescent infections.

In addition, to further characterize our model of HSV-1 latency, additional experiments were performed for Aim 1b: (iii) to investigate viral DNA chromatin accessibility to MCN at viral gene promoters during lytic and quiescent HSV-1 infections; and (iv) evaluate the association of heterochromatin protein-1 (HP1) to the viral genome in lytically infected cells.

3.4.1 Rationale of proposed experiments

3.4.1.1 Rationale of Experiment 1: qPCR assay to determine viral copy number

Viral DNA copy number was estimated by qPCR in acutely and latently infected iPSC-neurons and during viral reactivation. Furthermore, productive infection for the aforementioned conditions was analyzed. To rule out the possibility that the antiviral compounds (5BVdU+IFNα) used to establish quiescence in iPSC-neurons could have adverse effects on the earliest events of infection, two additional conditions were evaluated: i) human iPSC-neurons were pretreated with 5BVdU+IFNα for 24 hours and then infected with HSV-1 for 2 hours in the presence of these antivirals; and ii) human iPSC-neurons were infected with HSV-1 for 2 hours in the absence of 5BVdU+IFNα. The cells infected with a viral construct carrying the reporter genes EGFP and RFP under the control of viral promoters (Ramachandran et al., 2008). The HSV-1 viral DNA copy number was quantified as described in section 3.1.7 (FIGURE 19).

3.4.1.2 Rationale of Experiment 2: Fluorescent *in situ* hybridization (FISH) to evaluate the sub-nuclear compartments containing viral DNA during models of HSV-1 infection in iPSC-neurons

We employed 2D FISH to further evaluate our models of HSV-1 infection. In a time-course experiment, we evaluated the progression of viral infection in Vero cells (FIGURE 20). The cells were infected at an MOI=1 and blocked for FISH at the indicated time points. In iPSC-neurons, the same FISH technique was performed on a 24-hour lytic infection, quiescently-infected cells, and cells that were induced for viral reactivation. Given our inability to detect quiescent viral genomes by the original FISH protocol (FIGURE 21), we adopted a three-dimensional (3D) FISH technique (Cremer et al., 2007) with modifications (FIGURE 22).

A FISH procedure was optimized for infected cells that were not affixed to microscope slides. The original FISH procedure was carried out on cells that were in suspension (FIGURE 23). We evaluated the efficiency of this protocol to provide alternate methods of viral readout.

3.4.1.3 Rationale of Experiment 3: Evaluating the association of heterochromatin protein-1 (HP1) with the viral genome in lytically infected cells using Co-ICC/FISH

HSV-1 infected cells were evaluated for patterns of heterochromatin by utilizing 3D FISH paired with immunocytochemistry (Co-ICC/FISH; FIGURE 24). FISH was performed on Vero cells (MOI=1) and human iPSC-neurons (MOI=0.3) that were infected with HSV-1 for 24 hours with a probe that is complementary to the HSV-1 genome. Next, ICC was performed on the same cell preparations using an anti-HP1α mouse monoclonal antibody (heterochromatin protein-1 alpha). HP1α binds with H3K9me3, an indicator of transcriptional gene silencing, and is associated with heterochromatic structures (Jacobs et al., 2001).

3.4.1.4 Rationale of Experiment 4: CHART-qPCR to investigate chromatin accessibility of viral gene promoters to MCN during lytic and quiescent HSV-1 infections

This technique quantifies nuclease accessibility across the genome, by digesting DNA not bound to histone complexes and then amplifying with locus-specific promoters. Briefly, the cells were harvested, the nuclei were extracted, and then distributed evenly into 5 tubes. MCN was added to each tube in increasing concentrations (0.5, 1.0, 3.0, and 5.0 units). One sample was treated only with nuclease digestion buffer. Samples were incubated for 20 minutes at 39° C. DNA was then extracted from the samples and identical amount of DNA (5ng) were used for quantitative PCR assays.

The host loci encoding rhodopsin (*RHO*) and glyceraldehyde-3-phosphate dehydrogenase (*GAPDH*) were chosen for controls. *RHO* served as a locus that is less accessible to the micrococcal nuclease (MCN), as it is expressed primarily in ocular tissues. *GAPDH*, a housekeeping gene, served as a locus that is accessible to MCN. If the underlying DNA is protected from MCN digestion, more intact DNA will be available to be amplified in the qPCR (*RHO*); however, if the DNA is not protected, the nuclease will digest and result in poor qPCR amplification (*GAPDH*; FIGURE 25). By taking the difference of Ct values of the digested and undigested, the ΔCq value (quantification cycle) can be determined (ΔCq= Ct(-MCN) – Ct(+MCN)). The viral loci include amplifying a region of the promoter for i) immediate early gene ICP4, ii) immediate early gene ICP27, iii) late gene glycoprotein C, and iv) the latency associated transcript (LAT). In iPSC-neurons, the promoters for the control and viral genes were analyzed at 8-hour lytic infection and a 7-day quiescent infection (FIGURE 26). The 8-hour time point was chosen to eliminate analyzing secondary or tertiary infections that occur during a full 24-hour cycle.

3.4.2 Results of proposed experiments

3.4.2.1 Results for Experiment 1: qPCR assay to determine viral copy number

Viral copy number was assessed in iPSC-neurons under several experimental conditions (FIGURE 19, *left panel*). Following the 2 hour adsorption time, we observed no statistical difference in viral copy number when infecting in the absence or the presence of 5BVdU+IFNα ($p=0.2092$). The mean viral copy number for HSV-1 at 24 hours post infection was 212,163 copies in 5 ng of total DNA extracted from the neurons. After exposing the infected cultures to 5BVdU+IFNα for 7 days, the mean viral copy number was 1,743 copies. After sodium butyrate was applied to induce reactivation on quiescent cultures, the mean viral copy number increased to 81,039 ($p=0.00506$). The number of infectious viral particles released from these cells was later estimated using the plaque assay on Vero cells (FIGURE 19, *right panel*). No plaques were observed in any condition, with the exception of HSV-1 incubated for 24 H (mean plaque forming units per milliliter was 48,667) and Reactivation (5D; mean plaque forming units per milliliter was 27,333). Each group was tested for homogeneity of variance using Levene's test and found they had unequal variance, thus we tested for differences in group means using an unpaired two-tailed Welch's t-test ($\alpha=0.05$) in GraphPad Prism version 6.0f software.

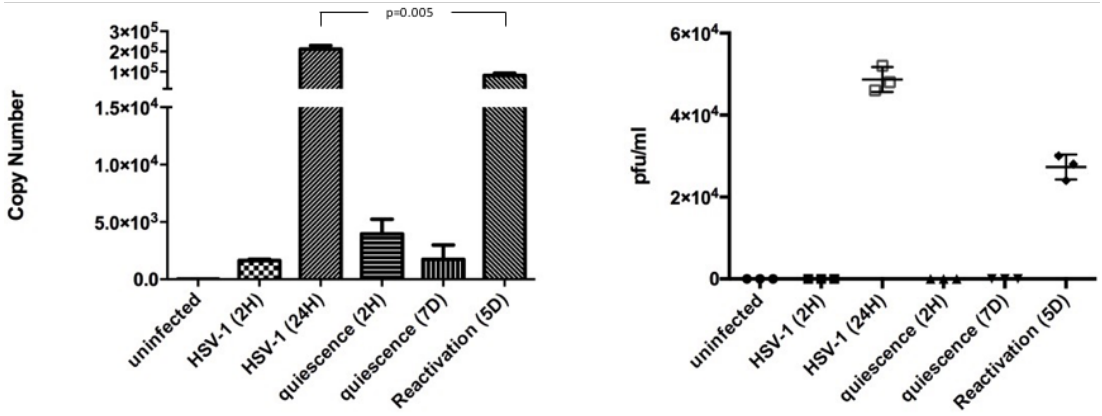

Figure 19. Viral DNA copy number in iPSC-neurons (*left*) and corresponding plaque assays of virions produced in the supernatant titrated on Vero cells, shown in PFU/ml (*right*).

The following groups of human iPSC-neurons were assayed: i) uninfected cells; ii) cells infected for 2 hours ("HSV-1_2H"); iii) cells infected for 24 hours ("HSV-1_24H"); iv) cells infected in the presence of 5BVdU+IFNα for 2 hours ("quiescence_2H"); v) infected cells cultured in the presence of 5BVdU+IFNα for 7 days ("quiescence_7D"); vi) infected cells cultured in the presence of 5BVdU+IFNα for 7 days followed by treatment with sodium butyrate to induce viral reactivation for 5 days ("Reactivation_5D").

3.4.2.2 Results for Experiment 2: Fluorescent *in situ* hybridization (FISH) to evaluate the sub-nuclear compartments containing viral DNA during models of HSV-1 infection in iPSC-neurons

The 2D FISH protocol was able to detect signals for HSV-1 gDNA in the lytic infection in Vero cells (FIGURE 20) and iPSC-neurons (FIGURE 21). Following a lytic HSV-1 infection in Vero cells, the viral genome was observed to replicate in distinct compartments in the nucleus as indicated by FISH probes (12 hours post infection, FIGURE 20). As infection proceeds, these replication compartments merge and completely occupy the interior of the nucleus (24 + hours post infection, FIGURE 20).

When using the 2D FISH protocol, numerous FISH hybridization signals were observed in the nuclei of acutely infected iPSC-neurons (MOI=0.3); conversely, no FISH signals were

observed in quiescently infected iPSC-neurons. (FIGURE 21). Upon treatment with sodium butyrate for 5 days the hybridization pattern was similar to what was observed in the acutely infected cells (FIGURE 21). To circumvent our inability to detect quiescent HSV-1 genomes using our 2D FISH procedure, we used 3-dimensional (3D) FISH. With this protocol, we were able to detect viral genomes in our model of latent HSV-1 infection in iPSC-neurons, as well as a 24-hour lytic infection (FIGURE 22).

Additionally, we performed FISH in suspension on Vero cells following a 24-hour infection (MOI=1.0; FIGURE 23). The protocol provided the groundwork to utilize FISH for use in future applications of flow cytometry quantification.

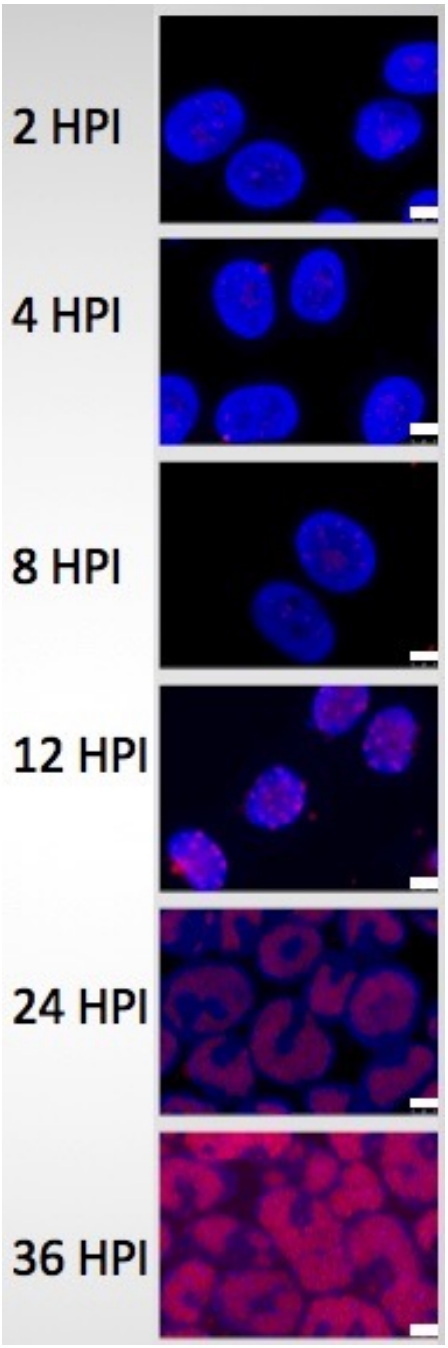

Figure 20. FISH on HSV-1 (strain KOS) infected Vero cells.

Cells were infected at MOI=1 and analyzed by 2D FISH at the indicated time points. The probe signal is shown in red. Nuclei are counterstained with Hoechst 33342 (blue). Scale bar is 5 μm.

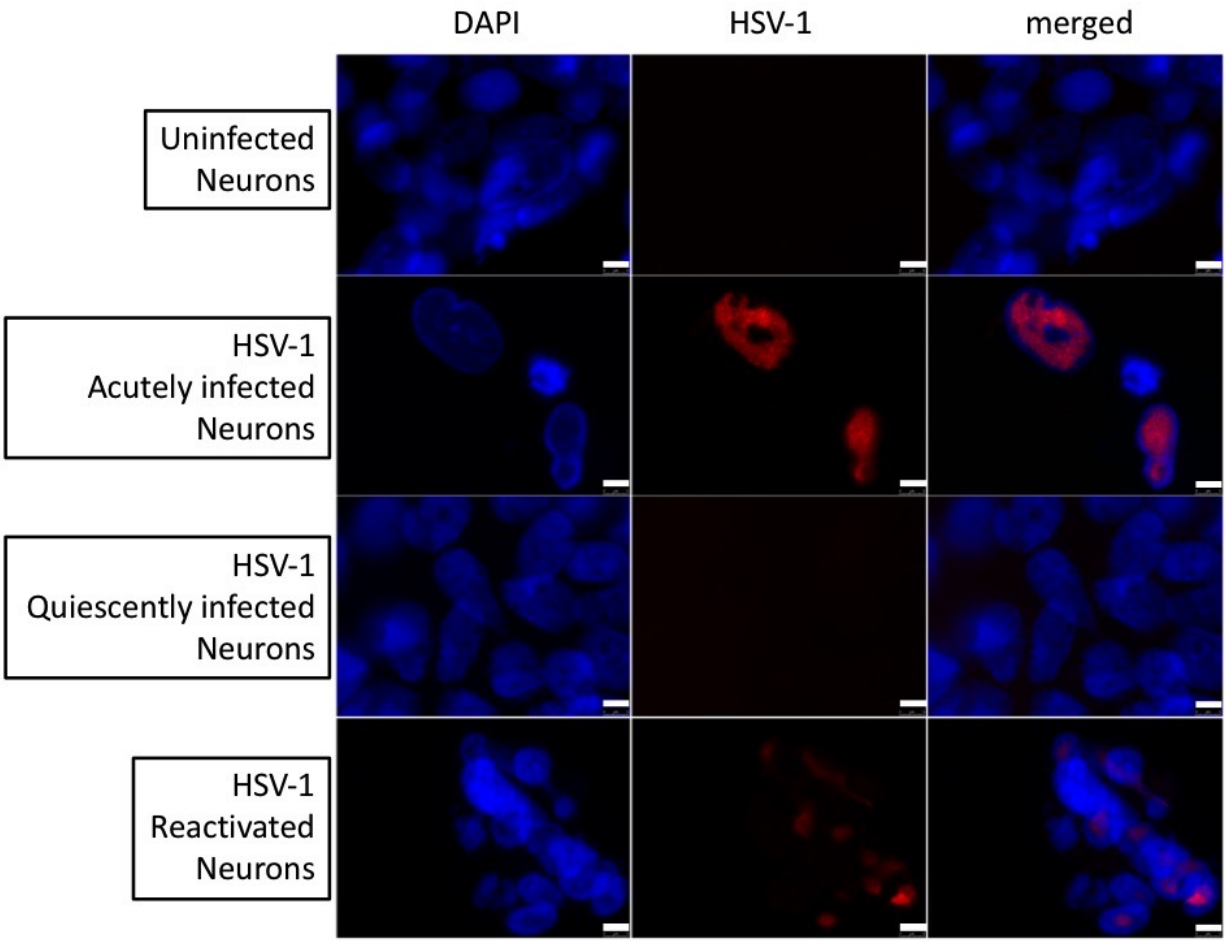

Figure 21. Location of HSV-1 genomes (strain KOS) in iPSC-neurons with lytic infection, quiescent infection, and reactivation by FISH analysis.

The probe signal is shown in red. Nuclei were counterstained with Hoechst 33342 (blue). Scale bar is 5 μm.

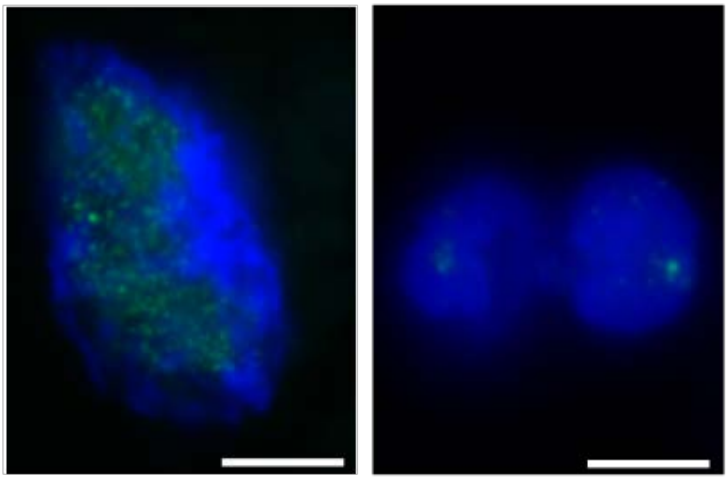

Figure 22. Location of HSV-1 genomes in lytically (*left*) and quiescently (*right*) infected neurons (strain KOS) using 3D FISH analysis.

A 3D FISH analysis was performed on iPSC-derived neurons that were acutely infected for 24 hours (*left)* or a 7-day quiescent infection (MOI=0.3). The probe signal is shown in green in the merged images. Nuclei were counterstained with Hoechst 33342. The scale bar is 5 μm**.**

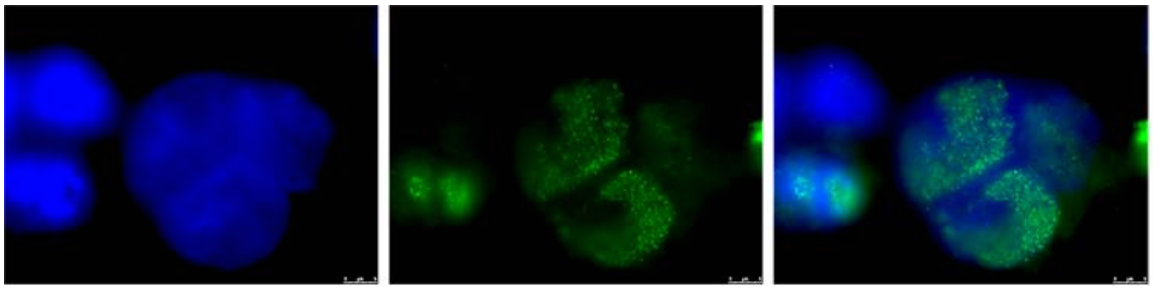

Figure 23. FISH in suspension performed on HSV-1 infected Vero cells.

FISH in suspension that was performed on Vero cells following a 24-hour infection with HSV-1 (strain KOS; MOI=1) utilizing the viral gDNA as a probe (green). Nuclei are counterstained with Hoechst 33342 (blue). The scale bar is 5 μm**.**

3.4.2.3 Results for Experiment 3: Evaluating the association of heterochromatin protein-1 (HP1) with the viral genome in lytically infected cells using Co-ICC/FISH

FISH (using a probe that was complementary to the viral genome) was combined with immunocytochemistry (Co-ICC/FISH) using an anti-heterochromatin protein-1 (HP1α) mouse monoclonal antibody. HP1α binds with H3K9me3, an indicator of transcriptional gene silencing, and is associated with heterochromatic structures (Jacobs et al., 2001). Co-localization of these signals may indicate the heterochromatizined viral genomes. In Vero cells, substantial overlap of HP1 was not observed with the viral DNA (FIGURE 24, *left*). However, acutely infected iPSC-neurons showed differing overlapping signals (yellow) from HP1 (green) and the viral DNA (red; FIGURE 24, *right*). Although the presence of overlapping signals may indicate binding of HP1 protein with some viral genomes, this needs careful evaluation using confocal microscopy, which will provide 3-dimensional resolution that is not evident in this thesis.

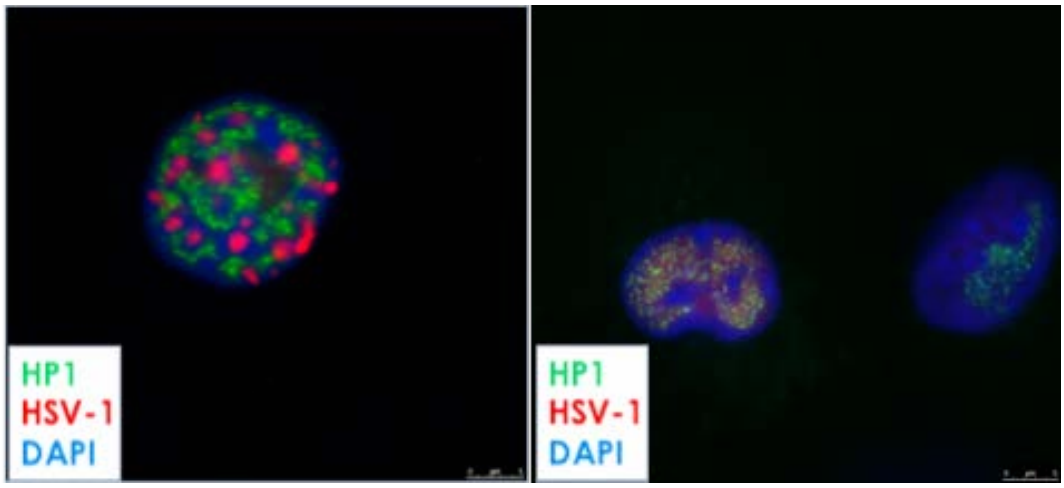

Figure 24. Co-ICC/FISH on HSV-1 infected cells.

Vero cells (*left*) and human iPSC-neurons (*right*) were infected with HSV-1 (strain KOS) for 24 hours at MOI=1.0 and 0.3, respectively. FISH was performed using HSV-1 gDNA as a probe (shown in red) and ICC was performed using an anti-HP1α mouse monoclonal antibody (shown in green; Millipore, catalog 05-689). Nuclei are counterstained with Hoechst 33342 (shown in blue). The scale bar is 5 μm.

3.4.2.4 Results for Experiment 4: CHART-qPCR to investigate chromatin accessibility of viral gene promoters to MCN during lytic and quiescent HSV-1 infections

In iPSC-neurons, CHART-PCR was performed following an 8-hour HSV-1 infection and a 7-day quiescent infection (MOI=0.3). Control genes showed different levels of MCN accessibility: the *RHO* promoter was less accessible than the *GAPDH* promoter (ΔCq was estimated at 0.63 and 7.37, respectively; FIGURE 25). The viral gene promoters of ICP27, glycoprotein C, and EGFP (that is under the control of ICP0 promoter) showed higher accessibility to MCN during acute HSV-1 infections (ΔCq was estimated at 2.18, 1.80, and 2.63, respectively) when compared to quiescent infections (ΔCq= 0.94, 0.90, and 1.17, respectively; FIGURE 26). LAT and ICP4 promoters showed higher MCN accessibility in quiescent infections (ΔCq was estimated at 1.93 and 2.05, respectively) when compared to acute infection (ΔCq was estimated at 1.07 and 0.88, respectively; FIGURE 26).

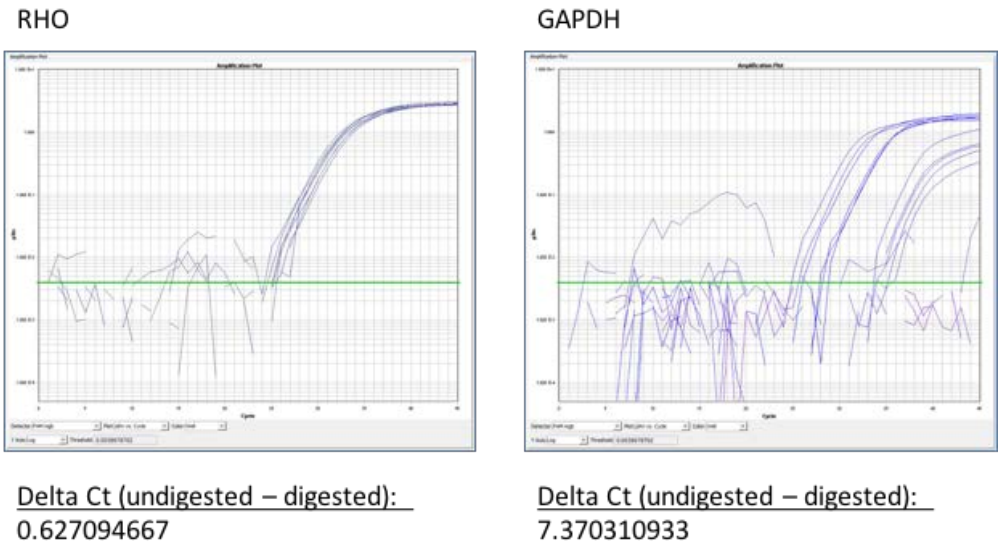

Figure 25. CHART-PCR performed on lytically infected human iPSC-neurons.

iPSC-neurons were infected with HSV-1 viral construct expressing reporter genes EGFP and RFP under the control of viral promoters for 8 hours (MOI=0.3). Following MCN digestion and DNA extraction, real-time qPCR was conducted using primers specific to promoter regions of host genes. *Left, RHO*, as a control for a transcriptionally silent gene in iPSC-neurons, is minimally susceptible to nuclease degradation (ΔCq was estimated at 0.63), compared with *Right*, housekeeping gene *GAPDH* (ΔCq was estimated at 7.37).

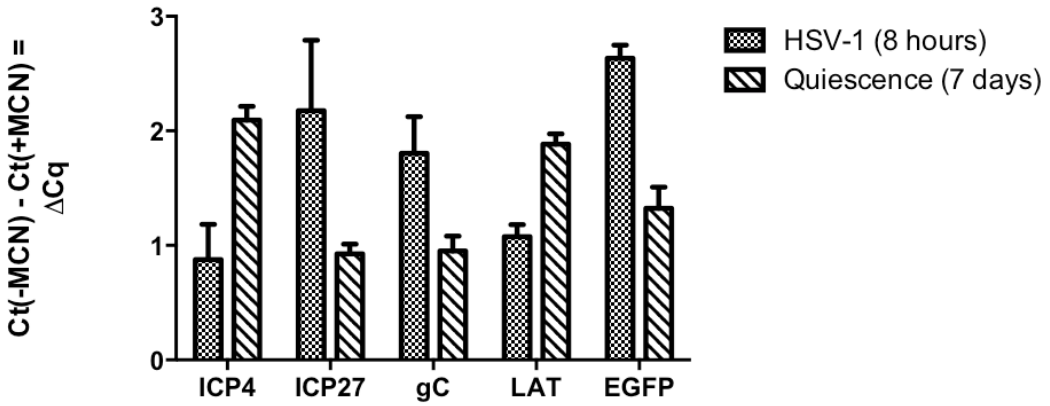

Figure 26. CHART-PCR performed on human iPSC-neurons amplifying viral gene promoters.

iPSC-neurons were acutely infected with HSV-1 viral construct expressing reporter genes EGFP and RFP under the control of viral promoters for 8 hours (MOI=0.3) and quiescently infected with HSV-1 for 7 days (MOI=0.3). Following MCN digestion and DNA extraction, real-time qPCR was conducted using primers specific to promoter regions of viral genes. MCN accessibility was determined by calculating the difference of the undigested DNA and the digested DNA (ΔCq). Error bars represent the standard deviation of the ΔCq values.

4.0 AIM 2. ANTIVIRAL SCREENING AND GROUNDWORK FOR MODERATE THROUGHPUT DRUG SCREENING

The primary goal is to identify drugs that potentially have a different mechanism of action than currently available antivirals for HSV-1 infections. The matter is acquiring urgency as viral resistance toward antivirals that target viral genes, such as viral DNA polymerase, viral DNA replication, or the helicase has been repeatedly documented (Burrel et al., 2013; Dropulic & Cohen, 2010; Malvy et al., 2005; Stránská et al., 2005). In immunocompromised individuals or organ transplant recipients, the frequency of viral reactivation of an antiviral-resistant virus is significantly higher compared with immunocompetent individuals, and can lead to devastating outcomes. Therefore, identifying small molecules with a novel mechanism of action will be part of our goal. Additionally, there is no drug directed toward the latent form of HSV-1. By using iPSC-neurons and the HSV-1 models of infection previously outlined, we tested molecules for antiviral effects and inhibition of reactivation from latency.

In order to enable a moderate throughput screening campaign for anti-HSV-1 compounds we propose scaling-up our efforts to generate a robust and cost-effective cellular platform. Drug screening campaigns require: (i) generation of large numbers of neurons in a multi-well culture system and (ii) meaningful readouts to test drug efficacy.

Sections 4.1 and 4.2 will cover two peer-reviewed manuscripts that detail our initial efforts to screen small compound libraries in HSV-1 infected human iPSC-neurons for antiviral effects i) using molecules that were previously reported to have lysosomotropic activities and ii) using novel, naturally occurring alkaloids derived from the Amaryllidaceae plant family. Section 4.3 follows these studies and details the groundwork required to culturing iPSC-neurons in 96- and 384-well culture plates and viral readout methods, which may be used in future studies to agnostically screen compounds for antiviral effects.

Aim 2a. Generation of culture plates containing homogeneously distributed human iPSC-neurons in monolayer fashion.

Aim 2b. Evaluate strategies that enable an automated analysis of the viral state in infected cells.

4.1 BROAD-SPECTRUM NON-NUCLEOSIDE INHIBITORS OF HUMAN HERPESVIRUSES

Lora McClain[a,b,1], Yun Zhi[a,c], Hoyee Cheng[a], Ayantika Ghosh[a], Paolo Piazza [d], Michael B. Yee [e],Santosh Kumar[g], Jadranka Milosevic[h], David C. Bloom[i], Ravit Arav-Boger[g], Paul R. Kinchington[e,f],Robert Yolken[j], Vishwajit Nimgaonkar[a,b], Leonardo D'Aiuto[a,⇑,1]

[a] Department of Psychiatry, WPIC, University of Pittsburgh School of Medicine, Pittsburgh, PA, USA

[b] Department of Human Genetics, Graduate School of Public Health, University of Pittsburgh, Pittsburgh, PA, USA

[c] Department of Pharmacology and Pharmaceutical Sciences, School of Medicine, Tsinghua University, Beijing, China

[d] Department of Infectious Diseases and Microbiology, University of Pittsburgh, Pittsburgh, PA, USA

[e] Department of Ophthalmology, University of Pittsburgh School of Medicine, Pittsburgh, PA, USA

[f] Department of Molecular Genetics & Biochemistry, University of Pittsburgh, Pittsburgh, PA, USA

[g] Department of Pediatrics, Johns Hopkins School of Medicine, Baltimore, MD, USA

[h] Division of Pulmonary, Allergy and Critical Care Medicine, University of Pittsburgh School of Medicine, Pittsburgh, PA, USA

[i] Department of Molecular Genetics and Microbiology, University of Florida College of Medicine, Gainesville, FL, USA

[j] Stanley Division of Neurovirology, Department of Pediatrics, Johns Hopkins University School of Medicine, Baltimore, MD, USA

McClain, L., Zhi, Y., Cheng, H., Ghosh, A., Piazza, P., Yee, M. B., Kumar, S., Milosevic, J., Bloom, D. C., Arav-Boger, R., Kinchington, P. R., Yolken, R., Nimgaonkar, V., & D'Aiuto, L. (2015). Broad-spectrum non-nucleoside inhibitors of human herpesviruses. *Antiviral research*, 16–23. doi: 10.1016/j.antiviral.2015.06.005.

4.1.1 Abstract

Herpesvirus infections cause considerable morbidity and mortality through lifelong recurrent cycles of lytic and latent infection in several tissues, including the human nervous system. Acyclovir (ACV) and its prodrug, the current antivirals of choice for herpes simplex virus (HSV) and, to some extent, varicella zoster virus (VZV) infections are nucleoside analogues that inhibit viral DNA replication. Rising viral resistance and the need for more effective second-line drugs have motivated searches for additional antiviral agents, particularly non-nucleoside based agents. We evaluated the antiviral activity of five compounds with predicted lysosomotropic activity using conventional and human induced pluripotent stem cell-derived neuronal (iPSC-neurons) cultures. Their potency and toxicity were compared with ACV and the lysosomotropic agents chloroquine and bafilomycin A1. Out of five compounds tested, micromolar concentrations of 30N12, 16F19, and 4F17 showed antiviral activity comparable to ACV (50 μM) during lytic herpes simplex virus type 1 (HSV-1) infections, reduced viral DNA copy number, and reduced selected HSV-1 protein levels. These compounds also inhibited the reactivation of 'quiescent' HSV-1 infection established in iPSC-neurons, but did not inhibit viral entry into host cells. The same compounds had greater potency than ACV against lytic VZV infection; they also inhibited replication of human cytomegalovirus. The anti-herpetic effects of these nonnucleoside agents merit further evaluation in vivo.

4.1.2 Introduction

Herpesvirus infections affect the vast majority of adults world-wide, with rates exceeding 95% for human cytomegalovirus (HCMV) and varicella zoster virus (VZV), and up to 60% for

herpes simplex virus type I (HSV-1; Xu et al., 2006; Cannon et al., 2010). These viruses can infect an array of human tissues including the peripheral and/or central nervous system (CNS), causing severe CNS disease (Schmutzhard, 2001; Steiner et al., 2007). Currently, the list of FDA approved antiviral drugs is limited, particularly for HCMV or VZV (Strasfeld & Chou, 2010), moreover, the available drugs can produce serious adverse effects. Acyclovir (ACV) or its prodrug valacyclovir (VACV) are the most widely used agents for HSV-1 and VZV. Both drugs are processed to nucleoside analogues that are selectively activated in virus-infected cells and then block viral DNA replication. Resistance to ACV can develop from mutations in the viral thymidine kinase and/or DNA polymerase (Burrel et al., 2013), with incidence rates of 0.3–7.1% (Malvy et al., 2005; Stránská et al., 2005). Though some new antiherpetic drugs target the viral helicase and primase, viral resistance to these agents has also been reported (Kleymann et al., 2002; Sukla et al., 2010). In addition, nephrotoxicity can occur following prolonged ACV treatment (Izzedine et al., 2005). Moreover, ACV is not clinically effective against HCMV. There is thus a compelling need to search for additional drugs to treat herpesvirus infections.

Here, we report on novel anti-herpetic compounds that are based on non-nucleoside agents initially proposed to have lysosomotropic activities. Our studies were motivated by earlier reports indicating the efficacy of lysosomotropic drugs like chloroquine (CQ) and bafilomycin A1 (BFLA) in inhibiting HSV-1 infections (Harley et al., 2001). Lysosomotropic agents increase intracellular pH and presumably inhibit viral packaging and maturation through the trans-Golgi network, although their precise mechanisms of action against herpesviruses remain unclear (Nieland et al., 2004). In the present study, the *in vitro* efficacy of selected agents for HSV-1, VZV, and CMV infections was tested. We focused particularly on HSV-1, including analyses of lytic infection, as well as a model of ‘quiescent’ infection in human iPSC-derived neuronal cells

that mimics several aspects of HSV-1 latent infections (D'Aiuto et al., 2014). We report on three promising agents that appear to have a broader spectrum of activity compared with ACV.

4.1.3 Materials and Methods

4.1.3.1 Drugs

Compounds 30N12, 16F19, 4F17 (95% purity), 16D20, and 17G7 (90% purity) were purchased from ChemBridge. CQ (≥98% purity), phosphonoacetic acid (PAA; ≥98% purity), and BFLA (≥90% purity) were purchased from Sigma. ACV (≥98% purity) was purchased from Spectrum Chemical Mfg Corp. The chemical structure of the compounds is depicted in FIGURE 27.

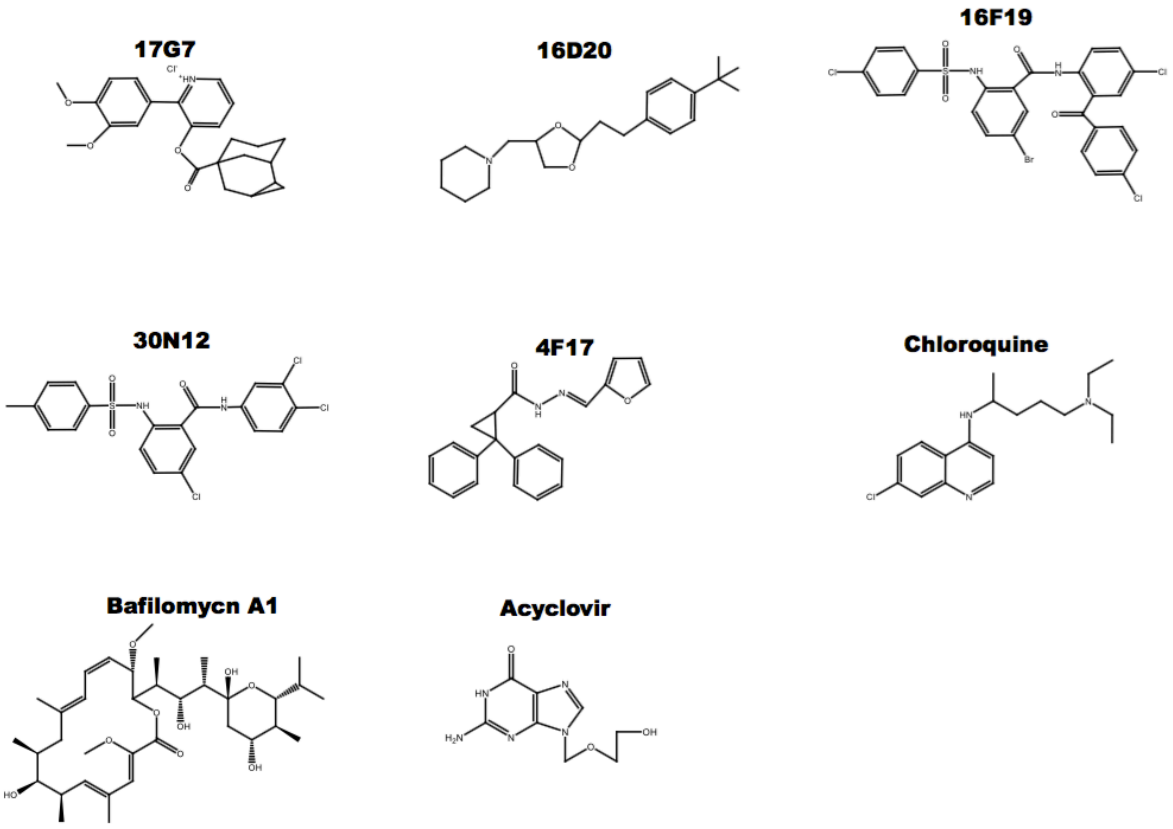

Figure 27. Structure of compounds tested against herpesviruses.

4.1.3.2 Cell lines and viral constructs

Vero cells were maintained in Eagle's minimum essential medium (EMEM) supplemented with 10% fetal bovine serum (FBS; HyClone) and 5% antibiotic/antimycotic (HyClone). VZV permissive human retinal pigmented epithelial cells (ARPE-19) were maintained in Dulbecco's modified Eagle medium/F12 (DMEM/12) supplemented with 10% FBS (HyClone) and 5% antibiotic/antimycotic (HyClone). Human foreskin fibroblasts (HFF; ATCC, CRL-2088) were maintained in Dulbecco's modified Eagle medium (DMEM) containing 10% FBS (HyClone). Human iPSC lines 73-56010-02 and HFF1-S were differentiated into

functional neurons (iPSC-neurons) as described (D'Aiuto et al., 2012). All cells were grown at 37°C, 5% CO_2, and 100% humidity.

The HSV-1 strain was based on the KOS virus (VR-1493; ATCC). This recombinant virus expresses the enhanced green fluorescent protein (EGFP) from the ICP0 promoter, and the monomeric red fluorescent protein (RFP) from the glycoprotein C promoter (Ramachandran et al., 2008). The VZV construct, derived from an infectious Bacterial Artificial Chromosome of the whole VZV genome of the Parent of Oka strain, was engineered to express the luciferase reporter as a fusion to the VZV ORF9 protein, as described recently (Bayer et al., 2015). The human cytomegalovirus (HCMV) recombinant virus, derived from the Towne strain, was engineered to express the luciferase under the control of the viral pp28 gene promoter (He et al., 2011).

4.1.3.3 Viral infections

To test the effects of the compounds during acute HSV-1 infection, cell-free virus was adsorbed onto cells for 2 hours (h) at a multiplicity of infection (MOI) of 1.0 for Vero cells and 0.3 for iPSC-neurons. The inocula were removed, cells were washed with PBS, and medium was exchanged. Compounds 30N12, 16F19, 4F17, 16D20, and 17G7 (Nieland et al., 2004) were added 2 h post infection (hpi) at the concentrations indicated. Parallel cultures were pretreated for 24 h with CQ (50 μM) or BFLA (0.1 μM; (Joubert et al., 2009). As positive controls, cultures were pretreated with ACV (50 μM; (D'Aiuto et al., 2014) for 24 h or pretreated with PAA, a HSV-1 DNA polymerase inhibitor (300 μg/ml; (Blaho et al., 1993) for 1 h prior to the infection.

We tested effects on HSV-1 attachment to the host cell membrane and host cell entry using a published protocol (Krepstakies et al., 2012); FIGURE 58).

To test the effect of the compounds on the HSV-1 reactivation, quiescence was established using (E)-5-(2-bromovinyl)-20-deoxyuridine + interferon alpha (5BVdU+IFN-α ; 30 μM, 125 U/ml, respectively) for 7 days as reported (D'Aiuto et al., 2014). After this period, the quiescence-inducers were withdrawn, and iPSC-neurons were cultured for 48 h in the presence or absence of the test compounds. HSV-1 infection was then reactivated by treatment with sodium butyrate (NaB; 5 mM) for 5 days (D'Aiuto et al., 2014). The number of cells expressing EGFP and RFP was determined by flow cytometry (FC) on Fortessa FACS analyzer (Becton Dickinson).

Inhibition of VZV was assessed on ARPE-19 cells, inoculated with 1000 PFU/well of a cell-associated high titer VZV stock for 2 h at 37 °C, in which >70% of cells were infected and infectious. Small molecules were added in the same manner as just detailed, and luciferase activities were assayed 48 hpi.

Inhibition of HCMV was evaluated by cell-free virus infection adsorbed on HFF cells for 90 min at MOI of 1.0, at which point, small molecule inhibitors were added in a manner as just detailed. Ganciclovir (5 μM) was used as control in all experiments. Luciferase activities were assayed 72 hpi.

4.1.3.4 qPCR assays for viral DNA

The EGFP sequence from the genetically engineered HSV-1 was utilized as the target for copy number analysis. Copy number qPCR was performed as previously reported (Kaufman et al., 2005), employing an EGFP plasmid standard curve, using 5 ng total DNA with biological and technical triplicates, along with corresponding non-template controls. The probe master mix had final concentrations of 18 μM EGFP forward primer (5'-`ccacatgaagcagcacgactt`-3'), 18 μM EGFP reverse primer (5'-`ggtgcgctcctggacgta`-3'), and 5 μM

probe (5'-6FAM-ttcaagtccgccatgcccgaa-TAMRA-3'). The reaction conditions were 95°C for 3 min followed by 45 cycles of 95°C for 15s and 55°C for 30s, and finished with 72°C for 30s. All qPCRs were conducted on a 7900HT Fast Real-Time PCR System (Applied Biosystems) and analyzed with manufacturer's software SDS 2.4.

4.1.3.5 Cytotoxicity assay

The viability of iPSC-neurons following exposure for 24 h at different concentrations of compounds 30N12, 16F19, and 4F17 was assayed by FC using the LIVE/DEAD® Fixable Aqua Dead Cell Stain Kit (Life Technologies). The cytotoxicity analysis was also performed in ARPE-19 cells as described for the iPSC-neurons, but the cells were incubated with the drugs for 48 h instead of 24 h. The drug-induced cytotoxicity in HFF cells used for HCMV infection was estimated using CellTiter-Glo Assay Kit following incubation with the drugs for 72 h.

4.1.3.6 Statistical analyses

Statistical analyses were conducted using the open source software R statistical package version 3.0.1, IBM SPSS v21, GraphPad Prism v5.02, and SigmaPlot. The drug concentration that reduced the number of fluorescent cells in cultures infected with HSV-1 or VZV by 50% (IC50) was estimated using the drc package in R (http://cran.r-project.org/web/packages/drc/drc.pdf; version 2.3– 96); briefly, model fit was first assessed by comparison to an ANOVA model using an F-test. Then, a Box-Cox transformation to fit a 4 parameter, log logistic model provided the best fit to the data (results not shown). The IC50 for HCMV was calculated from the dose response curve constructed by using SigmaPlot software. Statistical significance was calculated by first testing for equality of variance using Levine's test, where two-tailed Student's t-tests (where variances were not significantly different at $a < 0.05$)

or Welch's t-tests (where variances were significantly different at $a < 0.05$) were conducted. Data used represent three independent experiments.

4.1.4 Results

4.1.4.1 Antiviral activity of new drugs on HSV-1 infection

Vero cells

Vero (green monkey kidney epithelial) cells were infected with HSV-1 at MOI of 1 for 24 h in the presence or absence of the test compounds, as well as CQ, BFLA, and ACV (FIGURE 28a). FC analysis indicated that at 50 μM, compounds 30N12 and 16F19 displayed a 90- and 73-fold reduction of EGFP+ cells, respectively, compared with a 22-fold reduction at the same concentration of ACV. Compound 4F17 (50 μM) produced a more modest 2.7-fold decrease, while 16D20 and 17G7 did not reduce HSV-1 infection substantially. The presence of infectious particles in supernatant of treated infected cultures was analyzed by a conventional plaque assay using Vero cells. Consistent with the FC analysis, infectious particles were undetectable in the supernatants of the cultures incubated with 30N12, 16F19, 4F17, CQ, BFLA, or ACV (FIGURE 28b), while infectious particles were detected in the supernatants from cultures treated with compounds 16D20 and 17G7. Thus, at 50 μM concentrations, 30N12 and 16F19 showed greater potency than ACV.

For both viral attachment and entry, no statistically significant reduction in viral DNA copy number was observed in cells treated with the test compounds compared to the untreated HSV-1 group (FIGURE 58).

iPSC-neurons

In view of the toxic effects of HSV-1 on neuronal cells, we employed iPSC-derived neurons (iPSC-neurons) to test the antiviral effect of the aforementioned compounds. iPSC-neurons were infected with the HSV-1 construct at MOI of 0.3 and assayed at 24 hpi. FC analysis indicated that compounds 30N12 and 16F19 reduced fluorescent cells approximately 20-fold (approximately 1% of EGFP+ cells in drug-treated cultures, versus over 20% in the control, drug-free cultures), similar to the inhibition caused by ACV, CQ or BFLA (FIGURE 28c; all drugs at 50 μM except BFLA, which was 0.1 μM). Compound 4F17 resulted in a 6.3-fold reduction of EGFP+ cells (3.3%; FIGURE 28c). Compound 17G7 resulted in a modest 2-fold reduction of EGFP+ cells (9.9%; FIGURE 28c). Unlike CQ or BFLA, however, supernatants from cell cultures treated with 4F17, 30N12, or 16F19 produced no detectable infectious virus (FIGURE 28d). The patterns of effects produced by 4F17, 30N12, or 16F19 were moderately correlated in Vero cells and iPSC-neurons, motivating further analyses of these drugs in iPSC-neurons ($r=0.72$, 95% CI = 0.031–0.945, $p = 0.044$; FIGURE 55).

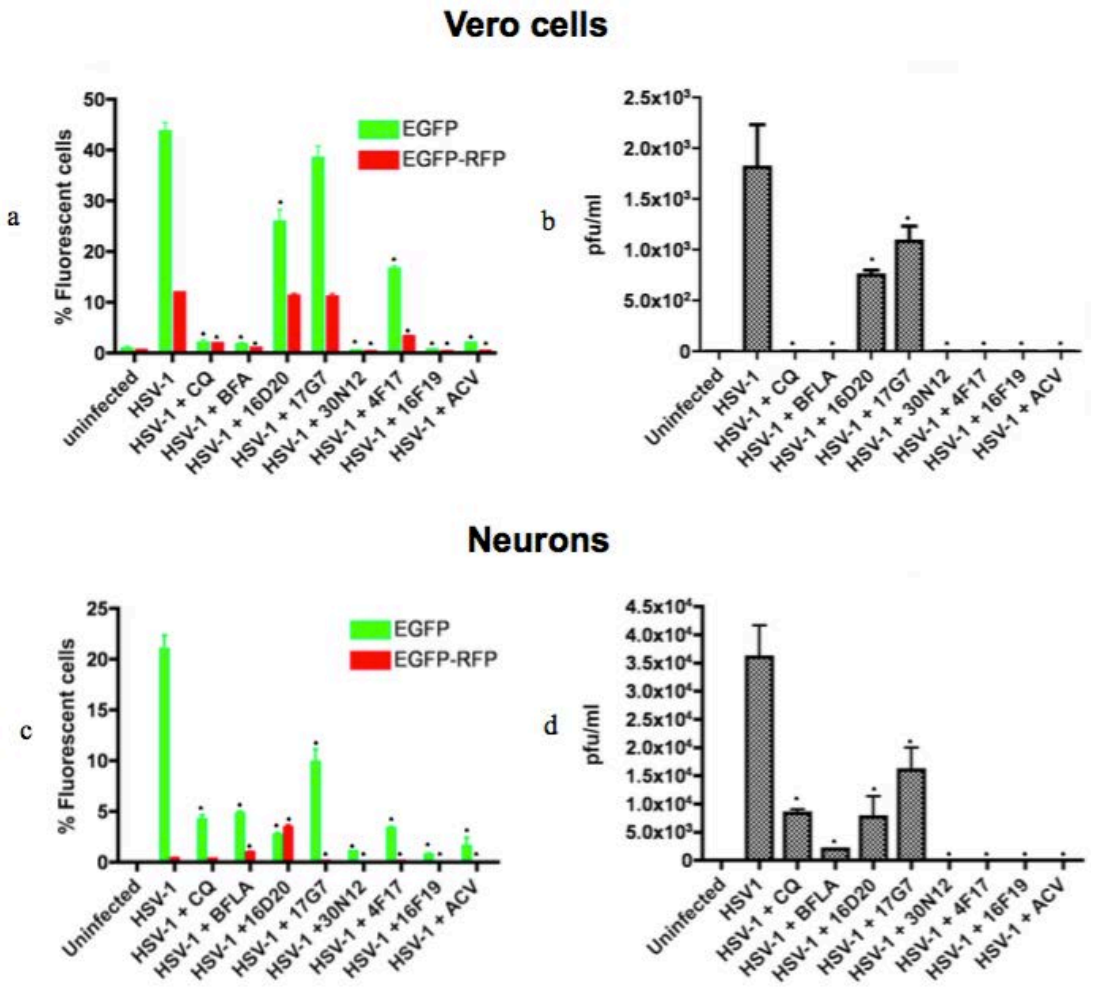

Figure 28. Comparison of inhibitory effects of test compounds on lytic HSV-1 infection.

(a) Flow cytometry (FC) analysis of uninfected and HSV-1 infected Vero cells in the presence or absence of test compounds using HSV-1 expressing EGFP from an IE gene promoter and RFP from a late gene promoter. The fractions of cells showing fluorescence of the appropriate color are indicated. *p≤0.0019. (b) Plaque assays of virus produced in the supernatant of HSV-1 infected Vero cells titrated on Vero cells, shown as plaque forming units per milliliter (pfu/ml). *p≤0.0017. (c) FC analysis of uninfected and HSV-1 infected iPSC-neurons in the presence or absence of test compounds. *p≤0.026. (d) Plaque assays of virus produced in the supernatant of HSV-1 infected iPSC-neurons titrated on Vero cells, shown as pfu/ml. *p≤0.045. The data represent an average of three independent experiments. CQ: chloroquine (50 μM); BFLA: bafilomycin A1 (0.1 μM); ACV: acyclovir (50 μM). Test compounds were used at a concentration of 50 μM. pfu: plaque forming units. Error bars represent standard deviations.

IC50 estimation

The IC50 concentration of 30N12, 16F19, and 4F17 in iPSC-neurons was 9.27, 0.42 and 41.35 μM, respectively (FIGURE 29a). The IC50 of ACV in iPSC-neurons is 0.27 μM (FIGURE 56).

4.1.4.2 Cellular toxicity

At concentrations up to 50 μM, 30N12, 16F19, or 4F17 caused less than 50% reduction in iPSC-neuron viability, precluding estimation of their therapeutic index (FIGURE 29b). At higher concentrations, compound 30N12 showed mild cytotoxicity at 100 and 500 μM (viable cells: 74.5% ± 4.95% and 67.1% ± 0.808%, respectively). Compound 16F19 produced relatively mild cytotoxicity at 100 μM (viable cells: 75.7% ± 2.05%), but substantially higher effects at 500 μM (viable cells: 38.6% ± 0.723%). Compound 4F17 did not show significant cytotoxicity at either 100 μM or 500 μM (viable cells: 97.1% ± 1.43% and 95.4% ± 0.289%, respectively; FIGURE 57).

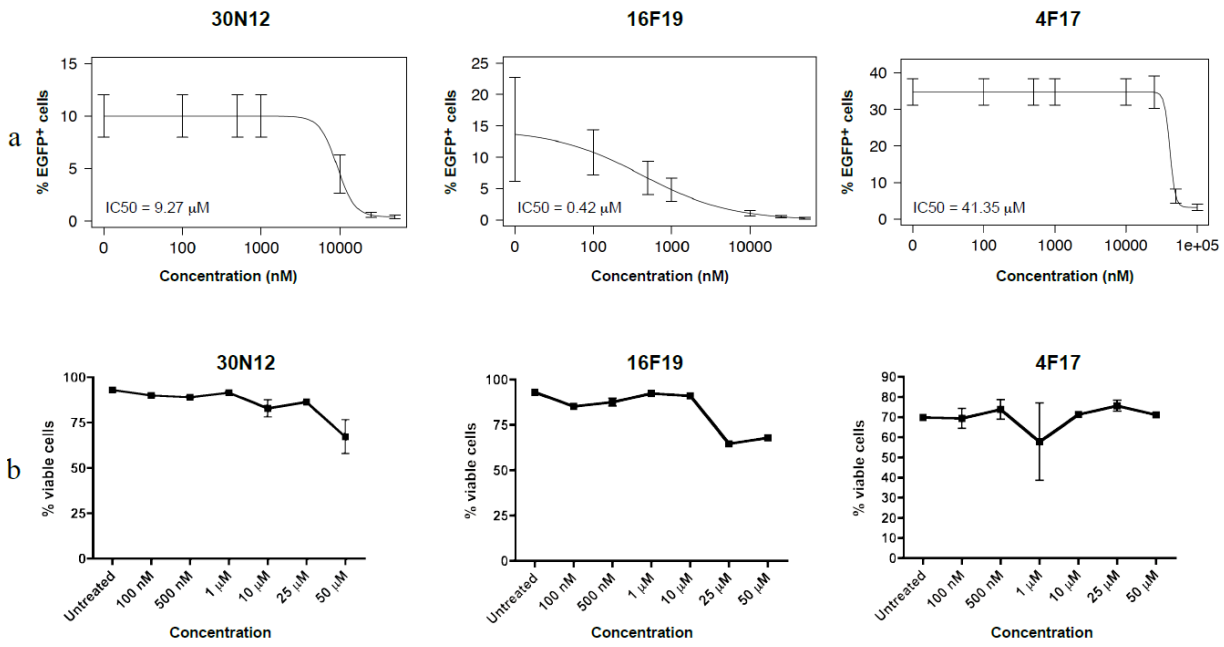

Figure 29. Antiviral efficacy and cytotoxicity of 30N12, 16F19, and 4F17 against HSV-1.

(a) Efficacy of varying drugs concentrations against HSV-1 lytic infection; FC performed 24 hpi. (b) Neurotoxicity of 30N12, 16F19, and 4F17 without HSV-1 infection was assessed by FC using fixable viability dye. The data represent an average of three independent experiments. Error bars represent (a) model-based standard error and (b) standard deviations.

4.1.4.3 Effects on HSV-1 DNA copy number in iPSC-neurons

Next, we analyzed HSV-1 copy number using quantitative PCR (qPCR) to investigate whether these compounds alter HSV-1 DNA replication. HSV-1 DNA copy number was estimated in acutely infected iPSC-neurons 24 hpi, using the EGFP sequence in the HSV-1 viral construct as a probe. In 5 ng of total DNA, the number of copies of viral DNA were as follows: HSV-1 infected, untreated iPSC-neurons (3,461,970), 30N12 (1,664), 16F19 (48,530), 4F17 (561,665), PAA (924), and ACV (483; FIGURE 30). Fluorescence in situ hybridization (FISH) analyses were consistent with the qPCR results: similar to ACV or PAA, a substantial reduction in viral DNA copy number was observed in infected cells treated with 30N12, or 16F19, and to a

lesser extent with 4F17, (FIGURE 53). Further, markedly reduced expression of the HSV-1 immediate early genes ICP0 and ICP4 was observed in separate immunocytochemistry experiments when infected cells were treated with ACV, PAA, 30N12, 16F19 or 4F17 (FIGURE 54).

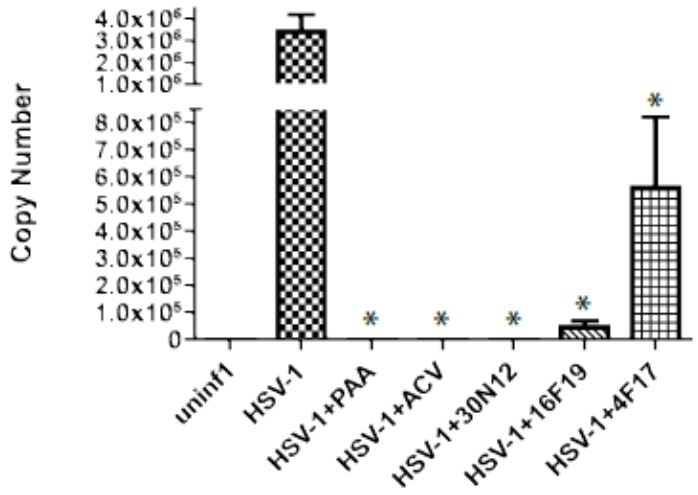

Figure 30. qPCR assays for HSV-1 genome copy number in iPSC-neurons.

Cells were infected with HSV-1 for 24 h in the presence or absence of test compounds (all at 50 μM). HSV-1 copy number calculated in 5 ng total DNA. ACV: acyclovir, PAA: phosphonoacetic acid. *p≤0.015. Error bars represent standard deviations.

4.1.4.4 Effects on reactivation of HSV-1 quiescent infection

Based on protocols for rodent models of HSV-1 latent infection, we have proposed a model of quiescent HSV-1 infection in iPSC-neurons (D'Aiuto et al., 2014). Treatment with 5BVdU + IFN-α causes a sustained reduction in the percentage of EGFP+ cells and EFGP+/RFP+ cells in HSV-1 infected iPSC-neurons; furthermore, HSV-1 can be reactivated

subsequently by incubation with sodium butyrate (NaB, 5 mM), a histone deacetylase inhibitor for 5 days (D'Aiuto et al., 2014). The pattern of infection, denoted ‘‘quiescent infection,’’ mimics several features of rodent latent infection models. In the present experiments, quiescent infection was induced with 5BVdU + IFN-α, the drugs were withdrawn, and cells were incubated for 48 h in the presence of the vehicle (DMSO) or test compounds. Subsequently, the infection was reactivated with NaB (5 days). FC analysis showed a 16-fold increase of EGFP+ cells and 850-fold increase of EGFP+/RFP+ cells in vehicle treated cells (FIGURE 31a). Following incubation with 30N12, 16F19, 4F17, or ACV for 48 h, a more modest reactivation was indicated by lower levels of EGFP+ cells (8-, 6-, 6-, and 2-fold, respectively) or EGFP+/RFP+ cells (201-, 97-, 26-, and 17-fold, respectively; FIGURE 31a). Compared to vehicle, treatment with ACV or test compounds also lowered the mean intensity of fluorescence (MFI; FIGURE 31b).

Consistent with these results, the supernatant culture medium from neuronal cultures treated with 5BVdU + IFN-α, followed by ACV or 4F17 had no detectable infectious viral particles, while treatment with 30N12 and 16F19 resulted in a 7.3- and 4-fold decrease in infectious virion production as compared to treatment with vehicle for 48 h (FIGURE 31c). Taken together, these results indicate that treatment with ACV or test compounds reduce HSV-1 reactivation.

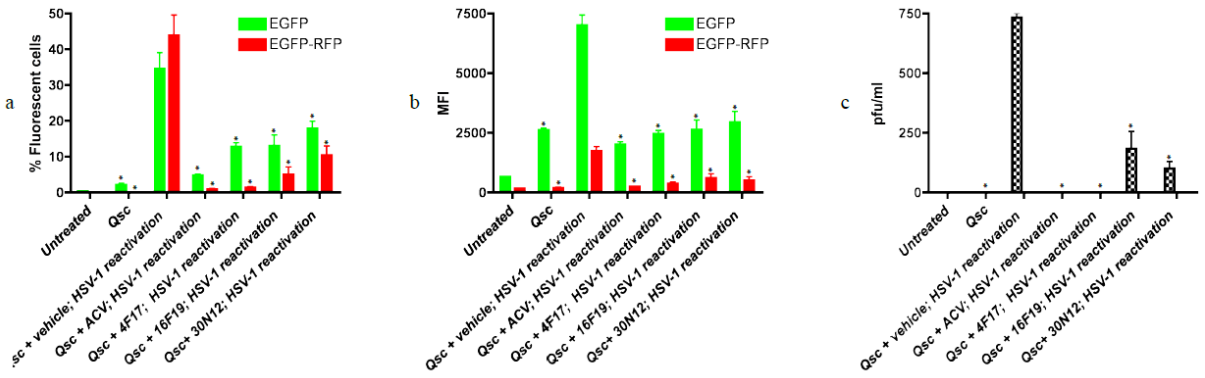

Figure 31. Effects of test compounds on reactivation of quiescent HSV-1 infection in iPSC-neurons.

FC was performed after reactivation of quiescently infected iPSC-neuronal cultures as described. (a) Percentage of fluorescent cells. *p≤0.027. (b) Mean fluorescence intensity (MFI). *p≤0.016. (c) Plaque assays of virus produced in the supernatant of reactivated cells titrated on Vero cells, shown as plaque forming units per milliliter (pfu/ml). *p≤0.002. The data represent an average of three independent experiments. 5BVdU: (E)-5-(2-bromovinyl)-20-deoxyuridine, IFN-α: interferon alpha, NaB: sodium butyrate, vehicle: DMSO. Error bars represent standard deviations. ‘‘Qsc’’: Quiescent HSV-1 infection established by infecting iPSC-neurons with HSV-1 and then culturing in neurobasal medium containing 5BVdU + IFN-α for 7 days (See methods). ‘‘Qsc + vehicle or compounds (ACV, 4F17, 16F19, or 30N12); HSV-1 reactivation’’: 5BVdU + IFN-α were withdrawn and cells were cultured in the presence of vehicle or compounds for 48 h; HSV-1 was then reactivated by treatment with NaB for 5 days.

4.1.4.5 Effects on VZV and HCMV infection

In the VZV permissive ARP19 line, infection with the VZV construct was monitored using luciferase activity. PAA effectively inhibited VZV infection, while ACV treatment caused a more modest 1.8-fold reduction at 50 µM. Incubation with 30N12, 16F19, and 4F17 resulted in 60.3-, 548.2-, and 2.7-fold reduction in luciferase activity, respectively, at 50 µM (FIGURE 32a). At these concentrations, none of the drugs were cytotoxic for ARPE-19 cells (FIGURE 32b). The IC50 values for 30N12 and 16F19 were estimated to be 11.52 and 2.43 µM (FIGURE 32c). At the highest concentration tested, 4F17 and ACV produced less than 50% inhibition.

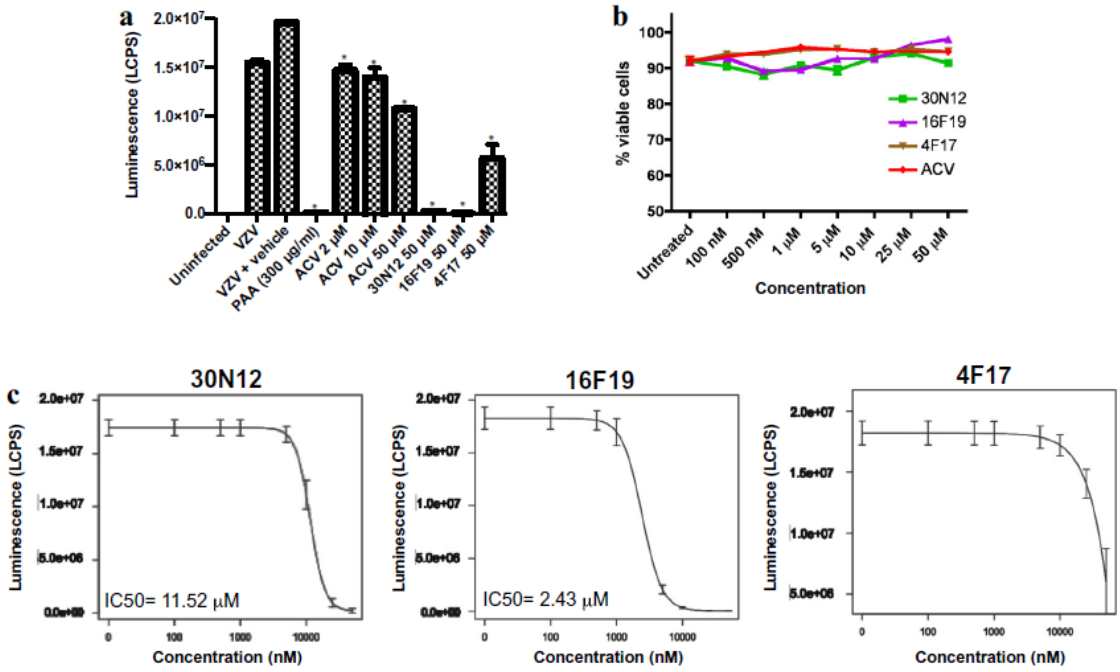

Figure 32. Analysis of VZV infection.

(a) ARPE-19 cell lysates were assayed for luciferase activity following infection with VZV-ORF63fluc in the presence or absence of drugs for 48 hpi. LCPS: luciferase counts per second. *p≤0.013. (b) Cytotoxicity of the compounds in the absence of VZV in ARPE-19 cells. (c) Efficacy of 30N12, 16F19, and 4F17 at different concentrations; with the luciferase assay performed at 48 hpi. The data represent an average of three independent experiments. Error bars represent standard deviations.

In permissive HFF cells infected with HCMV (MOI of 1), the IC50 and the concentration that reduced the HFF cell viability by 50% (CC50) for 4F17 were estimated at 8.85 and 123.68 µM, respectively (selectivity index: 13.98; FIGURE 33). IC50 and CC50 were estimated for compounds 30N12 (10.4, 37.8 µM; selectivity index: 3.63) and 16F19 (4.1 µM, 12.3 µM; selectivity index: 3). However, both compounds exhibited a low selectivity index.

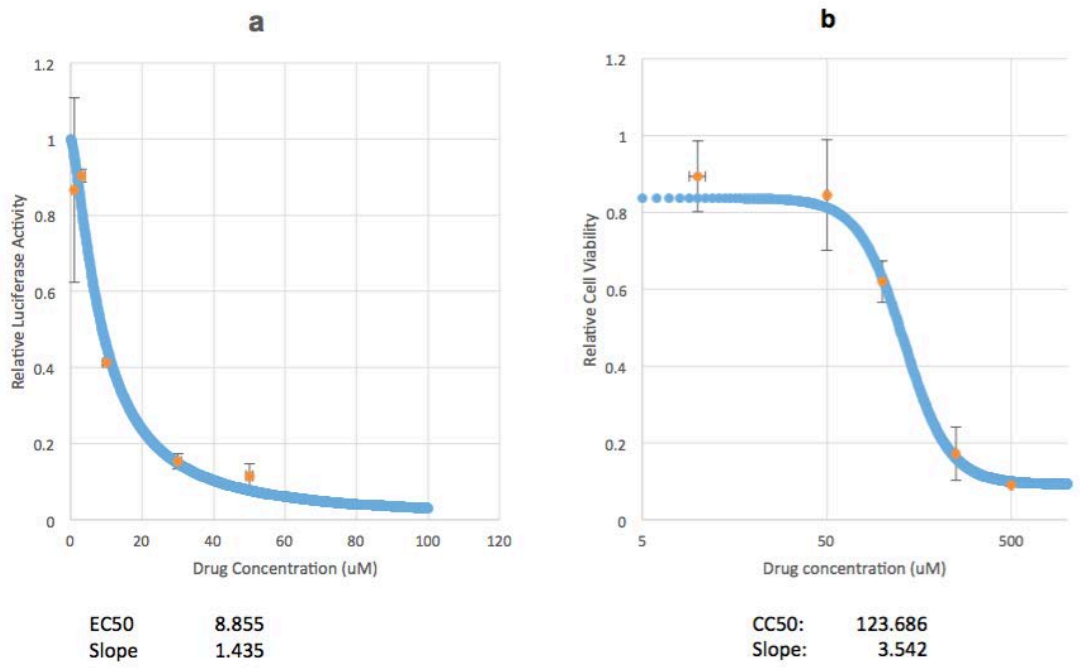

Figure 33. Anti-HCMV activity of 4F17.

(a) Dose response of HCMV inhibition based on luciferase expression. (b) Cellular toxicity in non-infected HFF cells as determined by Cell- titer GLo assay. The data represent an average of three independent experiments. Error bars represent standard deviations.

4.1.5 Discussion

We assessed the potency and cytotoxicity of five novel non-nucleoside drugs for inhibiting infections with HSV-1, VZV, and CMV. Of these, compounds 30N12, 16F19, and 4F17 inhibited lytic HSV-1 with potencies similar to ACV, CQ, and BFLA. Like ACV, these compounds also inhibited viral reactivation in iPSC-neurons with prior quiescent HSV-1 infection. Furthermore, they were efficacious against VZV and compound 4F17 was also effective *in vitro* for HCMV infection. To our knowledge, these antiviral effects have not been reported before.

The mechanism of action of these drugs is unknown. The present investigations were motivated by the reported efficacy of lysosomotropic agents like CQ and BFLA against lytic HSV-1 infection (Harley et al., 2001). It was hypothesized that the antiviral activity of CQ and BFLA is due to increase in the pH of the trans-Golgi network (TGN) and endosomes–organelles that are critical for HSV-1 egress (Johnson & Baines, 2011). As the test compounds were previously reported to interfere with Golgi-to-cell surface traffic (Nieland et al., 2004), we predicted that they would inhibit productive HSV-1 infection. Productive infection was indeed reduced by 30N12, 16F19, and 4F17. In addition, these agents also reduced the proportion of IE-expressed EGFP+ cells, with concomitant reduction in MFI. Further, FISH analyses also indicated a substantial reduction in viral DNA load (FIGURE 53). Several recent reports have strongly implied that, at least for HSV-1, viral entry may utilize the endosomes in some cell types (Döhner et al., 2002; Nicola, et al., 2005; Harkness, et al., 2014). It is unlikely these lysosomotropic compounds may affect HSV-1 entry in Vero cells and neurons, as all the drugs were added to cell cultures 2 h after HSV-1 infection, when most of the nucleocapsids are expected to be transported to the nuclear membrane; further, viral entry was previously reported to be pH-independent in neurons (Nicola et al., 2005). These compounds do not appear to affect viral attachment and entry (FIGURE 58). Taken together, these results indicate that 30N12, 16F19, and 4F17 exert their antiviral effects by influencing one or more stages of the early phase of the HSV-1 lytic cycle and late stages of infection. Although our data clearly indicate that 30N12, 16F19, and 4F17 efficiently block events at or before DNA replication, the exact stage of the block remains to be determined. While our analyses suggest that these compounds reduce IE gene expression consistent with earlier reports, the repression may be a secondary effect of multiple rounds of replication (Park et al., 2013; Pierce et al., 2005; Zambrano et al., 2008).

The patterns of the effects on HSV-1 infection may differ between the compounds. For example, the IC50 for 1619 is 10- to 100-fold lower than the other compounds, the slope of the dose response curve is more gradual, and the values are more variable. This suggests a different mechanism of action compared with 30N12 and 4F17. Indeed, 16F19 may have multiple targets in Vero cells, although it is not possible to identify them at present.

The spectrum of antiviral activity of these compounds is also noteworthy. 30N12, 16F19, and 4F17 inhibited lytic VZV infection with greater potency than ACV (FIGURE 32a). These compounds also effectively inhibited HCMV infection; however, 30N12 and 16F19 showed a low selectivity index. It is not known whether the mechanisms of action against VZV and HCMV are similar to their effects against HSV-1 infection. It is likely to be different at least for 16F19, as the IC50 curve for this compound is typical, in contrast to a more complex effect against HSV-1 (FIGURE 32).

In summary, we identified three non-nucleoside compounds with potent antiviral effect comparable to that of ACV against HSV-1. Consistent with prior reports of relatively low efficacy of ACV against VZV vis a vis HSV-1 infection (Iwayama et al., 1998), the test compounds showed a higher potency than ACV against VZV, at concentrations that produced relatively low cellular toxicity. In addition, HCMV infection was inhibited effectively. The selective activities for individual herpesviruses suggest the agents have different mechanisms of activity, or influence cellular processes that are more important for one herpesvirus over another. Further studies are needed to investigate the underlying mechanism/s accounting for the antiviral activity of these compounds.

4.1.6 Acknowledgments

The authors acknowledge the following colleagues for the critical reading of the manuscript and technical support: Joel Wood, Chowdari Kodavali, Peter Dimitrion, Benjamin Treat, and Rebecca Lipski. This study was funded by the Stanley Medical Research Institute (SMRI) grant ID 07R-1712 and NIH MH63480 to VLN and NIH 5R01AI093701 to RAB. PRK acknowledges support from EY08098, Research to Prevent Blindness Inc. and the Eye & Ear Foundation of Pittsburgh. The funding source had no involvement in the collection, analysis, and interpretation of the data; the conduct of this research; nor the preparation of the article.

4.2 IPSC NEURONAL ASSAY IDENTIFIES AMARYLLIDACEAE PHARMACOPHORE WITH MULTIPLE EFFECTS AGAINST HERPESVIRUS INFECTIONS

James McNulty[*,†,#], Leonardo D'Aiuto[‡,#], Yun Zhi[‡,#,△], Lora McClain[‡,‖], Carlos Zepeda-Velaźquez[†], Spencer Ler[†], Hilary A. Jenkins[†], Michael B. Yee[§], Paolo Piazza[‖], Robert H. Yolken[⊥], Paul R. Kinchington[§], and Vishwajit L. Nimgaonkar[*,‡,‖]

† Department of Chemistry and Chemical-Biology, McMaster University, 1280 Main Street, West Hamilton, Ontario L8S 4M1, Canada

‡ Department of Psychiatry, University of Pittsburgh, School of Medicine, 3811 O'Hara Street, Pittsburgh, Pennsylvania 15213, United States

§ Department of Ophthalmology, University of Pittsburgh School of Medicine, 203 Lothrop Street, Pittsburgh Pennsylvania 15213, United States

‖ Department of Human Genetics, University of Pittsburgh, Graduate School of Public Health, 130 De Soto Street, Pittsburgh, Pennsylvania 15213, United States

⊥ Department of Pediatrics, Johns Hopkins University School of Medicine, 600 North Wolfe Street, Baltimore, Maryland 21287, United States

McNulty J, D'Aiuto L, Zhi Y, McClain L, Zepeda-Velázquez C, Ler S, Jenkins HA, Yee MB, Piazza P, Yolken RH, Kinchington PR, Nimgaonkar VL. iPSC neuronal assay identified Amaryllidaceae Pharmacophore with multiple effects against Herpesvirus infections. ACS Med Chem Lett. 2015 Nov 19;7(1):46-50. doi: 10.1021/acsmedchemlett.5b00318. eCollection 2016.

NOTE. Dr. James McNulty and his research group designed, performed, and analyzed the chemical synthesis studies, which are not within the scope of this thesis.

4.2.1 Abstract

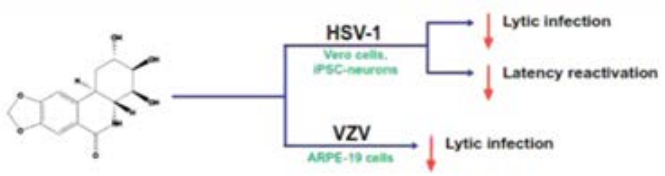

The Amaryllidaceae alkaloid trans-dihydrolycoricidine 7 and three analogues 8−10 were produced via asymmetric chemical synthesis. Alkaloid 7 proved superior to acyclovir, the current standard for herpes simplex virus, type 1 (HSV-1) infection. Compound 7 potently inhibited lytic HSV- 1 infection, significantly reduced HSV-1 reactivation, and more potently inhibited varicella zoster virus (VZV) lytic infection. A configurationally defined (3R)-secondary alcohol at C3 proved crucial for efficacious inhibition of lytic HSV-1 infection.

Herpes simplex virus, type 1 (HSV-1) is a ubiquitous DNA virus from the Herpesviridae family that causes substantial human morbidity and mortality (Kinchington et al., 2012). With seropositivity rates exceeding 70% in elders, it causes recurrent cold sores, corneal infection, blindness, and, rarely, encephalitis (Kinchington et al., 2012). It establishes latent infection in sensory neurons that is refractory to clearance, producing an intractable lifelong reservoir that cycles with lytic infections. Though acute HSV-1 infection is readily treatable with nontoxic nucleoside analogues such as acyclovir (ACV), no drug successfully eliminates the latent infection. In addition, growing ACV drug resistance has further fueled the search for novel antivirals (Burrel et al., 2013).

Plants of the Amaryllidaceae family produce numerous structurally diverse, biologically active alkaloids (Evidente et al., 2009; Jin 2013). In particular, alkaloids of the lycorane subclass including lycorine **1**, pseudolycorine **2**, pancratistatin **3**, its 7-deoxy analogue **4**, and the

unsaturated derivatives narciclasine **5** and deoxy analogue **6** have demonstrated a variety of antiviral activities (FIGURE 34) (Gabrielsen et al., 1992; Hwang et al., 2008; Ieven et al., 1982; Li et al., 2005; McNulty & Zepeda-Velázquez, 2014; Renard-Nozaki et al., 1989; Vrijsen et al., 1986; Zou et al., 2009). The restricted availability of other natural lycorane-type alkaloids and the absence of a rapid synthetic route toward structural analogues has impeded further development of the antiviral pharmacophore.

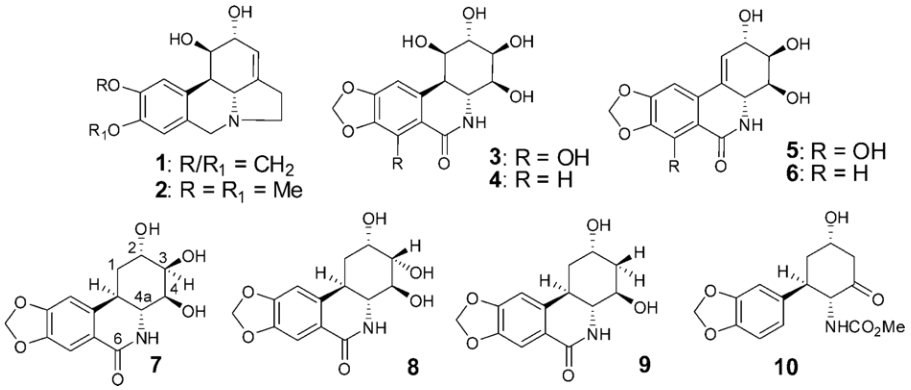

Figure 34. Structure of antiviral Amaryllidaceae alkaloids.

Alkaloids **1**−**7** are natural products. Compounds **7**−**10** were accessed via total synthesis. Lycorine **1**, pseudolycorine **2**, pancratistatin **3**, 7- deoxypancratistatin **4**, narciclasine **5**, 7-deoxynarciclasine **6**, trans-dihydrolycoricidine **7**, 3-epi-trans-dihydrolycoricidine **8**, and 3-deoxy- trans-dihydrolycoricidine **9**.

The development of synthetic strategies that allow rapid access to functionally dense, stereochemically defined cores not only enables the asymmetric synthesis of biologically active natural products, but opens synthetic entry to non-natural analogues. These analogues expand the structural diversity available for biological assessment facilitating the discovery of previously unknown effects, improving our understanding of the structural requirements for such biological activity.

We recently reported the total asymmetric synthesis of trans- dihydrolycoricidine **7** employing a convergent, stepwise organocatalytic [3 + 3]-Michael-aldol annulation of substituted acetone derivative **13a** onto functionalized cinnamaldehyde **12** (McNulty & Zepeda-Velázquez, 2014), catalyzed by diarylprolinol ether **11** (TMS = trimethyl- silyl). This crucial step allows for the asymmetric entry to functionalized, nitrogen-substituted cyclohexanes, in one step, and could be conducted at gram scale. In this case (McNulty & Zepeda-Velázquez, 2014), compound **14a** was converted to alkaloid **7** in a short sequence of subsequent transformations involving epoxidation and 2,3- diaxial diol installation, FIGURE 35).

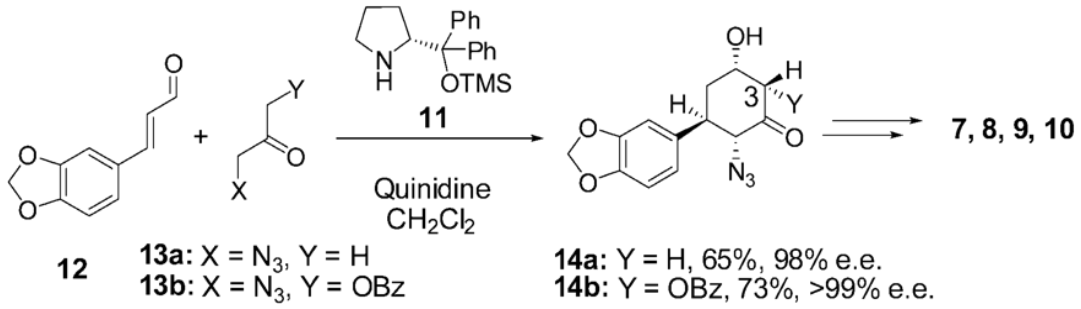

Figure 35. Scheme 1a.

Asymmetric organocatalytic Michael-aldol [3 + 3]-cycloaddition reaction of cinnamaldehyde derivative 12 and azido-acetone derivatives 13a allows a one-step access to stereochemically defined cyclohexanol 14a permitting rapid asymmetric entry to natural alkaloid 7, while reaction of 13b leads to 14b, permitting access to C3-epimeric and deoxy analogues 8, 9, and 10.

In order to extend the [3 + 3]-Michael-aldol methodology to obtain more oxygenated cyclohexane derivatives directly, we have now investigated the reaction of **12** with the nonsymmetrical 1,3-disubstituted benzoyloxy-azidoacetone derivative **13b** (FIGURE 35). To our delight, this reaction was found to proceed in a highly regioselective fashion with the initial

Michael-addition being fully directed by the azido group, allowing a direct entry to cyclohexanol **14b**. The complex cyclohexane product **14b** was obtained directly as a precipitate that formed during the reaction in 73% isolated yield and did not require chromatographic purification. The reaction also proved to be highly diastereoselective (dr = 96%) with the major diastereomer being essentially homochiral (>99% ee). The relative and absolute stereochemistry of this major cycloadduct was determined as α-benzyloxy at C3 as shown in **14b**. This data was confirmed by single crystal X-ray analysis of the 4-bromobenzoate analogue **15** (see FIGURE 36 and Supporting Information in Appendix D).

With rapid access to compounds of the C3-epimeric series now available (in comparison to natural products **3**−**7**), we converted **14b** to compound **8**, the C3-epimer of natural product **7**, as shown in FIGURE 36. Catalytic hydrogenation of the azido group and in situ protection as the methoxycarbonylamino ketone **16** was successfully achieved from **14b** using dimethoxydicarbonate (DMDC). The ketone **16** was subjected to axial hydride reduction and the desired C4-equatorial alcohol protected alongside the C2-axial hydroxyl group to give the orthogonally protected triol **18**. Cyclization of **18** was achieved using the Banwell modification of the Bischler−Napieralski reaction to give **19** with high regioselectivity (no minor diastereomer detected), which was now deprotected to give the target molecule **8**.

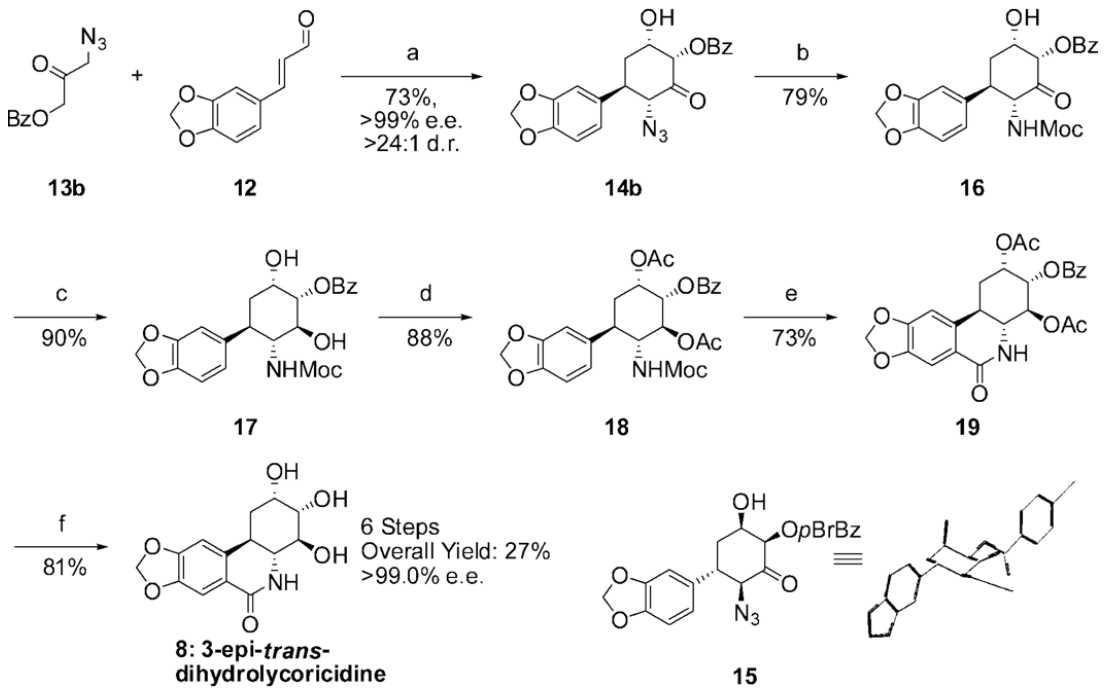

Figure 36. Scheme 2a.

Reagents and conditions: Yields of isolated products (%) are indicated. (a) 13b (1.00 equiv), 12 (1.05 equiv), 11 (10 mol %), quinidine (10 mol %), CH_2Cl_2, −10 °C → RT, 73%. (b) DMDC (3.0 equiv), H_2, 10% Pd/C (0.075 equiv), EtOAc, 50 psi, RT, 79%. (c) $Me_4NHB(OAc)_3$ (4.0 equiv), AcOH (10.0 equiv), MeCN, RT, 90%. (d) AcCl (100 equiv). (e) Tf_2O (5.0 equiv), DMAP (3.0 equiv), CH_2Cl_2, 0 °C → RT, 73%. (f) K_2CO_3 (0.10 equiv), H_2O/MeOH 9:1, RT, 81%. DMDC = dimethyl dicarbonate, Tf = triflic, DMAP = 4- dimethylaminopyridine, Moc = methyloxycarbonyl.

Access to compound **8** was exceedingly efficient given the one-pot asymmetric entry to the azido-cyclitol **14b** and high yields obtained in conversion to **8** as shown in FIGURE 36. The C3-deoxy analogue **9** and the acyclic intermediate **10** were now prepared via a similar [3 + 3]-Michael-aldol annulation of azidoacetone **13** and cinnamaldehyde derivative **12**, as outlined in Supplemental Schemes 1 and 3 in Appendix D.

With synthetic access to the natural alkaloid **7**, C-3-epimer **8**, C-3-deoxy analogue **9**, and acyclic compound **10** now on-hand and, in conjunction with natural products **3** and **5**, we proceeded with their antiviral assessment.

Based on an earlier report showing the anti-HSV-1 activity of alkaloids derived from Amaryllidacea (Renard-Nozaki et al., 1989), we initially evaluated the efficacy of compounds **3**, **5**, **7**, **8**, **9**, and **10** against HSV-1 infection. We employed a genetically engineered HSV-1 construct, incorporating enhanced green fluorescent protein (EGFP) and red fluorescent protein (RFP) as reporter genes, whose expression is driven by the viral promoters ICP0 and glycoprotein C (gC), respectively (Ramachandran et al., 2008). ICP0 is an HSV-1 immediate early (IE) gene, while gC is expressed only after onset of viral DNA replication. Vero cells initially infected with HSV-1 at multiplicity of infection (MOI) 1 were cultured at 2 h postinfection (hpi) in media containing compounds **3**, **5**, **7**, **8**, **9**, or **10** (10 μM) or ACV (50 μM). Flow cytometry analysis (FC) showed that the percentage of EGFP positive ($EGFP^+$) cells in infected cultures exposed to **3**, **5**, and **7** was reduced 8.3-, 10.6-, and 19.6-fold, respectively, compared with un- treated, HSV-1 infected cultures 24 hpi (FIGURE 37a), while ACV caused 4.3-fold reduction of $EGFP^+$ cells. Productive infection, estimated in the culture supernatant by virus yield reduction assay using Vero cells 48 hpi was also suppressed in cell cultures treated with **3**, **5**, and **7** (10 μM), similar to ACV (50 μM) (FIGURE 37b). Conversely, compounds **8**, **9**, and **10** (10 μM) did not inhibit HSV-1 infection (FIGURE 37a); furthermore, these compounds did not suppress productive infection (FIGURE 37b). These results reveal a critical role played by the C3-β-hydroxyl group, found only in natural products **3**, **5**, and **7**, as a requirement for antiviral activity.

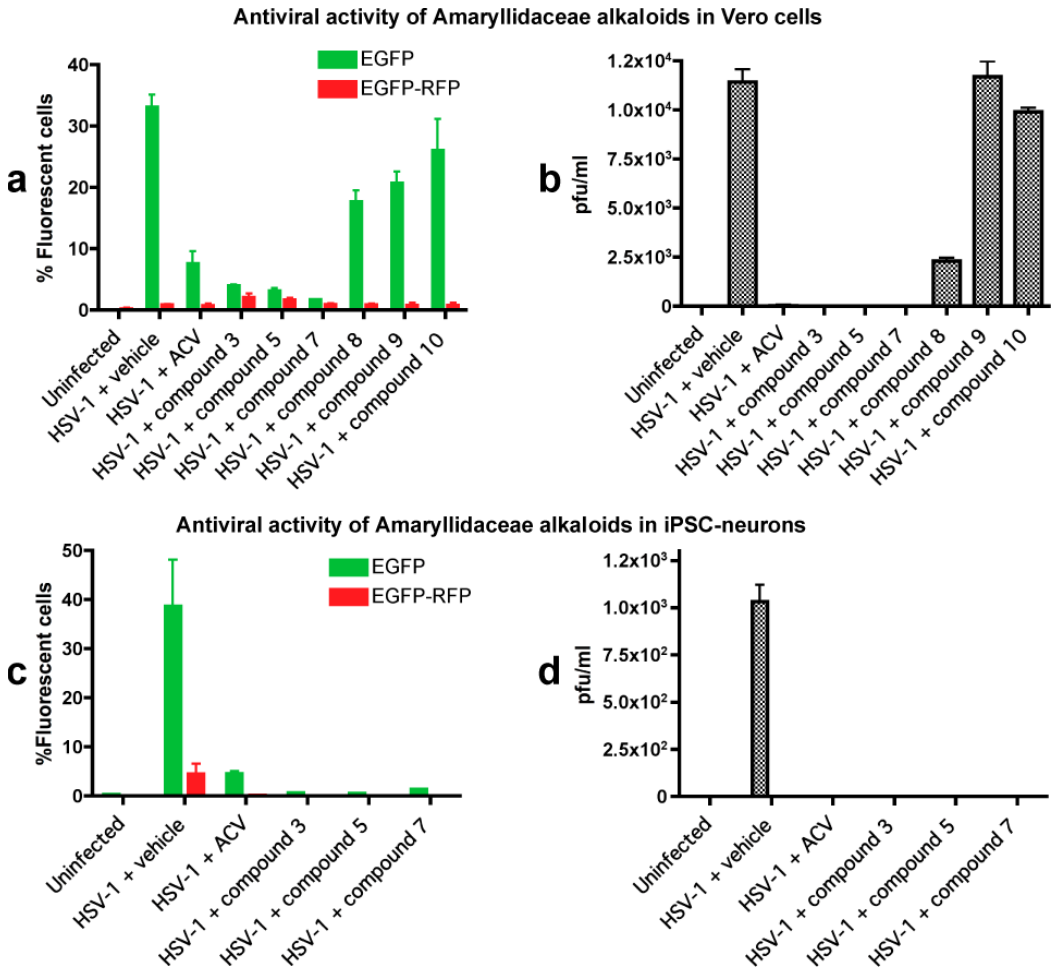

Figure 37. Natural and synthetic Amaryllidaceae alkaloids selectively inhibit HSV-1 infection in Vero cells and iPSC-neurons.

(a) Flow cytometry (FC) analysis of uninfected and HSV-1 infected Vero cells (MOI 1) 24 hpi. (b) Viral titer in Vero cell culture supernatants estimated with virus yield reduction assay using Vero cells 48 hpi. Plaques were not observed in cultures treated with compounds **3**, **5**, and **7**. A very low titer was observed for ACV (33.3 pfu/mL). (c) FC analysis of uninfected and HSV-1 infected iPSC-neurons (MOI 0.3) 24 h postinfection (hpi). (d) Viral titer in iPSC-neuronal culture supernatants estimated with virus yield reduction assay using Vero cells 48 hpi. Plaques were observed only in cultures infected with supernatants deriving from untreated, infected neurons. Dimethyl sulfoxide (DMSO) is the vehicle. The data represent an average of three independent experiments. Error bars represent standard deviations.

As humans are the natural hosts for HSV-1, and human neurons are the only known reservoir of HSV-1 infection, compounds **3**, **5**, and **7** were also tested in neurons derived from

human induced pluripotent stem cell (iPSCs) (D'Aiuto et al., 2012; D'Aiuto et al., 2014). iPSC-neuronal cultures were infected with the genetically engineered HSV-1 construct (MOI 0.3) and subsequently treated with **3**, **5**, **7**, or ACV 2 hpi. FC analysis showed ~62-, 69-, and 28-fold reduction in the percentage of $EGFP^+$ cells in iPSC-neuronal cultures treated with **3**, **5**, and **7** (10 μM) 24 hpi, respectively, while ACV caused more modest inhibition (~8.5-fold at 50 μM; FIGURE 37c). Suppression of productive infection in iPSC- neurons treated with compounds **3**, **5**, and **7** (10 μM) was also noted (FIGURE 37d).

Next, using fluorescent in situ hybridization (FISH) we investigated whether the test compounds affected HSV-1 DNA replication in iPSC-neurons similar to ACV. FISH analysis of HSV-1 infected iPSC-neurons treated with **3**, **5**, **7** (10 μM), or ACV (50 μM) indicated no hybridization with HSV-1 DNA, whereas infected cells treated with **8**, **9**, or **10** (10 μM) showed numerous hybridizing signals, suggesting ongoing viral replication (FIGURE 59). Thus, compounds **3**, **5**, and **7** appear to exert an inhibitory effect on HSV-1 DNA replication like ACV. Since compound **7** is the simplest analogue from a functional and stereochemical perspective to exhibit these novel antiviral effects and is readily available through our total synthetic strategy, we selected it for further analyses (McNulty & Zepeda-Velázquez, 2014).

iPSC-neurons were infected with HSV-1 as described above, and DNA was extracted 24 hpi. Quantitative PCR (qPCR) analysis indicated dramatic reduction in viral DNA copy number in cells treated with **7** (over 1,800-fold reduction at 10 μM) and ACV (2,300-fold reduction at 50 μM), compared with infected, untreated cells (FIGURE 59b). The HSV-1 immediate early gene ICP4 is essential for viral replication (Bates & DeLuca, 1998); therefore, we utilized RT-qPCR to test the expression of ICP4 and viral DNA polymerase 24 hpi in infected iPSC-neurons treated with **7** or ACV.

A substantial reduction in the expression of ICP4 and viral DNA polymerase was observed in iPSC-neurons treated with **7** (10 μM) and ACV (50 μM; FIGURE 59c). The reduction of ICP4 expression level was further confirmed by Western blotting (FIGURE 59d). Taken together, these results indicate that **7** influences one or more stages of HSV-1 lytic cycles at or before DNA replication. Alternatively, the reduced expression of IE genes and viral DNA polymerase with both drugs may result from the inhibition of multiple rounds of viral replication. As the drugs were added 2 hpi, it was unnecessary to test effects on viral entry. The concentration of **7** that caused a decrease in the percentage of $EGFP^+$ cells by 50% (EC50) was estimated to be 0.10 μM, similar to ACV (EC_{50} = 0.07 μM; FIGURE 60a). At concentrations from 100 nM to 50 μM, **7** or ACV did not significantly affect iPSC-neuronal viability (FIGURE 60b).

Given the remarkable anti-HSV-1 activity of **7**, we next investigated its effect on nonlytic HSV-1 infection. By adapting conventional rodent latency protocols, we have previously used an antiviral cocktail of (E)-5-(2-bromovinyl)-2′-deoxyuridine (5BVdU, 30 μM) + interferon-α (IFN-α, 125 U/mL) for 7 days to induce "quiescent" infection in iPSC-neurons that mimics several aspects of HSV-1 latency (D'Aiuto et al., 2014). As reported before, up to 5 days after 5BVdU + IFN-α were withdrawn, only low levels of productive infection were noted (FIGURE 38c), but HSV- 1 could be reactivated using sodium butyrate (NaB, 5 mM), a histone deacetylase inhibitor (D'Aiuto et al., 2014). Cells treated with **7** (10 μM) or **7** + IFN-α showed 2.9- and 2.1-fold greater increase, respectively, in the percentage of $EGFP^+$ cells compared with 5BVdU + IFN-α treated cells after withdrawal of agents for 5 days (FIGURE 38a), but infectious viral particles were nevertheless undetectable in the supernatant harvested from any of the cells (FIGURE 38c). Unexpectedly, the EGFP mean fluorescence intensity (MFI) in cells treated with **7** or **7** + IFN-α

was approximately 1.6- and 2.5-fold lower than the 5BVdU + IFN-α treated cells, 5 days after the drugs were withdrawn (FIGURE 38b). Cells treated with **7** or **7** + IFN-α also differed from the 5BVdU + IFN-α treated cells following incubation with NaB; whereas the latter showed robust reactivation with respect to percentage of $EGFP^+$ cells or EGFP MFI, cells treated with **7** or **7** + IFN-α did not show significant reactivation (FIGURE 38a,b). Similarly, the proportion of EGFP-RFP+ cells and EGFP-RFP MFI were significantly reduced in cells treated with **7** or **7** + IFN-α after treatment with NaB when compared to the cells treated with 5BVdU + IFN-α (FIGURE 38a,b). Taken together, these experiments suggest that the repression induced by **7** or **7** + IFN-α is distinct from BVdU + IFN-α or ACV, as it is not reactivated to the same extent by NaB.

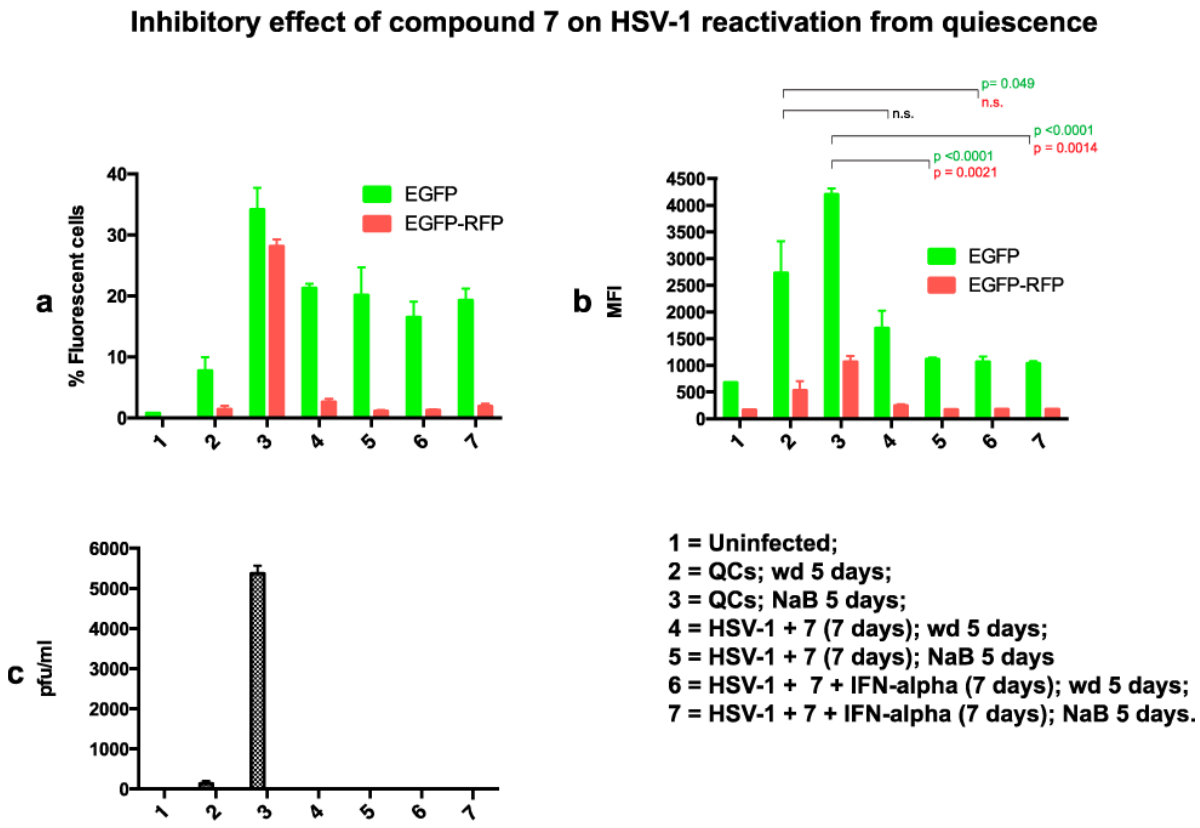

Figure 38. Compound 7 significantly reduces HSV-1 reactivation and inhibits VZV lytic infection (a−c).

Sodium butyrate (NaB) induces HSV-1 reactivation in quiescent neuronal cultures (QCs) but not in infected cultures treated with **7** or **7** + IFN-α. Quiescent neuronal cultures were produced by incubating iPSC-neurons with HSV-1 in the presence of 5-bromodeoxyuridine (5BVdU) and interferon-α (IFN-α). Cells were also infected with HSV-1 in the presence of **7** or **7** + IFN-α. After 7 days, drugs were withdrawn (wd) and cells were either cultured in the presence of NaB to induce HSV-1 reactivation or vehicle for an additional 5 days. (a) Percentage of EGFP+ and EGFP- RFP+ cells. (b) Mean fluorescence intensity (MFI) of EGFP+ cells and EGFP-RFP+ cells. (c) Viral titer in culture supernatants estimated with virus yield reduction assay using Vero cells 48 hpi. Indicated p- values for comparisons in panel b involving EGFP and EGFP-RFP are depicted in green and red, respectively. The data represent an average of three independent experiments. Error bars represent standard deviations.

To explore whether the antiviral effects of **7** extend beyond HSV-1, we compared **7** and ACV against varicella zoster virus (VZV), another common herpes virus that causes chicken pox, shingles, and neuralgia (Smith et al., 2011). We used a VZV construct expressing luciferase

from the late ORF9 promoter (Bayer et al., 2015). ARPE-19 retinal pigment epithelial cells were infected with VZV at 1000 PFU/ well. Compound **7** or ACV were added 2 hpi and assayed 48 hpi. Compound **7** caused ~220-fold reduction at 10 μM in luciferase counts per second and showed an EC_{50} of 0.15 μM, while ACV (50 μM) caused only 1.8-fold reduction (FIGURE 60c). No significant changes in cell viability were observed at tested concentrations for **7** and ACV (FIGURE 60d).

Various antiviral activities of Amaryllidaceae alkaloids have been reported over the last three decades (Ieven et al., 1982). A comprehensive evaluation on the antiviral activity of several of these alkaloids revealed that pancratistatin **3**, narciclasine **5**, trans-dihydrolycoricidine **7**, and its 7-hydroxy analogue were active against Japanese encephalitis, yellow fever, and dengue viruses (Gabrielsen et al., 1992). Antiviral activity of lycorine **1** against the avian influenza virus was recently reported (He et al., 2013). Lycorine can also inhibit other RNA-viruses, including severe acute respiratory syndrome (SARS)-associated coronavirus (Li et al., 2005), poliovirus (Hwang et al., 2008), and West Nile virus. The present work significantly expands knowledge on the antiviral activity of these alkaloids by identifying derivatives that exhibit novel, distinctive, and diverse inhibitory effects against HSV-1 and VZV infection that are superior to ACV. The facile method reported here for the rapid asymmetric synthesis of natural and non-natural lycorine-type alkaloids permitted discovery of a clear structure−activity pattern, demonstrating that a crucial role is played by the (3R)-hydroxy substituent in these alkaloids as a requirement for this antiviral activity. Only compounds **3**, **5**, and **7** containing the (3R)-stereochemistry demonstrate potent antiviral activity, the C3-epimeric compound **8** and C3-deoxy derivative **9** are significantly less active.

This allowed identification of alkaloid **7** as a functionally minimum antiviral pharmacophore. Further applications on harnessing the iPSC-neuron based platform with additional pathogens with the current and additional analogues prepared through refinements on the synthetic protocol are under active investigation. Most importantly, as latent HSV-1 infection is lifelong and drug-refractory, the multiple effects of compound **7** on HSV-1 infection, including its ability to significantly reduce HSV-1 reactivation from quiescence, motivate additional studies of viral entry and viral heterochromatinization. Additional studies are needed to evaluate whether compound **7** alone or in combination with currently known antiherpetic drugs can repress HSV-1 irreversibly to confer protection of immunocompromised individuals who may be at risk for ACV-resistance (Antoine et al., 2013) or patients with renal failure.

Associated Content

Full details on the biological and synthetic procedures and characterization data for all compounds reported; crystallographic data for compound 15 are deposited under CCDC 1001464.

Author Contributions

[#]These authors contributed equally. The manuscript was written through contributions of all authors. J.McN. designed and C.Z.V. and S.L. performed all synthetic organic experiments. H.A.J. performed X-ray analysis. V.L.N., L.D., Y.Z., and L.M. designed/performed the HSV-1 studies. P.R.K., M.B.Y., L.D., and L.M. designed/performed the VZV studies. All authors aided in manuscript preparation and editing. All authors have given approval to the final version of the manuscript.

Funding

This work was supported by NSERC (to J.Mc.N.), the Stanley Medical Research Institute (to J.Mc.N., V.L.N.), and NIMH (MH63480). C.Z.V. thanks CONACyT for a graduate fellowship. P.R.K. acknowledges EY015291, EY08098, Research to Prevent Blindness Inc., and the Eye and Ear Foundation of Pittsburgh.

4.3 GROUNDWORK FOR MODERATE THROUGHPUT DRUG SCREENING

Generation of neuronal cultures in 384-well plates is *condicio sine qua non* start for a moderate or high throughput drug screening campaign aiming to identify novel compounds exhibiting antiviral activity able to inhibit HSV-1 lytic infection or inhibit viral reactivation from latency; therefore, we propose to i) generate human iPSC-neuron cultures in 384-well plates and ii) develop a sensitive and cost-effective read-out method for HSV-1 infections. This section will describe these methods.

4.3.1 IPSC-Neuronal Cultures for 384-Well Plates

In Aim 1 (Section 3.2), we described a method for large-scale generation of neural stem cells/early neural progenitor cells (NSCs/eNPCs) from induced pluripotent stem cells (iPSCs) and their differentiation into neurons (iPSC-neurons; D'Aiuto et al., 2015). Cultures displaying a high percentage of flat, non-neuronal cells were purified by a rapid and easy method as previously described (Azari et al., 2014) with modifications.

4.3.1.1 Purification of NSCs/eNPCs

In each well of a 6- well plate, the medium was aspirated and 500 µl accutase was added. Cells were observed under the microscope for a rounded-up morphology (approximately 90 seconds). One milliliter of DMEM/F12 (Lonza, catalog 12-719F) was added very slowly to the side of the wells, and then all the medium was carefully removed and discarded. One milliliter

of mTeSR1™ cell culture medium was dispensed into each well, the edges were sealed with parafilm, and the plate was wrapped in aluminum foil to protect from light. The plate was placed on a VWR OS-500 orbital shaker for 30 minutes on speed 4.

The cells that detached during the 30-minute shake were collected and dispensed onto a new 6-well matrigel-coated plate. The cells were propagated and mTeSR1™ medium changed daily. Once the cells reached 80% confluency, cells were treated with accutase for propagation into a new matrigel-coated 6-well plate, or the medium was exchanged with neurobasal for neuronal differentiation (FIGURE 39).

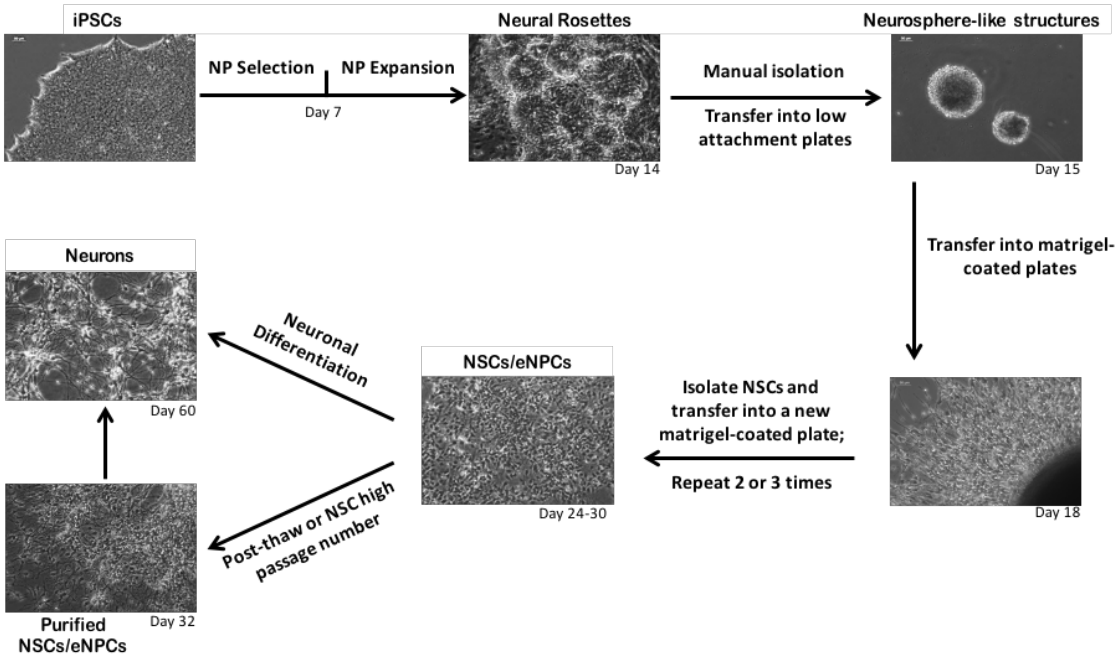

Figure 39. Schematic flow diagram to depict the stages of differentiation into neurons from induced pluripotent stem cells (iPSC).

NSC: neural stem cells; eNPC: early neural progenitor cells. Adapted from "Large-scale generation of human iPSC-derived neural stem cells/early neural progenitor cells and their neuronal differentiation," by D'Aiuto et al., 2014, *Organogenesis, p. 365-77*. Copyright © 2014 Taylor & Francis Group, LLC. Adapted with permission.

4.3.1.2 Cell seeding

Human iPSC-derived NSCs were cultured as reported (D'Aiuto et al., 2015) with modifications for NSC purification. Purified NSCs were plated onto matrigel-coated 6-well plates and grown to approximately 80% confluency with mTeSR1™ cell culture medium. The medium was exchanged to neurobasal medium for 4-6 weeks to enable neuronal differentiation. iPSC-neurons cultured in 6-well plates were dissociated using 1 ml accutase (ThermoFisher, catalog a11105-01) for 2-3 minutes. The accutase was diluted by adding 1 ml of DMEM/F12 and cells were very gently triturated by pipetting with a p1000 Pipetman. The cell suspension was transferred into a 15 ml conical and centrifuged at 1,200 rpm for 5 minutes. The supernatant was carefully removed and the cell pellet was gently disturbed by flicking the tube. The cells were re-suspended in neurobasal medium. An aliquot of cells was removed for determining the cell count using a haemocytometer following trypan blue stain. Cells were then seeded into a matrigel-coated 384-well plate at a density of 5,000 cells/well for lytic infections (FIGURE 40) or 20,000 cells/well for quiescent infections (FIGURES 47 and 48). The plates were then centrifuged at 500 rpm for 30 seconds to deposit the cells to the bottom of the wells. The plate was incubated in standard cell culture conditions.

NOTE. Since 384-well culture medium in cell culture plates tends to evaporate relatively quickly along the wells on the periphery of 384-well culture plates, the stack of plates were placed in a second, smaller water bath that was positioned on the bottom shelf close to the main water reservoir dish.

The cells were cultured for a minimum of 7 days to recover from the transferring process and half-volume of neurobasal medium was replaced every other day using a multichannel pipette or Hydra 96-well liquid transfer machine. The iPSC-neurons plated at a density of 5,000 cells per well were immunostained for neuronal markers TUJ1 and MAP2 (FIGURE 41 and 42).

4.3.2 384-Well Plate Infection

4.3.2.1 Lytic Infections

Lytic HSV-1 infections were performed at MOI = 5 for 2 hours using the HSV-1 viral construct incorporating reporter genes EGFP and RFP under the control of the promoters for ICP0 and gC, respectively (FIGURE 43). Increased cell seeding densities used in the quiescent infection were also able to be acutely infected with HSV-1 (FIGURE 47 *left).* The antiviral compounds acyclovir (ACV 50 µM) or phosphonoacetic acid (PAA 300 µg/ml) were included as controls, and cells were pretreated as previously described (McClain et al., 2015). At 2 hours post infection (hpi), the inoculum was removed and replaced with either neurobasal or neurobasal with drug. At 48 hpi, the medium was removed, the cells were washed with PBS, and fixed with 4% paraformaldehyde for 20 minutes. Hoescht 33342 solution (1:1,000 in PBS) was added to the wells for 2 minutes to counterstain the nuclei. Cells were washed twice with PBS, followed by addition of PBS (80 µl). Plates were wrapped in aluminum foil to protect from light prior to analysis. Fluorescent cells were analyzed using the ImageXpress Ultra (IXU) High Content imager with 20x objective. Imaged cells were analyzed with Multiwavelength Cell Scoring application within the MetaXpress software at the University of Pittsburgh Drug Discovery Institute in collaboration with Dr. Mark Schurdak, Ph.D.

A parallel experiment was performed using a different virus (KOS, wild-type) at MOI=5.0 and imaged 48 hours post infection to evaluate reproducibility. HSV-1 positive cells were detected by ICC utilizing an anti-HSV-1 ICP4 monoclonal antibody (Abcam, catalog ab6514; FIGURE 44).

Small molecules that were previously tested for antiviral activity against HSV-1 by flow cytometry (McClain et. al., 2015; McNulty et. al., 2016) were also tested for anti-lytic activity using the high content imaging at the DDI. Human iPSC-neurons were infected with KOS strain at MOI=5.0 and imaged 48 hours post infection. Mode of detection was ICC utilizing an anti-HSV-1 ICP4 monoclonal antibody (Abcam, catalog ab6514; FIGURE 45).

4.3.2.2 Quiescent Infections

The iPSC-neurons were pretreated with 5BVdU+IFNα (30 μM and 125 u/ml, respectively) for 24 hours. The following day, cells were infected with an HSV-1 viral construct that expresses fluorescent reporter genes EGFP and RFP under the control of viral promoters ICP0 and glycoprotein C, respectively in neurobasal medium containing 5BVdU+IFNα (MOI=5.0). The plate was centrifuged for 30 seconds at 500 rpm and the plate was returned to the incubator for 2 hours. At 2 hours post infection, the infectious medium was removed and replaced with neurobasal medium supplemented with 5BVdU+IFNα. Half the volume of medium was exchanged every other day for a total of 7 days. The quiescent wells were monitored on a daily basis for indication of spontaneous reactivation, indicated by EGFP/RFP expression (FIGURES 46 AND 47 *right*).

4.3.2.3 HSV-1 Reactivation

Following the induction of a 7-day quiescent infection, the quiescent inducing medium was removed, the cells were washed with DMEM/F12, and the reactivation was induced by culturing cells in the presence of sodium butyrate (NaB; 5 mM; an HDAC inhibitor) for 5 days. Alternative means of reactivation were investigated, which included the substitution of NaB with trichostatin A (TSA; 1 μM; an HDAC inhibitor) or LY294002 (PI3Ki; 20 μM; phosphoinositide 3-kinase inhibitor; FIGURE 48). To evaluate spontaneous reactivation in the absence of 5BVdU + IFNα, withdrawal of these compounds was followed by culturing cells in regular neurobasal medium for 7 days (FIGURE 48). The cells were monitored on a daily basis for induced reactivation, indicated by EGFP/RFP expression and cytopathic effect.

4.4 RESULTS FOR AIM 2

4.4.1 Cell Seeding in 384-Well Plates

Cells were titrated to obtain a monolayer culture of cells. Seeding 5,000 cells per well yielded a monolayer culture of cells that recovered well and was able to be analyzed with the Multiwavelength Cell Scoring application within the MetaXpress software (FIGURE 40).

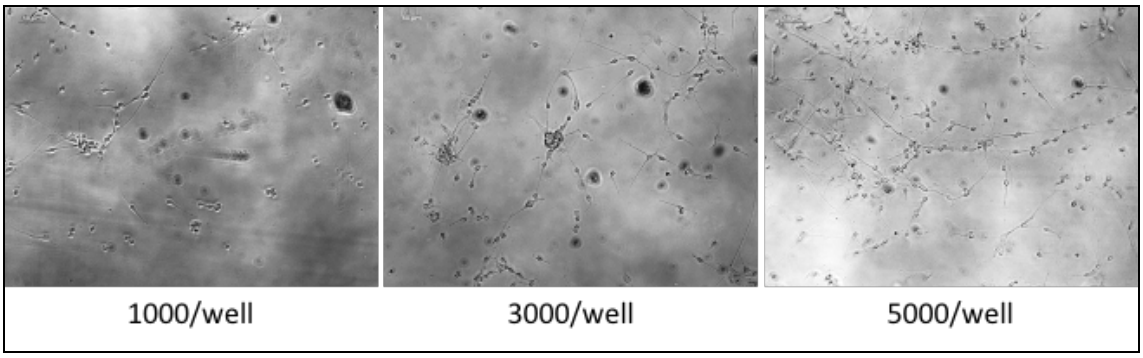

Figure 40. iPSC-neurons plated in 384-well culture plates.

iPSC-neurons were differentiated in 6-well matrigel-coated plates. Following accutase treatment, cells were seeded into matrigel-coated 384-well plates at the following densities per well: 1,000; 3,000; and 5,000.

4.4.2 Immunocytochemistry Analysis of iPSC-Neurons

Immunocytochemisry (ICC) was performed on cells seeded in the 96- and 384-well plates for neuronal markers beta tubulin III (TUJ1) and microtubule associated protein-2 (MAP2) using an inverted fluorescent microscope (FIGURE 41), and using the ImageXpress Ultra (IXU) High Content imager at the DDI (FIGURE 42). ICC analyses indicate expression of both proteins in cells plated on 96- and 384-well culture plates.

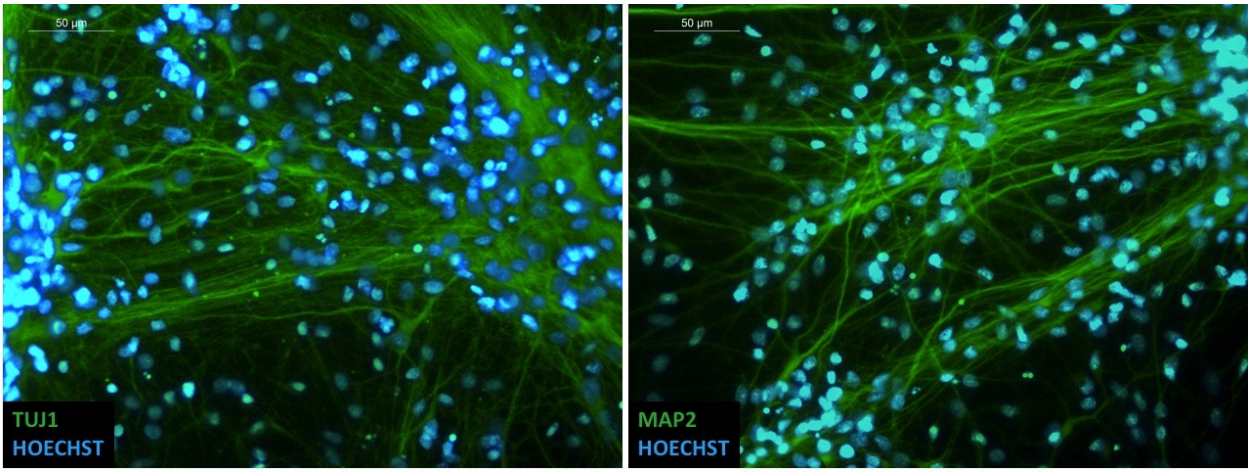

Figure 41. Human iPSC-neurons cultured in a 96-well plate for 4 weeks' differentiation.

Cells were immunostained with neuronal markers beta tubulin III (TUJ1, *left*) and microtubule-associated protein-2 (MAP2, *right*). Nuclei were counterstained with Hoechst 33342. Images were acquired using Leica LAS AF. Scale bar is 50 µm.

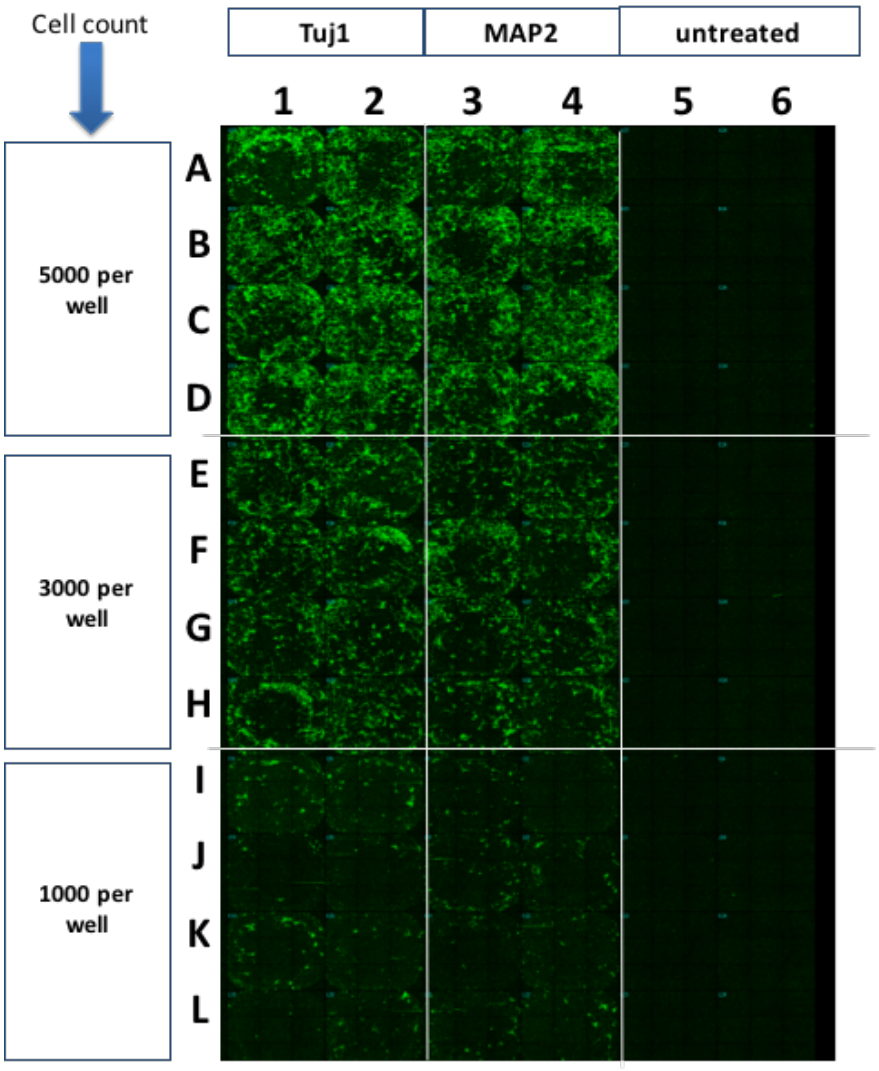

Figure 42. Immunostaining of iPSC-neurons in 384-well plates with TUJ1 and MAP2.

Cells were imaged using the ImageXpress Ultra (IXU) High Content imager with 20x objective. Imaged cells were analyzed with Multiwavelength Cell Scoring application within the MetaXpress software at the University of Pittsburgh Drug Discovery Institute.

4.4.3 HSV-1 Infections in 96- or 384-Well Plates

To test the robustness of the DDI analysis program to detect viral inhibition and to evaluate the readout method, iPSC-neurons were infected with either the HSV-1 viral construct that expresses EGFP and RFP reporter genes or with KOS wild-type virus in 384-well culture plates at MOI=5 for 48 hours (FIGURES 43 AND 44). Immunocytochemistry was used to detect virally infected cells using an anti-HSV-1 ICP4 monoclonal antibody. FIGURES 44 and 45 show the effects of antiviral, acyclovir and viral DNA inhibitor, phosphonoacetic acid on a lytic HSV-1 infection. Compounds that were previously tested for antiviral effects (McClain et al., 2015; McNulty et al., 2016) showed an anti-HSV-1 effect in the 384-well culture plates following a 48-hour infection (FIGURE 45).

Next, the models of HSV-1 quiescence and viral reactivation were evaluated in human iPSC-neurons seeded in 96- or 384-well culture plates. In 96-well plates, HSV-1 infected cells that were treated with 5BVdU+IFNα for quiescence resulted in an absence of EGFP and RFP expression; conversely, viral reactivation of HSV-1 in iPSC-neurons was evident following a 5-day exposure to sodium butyrate, trichostatin A, or PI3K inhibitor (FIGURE 46). In the 384-well plates analyzed with the high content imaging at the DDI, lytic HSV-1 infection and quiescently-infected cells were observed (FIGURE 47) and quantified in addition to the aforementioned methods of viral reaction (FIGURE 48). Compounds that function as histone deacetylase inhibitors (trichostatin A and sodium butyrate) produced more robust viral reactivation (FIGURE 48). These findings were consistent with our previously reported data that used flow cytometry to detect EGFP-positive HSV-1 infected iPSC-neurons that were cultured in 12-well plates (D'Aiuto et al., 2015).

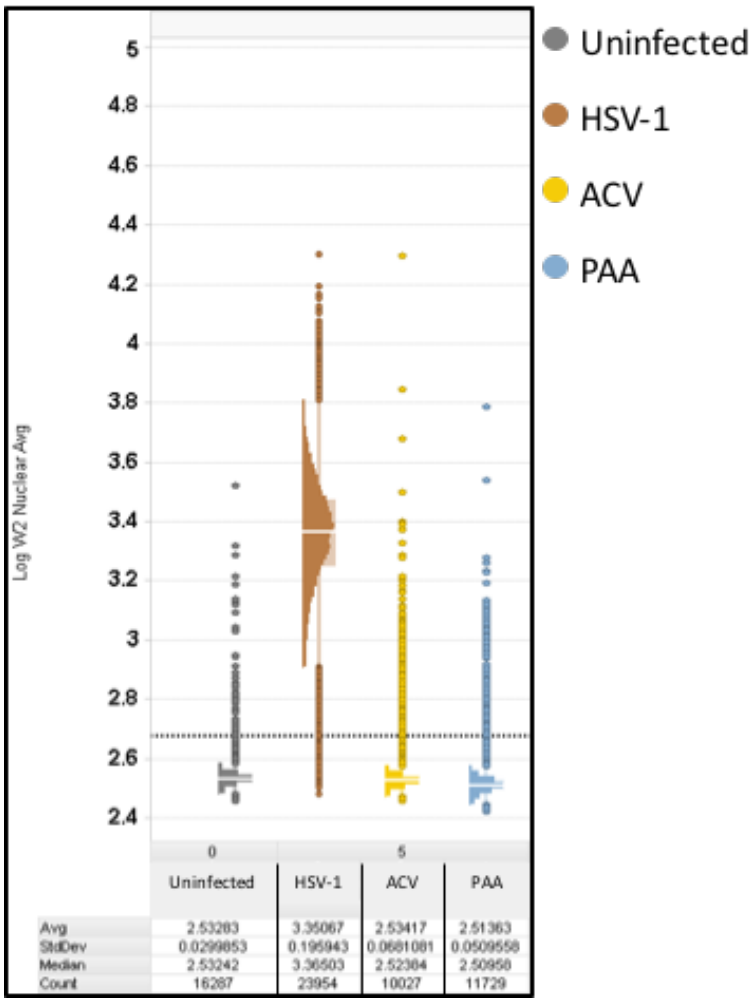

Figure 43. Inhibition of lytic infection with antiviral drugs using HSV-1 viral construct.

Acyclovir (ACV; 50 µM; yellow) and phosphonoacetic acid (PAA; 300 µg/ml; blue) inhibit HSV-1 lytic infection (brown) at MOI = 5.0 on 384-well plates. Cells were imaged 48 hours post infection for EGFP expression. Untreated, uninfected neurons (gray) provide the basis of inhibition detection in 384-well plates, which is 3 standard deviations above its mean (gray dotted line). The distribution of EGFP-positive cells is shown in the histograms. The table below the histograms indicate the number of cells measured in each population (Count), the average (Ave), the median (Median) and the standard deviation (StdDev) of overall EGFP expression in the population.

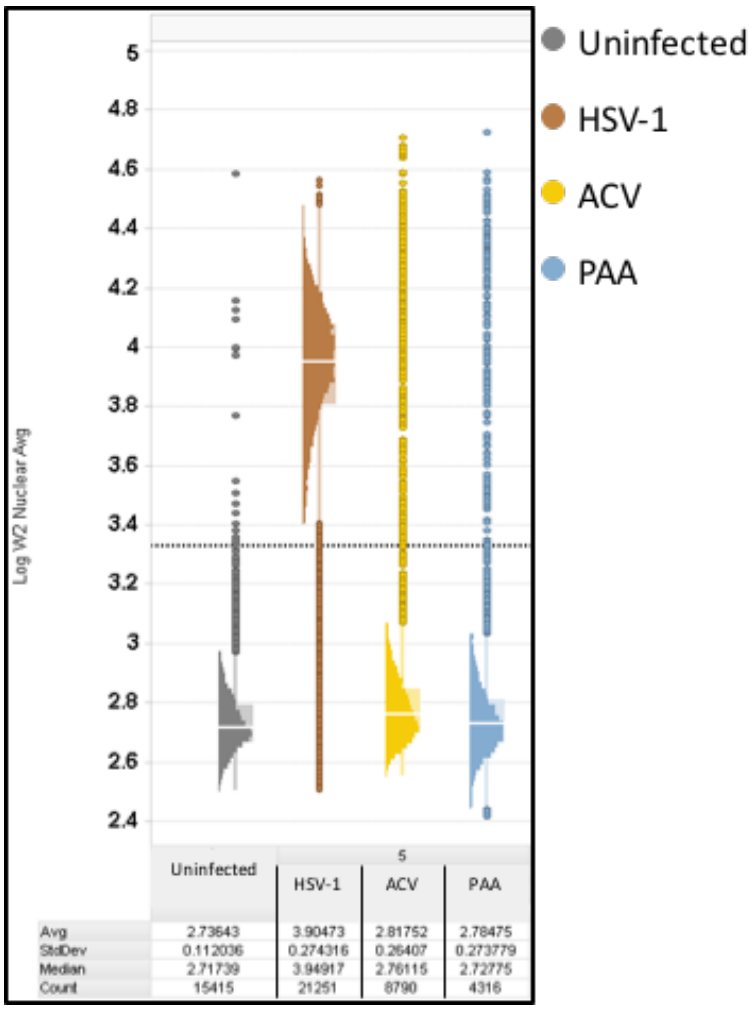

Figure 44. Inhibition of lytic infection with antiviral drugs using HSV-1 KOS strain and immunocytochemistry.

Cells were imaged 48 hours post infection. Inhibitors Acyclovir (ACV; 50 µM; yellow) and phosphonoacetic acid (PAA; 300 µg/ml; blue) were used to inhibit HSV-1 lytic infection (KOS; MOI=5.0; brown). Untreated, uninfected neurons (gray) provide the basis of inhibition detection in 384-well plates, which is 3 standard deviations above its mean (gray dotted line). ICC was performed to detect HSV-1 positive cells using an anti-HSV-1 ICP4 monoclonal antibody. The distribution of ICP4-positive cells is shown in the histograms. The table below the histograms indicate the number of cells measured in each population (Count), the average (Ave), the median (Median) and the standard deviation (StdDev) of overall ICP4 expression in the population.

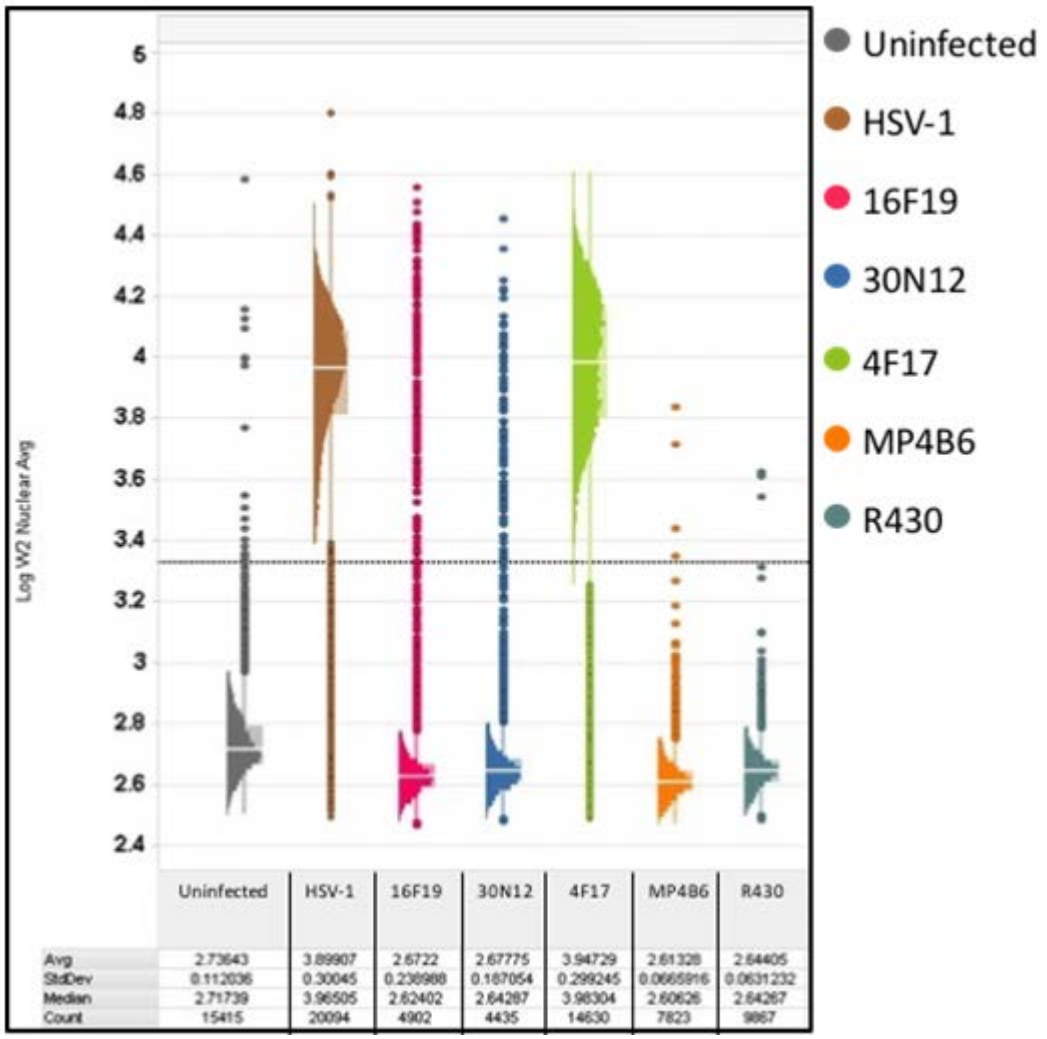

Figure 45. Novel compounds inhibit HSV-1 lytic infection.

Human iPSC-neurons were infected with KOS strain at MOI=5.0 and imaged 48 hours post infection. Untreated, uninfected neurons (gray) provide the basis of inhibition detection in 384-well plates, which is 3 standard deviations above its mean (gray dotted line). ICC was performed to detect HSV-1 positive cells using an anti-HSV-1 ICP4 monoclonal antibody. The distribution of ICP4-positive cells is shown in the histograms. The table below the histograms indicate the number of cells measured in each population (Count), the average (Ave), the median (Median) and the standard deviation (StdDev) of overall ICP4 expression in the population.

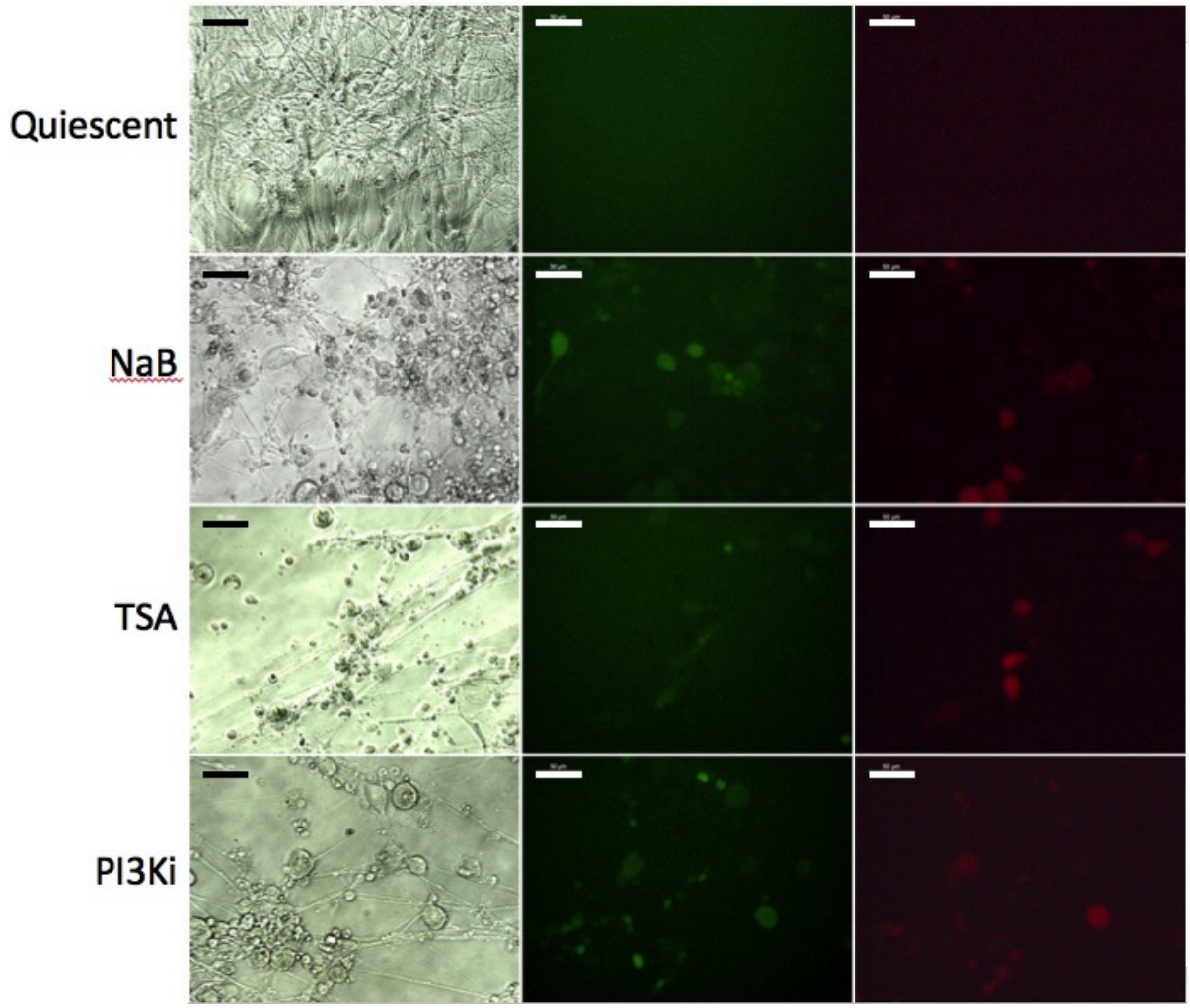

Figure 46. Induced reactivation models of HSV-1 quiescently infected iPSC-neurons in a 96-well plate.

Following the 7-day quiescent infection (HSV-1 expressing reporter genes for EGFP and RFP; MOI 5.0), the cells were exposed to sodium butyrate (NaB), trichostatin A (TSA), and PI3K-inhibitor (PI3Ki) for 5 days. Cells were imaged on a Leica DM IL LED inverted, fluorescence microscope. Scale bar is 50 μm.

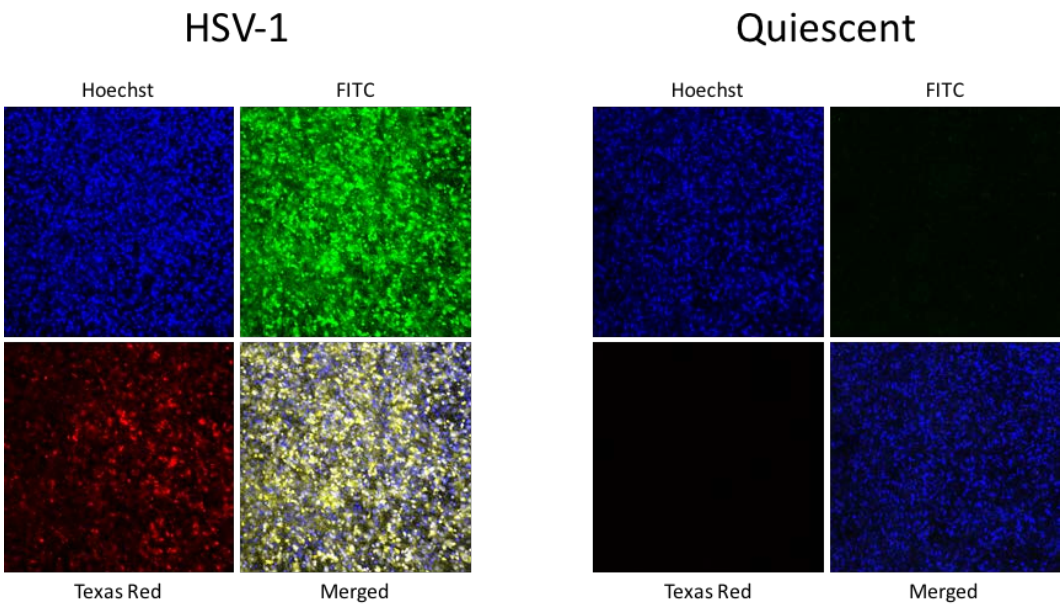

Figure 47. HSV-1 models of lytic and latent infection on iPSC-neurons seeded into 384-well culture plates.

Human iPSC-neurons were infected (MOI=5) with HSV-1 viral construct that expresses reporter genes EGFP and RFP under the control of viral promoters ICP0 and glycoprotein C, respectively for 48 hours (*left*). Human iPSC-neurons were quiescently infected for 7 days with HSV-1 (MOI=5; *right*).

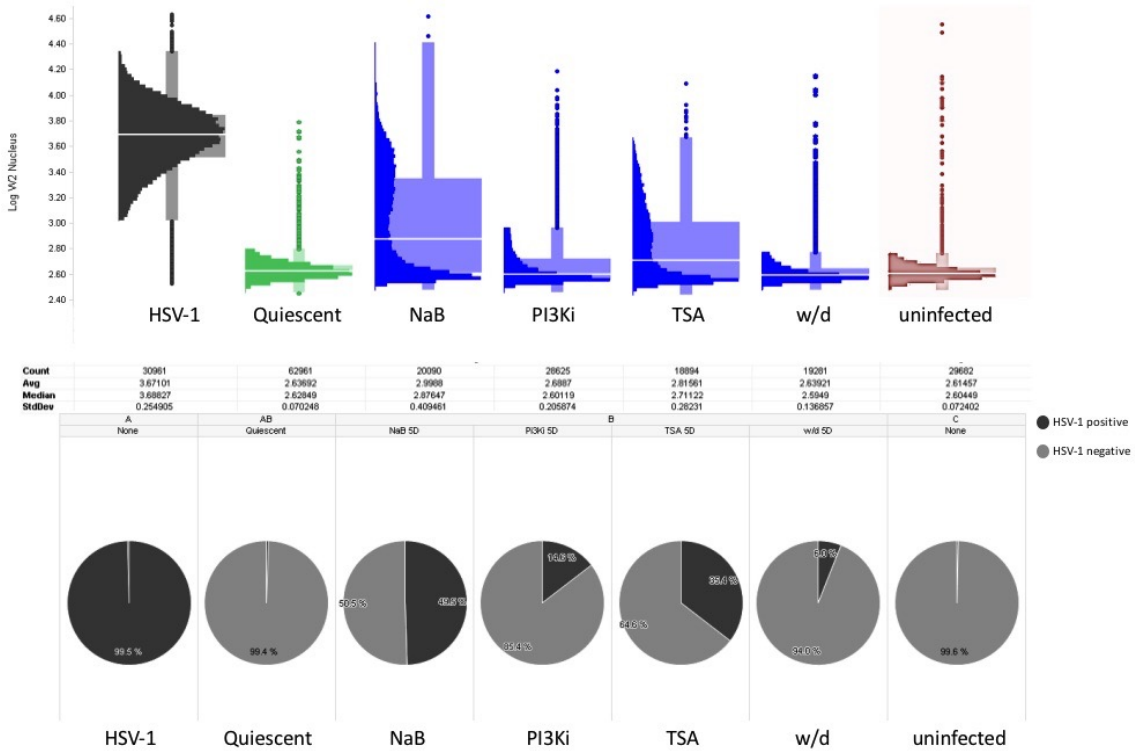

Figure 48. Alternate modes of HSV-1 reactivation analyzed with high content imaging.

HSV-1 quiescence was induced in iPSC-neurons for 7 days and then removed. The reactivation compounds were added for 5 days. *TOP*. Histograms depicting the EGFP intensity in lytically infected cultures (black histogram), quiescently infected cultures (green histogram), HSV-1 reactivation from quiescence (blue histograms; NaB, PI3Ki, TSA, or withdrawal of quiescent-inducing compounds), and uninfected/untreated iPSC-neurons (orange histogram). *BOTTOM:* Percentage of EGFP-positive cells (black) and EGFP-negative cells (gray). The distribution of EGFP-positive cells is shown in the histograms. The table below the histograms indicate the number of cells measured in each population (Count), the average (Ave), the median (Median) and the standard deviation (StdDev) of overall EGFP expression in the population.

5.0 DISCUSSION

Research on human neurological diseases, neurodegenerative diseases, or neuroinvasive infections has previously been hampered by the inability to obtain sufficient amounts of human neurons to investigate pathogenesis or conduct drug screens in cultured cells. Therefore, many groups relied either on animal models or on human post-mortem brain tissues. Even such sources do not conveniently provide substantial quantity of neural tissue needed for drug screens. iPSC technologies have revolutionized this field of research by enabling virtually limitless supplies of iPSC-neurons that resemble human neuronal cells and related non-neuronal tissues. The utility of iPSC neurons for modeling and drug screens related to human HSV-1 infections was explored in the present thesis.

In Aim 1a, I have described the generation of neural stem cells/early neural progenitor cells (NSCs/eNPCs) from human iPSCs using a method that is scalable, cost effective, and relevant for studying human-specific neurotropic viruses. NSCs/eNPCs are mitotically active, multipotent stem cells that can be differentiated into large-scale quantities of neuronal cells. The method eliminated previously reported steps of embryoid body generation, saving time and cost. The adherent cultures of NSCs/eNPCs was also favored over embryoid bodies as it enabled more uniform contact of each cell with the cell culture medium. The use of B27 and BDNF in the cell culture medium resulted in a cell population that had 90% TUJ1 positive cells. The neurons also expressed other neuronal markers like MAP2, VGLUT1, and NR1 (subunit of the glutamate

receptor). A modest proportion of the cell population also expressed proteins that are found in layer 3 of pyramidal cells in the dorsolateral prefrontal cortex (DLPFC) in the human brain. These 'iPSC-neurons' express proteins found in human cortex tissues and have functional ligand-gated channels (D'Aiuto et al., 2014). Furthermore, the iPSC-neurons express glutamate receptors (D'Aiuto et al., 2014), which are also found on neurons from the trigeminal ganglia and the CNS, the site of HSV-1 latent reservoirs (Lazarov, 2002).

Further on in Aim 1a, the neuronal cells derived from human iPSCs were used to model lytic and latent HSV-1 infections with an HSV-1 viral construct that expresses two fluorescent reporter genes. Neural progenitor cells (NPCs) and iPSC-neurons were permissive to HSV-1 lytic infection. HSV-1 quiescence was established in human iPSC-neurons with the use of antivirals (E)-5-(2-bromovinyl)-2-deoxyuridine and interferon-alpha (5BVdU+IFNα). 5BVdU is an analog of the nucleoside thymidine that shares a common mechanism of action as acyclovir (ACV). IFNα is a signaling molecule that is secreted in virally-infected cells that promotes an 'antiviral state' (Ivashkiv & Donlin, 2014). Together, 5BVdU+IFNα act synergistically to inhibit HSV-1 infection *in vitro* and *in vivo* (van Bijsterveld et al., 1989). In our models of HSV-1 infection, these compounds were used to induce quiescence for a 7-day period of time. The quiescently infected cells showed the following features of latent HSV-1 infections that have been described in other model systems.

i) Viral replication is decreased: Of the total population of cells, 9% expressed EGFP. Upon withdrawal of the antiviral compounds, a ~3-fold increase in EGFP expressing cells were detected. Further, qPCR assays indicated a marked reduction in mean viral copy numbers during quiescence when compared with lytic infections (1,747 and 212,163, respectively).

ii) Productive infection is absent: The cell culture supernatants from the quiescent infections were used to infect fresh Vero cells, which failed to produce any plaques, indicating the absence of productive infection. Withdrawal of the antiviral compounds resulted in a significant, continued suppression in infectious virions (1 plaque each in 3 wells of 9 examined).

iii) Viral DNA is retained in the nucleus: Quiescent viral genomes located in the nuclear periphery were detected as distinct foci of hybridization signals using 3D-FISH; in acutely infected cells, these hybridization signals formed replication compartments closer to the interior of the host nuclei, which eventually merged to completely occupy the host nucleus.

iv) Expression of LAT during infection: The quiescently-infected neurons expressed LAT. Interestingly, consistent with prior publications, LAT was also expressed at higher levels during lytic infection.

v) Quiescent viral infections can be reactivated. HSV-1 quiescent cultures were exposed to the histone deacetylase inhibitor sodium butyrate (Davie, 2003) to induce viral reactivation. This resulted in a 2-fold and 6-fold increase of EGFP- and EGFP/RFP-positive cells, respectively. Additionally, viral copy numbers are increased when compared with quiescent infections (81,039 and 1,747, respectively).

vi) Quiescent genomes exist as a heterochromatinized fragment of DNA within host nuclei. In acutely infected Vero cells, we did not observe co-localization of a protein associated with heterochromatin (HP1) with viral genomes, indicating that a substantial fraction of viral DNA does undergo heterochromatization. The

pattern in acutely-infected iPSC neurons may show some co-localization. However, it could not be determined at this time for quiescently-infected iPSC neurons. Fine-grain analyses of nuclease accessibility on promoter regions of the viral genome were performed with CHART-PCR. Viral lytic gene promoters were more accessible to nuclease degradation during lytic infections, with the exception of ICP4. LAT was more accessible to nuclease degradation during quiescent infections.

During latency, LAT expression is commonly reported. Mouse explant cultures that were latently infected showed LAT promoter genomic regions associated with H3K9 and H3K14 acetylation, indicative of gene transcription (Kubat et al., 2004); however, LAT has been reported to be expressed late during infection cycles, in addition to latency (Spivack & Fraser, 1988; Roehm et al., 2011; Ma et al., 2014). In the iPSC-neuron cultures, we have reported LAT expression during both the quiescent infections, as well as a 24-hour acute infection. During viral quiescence, there may be subpopulations of cells that show quiescent infection, others that are resistant to viral infection, or still others with lytic infection. As our RT-qPCR assays used to derive LAT expression were performed on pools of cells, this question could be resolved through single-cell analysis. In 2008, Umbach and colleagues described viral miRNAs originating from latently-infected mouse trigeminal ganglia that were antisense to viral genes ICP0 and ICP34.5 (Umbach et al., 2008). It would be instructive to see if the same miRNAs can be detected in this model of HSV-1 latency.

The iPSC-neuron model of HSV-1 latency was further analyzed using copy number qPCR. In Aim 1 of this thesis, we used several methods to evaluate viral infections. Our

primary readout method using qPCR was to quantify the EGFP locus expressed in the genomes of the viral construct. The standard curve was generated using an EGFP plasmid that was serially diluted. The resulting standard curve had an R^2 of 0.991, indicating the data points were a good fit with minor variation to the regression line. The standard curve was similar to previously reported assays using qPCR-based means to estimate viral copy number (Cohrs et al., 2000). The uninfected Vero cells had a mean Ct of 38.407 (SD 0.306), which corresponded to a mean copy number of 15.41 (SD 7.54). Thus, the lower detection limit of this assay was set to approximately 100 copies per 5 ng total DNA.

To induce quiescence, the iPSC-neurons are pretreated with 5BVdU+IFNα for 24 hours prior to infection. There was no significant difference in viral copy number when infecting iPSC-neurons in the presence or absence of 5BVdU+IFNα during the 2-hour adsorption period, indicating the compounds did not interfere with the earliest events of the viral lifecycle ($p=0.21$). A 7-day quiescent infection resulted in a decrease in viral copy number compared with a lytic, 24-hour infection (1,743 and 212,163 in 5 ng of total DNA, respectively). A moderate increase of viral copy numbers was observed when sodium butyrate was used to induce reactivation for 5 days (81,038 copies in 5 ng of total DNA). There was a statistically significant difference in the mean copy numbers of the lytic infection and in cells that experienced viral reactivation ($p=0.005$). This may indicate i) some viral genomes are persisting in the quiescent state, even in the presence of sodium butyrate, ii) loss of cells that harbor quiescent genomes, or iii) aborted reactivation. The corresponding plaque assay that quantified the presence of infectious viral particles was consistent with the copy number assays. After the 2-hour adsorption period, acutely infected neurons (in the presence or absence of 5BVdU+IFNα) did not release infectious virions, but infectious particles were observed in a 24-hour lytic infection and viral reactivation

(48,667 PFU/ml and 27,333 PFU/ml, respectively). The use of sodium butyrate has been previously used to induce viral reactivation in quiescently infected PC-12 cells (Danaher et al., 2005); as well as *in vivo* mouse models of reactivation, where upwards of 75% of latently infected mice experienced viral reactivation (Neumann et al., 2007).

Fluorescent in situ hybridization (FISH) was used as an additional method to evaluate the latency model. Acutely infected Vero cells were blocked for FISH in a time course experiment, which showed the first reported hybridization signals at 12 hours post infection. By 24+ hours, the viral genome occupied the majority of the interior of the nuclei whilst the host chromatin was displaced to the periphery. Like acutely infected Vero cells, acute HSV-1 infections in neurons resulted in similar patterns of FISH probes at 24 hours post infection. However, the method was not sensitive enough to detect quiescent viral genomes, even though the same inoculum was used to infect both the quiescently infected cells and the cells that experienced viral reactivation in that particular experiment. Therefore, a 3D FISH method was optimized and used to detect viral genomes during quiescence. During quiescence, the hybridization signals were observed as discrete foci at the host nuclear periphery, where transcription may be repressed, similar to a 28-day latently-infected mouse model following TG sectioning (Catez et al., 2014). The nuclear periphery is mostly considered a region of repressed transcription, however there is evidence some loci do transcribe if localized at the periphery (Deniaud & Bickmore, 2009). This method may be applied to provide quantitative data if paired with flow cytometry, but must be optimized for cost-effectiveness and efficacy.

Withdrawing the quiescence-inducing drugs resulted in low-level viral replication, possibly due to a few number of spontaneous reactivation events that spread to neighboring cells. The flow cytometry data indicate that ~25% of cells are expressing EGFP from the viral

immediate early promoter, but only a third of those are expressing RFP from a late gene promoter. The plaque assays showed 1 each in 3 of 9 wells. Together, these data suggest the viral remains latent in the majority of infected cells in the absence of 5BVdU+IFNα.

A quiescent HSV-1 infection was not observed in NPCs, nor was it observed when infecting iPSC-neurons with the replication-defective virus, indicating both cell-type and virus-strain specificities. Using a replication defective virus (provided by Dr. Fred Homa), we hoped to avoid infecting neighboring cells (and thus potentially leading to lytic infection in other cells); however, quiescence could not be established using the same protocols. Following the day of infection and in the presence of 5BVdU+IFNα, the cell cultures showed widespread necrosis and further culture of live cells was not possible. The reasons for the toxic effects are uncertain. Further studies may be able to optimize the quiescent inducing conditions for this virus.

In iPSC-neurons, microarray analyses show both the acute infection and viral reactivation caused altered gene expression, but consistent with other models of latency, the quiescently-infected neurons show less extensive gene changes. Pathway analyses show the top significantly functions affected during quiescent infection are axonal guidance signaling ($p=5.21 \times 10^{-4}$), complement system ($p=8.74 \times 10^{-4}$), and NFκB signaling ($p=4.9 \times 10^{-3}$). Additional studies are needed to tease out the effects of a quiescent HSV-1 infection on neuronal function and survival.

In latent infections, HSV-1 exists as an extrachromosomal fragment that is silenced, in part, by the formation of heterochromatin. This was initially described by Deshmane and Fraser, who showed latent viral genomes are coupled with histones in a manner similar to host DNA (Deshmane & Fraser, 1989). Therefore, in Aim 1b, I sought to analyze patterns of heterochromatin by utilizing 3D FISH paired with immunocytochemistry (Co-ICC/FISH) and performing CHART-PCR on viral gene promoters. The ICC was specific for an anti-HP1α

monoclonal antibody and FISH probes were complementary to viral genomic DNA. HP1α binds to trimethylated H3K9, an indicator of transcriptional repression (Jacobs et al., 2001). In acutely infected Vero cells, substantial overlapping signals were not observed, indicating that a considerable fraction of viral DNA is not heterochromatinized. In acutely infected iPSC-neurons, overlapping signals were not as clear. Co-localization of HP1 protein on viral genomes in quiescently infected cultures also proved to be technically challenging (data not shown). The co-ICC/FISH protocol needs to be optimizing using confocal microscopy.

CHART-PCR analyses indicated that host control gene promoters that are transcriptionally active (*GAPDH*) or transcriptionally repressed (*RHO*) were more and less susceptible to digestion by MCN, respectively. In the qPCR assays of the digested samples, this resulted in low level amplification of *GAPDH* and when compared with the undigested sample, there was a mean difference in Ct values (ΔCq) of 7.37. On the other hand, *RHO* was protected from the digestion of the nuclease and amplified similar to its undigested counterpart (ΔCq = 0.63). The difference in the resulting cycle threshold values was as expected for these control genes (Cruickshank et al., 2008). In iPSC-neurons that were infected with HSV-1 for 8 hours, viral gene promoter regions that are active during acute infections were more accessible to MCN digestion during lytic infections than during quiescent infections, with the exception of ICP4. The EGFP locus (downstream of the promoter) was digested the most during lytic infections, indicating more permissive regions for MCN digestion (ΔCq was 2.63). The promoter region for LAT and ICP4 were more accessible to MCN during quiescent infection (ΔCq was estimated at 1.93 and 2.05, respectively) than during lytic infection (ΔCq was estimated at 1.07 and 0.88, respectively). The HSV-1 genome incorporates seven clusters of sequences that are bound by CTCF (CCCTC-binding factor, a chromatin insulator protein) and partitions the genome into

distinct compartments of transcriptional permissiveness or repression (Bloom et al., 2010). Each immediate early gene is bounded by these elements and may be regulated independently (Amelio et al., 2006). In our model of HSV-1 latency, these CTCF proteins may block the spread of heterochromatin on the promoter region of ICP4. In addition, the promoter region may be more accessible to MCN during quiescent infections because there may be insulating elements organized on the viral genome downstream of the promoter. Alternatively, ICP4 may be transcribed. Further analysis on this locus is needed. Estimating levels of ICP4 mRNA by RT-qPCR, as well as chromatin immunoprecipitation (ChIP) would be useful to gain further understanding of ICP4 heterochromatization and transcription during viral latency.

In Aim 2, we tested novel compounds for antiviral effects and compared them with acyclovir. These initial attempts to screen compounds yielded several promising results. We sought novel compounds to combat viral resistance in individuals who are immunocompromised or the recipients of organ transplants. We used conventional Vero cells, as well as human iPSC-neurons to evaluate the antiviral effects. Compounds 30N12, 16F19, 4F17, and R430 ("compound **7**") inhibited lytic viral infections comparable to or better than acyclovir. In lytic HSV-1 infections, these four compounds i) reduced viral DNA copy numbers, ii) reduced selected HSV-1 protein levels, and iii) inhibited productive infection. Additionally, these compounds decreased sodium butyrate-induced HSV-1 reactivation. These compounds were also more efficacious against lytic varicella zoster virus (VZV) infections than acyclovir and 4F17 inhibited lytic human cytomegalovirus infections. Currently, the mechanism/s of action of these novel compounds is unknown.

Three of these new antiviral compounds were reported in the literature to have lysosomotropic activities (Nieland et al., 2004). Agents that were previously reported to have

lysosomotropic activity, like chloroquine (a drug used to treat malaria infections) or bafilomycin A1 were also reported to have antiviral activity on HSV-1 infections (Harley et al., 2001). Though the precise mechanism has not been elucidated, they may affect viral activities by increasing intracellular pH. Increasing intracellular pH produces an inhibitory effect on the trans-Golgi network, and since the trans-Golgi network is critical for HSV-1 egress, these compounds may inhibit viral packaging or maturation in the trans-Golgi network (Johnson & Baines, 2011). Compounds 30N12, 16F19, and 4F17 were previously reported to interfere with trans-Golgi trafficking, but were not tested for antiviral effects. The inhibitory concentration of 30N12, 16F19, and 4F17 that reduced the number of virally-infected iPSC-neurons by 50% was 9.7 μM, 0.42 μM, and 41.35 μM, respectively. Of the three compounds, 16F19 has an inhibitory concentration curve with a more gradual slope than the others. It is likely this compound has more than one target, but the identity of these target(s) are unknown. For all three compounds, the cytotoxic dose that reduces cellular viability by 50% could not be calculated. The highest concentration of compound added to cells (500 μM) did not significantly reduce viability when testing uninfected, treated cells with LIVE/DEAD® Fixable Aqua Dead Cell Stain Kit (Life Technologies); however, 16F19 showed the most cytotoxicity at 500 M, where cell viability was decreased to 38%. When testing cell viability with concentrations greater than 500 μM, partial product precipitation (data not shown) occurred. As a result, accurate therapeutic indices could not be calculated.

R430, the fourth compound with antiviral effects is the synthetic version of a naturally occurring alkaloid isolated from plants of the *Amaryllidaceae* family. R430 (previously identified as "compound **7**") was chosen for anti-HSV-1 testing in our model system as prior studies report compounds from this family have inhibitory effects against other viruses. The

IC50 for R430 in HSV-1 acutely infected iPSC-neurons was 0.1 μM, which was very similar to the IC50 of acyclovir (0.07 μM). Most interesting is the effect of R430 on viral reactivation. When R430 or R430+IFNα was added to infected cells for 7 days and then withdrawn for 5 days, it showed a 2.9- and 2.1-fold increased EGFP-positive cells than infected cells treated with 5BVdU+IFNα for 7 days and then withdrawn for 5 days, however, the mean fluorescence intensity of each cell expressing EGFP was lower ($p=0.49$ for R430+IFNα). We compared viral reactivation induced by sodium butyrate following a 7-day period of time where quiescence was induced with 5BVdU+IFNα or viral silencing with R430. R430 reduced viral reactivation with statistically significant mean fluorescence intensity ($p<0.0001$). The mechanism of viral silencing by R430 is distinct from 5BVdU+IFNα (McNulty et al., 2016).

The precise mechanism of action for these four compounds is unknown at this time. Since the compounds were added two hours post infection, the inhibition reported here is not likely due to blocking viral attachment or entry. I tested for the effects of compounds 30N12, 16F19, and 4F17 on viral attachment and entry, but did not observe a statistical significance in the mean copy numbers of the groups when comparing infected, treated cultures with infected cultures alone. Future studies are needed to determine the mechanism of action. This work will include comparing cells treated or untreated with the aforementioned compounds using RNAseq or a proteomics approach (mass spectrometry). Performing a pathway analysis may reveal candidate pathways that are affected by the compound; further fine-grain evaluation of the individual molecules in candidate pathways may lead to identifying the mechanism of action. Mass spectrometry may indicate intracellular proteins that specificall interact with these compounds. In addition, future studies could include synthesizing pharmacophores based on these lead molecule hits and its respective mechanism of action; even minimal molecular

modifications may improve efficacy and decrease toxicity. Broad spectrum compounds that operate with mechanism of action different than the current arsenal of antivirals are highly desirable, especially for individuals with drug-resistant HSV-1 infections. Moreover, broad-spectrum compounds could be very beneficial during acute fulminant infections in individuals before precise diagnoses can be established. Further testing of other viruses and *in vivo* models of infections is warranted.

To extend the small scale drug screens initiated in Aim 2, additional experiments were conducted to lay the groundwork for generating large numbers of neurons in multi-well culture plates and methods of readout. In order to generate 96- or 384-well plates of human iPSC-neurons, neural stem cells/early neural progenitor cells (NSC/eNPCs) were differentiated from iPSCs and purified to eliminate unwanted cell types. The cells were then expanded and differentiated into iPSC-neurons in 6-well plates. Following a 4- to 6-weeks period of differentiation, the cultures were dissociated with accutase and seeded into 96- or 384-well culture plates at a density of 20,000 or 5,000 cells per well, respectively. These cells are TUJ1- and MAP2-positive, suggesting neuronal morphology. We favored 5,000 cells per well since seeding less cells compromises the ability of the neurons to reform their complex neurite network with neighboring cells and seeding higher cell densities resulted in cell aggregation and the formation 3-dimensional structures, which introduced some error for the analysis software algorithm.

The advantage of differentiating the NSC/eNPCs into neurons in the 6-well plates instead of directly into the 384-well plates was i) ease of changing cell culture medium; ii) the 6-well plates showed less evaporation of cell culture medium in the wells than cells cultured in 384-well plates; iii) cells could be counted prior to seeding into the 384-well plates to contain cell counts

that were consistent. Our attempts to differentiate iPSC-neurons directly in 384-well plates resulted in greater well-to-well variability; however, the neurons differentiated well in these plates (data not shown) and were only limited for use by the software utilized to analyze the data. Current analysis algorithms rely on the use of imaging cells on a single, flat plane. Future studies to reduce the well-to-well variability are needed to titrate NSC/eNPCs directly into the 384-well culture plates and then differentiate them into neurons, as well as investigate new methods to analyze these cells.

Following the cell titration experiments, we optimized viral infections. We tested two viruses with different methods of readout in virally infected iPSC-neurons. We compared the HSV-1 viral construct that express reporter genes EGFP and RFP under the control of ICP0 and glycoprotein C, respectively with HSV-1 KOS wild-type virus. The detection method for the KOS virus was immunocytochemistry (ICC) for the anti-HSV-1 mouse monoclonal ICP4 primary antibody. ICP4 is an immediate early viral protein that is abundantly expressed in lytically infected cells. EGFP expression or secondary antibody fluorescence was detected for the viral construct and the KOS viruses, respectively. We found the optimal condition for assessing lytic HSV-1 infections in the multi-well plates is a 48-hour infection at an MOI=5. Two readout methods for viral inhibition consistently produced similar results.

The resulting histograms display all of the cell population where the dots represent outliers. (FIGURES 43, 44, and 45). We based the detection of infection to be 3 standard deviations of the mean fluorescent intensity of the uninfected population. In section 4.4.3., we found that either infection model is suitable to discriminate uninfected from acutely-infected iPSC-neurons. Furthermore, after adding the antiviral drugs ACV or PAA, the levels of fluorescence detected is similar to the uninfected condition (mean nuclear fluorescence is

log(2.534), log(2.514), and log(2.533), respectively). Some of the novel antivirals identified earlier in this work inhibited HSV-1 infection and were distinguishable from the acutely-infected iPSC-neurons on the 384-well plates; however, compound 4F17 showed some variance compared with the flow cytometry readouts (~1-fold and 6.3-fold, respectively). Quiescent HSV-1 infections and viral reactivation was observed in these culture plates, albeit at a higher cell density (20,000 cells per well in the 384-well plate). Inducing reactivation with histone deacetylase inhibitors produced the most robust reactivation in both 96-and 384-well plates and future studies using adenovirus to supply ICP0 may provide alternate means to reactivate these virally infected cultures (Halford et al., 2001).

Given the need for reproducibly generate cell culture plates with low variability (well-to-well, plate-to-plate, day-to-day, and assay-to-assay) to screen a large number of compounds for antiviral effects, other cell types were considered as follows:

i. Vero cells. Vero cells are a lineage of cells isolated from African green monkey kidney epithelium that are frequently used in herpesvirus research. These cells form monolayer cultures and have predictable doubling rates; features that would be advantageous to high throughput screening campaigns. However, it is not possible to generate viral latency in Vero cells. Employing a mutant virus defective in the immediate early genes may be a solution, however the use of such a virus may not recapitulate the native virus and differences in drug effects may become pronounced. Other methods to induce a quiescent herpesvirus infection in fibroblast that have been previously described by others is to incubate the cells at a higher temperature (42°C) and low multiplicity of infection (MOI=0.003; Russell, 1986). However, these experiments were based on using low MOIs,

which could introduce difficulties in data interpretation. Also, virally-infected Vero cells do not synthesize interferon due to a genetic defect, and thus cannot intrinsically circumvent viral infection in a manner similar to other cell types (Emeny & Morgan, 1979).

ii. NSC/eNPCs. These cells are closely related to neurons and are mitotically active, enabling us to generate large numbers of cells rapidly, but data must be generated to show a positive correlation of antiviral effects with the iPSC-neurons and/or the Vero cells. Still, testing compounds for reducing viral reactivation from latency is not possible as HSV-1 latency could not be established in these cells.

If a drug-screening protocol using these cells could identify anti-lytic compounds, it would provide a relatively rapid preliminary filter for the next round of screening in iPSC-neurons. Furthermore, as latency can be established in the iPSC-neurons, the leading hit compounds would be added for 2 days, and then viral reactivation would be induced with sodium butyrate. Compounds that are refractory to viral reactivation would be selected for further analyses. The methods outlined in previous chapters, such as viral copy number qPCRs, 3D-FISH, and CHART-PCR would provide confirmatory measures of the antiviral activity. Additionally, the use of Campenot chambers may be used to assess viral transport in neuronal cultures exposed to novel drugs or to assess differences in viral kinetics when infecting neuronal projections but not the soma, and vice versa (Curanović et al., 2009).

What types of compounds should be sought in future drug screens? Acyclovir and valacyclovir are efficacious antiviral compounds for HSV-1 lytic infections that have excellent safety profiles. Other antiviral compounds, such as nucleoside inhibitors, helicase/primase

inhibitors, or terminase inhibitor are newly reported potent inhibitors of HSV-1. However, since these antiviral compounds exert their inhibitory effects on viral DNA replication or DNA packaging into the capsid, viral resistance could arise through selection pressure. The use of these antivirals in immunocompetent individuals does not frequently result in the development of viral resistance. Conversely, the frequency of antiviral resistance to acyclovir is increased among AIDS patients, individuals undergoing chemotherapy, or organ transplant recipients. The development of methods to screen molecules for anti-lytic effects with a different mechanism of action would be beneficial for those individuals. Examples of these types of molecules include translation inhibitors or molecules that impair Golgi trafficking. A second option is to find a compound that reduces the frequency of viral reactivation. Herpes keratitis is the leading cause of corneal blindness in the world. After many cycles of HSV-1 reactivation, infected corneal tissue becomes scarred and opaque, resulting in decreased visual acuity and ultimately blindness. Additionally, herpes labialis, herpes genitalis, or herpes simplex encephalitis may also be exacerbated by reactivation, resulting in decreased quality of life or mortality. Compounds that result in reduced viral reactivation may operate epigenetically to keep the virus in a semi-permanent state of heterochromatization (Kristie, 2015). During infection, viral DNA is rapidly associated with histones bearing repressive marks (H3K9 and H3K27 methyl; Wang et al., 2005; Kwiatkowski et al., 2009). Modulation of histone repressive marks that can result in gene expression, and ultimately viral infection, is carried out by molecules that shape the epigenetic landscape (i.e., histone demethylases or methyltransferases; Narayanan et al., 2007). In fact, inhibitors of such molecules (lysine-specific demthylase 1 (LSD1)) and Jumonji C domain-containing protein 2 (JMJD2)) have potent antiviral effects due to heterochromatic repression, resulting in anti-lytic effects, as well as reduced viral reactivation from latency (Liang et al.,

2013; Hill et al., 2014). Hypotheses focusing on the correlation of cognitive impairment with HSV-1 seropositivity may also be tested following use of such a compound. A third type of compound is one that eradicates the virus in its latent form, and thus completely purges HSV-1 from the human body. An example of such a molecule could be an HSV-1 meganuclease, i.e., a sequence-specific endonuclease could be tailored to target the latent viral genome. While their large target size increases specificity, the mode of delivery of such a molecule must be considered. Currently, adeno-associated virus (AAV) vectors are popular; however, safety concerns and nuclease efficiency need to be addressed (Elbadawy et al., 2014). In addition, clustered regularly interspaced short palindromic repeat/ CRISPR associated protein 9 (CRISPR/Cas9) function to protect bacterial cells from viral infection by nuclease cleavage in a sequence-specific manner. This system has been optimized to be sequence-specific to viruses in mammalian cells with the use of guide RNA to induce cleavage of viral DNA by the Cas9 nuclease (Wang & Quake, 2014; Bi et al., 2014; Kennedy & Cullen, 2015). Use of the CRISPR/Cas9 system to specifically target viral genomes may be a method used in future studies to eradicate latent HSV-1 genomes. A compound that can accomplish a complete viral purge has thus far proved elusive, and future studies may shed light on such molecules to accomplish this feat.

Some shortcomings in the present studies should be noted. The differentiation process to generate the NSCs/eNPCs from iPSCs produces unwanted cell types. Further characterization of the iPSC-neurons is desirable. Additionally, the cells that comprise the brain are a complex, 3-dimensional structure, and optimization to a 3-dimensioanl culture system may provide a better model fit (Zhang et al., 2014). Our models outlined here do not contain all the aspects of the human immune system, which may not be conducive for some studies. However, other studies

investigating host-virus interactions may find its absence to be beneficial. The CHART-PCR method outlined here cannot conclusively demonstrate viral genome heterochromatization during quiescent infection, though it can quantify the accessibility of a DNA nuclease (MCN) at specific locations in the viral genome. Since many proteins have the ability to bind directly with DNA, chromatin immunoprecipitation (ChIP) or ChIPseq would provide such specificity. Of interest would be to analyze antibodies specific for acetylation or methylation of H3K9, H3K27, and H3K4. These studies have been initiated with our collaborators at the University of Florida (Dr. David Bloom). The antiviral studies are also limited by the absence of *in vivo* animal data and testing for antiviral effects on other viruses *in vitro*. Given their potent antiviral activity and favorable toxicity profile, such studies are warranted. To further elucidate their spectrum of effect, *in vitro* testing of these compounds for antiviral activities for other viruses would be beneficial.

In Aim 2, the effect of dissociating the neuronal cells prior to seeding them on 384 well plates is a serious limitation. Treatment with accutase breaks the neurite connections in the neuronal network. The 7-day recovery time does result in the growth and reconnection of these structures; however, it is unknown how the accutase treatment affects the neuronal network that is re-established. This may be due to the period of time from the beginning of neuronal differentiation to cell seeding into the 384-well plates. Neuronal cultures that remained in the 6-well plates for greater than 8 weeks were variable; these cultures were more difficult to dissociate, leading to more forceful pipetting to obtain single-cell suspensions. Additional characterization of non-neuronal cells in these cultures will be informative.

In addition, we are testing how we can make the readout more accurate. To directly test compounds that reduce viral reactivation, an alternative infection method could be utilized.

Following HSV-1 infection on iPSC-neurons, novel compounds would be added for a specified time (perhaps 2 to 3 days), and then removed. Fresh, drug-free medium would be added to the cells for a specified time (perhaps 5 to 7 days) and then analyzed for reduction in EGFP fluorescence. For this type of experiment, one could use a compound that has known effects on reducing viral reactivation, like compound R430.

Thus, several additional studies are needed to enable an increased throughput for future drug screening campaigns. Such studies are worthwhile not only to identify antiviral drugs for HSV-1 infections, but also because the iPSC-neuron based models could be used for drug screens against other viruses, to model infections in individuals with specific genomic changes, and indeed for patient-specific personalized medicine.

6.0 FUTURE DIRECTIONS

6.1 FURTHER INVESTIGATIONS OF THE LATENCY MODEL

As noted in the results related to Aim 1, it is difficult to resolve the status of cells in the latency model that apparently show fluorescence during the initial days of incubation with the antiviral drug cocktail. Therefore, further clarity could be obtained by single cell analysis, while inducing latency in a heterogeneous population of cells that are comprised of both neuronal cells and non-neuronal cells. It should be feasible to identify and analyze single cells in culture through laser capture dissection and single cell analysis of the transcriptome and proteome. Separately, further analysis of the patterns of heterochromatin and understanding of the mechanisms for viral gene silencing in the latency model would be instructive. Previously, investigators who used chromatin immunoprecipitation (ChIP) showed an enrichment of trimethylated H3K9 or H3K27 with promoter regions of viral lytic genes during latency. It would be informative to conduct similar ChIP experiments. Several miRNAs are expressed during HSV-1 latency; future work to quantifying such entities in this model of latency would be desirable. Applying this model of latency to 3-dimensional iPSC-neuronal cultures may lead to a more superior model, which may also be beneficial for future work in drug discovery.

6.2 MODIFICATIONS IN THE DRUG SCREENING PROTOCOL

We plan to follow up the small scale antiviral studies by developing more efficient methods for identifying larger numbers of compounds that target latent infection – including derivatives of current lead compounds, as well as small molecule screening libraries. Further modifications in the 'readout' for determining efficacy against latent infections are also needed. Third, it will be important to use strains resistant to acyclovir in these screens.

6.2.1 Primary Moderate Throughput Screen For Antiviral Drugs Against HSV-1 in iPSC-Neurons

Based on our preliminary data for the initial primary anti-lytic screening, we would infect iPSC-neurons in the 384-well plates at an MOI=5.0 for a 2-hours. The cell culture medium will be removed and cells washed with PBS, and then medium containing novel compounds will be added. This can be accomplished using multichannel pipettes or Hydra liquid transfer machines. Cells will be analyzed after 48 hours to test HSV-1 anti-lytic effect. The HSV-1 viral construct that we employed in our initial experiments express fluorescent reporter genes, EGFP and RFP, under the control of viral promoters. The primary readout will be reduction in cells expressing EGFP as compared to vehicle-treated cells. We propose an initial compound library such as the Library of Pharmacologically Active Compounds collection (LOPAC®^{1280}; Sigma, catalog LO1280-1KT), which includes 1,280 small molecules. We will examine each compound at three concentrations (50 µM, 10 µM, and 1 µM) during the primary screen. Known antiviral acyclovir (ACV 50 µM) or viral DNA inhibitor phosphonoacetic acid (PAA 300 µg/ml) will be included as controls and pretreated as previously described (McClain et. al., 2015). Subsequently, we will

analyze other compound libraries available through the Drug Discovery Institute of the University of Pittsburgh and Dr. James McNulty, Ph.D. from McMaster University.

The lead compounds that inhibit lytic infection with similar or greater potency than ACV will undergo a second screening at a range of concentrations ranging from 100 nM to 250 μM in a ten-point IC50 curve (the drug concentration that reduce the number of EGFP-positive cells by 50%). Furthermore, the CC50 (the concentration that reduce cell viability by 50%) curve will be determined. Cells will be imaged using the ImageXpress Ultra (IXU) High Content imager and analyzed with Multiwavelength Cell Scoring application within the MetaXpress software. The therapeutic index (TI) will be calculated [(CC50/IC50) * 100%]. Compounds with a high antiviral effect and low cytotoxicity (TI > 100) will be selected for secondary analyses and considered a lead or "hit" molecule.

6.2.2 Secondary Analysis of Antiviral Effects Following Lead Hit Analyses

Once a lead hit compound(s) is identified against lytic infection, further analyses will be performed to assess the extent of the antiviral effect in a low- or moderate throughput manner. We will employ secondary, orthogonal studies to further confirm the antiviral activity, as well as provide insights into potential mechanisms of action. Orthogonal studies (Table 4) will address the following questions when comparing vehicle-treated cells with the compound-treated cells:

Table 4. Secondary studies to confirm antiviral activity.

Does the compound inhibit the production of infectious virions?	Productive infection will be analyzed by Vero plaque assay.
Can the compound inhibit HSV-1 reactivation?	Quiescently infected cells will be treated with the test compounds for 48 h, followed by exposure to NaB, TSA, and PI3Ki for 5 days. Reactivation will be investigated by flow cytometry and 3D FISH.
What is the extent of viral reduction following exposure of infected cells to test compounds?	Viral DNA copy number will be estimated by qPCR.
Is there a reduction in viral gene expression?	Expression of viral genes will be investigated by RT-qPCR, immunocytochemistry, and Western blotting.
Is there a change in the state of viral chromatin?	Changes in the chromatin state will be evaluated by CHART-PCR, Co-ICC/FISH, and ChIP.

7.0 CONCLUSIONS

Herpes simplex virus, type 1 (HSV-1) is a common human pathogen that causes life-long latent infection, with recurrent cycles of reactivation that lead to immense public health burden. HSV-1 can cause productive (lytic) infection in virtually any type of cell in humans and other mammals; but by definition, latent HSV-1 infections is restricted to human neurons. The advent of induced pluripotent stem cell (iPSC) technologies provides us with the ability to differentiate human iPSCs into large numbers of neuron like cells that we call iPSC-neurons. In this thesis, iPSC-neurons were used to model lytic and latent HSV-1 infection, and for drug discovery.

We generated neural stem cells/early neural progenitor cells (NSC/eNPCs) in 6-well culture plates. The method also produced non-neuronal cells that could be eliminated. The NSC/eNPCs express neural stem cell-specific markers and can be differentiated into iPSC-neurons that also express functional ligand-gated channels, pre- and post-synaptic proteins, and intracellular proteins specific to human neurons. Thus, we developed relatively homogenous cultures of iPSC-neurons that share many properties of human neurons.

HSV-1 lytic and latent infections were modeled in human iPSC-derived neural precursors and neurons, using an HSV-1 construct with dual fluorescent promoter readouts. HSV-1 caused lytic infection in both types of cells. Only in the human iPSC-neurons were we able to maintain ‘quiescent’ infection with HSV-1 when co-incubated with an antiviral drug combination. The latency associated transcript (LAT), an indicator of latent infection, was expressed during the

quiescent infection. Even after withdrawal of the antiviral compounds, quiescence was maintained in most cells for five days, though some cells continued to show lytic infection from the first day. Reactivation of quiescently-infected iPSC-neurons was also induced by co-incubation with sodium butyrate, a histone deacetylase inhibitor. In addition, copy number analysis and viral genome patterns in the FISH experiments were consistent, as well as levels of infectious virions in the cell supernatants. Quiescence could not be induced in iPSC-neurons with a replication defective HSV-1 construct.

Previous reports indicate heterochromatization of viral DNA during latency; therefore, a protein associated with heterochromatin was evaluated during HSV-1 quiescent infection. Co-localization was not observed in Vero cells with lytic infection, but the pattern observed in iPSC-neurons is consistent with predictions of latency; further analysis is needed. Viral gene promoters were quantified for nuclease accessibility during lytic and quiescent infections in iPSC-neurons. Viral genes transcribed during acute infections were more accessible to nuclease degradation, with the exception of ICP4. LATs were more accessible to nuclease degradation during quiescent infections, as expected. These data could indicate transcriptional permissiveness with loci that have greater nuclease accessibility. If lytic genes are found to be heterochromatic during the quiescent infection, previously published criteria for HSV-1 latency will be satisfied. Thus, the quiescent infection resembles the majority of classical criteria for latent infection, but further optimization of this model is necessary.

The aforementioned HSV-1 infection models were used to investigate antiviral effects of novel compounds. Four compounds had potent antiviral effects on lytic HSV-1 infections in iPSC-neurons, with minimal cytotoxicity. Viral copy number was significantly reduced, and FISH experiments provided data consistent with this conclusion. The compounds decreased

viral reactivation induced by HDAC inhibitors in iPSC-neurons. Further, two compounds (4F17 and R430) inhibited productive infection during viral reactivation from quiescence. These compounds also inhibited acute varicella zoster virus (VZV) infection with greater potency than acyclovir while causing minimal host cell cytotoxicity; 4F17 inhibited human cytomegalovirus also. The mechanism of action is unknown, but it is likely that they have several effects.

We next scaled up our drug screening efforts. iPSC-neurons were cultured in 96- and 384-well culture plates. The cultured cells showed lytic and quiescent infection with HSV-1; the latter could be reactivated. We evaluated viral infection using two assays. Further methods for each hit compound identification are outlined.

In summary, iPSC-neurons can be used to model lytic and latent HSV-1 infections. These models are suitable for moderate throughput screening of compounds for neurotropic viruses or neurological diseases.

APPENDIX A: SUPPLEMENTAL INFORMATION FOR "LARGE-SCALE GENERATION OF HUMAN IPSC-DERIVED NEURAL STEM CELLS/EARLY NEURAL PROGENITOR CELLS AND THEIR NEURONAL DIFFERENTIATION"

Cryopreservation of iPSCs

Aspirate mTeSR1™ medium from 50-60% confluent 6-well plate culture wells. Add 1 ml of fresh mTeSR1™ and place the plate under the microscope. Eliminate the differentiated areas from colonies by scraping with a pipette tip. Aspirate the medium and wash twice with 2 ml of DMEM/F12. Add 1 ml/well of mTeSR1™ and cut iPSC colonies as described in 1(ii). Take an aliquot, dissociate cell clumps by digestion with accutase, and count viable cells using trypan blue. Pellet the cells by centrifugation at 1200 rpm for 5 min. Discard the supernatant and shake the pellet gently by flicking. Re-suspend the cells in CryoStore freezing solution to a density of $4x10^6$ cells/ml. Aliquot 500 µl of cell suspension in cryovials, place in alcohol-free cell freezing containers (CoolCell®) and transfer immediately at -80°C. The following day, transfer cryovials to a -135°C freezer or into liquid nitrogen containers.

NOTE: To improve post-thaw recovery, transfer cryovials to -80°C within 3-5 minutes after re-suspending iPSCs in freezing solution.

Cryopreservation of NSCs/NPCs

Aspirate NP expansion medium and rinse with DMEM/F12. For 6-well cultures, add 1 ml of StemPro Accutase per well and incubate for 3 min at 37°C. Add 2 ml of DMEM/F12 medium

and gently detach cells by pipetting up and down with a p1000 tip. Count viable cells using trypan blue. Pellet the cells by centrifugation at 1200 rpm for 5 min. Discard the supernatant and disturb the pellet by flicking. Re-suspend the cells in CryoStore freezing solution to a density of $4x10^6$ cells/ml. Aliquot 500µl of cell suspension in cryovials, place in alcohol-free cell freezing containers (CoolCell®) and transfer immediately to -80°C. On the following day, transfer cryovials to a -135°C freezer or into a liquid nitrogen cylinder.

Thawing NSCs/NPCs

Take a cryovial from freezer storage and clean the surface by spraying with 70% ethanol. Transfer 5 ml of ice-cold DMEM/F12 medium into a 15 ml conical tube. Remove the cap from the cryovial and break the frozen cell suspension by making pressure from the top with 1 ml or 5 ml plastic pipette (this procedure allows a quick transfer of frozen cells into the culture medium, that ensures a high cell recovery). Add 500 µl of cold DMEM/F12 medium and transfer all the content of the vial to the 15 ml conical tube. Centrifuge at 1200 rpm for 5 min. Discard the supernatant, wash the cells with 2ml of DMEM/F12 medium, re-suspend the cells in 8 ml of mTeSR1™ medium, and then seed 2 ml cell suspension/well in a matrigel-coated 6-well plate. Culture until the cells are confluent, changing the medium every other day.

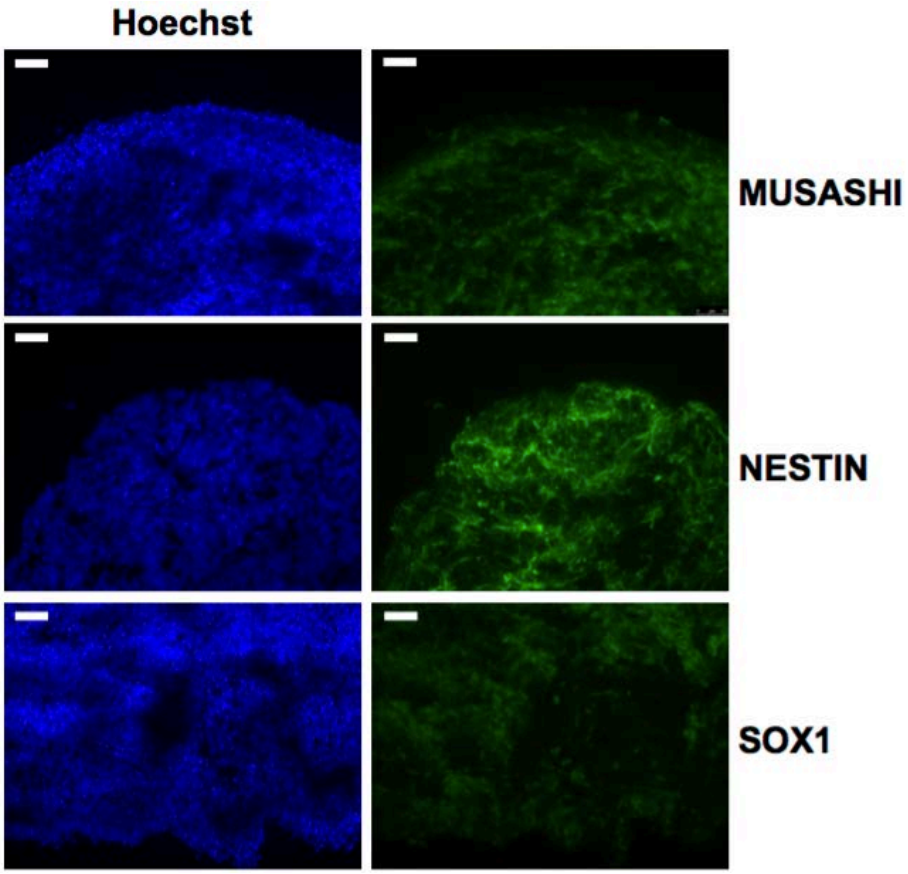

Figure 49. Immunocytochemical analysis of NLSs. Scale bar is 50 µM.

APPENDIX B: SUPPLEMENTAL INFORMATION FOR "PERSISTENT INFECTION BY HSV-1 IS ASSOCIATED WITH CHANGES IN FUNCTIONAL ARCHITECTURE OF IPSC-DERIVED NEURONS AND BRAIN ACTIVATION PATTERNS UNDERLYING WORKING MEMORY PERFORMANCE"

Immunocytochemistry and Microscopy

Immunocytochemistry was performed as previously described (D'Aiuto, et al., 2008). Primary antibodies used were mouse anti-β Tubulin III monoclonal antibody (clone Tuj-1, R&D System, 1:50 dilution), mouse monoclonal anti-MAP2 (Millipore, dilution 1:200), mouse monoclonal anti-human nestin antibody (R&D Systems, 1:1000 dilution), rabbit polyclonal anti-VGLUT1 antibody (Synaptic Systems, 1:200 dilution), and rabbit polyclonal anti-S100 beta antibody (Abcam, 1:200 dilution). Fluorescently labeled secondary antibodies were used for detection. Counterstaining was done with Hoechst 33342. Images were acquired using a Leica IL MD LED inverted fluorescence microscope and a LEICA DM5500 B fluorescence microscope.

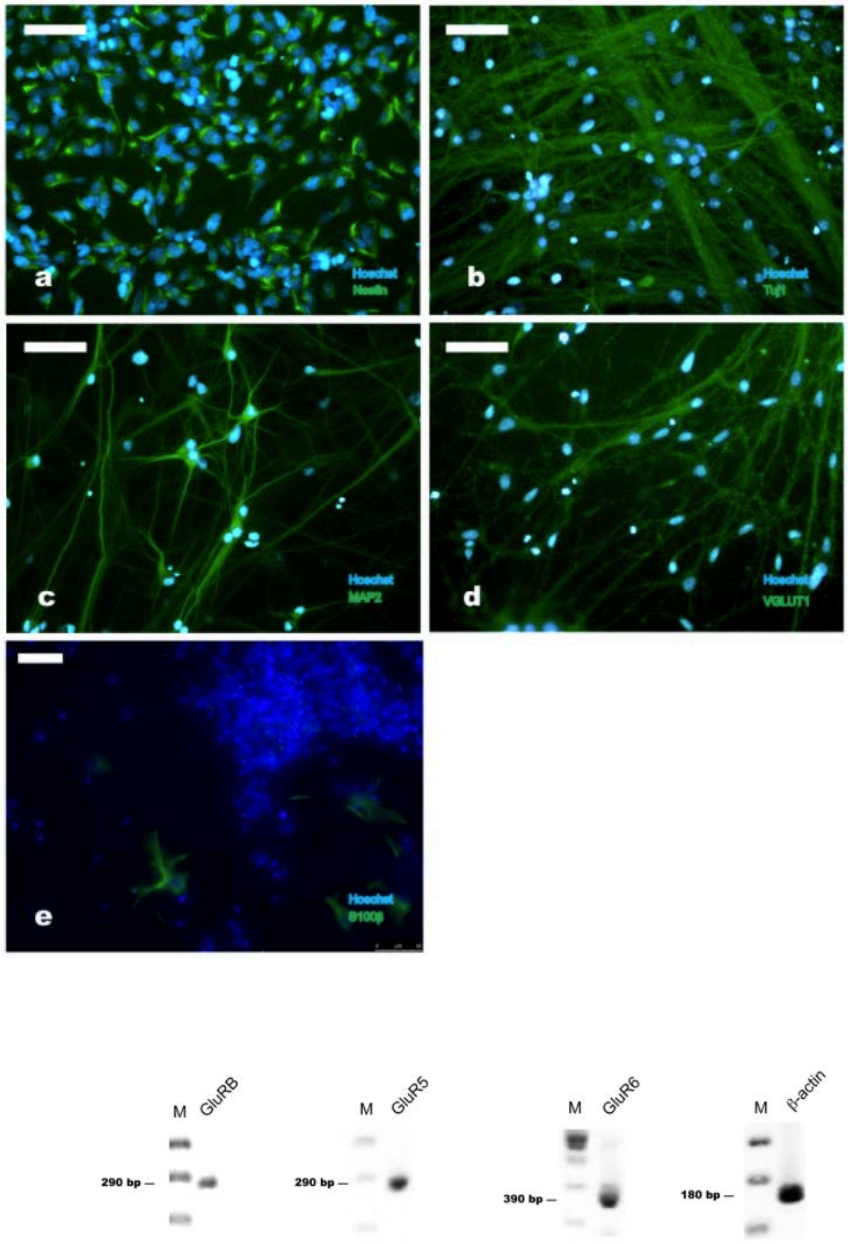

Figure 50. ***Top panel:*** **Immunocytochemical analysis of iPS-derived neural progenitor cells (a), neurons (b-d), and astrocytes (e).**

Bottom panel: Expression of glutamatergic receptors in iPSC-derived neurons. RNA was prepared iPSC-derived neurons. Total RNA was converted into cDNA, which was used as a template to PCR-amplify edited regions of glutamatergic receptors GluRB, GluR5, and GlurR6. Scale bar is 50 μm.

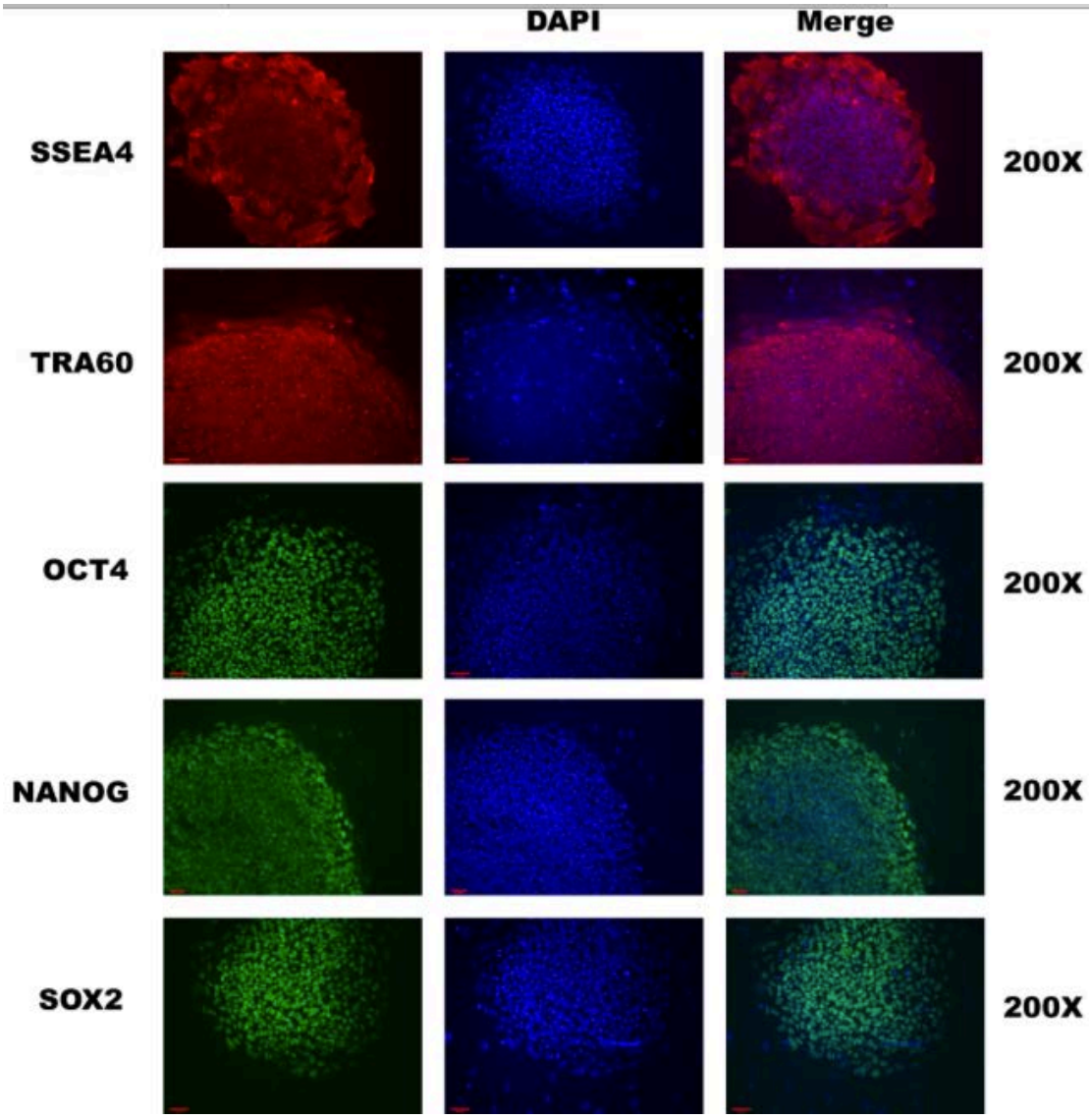

Figure 51. Expression of pluripotency markers in 5404 iPSC cell line by immunocytochemistry.

Movie a:

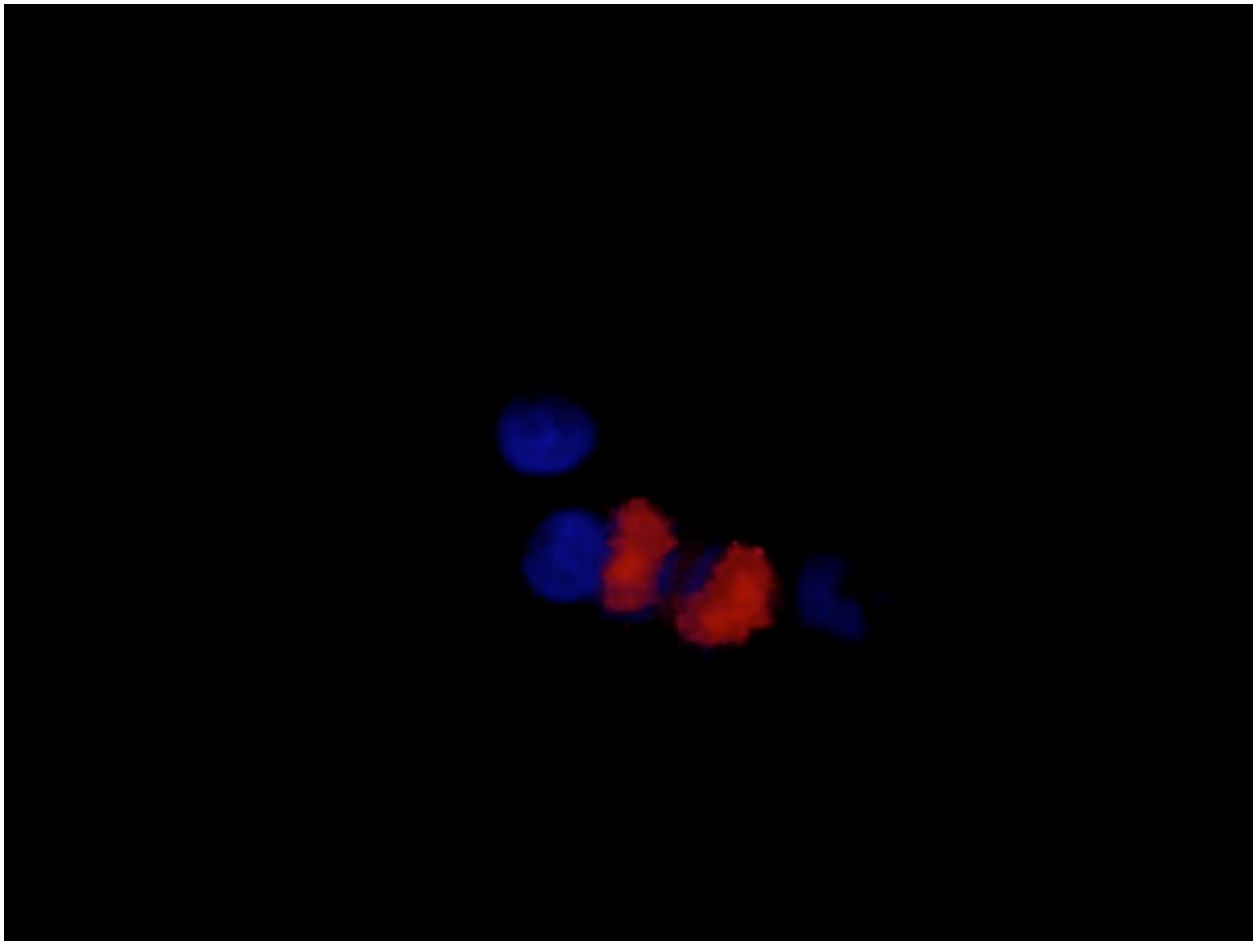

Movie b:

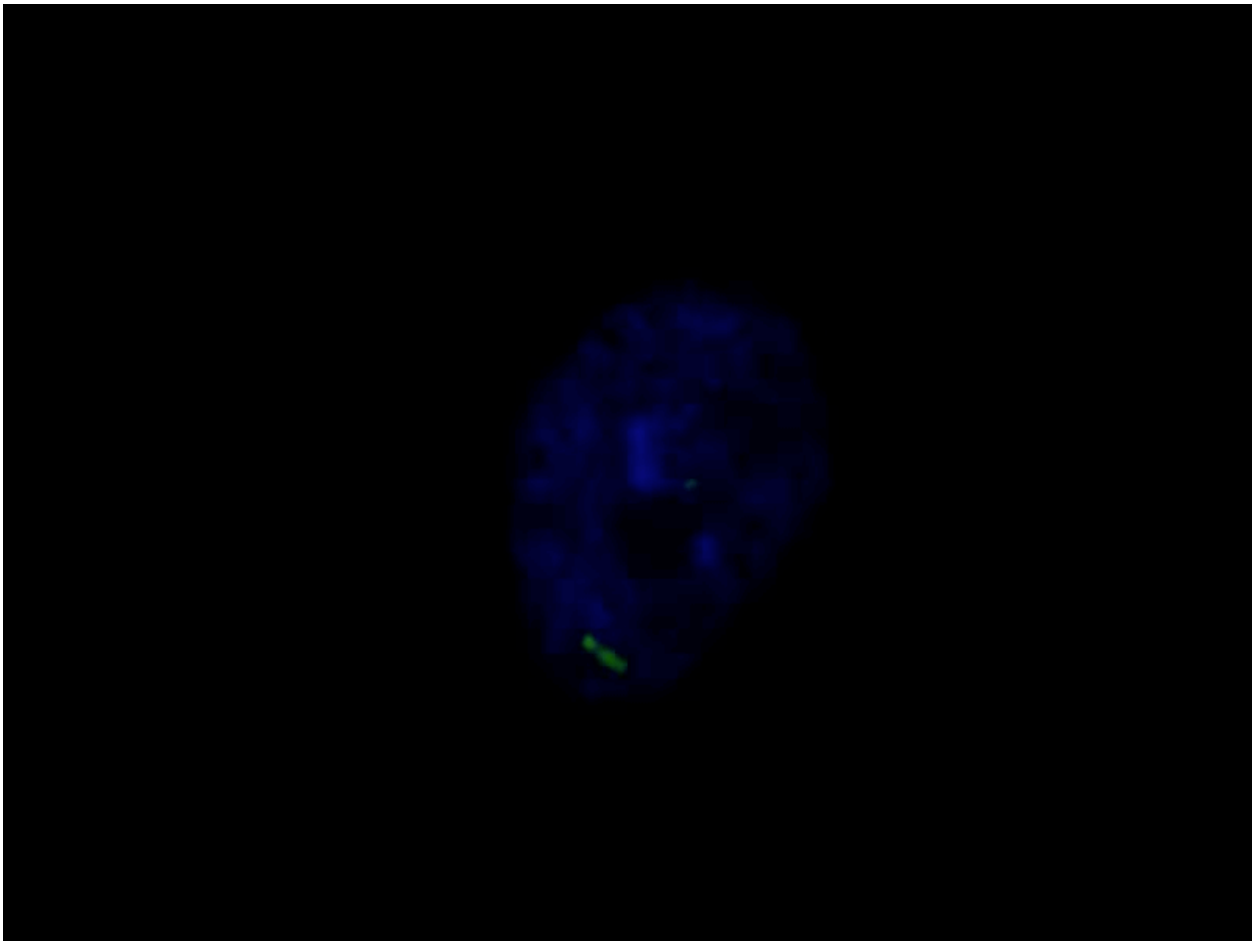

Figure 52. Location of HSV-1 genomes in neurons with (a) lytic and (b) quiescent infection.

iPSC derived neurons underwent lytic or quiescent infection in the absence or presence of 5BVdU +IFN-α as described (MOI 0.3). Cells were fixed to preserve the three-dimensional structure of the nuclei and probed using the entire HSV-1 genome. Signal specificity was assessed through FISH analysis of uninfected neurons (data not shown). Cells were probed at 24 h p.i for lytic infection. The probe signal is pseudo-colored in red in the merged images, with DAPI counterstaining.

APPENDIX C: SUPPLEMENTAL INFORMATION FOR "BROAD-SPECTRUM NON-NUCLEOSIDE INHIBITORS OF HUMAN HERPESVIRUSES"

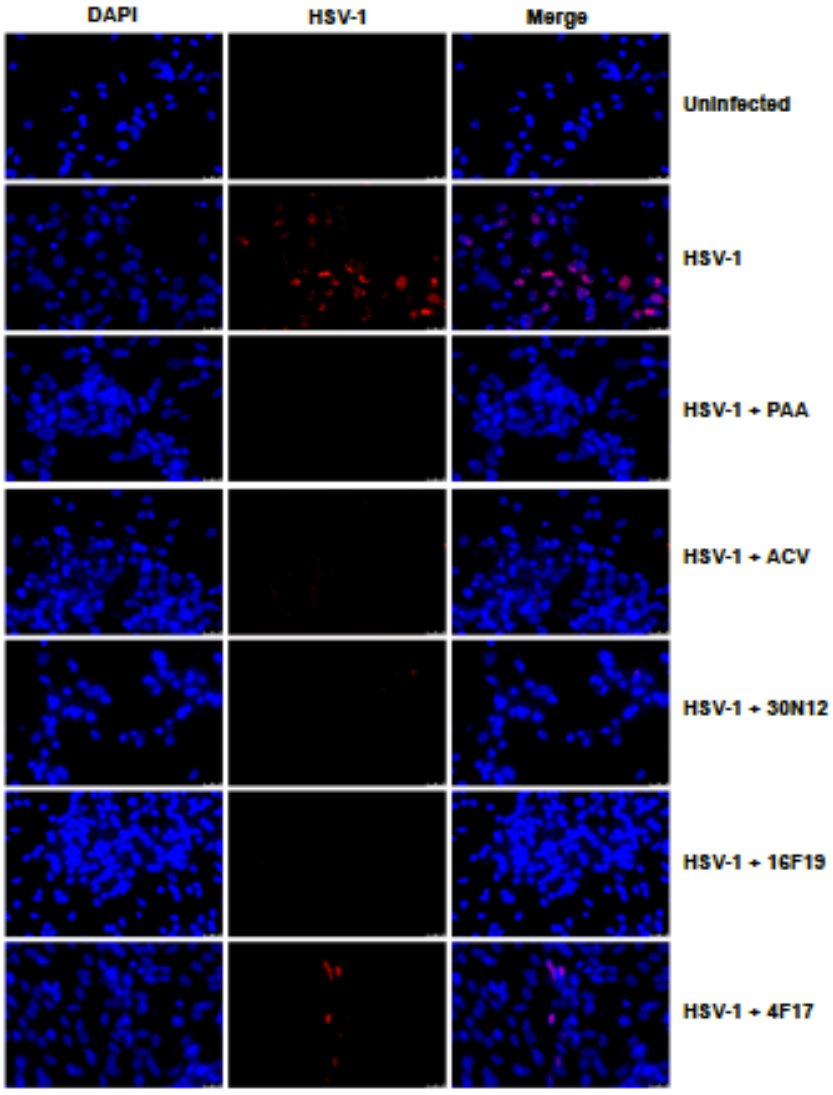

Figure 53. Analysis of HSV-1 genome in iPSC-neurons infected for 24 h in the presence or absence of test compounds.

FISH was performed on iPSC-neurons infected with HSV-1 (KOS strain, MOI 0.3) as previously described (D'Aiuto, Antonacci, Marzella, Archidiacono, & Rocchi, 1993), using the HSV-1 genome as a probe. HSV-1 genome was labeled with red-dUTP (0.2 mM; Abbott), by nick translation (Amersham™ Nick Translation Kit (GE Healthcare), both following manufacturer's instructions. On average, 100 nuclei from each cellular preparation were scanned. Digital images were generated using Leica LAS AF. Hybridization signals (red) were subjected to uniform thresholding to demarcate the signals. In infected, untreated cells, numerous hybridization signals for viral DNA probes were present in the central region of the nuclei, whereas the host chromatin (blue) was displaced toward the nuclear periphery. In contrast, viral DNA could not be detected in infected cultures treated with 30N12 and 16F19, similar to ACV or PAA. Hybridization signals were observed in a small fraction of infected neuronal cultures treated with 4F17. Nuclei were counterstained with DAPI (blue). ACV: acyclovir, PAA: phosphonoacetic acid.

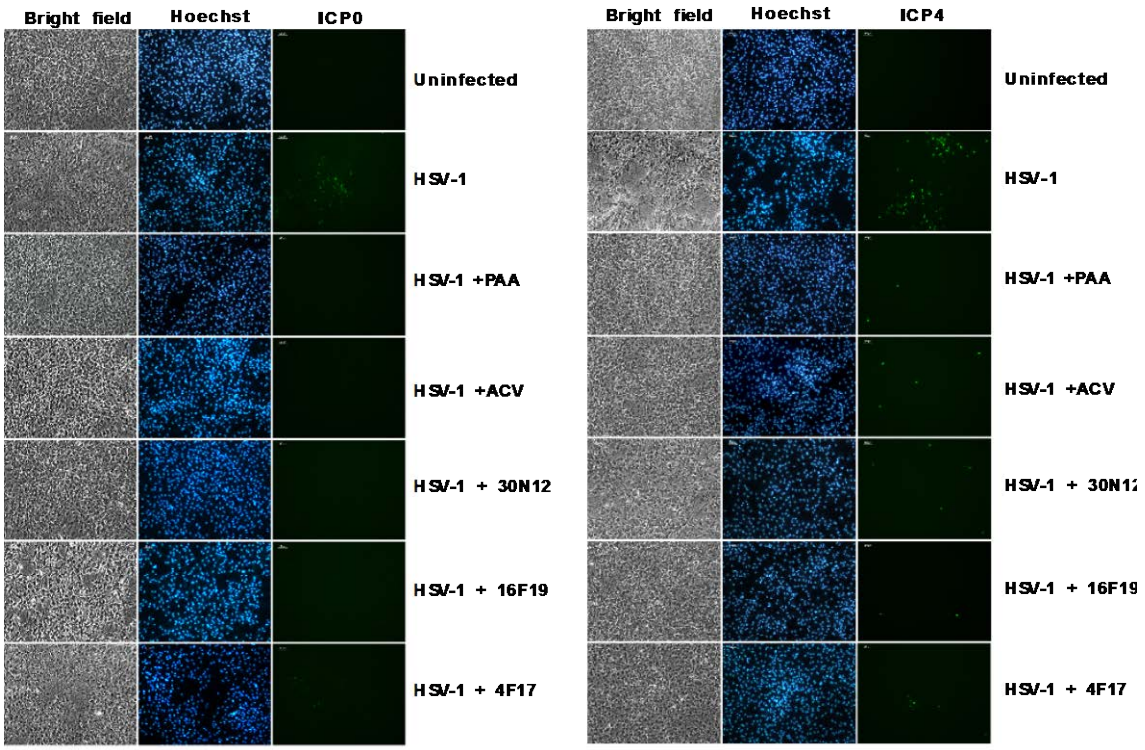

Figure 54. Immunocytochemistry analysis of uninfected and infected iPSC-neurons with ICP0 (green, left panel) and (b) ICP4 (green, right panel).

Immunocytochemistry was performed as previously described (D'Aiuto et al., 2008) following a 24 h infection protocol.

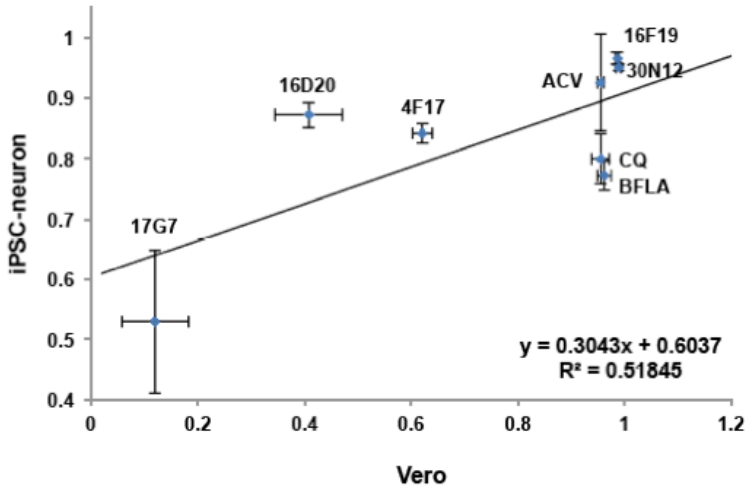

Figure 55. Correlation of drug inhibition effects on acute HSV-1 infection in Vero cells and iPSC-neurons.

Antiviral effects of the aforementioned compounds on acute HSV-1 infection show a moderate correlation when comparing the mean percent EGFP+ cells in iPSC-neurons and Vero cells (p=0.044, r=0.72, 95% CI 0.031-0.945). Error bars indicate the 95% confidence intervals of mean percent EGFP+ cells for each compound; vertical bars in iPSC-neurons and horizontal error bars in Vero cells. Specified drug concentrations are 50 µM, except BFLA, which is 0.1 µM.

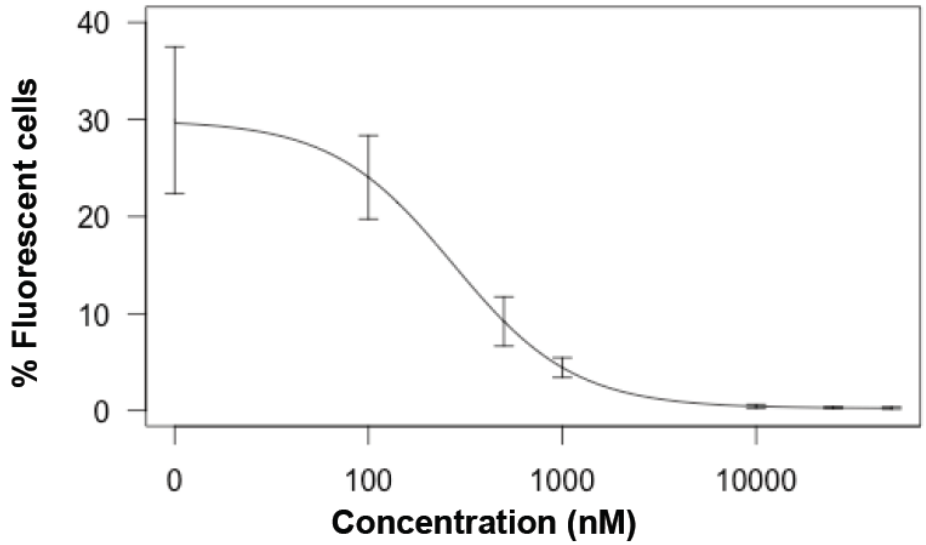

Figure 56. Dose response curve of Acyclovir on HSV-1 lytic infection.

Efficacy of varying drug concentrations against HSV-1 lytic infection in iPSC-neurons; FC performed 24 hpi. The data represent an average of three independent experiments. Error bars represent model-based standard error.

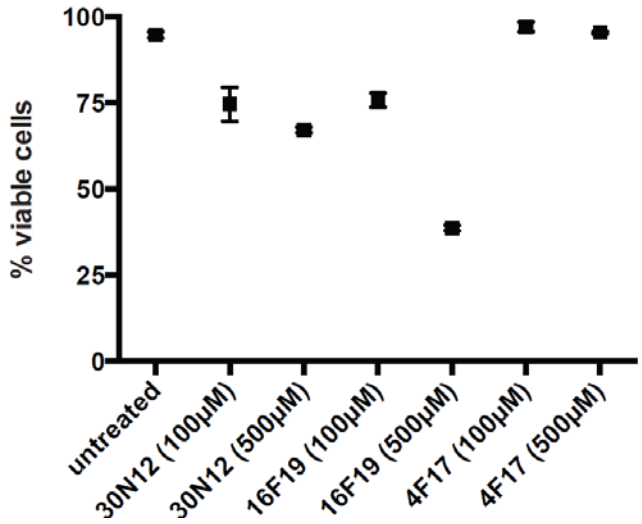

Figure 57. Cytotoxicity of 30N12, 16F19, and 4F17 in iPSC-neurons.

Neurotoxicity of 30N12, 16F19, and 4F17 was assessed by FC using fixable viability dye. The data represent an average of three independent experiments. Error bars represent standard deviations.

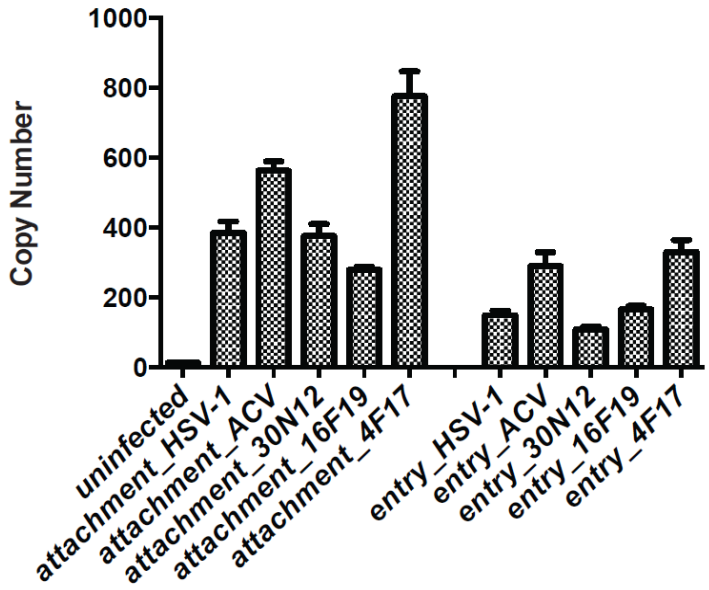

Figure 58. Analysis of drug inhibition effect on HSV-1 attachment and entry.

We tested effects on HSV-1 attachment to the host cell membrane, as well host cell entry using a published protocol (Krepstakies, et al., 2012, J Infect Dis. 205:1654-64).

Cell attachment: Vero cells were pre-treated with each compound or vehicle for 1 hour at 37°C. Cells were next infected with HSV-1 (MOI 1.0) and incubated on ice for 2 hours. This procedure likely enables attachment, but prevents viral entry. Cells were collected after the 2 hours infection on ice. DNA was extracted, and viral copy number was estimated by qPCR. We observed no statistically significant reduction in viral DNA copy number in cells treated with the different compounds compared to the untreated HSV-1 group.

Cell entry: Vero cells were pre-treated with each compound or vehicle for 1 hour at 37°C. Cells were then infected with HSV-1 (MOI 1.0) and incubated on ice for 2 hours. The inocula were removed, the Vero cells were washed, and cultured in Vero medium supplemented with compounds/ vehicle for 1 hour at 37°C to enable viral particles to enter the cell. To remove residual viral particles attached to the cell membrane, proteinase K (2 mg/ml) was added to the culture, and cells were incubated on ice for 1 hour. Next, protease inhibitor cocktail (1mM) was added to the cultures, and cells were harvested. Total DNA was extracted, and viral copy number was estimated by qPCR. There was no statistically significant reduction in viral DNA copy number observed in cells treated with the different compounds compared with the untreated HSV-1 group.

APPENDIX D: SUPPLEMENTAL INFORMATION FOR "IPCS NEURONAL ASSAY IDENTIFIES AMARYLLIDACEAE PHARMACOPHORE WITH MULTIPLE EFFECTS AGAINST HERPESVIRUS INFECTIONS"

Biological Assays

Cell lines and viral constructs

Human skin fibroblast line 73-56010-02 was reprogrammed into induced pluripotent stem cells (iPSC) using Sendai viral vectors, quality control assays were performed, and the iPSCs were further differentiated into iPSC-neurons as previously described (D'Aiuto, et al., 2012; D'Aiuto, et al., 2014). Vero and human retinal pigmented epithelial cells (ARPE-19) were maintained in Dulbecco's modified essential medium/F12 (DMEM/12) supplemented with 10% FBS (Hyclone) and 5% antibiotic/antimycotic (HyClone). HSV-1 strain KOS (VR-1493; ATCC) was utilized. A separate strain of KOS was modified to express EGFP and RFP under the control of viral promoters ICP0 and glycoprotein C, respectively (Ramachandran, et al., 2008). VZV derived from an infectious Bacterial Artificial Chromosome of the whole genome of the Parent of Oka strain expressing firefly luciferase as a fusion to the ORF9 promoter at the native locus was described previously (Bayer et al., 2015).

Viral infection

Vero and iPSC-neurons were infected with the HSV-1 at a multiplicity of infection (MOI) of 1.0 or 0.3 PFU/cell, respectively. Two hours post infection (hpi), the inocula were

removed, infected Vero cells or iPSC-neurons were washed twice with PBS, and cultured with the appropriate media with or without indicated compounds. Control cultures were pretreated with ACV (50 uM) for 24 h prior to infection (Joubert et al., 2009). All assays were conducted 24 hpi.

HSV-1 quiescent infection was established in iPSC-neurons using (E)-5-(2-bromovinyl)-2'- deoxyuridine and interferon alpha (5BVdU+IFNα; 30 μM, 125 U/ml, respectively) for 7 days, followed by treatment with sodium butyrate (NaB, 5 mM) for 5 days to induce viral reactivation (D'Aiuto, 2014). Separately, 5BVdU+IFNα were replaced with 7 (10 μM) or 7+IFNα (10 μM, 125 U/ml, respectively).

ARPE-19 cells were infected at a density of approximately 1.5x10^5 cells/well with VZV at 1000 PFU/well. Following 2 h adsorption, fresh medium containing indicated compounds was added. Viral inhibition was determined 48 hpi.

Flow Cytometry (FC)

Cells were trypsinized and resuspended in PBS containing Live/Dead® Fixable Aqua Dead Cell Stain kit (Life Technologies) 24 hpi with HSV-1/EGFP/RFP construct, following manufacturer's instruction. Cells were fixed in 4% formalin. The proportion of live cells and cells expressing EGFP and RFP was determined by FC (Fortessa FACS analyzer, Becton Dickinson).

Cytotoxicity assays

Human iPSC-neurons or ARPE-19 cells were treated with stated concentrations of 7 or ACV for 24 h or 48 h, respectively, and the proportion of live cells was measured by FC using Live/Dead® Fixable Aqua Dead Cell Stain kit following manufacturer's instruction.

Fluorescent *in situ* hybridization (FISH)

FISH was performed using probes generated from whole genome HSV-1. The HSV-1 genome (strain KOS) was amplified using Illustra GenomiPhi V2 amplification kit (GE Healthcare) and labeled with red-dUTP (0.2 mM; Abbott), by nick translation (AmershamTM Nick Translation Kit (GE Healthcare), following manufacturer's instructions. Human iPSC-neurons were infected with HSV-1 strain KOS at MOI 0.3 as described above and fixed 24 hpi. FISH was performed as previously described (D'Aiuto et al., 1993). On average, 50 nuclei for each cellular preparation were scanned. Digital images were obtained using Leica LAS AF with uniformed thresholding.

Copy number PCR (qPCR)

Human iPSC-neurons were infected with HSV-1/EGFP/RFP construct for 24 h, followed by total DNA extraction (QIAamp DNA Blood Mini Kit; Qiagen) and quantification (Quant-iT TM PicoGreen® ds DNA Assay Kit; Life Technologies) following the manufacturer's instructions. Copy number qPCR was performed as previously described (Kaufman et al., 2005) using 5 ng total DNA. EGFP forward primer (18 μM; 5′- ccacatgaagcagcacgactt-3'), EGFP reverse primer (18 μM; 5′-ggtgcgctcctggacgta-3′), and probe (5 μM; 5′- 6FAM-ttcaagtccgccatgcccgaa-TAMRA-3′) were used in the probe mix. The reaction conditions were 95°C for 3 min, followed by 45 cycles of 95° C for 15 sec and 55° C for 30 sec, and finished with 72° C for 30 sec. qPCRs were performed on a 7900HT Fast Real-Time PCR System (Applied Biosystems) and analyzed with manufacturer's software SDS 2.4.

Western blotting

Human iPSC-neurons were infected with HSV-1 (strain KOS), and cells were lysed 24 hpi with 10 volumes of RIPA (25 mM Tris–HCl pH 7.6,150 mM NaCl, 1% NP-40, 1% sodium

deoxycholate, and 0.1% SDS). Cell lysates were denatured by heating at 95°C and then separated by electrophoresis on Mini-PROTEAN@ TGXTM Precast gel (BIO-RAD), transferred onto an immobilon membrane (Millipore), and probed with mouse monoclonal HSV-1 ICP4 primary antibody [10F1] (Abcam (ab6514), 1:500 dilution). The blots were then probed with corresponding secondary antibody (Li-Cor) and visualized by using ClarityTM Western ECL substrates (BIO-RAD).

RT-qPCR

Human iPSC-neurons were infected with HSV-1 (strain KOS). Cells were collected 24 hpi and RNA was extracted using using RNeasy mini kit (Qiagen) followed by cDNA synthesis using QuantiTect Reverse Transcription kit (Qiagen) following manufacturer's instructions. A separate round of cDNA synthesis was made on RNA in a reaction that lacked the enzyme. RT-qPCR was performed as previously described in triplicate (Liu et al., 2015). The reaction conditions are: 95°C for 12 min, followed by 40 cycles of 95°C for 15 sec and 55°C for 1 min. Each reaction analyzed beta actin for normalization and the relative expression of viral transcripts ICP4 and viral DNA polymerase was calculated using the 2-ΔCt method (Livak et al., 1999). The sequences used for ICP4 are as follows: forward primer 5'-CGA CAC GGA TCC ACG ACC C-3', reverse primer 5'-GAT CCC CCT CCC GCG CTT CGT CCG-3', and probe 5'-VIC-ACC GCC AGA GAC AGA CCG TCA GA-MGB-NFQ-3'. The sequences used for HSV-1 DNA polymerase are as follows: forward primer 5'- AGA GGG ACA TCC AGG ACT TTG T-3', reverse primer 5'- CAG GCG CTT GTT GGT GTA C-3', and probe 5'-FAM- ACC GCC GAA CTG AGC A-MGB-NFQ- 3'. Human beta actin endogenous control probes are TaqMan ready-mix (NM_001101.2) that span exons 2 and 3 (Applied Biosystems).

Virus Yield Reduction Assay

In the HSV-1 infected cultures, supernatant was reserved just prior to cell collection for flow cytometry analyses. Confluent Vero cell monolayers in 6-well plates were infected with 10 microliters of the aforementioned supernatant in 1 mL Vero medium in triplicate. Following a 2-hour adsorption at room temperature, the medium was removed, washed twice in PBS, and replaced with 3 mL of 1% carboxy methylcellulose in Vero medium. Cultures were incubated at standard cell culture conditions for 48 hours. The mean plaque count for each condition was calculated and the mean infective titer was generated.

Statistical Analyses

Statistical analyses were conducted using the open source software R statistical package version 3.0.1, IBM SPSS v21, and GraphPad Prism v5.02. The EC50 (drug concentrations that reduced the percentage of EGFP+ cells in HSV-1 infected cultures by 50% or reduced the LCPS in the VZV-infected cultures by 50%) was estimated using the R program with the drc package (http://cran.r- project.org/web/packages/drc/drc.pdf; version 2.3–96). We first assessed model fit using an F-test by comparing to an ANOVA model. We chose a 4 parameter, log logistic model that provided the best fit to the data (results not shown). Statistical significance was calculated by first testing for equality of variance using Levine's test, where two-tailed Student's t-tests (where variances were not significantly different at $\alpha < 0.05$) or Welch's t-tests (where variances were significantly different at $\alpha < 0.05$) were conducted. Data used represent three independent experiments.

Supplemental Figures from the journal article

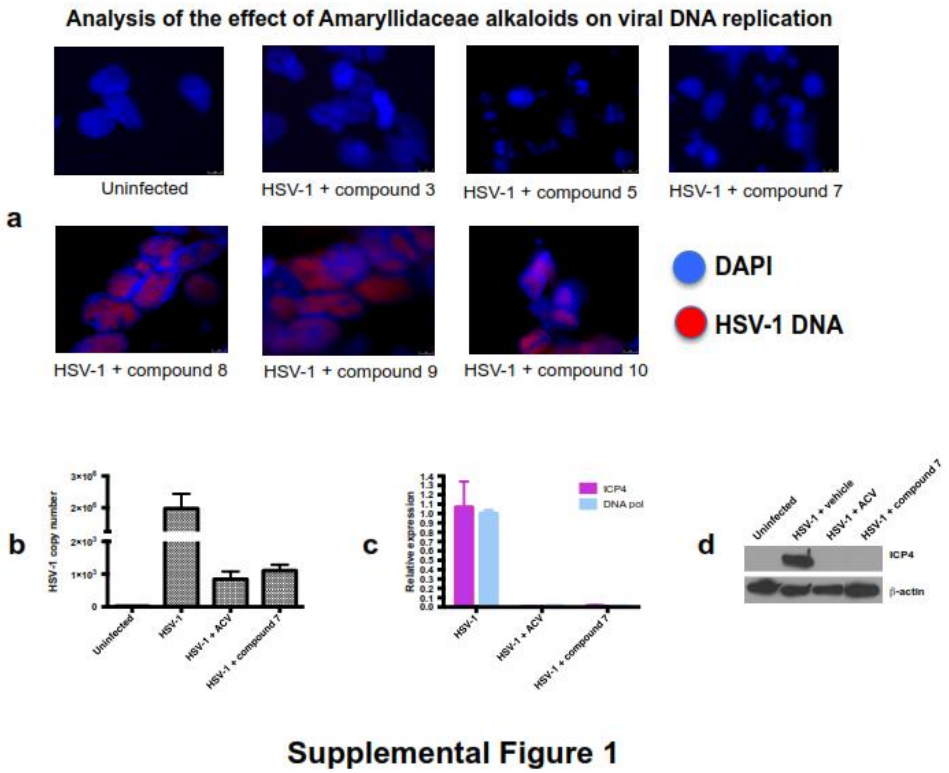

Figure 59. Supplemental Figure 1.

a) Detection of HSV-1 genome (red) by fluorescent *in situ* hybridization (FISH) in iPSC-neurons 24 hpi in the presence or absence of test compounds. Nuclei were counterstained with DAPI (blue). The data represent an average of three independent experiments. b) HSV-1 copy number in iPSC-neurons exposed to compound 7 and acyclovir (ACV). c) Analysis of HSV-1 DNA polymerase and immediate early gene ICP4 by RT-qPCR. d) ICP4 Western blot analysis. Vehicle is DMSO. The data represent an average of three independent experiments. Error bars represent standard deviations.

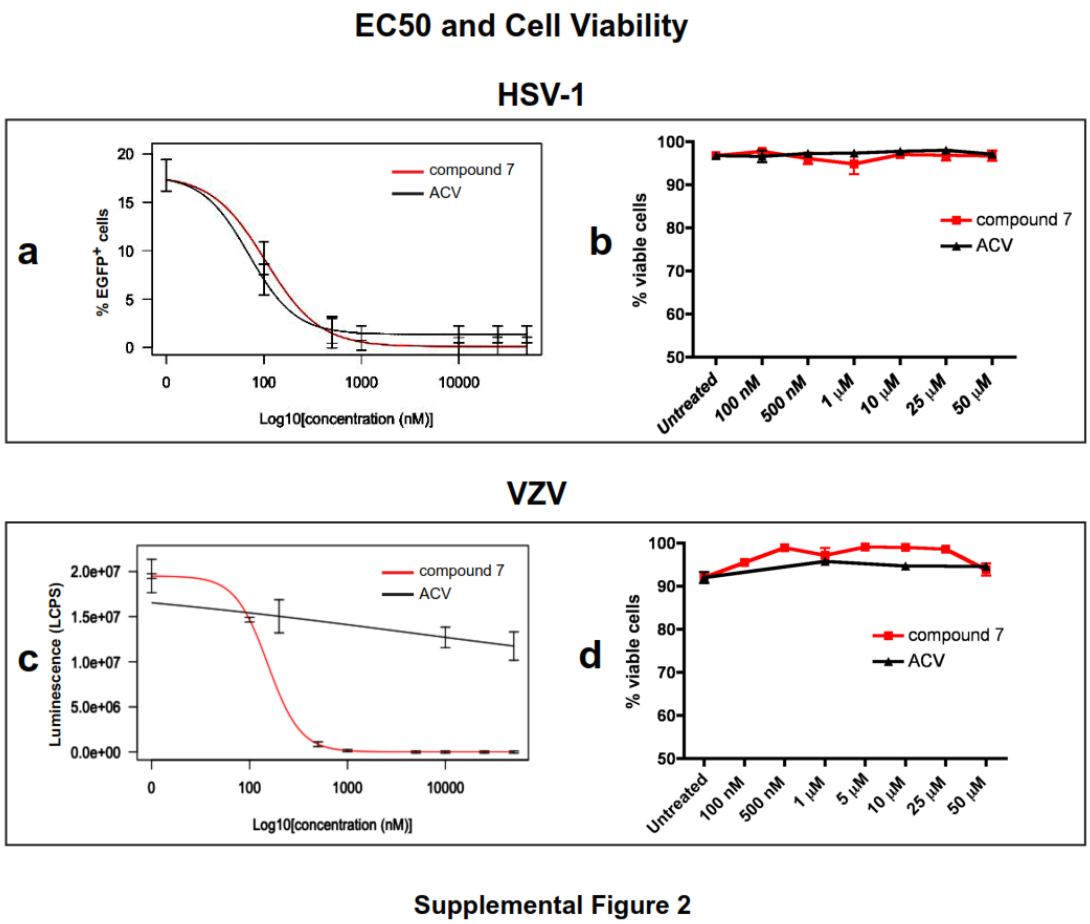

Figure 60. Supplemental Figure 2

a) EC50 estimation for 7 and ACV in iPSC-neurons. b) Comparison of cytotoxicity of 7 and ACV in iPSC-neurons. c-d) VZV infectivity at different concentrations of 7 or acyclovir (ACV). c) ARPE-19 cell lysates were assayed for luciferase following infection with VZV in the presence or absence of 7 for 48 h. LCPS: luciferase counts per second. d) Cytotoxicity of 7 in ARPE- 19 cells. Cytotoxicity was assessed by flow cytometry using fixable viability dye. The data represent an average of three independent experiments. Error bars represent model-based standard error.

Chemical Synthesis

Solvents and reagents

All chemicals and solvents were purchased from Acros, Aldrich, J.T. Baker, Caldeon, Cytec Industries and Fluka and used as received with the following exceptions: deuterated solvents were obtained from ACP Chemicals, Toronto, Canada; tetrahydrofuran (THF), diethyl

ether (Et_2O), and toluene were distilled from sodium/benzophenone under an atmosphere of dry nitrogen; dichloromethane (CH_2Cl_2) was distilled from calcium hydride under an atmosphere of dry nitrogen; methanol (MeOH) was distilled from magnesium turnings under an atmosphere of dry nitrogen; triethylamine (NEt_3), N,N- diisopropylethylamine (Hünig's base) and pyridine were distilled from potassium hydroxide under an atmosphere of dry nitrogen; solid sodium hydride (NaH) was obtained by filtration and washing with n- hexanes.

Reaction handling

All non-aqueous reactions were performed in flame dried round bottom flasks or in non-flame- dried amber 1.5-dram vials. Reactions were magnetically stirred and monitored by thin-layer chromatography (TLC) unless otherwise noted. TLC was performed on Macherey-Nagel silica gel 60 F_{254} TLC aluminum plates and visualized with UV fluorescence quenching and/or potassium permanganate ($KMnO_4$) or 2,4-dinitrophenylhydrazine or p-anisaldehyde stains (Sherma et al., 2003). Concentrations under reduced pressure were performed by rotary evaporation at 40 °C at the appropriate pressure, unless otherwise noted. Column chromatographic purification was performed as flash column chromatography with 0.3–0.5 bar pressure using Silicycle silica gel (40–63, 60 Å) or EcoChrom silica gel (12–26, 60 Å; Still et al., 1978). Distilled technical grade solvents were employed. The yields given refer to chromatographically purified and spectroscopically pure compounds, unless stated otherwise.

Melting points

Melting points were measured on a melting point apparatus using open glass capillaries and are uncorrected.

Nuclear Magnetic Resonance (NMR) spectroscopy

^{1}H, $^{13}C[1H]$, DEPTq, COSY, HSQC and HMBC NMR spectra were obtained on Bruker DRX- 500, AV-600 and AV-700 spectrometers. All ^{1}H NMR spectra were referenced relative to $SiMe_4$ through a resonance of the employed deuterated solvent or proteo impurity of the solvent; chloroform (7.26 ppm), acetone (2.05 ppm), DMSO (3.33 ppm) and methanol (3.31 ppm) for ^{1}H NMR; chloroform (77.00 ppm), acetone (29.84 ppm), DMSO (39.52 ppm) and methanol (49.00 ppm) for ^{13}C NMR. All NMR spectra were obtained at RT (ca. 22 °C) unless otherwise specified. The data is reported as (s = singlet, d = doublet, t = triplet, m = multiplet or unresolved, br = broad signal, coupling constant(s) in Hz, integration). ^{13}C-NMR spectra were recorded with complete ^{1}H-decoupling. Service measurements were performed by the NMR service team of the Nuclear Magnetic Resonance Facility at McMaster University by Dr. Bob Berno, Dr. Dan Sorensen and Dr. Hilary A. Jenkins.

Mass spectrometry

Mass spectrometric analyses were performed as high resolution ESI measurements on a Waters/Micromass QTof Global Ultima (quadrupole time-of-flight mass spectrometer) or high resolution EI in a Waters/Micromass GCT (time-of-flight mass spectrometer) instrument by the mass spectrometry service of the McMaster Regional Centre for Mass Spectrometry (MRCMS) at McMaster University by M.Sc. Sujan Fernando, Tadek Olech and Leah Allan under the supervision of Dr. Kirk Green.

Enantiomeric ratios

Enantiomeric ratios were determined using an Agilent 1220 Infinity HPLC manual injection with a variable wavelength detector, using a Daicel Chiralpak® AD-H column (150 x

4.6 mm, 5μ), n- hexane/iPrOH (75:25) as a mobile phase; flow rate 0.75 mL/min, column temperature 40°C, λ236 or 287 nm, sample 0.5 mg/mL dissolved in the mobile phase, or a Daicel Chiralpak® AS-RH column (150 x 4.6 mm, 5μ), water/ACN (50:50) as a mobile phase; flow rate 0.75 mL/min, column temperature 20 °C, λ236, sample 0.02 mg/mL dissolved in the mobile phase. The sample was filtered through Parr 0.2 μm GHP Acrodisc (13 mm) syringe filters prior to injections.

Diastereomeric ratios

Diastereomeric ratios were determined using an Agilent 1220 Infinity HPLC manual injection with a variable wavelength detector, using a ZORBAX SB-C18 column (150 x 4.6 mm, 5μ), water/ACN (75:25 to 35:65, 30 min) as a mobile phase; flow rate 1.0 mL/min, column temperature 20 °C, λ236, sample was evaporated and dissolved (0.01 mg/mL) in the mobile phase. The sample was filtered through Parr 0.2 μm GHP Acrodisc (13 mm) syringe filters prior to injections.

Optical rotations

Optical rotations were measured with a Perkin-Elmer 241 MC polarimeter, [α] is given in $deg cm^3 g^{-1} dm^{-1}$ and c is given in $g cm^{-3}$.

Fourier Transform Infrared Spectroscopy (FTIR).

FTIR spectra were obtained from the Combustion Analysis and Optical Spectroscopy (CAOS) facility using a Thermo, Nicolet 6700 FTIR.

Differential Scanning Calorimetry (DSC).

DSC was performed using a DSC Q20 coupled with a refrigerated cooling system 40 form TA instruments by Laura Dodge.

Synthesis of (+)-trans-Dihydrolycoricidine (7).

The title compound was prepared following the procedure of McNulty et al., 2013. (+)-trans-Dihydrolycoricidine (7). 2,3,4-Triacetoxy-trans-dihydrolycoricidine 0.0058 g (0.012 mmol) and potassium carbonate (0.0002 g, 0.001 mmol, 0.10 equiv) were dissolved in water (0.104 mL) and MeOH (0.011 mL) and stirred at RT until a white solid precipitated. TLC analysis showed full conversion after 6 h. The mixture was concentrated under a flow of N_2. The white product was dissolved in 9:1 CH_2Cl_2 / MeOH and filtered through a pad of silica. The white solid was recrystallized from methanol to afford 0.0035 g of fine white needles.

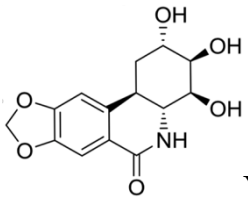

Yield: 92%; M.P.: 296-299 °C (solidified material from MeOH) [lit.[14] 303-304 °C (recrystallized from MeOH), lit.[15] 303-304 °C (recrystallized from $CHCl_3$:MeOH), lit.[16] 294-297 °C]; TLC: R_f = 0.10 (CH_2Cl_2 / MeOH; 95:5; UV); $[\alpha]^{22}_D$ = +61 (c = 0.18, DMSO, l = 1 dm); ^{1}H NMR (600 MHz, DMSO) δ 7.28 (s, 1H, H-Ar), 6.90 (br, 2H , H-Ar, NH), 6.05 (s, 2H, OCH_2O), 4.97 (s, 1H, CH_2-CH-OH), 4.92 (s, 1H, OH), 4.80 (s, 1H, OH), 3.86 (s, 1H, CH_2-CH-OH), 3.70 (br, 2H, CH-OH, CH-OH), 3.31 (dd, J = 12.6, 9.8 Hz, 1H, CH-NH), 2.86 (td, J = 12.6, 3.6 Hz, 1H, CH-Ar), 2.12 (dt, J = 13.3, 3.1 Hz, 1H, CH_{2eq}), 1.62 (td, J = 12.7, 2.3 Hz, 1H, CH_{2ax}); ^{1}H NMR (600 MHz, DMSO, D_2O) δ 6.69 (s, 1H, H-Ar), 6.29 (s, 1H, H-Ar), 5.43 (d, J = 4.0 Hz, 2H, OCH_2O), 3.31 (s, 1H, CH-OD), 3.12 (m, 2H, CH-OD, CH- OD), 2.70 (dd, J = 12.5, 10.0 Hz, 1H, CH-N), 2.28 (td, J = 12.5, 3.3 Hz, 1H, CH-Ar), 1.54 (dt, J = 13.6, 2.7 Hz, 1H, CH_{2eq}), 1.04 (td, J = 12.1, 1.7 Hz, 1H, CH_{2ax}); ^{13}C NMR (151 MHz, DMSO) δ 164.30, 150.65, 145.95, 138.04, 123.26, 106.92, 104.33, 101.58, 71.68, 69.70, 68.61, 55.12, 34.27, 28.32; IR (KBr, cm^{-1}) ν 3206, 2948, 1657, 1577. 1403, 1307, 1079, 1040, 900, 645; HRMS (ESI): exact mass calculated for $C_{14}H_{16}NO_6$ [$(M + H)^+$], 294.0978; found 294.0966.

(+)-trans-3-Epi-dihydrolycoricidine

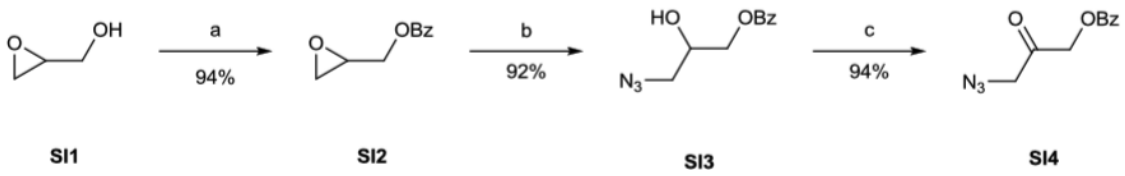

Figure 61. Supplementary Scheme 1.

Reagents and conditions: Yields of isolated products (%) are indicated. a) BzCl (1.05 equiv), DMAP (0.05 equiv), py (1.05 equiv), CH_2Cl_2, 0 °C, 94%. b) NaN_3 (8.0 equiv), NH_4Cl (2.0 equiv), MeOH and water 8:1, RT, 24h, 92%. c) TEMPO (0.02 equiv), NaOCl (5.0 equiv), NaBr (0.1 equiv), $NaHCO_3$ (5.6 equiv), CH_2Cl_2, 0°C →RT, 74%. BzCl = Benzyl chloride, DMAP = 4- Dimethylaminopyridine, py = Pyridine, TEMPO = (2,2,6,6-Tetramethylpiperidin-1-yl) oxy.

2,3-Epoxypropyl benzoate (SI2).

Benzoyl chloride (1.668 mL, 14.373 mmol, 1.05 equiv) and DMAP (0.084 g, 0.68 mmol, 0.05 equiv) were added to a solution of (±)-glycidol SI1 (1.014 g, 13.69 mmol) and pyridine (1.162 mL, 14.37 mmol, 1.05 equiv) in CH_2Cl_2 (10 mL) at 0 °C. The reaction mixture was further stirred at 0 °C for 4 h after which TLC (CH_2Cl_2) showed full conversion. The solvent was removed in vacuo (35 °C, 0.1 mbar) to produce a yellow oil that was dissolved in EtOAc (20 mL). The organic layer was washed with ammonium chloride (10 mL), sodium bicarbonate (2 X 10 mL), and brine (10 mL). The organic layer was dried with Na_2SO_4 and concentrated to yield 2.293 g of a translucent oil. NMR analysis showed that the product was pure enough for the subsequent reaction, and the crude mixture was used without further purification. To obtain spectroscopic data, a small portion of the crude was purified by flash column chromatography (CH_2Cl_2) to afford a white semisolid. This compound is known and matches the reported spectroscopic data (Cisneros et al., 2007).

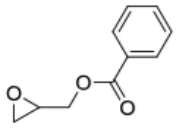

Yield: 94%; TLC(CH_2Cl_2, UV): R_f = 0.30; ^{1}H NMR (600 MHz, $CDCl_3$) δ 8.07 – 8.00 (m, 2H, H-Bz), 7.57 (t, J = 7.4 Hz, 1H, H-Bz), 7.43 (t, J = 7.8 Hz, 2H, H-Bz), 4.46 (d, J = 5.2 Hz, 2H, CH_2-OCO), 4.21 (p, J = 5.2 Hz, 1H, CH), 3.70 (ddd, J = 17.2, 11.3, 5.4 Hz, 2H, CH_2-O); ^{13}C NMR (151 MHz, $CDCl_3$) δ 166.60, 133.32, 129.64, 129.38, 128.41, 69.65, 65.64, 45.97; IR (neat, cm^{-1}) ν 3459, 2958, 1721, 1275, 1122, 710; HRMS (ESI): exact mass calculated for $C_{10}H_{10}O_3Na$ [$(M + Na)^+$], 201.0528; found 244.0520.

3-Azido-2-hydroxypropyl benzoate (SI3).

To a mixture of 2,3-epoxypropyl benzoate (2.012 g, 11.29 mmol) and NH_4Cl (1.208 g, 22.58 mmol, 2.0 equiv) in MeOH and water (13.3 mL/1.6 mL, 8:1) was added NaN_3 (5.872 g, 90.33 mmol, 8.0 equiv) and the reaction mixture was stirred at room temperature for 24 h. The reaction mixture was concentrated to 1/10 its volume, diluted with water and extracted with EtOAc (20 mL). The combined organic layers were washed with brine (2 X 10 mL), dried over Na_2SO_4, filtered and concentrated to yield 2.298 g of a yellow oil. NMR analysis showed that the product was pure enough for the subsequent reaction, and the crude mixture was used without further purification. To obtain spectroscopic data, a small portion of the crude was purified by flash column chromatography (35% EtOAc in hexanes) to obtain a yellow oil. This compound is known and matches the reported spectroscopic data (Acquaah-Harrison et al., 2010).

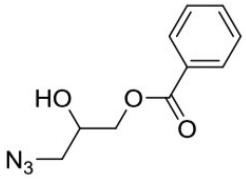

Yield: 92%; TLC(CH_2Cl_2:MeOH, 98:2 v/v; UV): R_f = 0.47; ^{1}H NMR (600 MHz, $CDCl_3$) δ 8.04 (dd, J = 8.3, 1.2 Hz, 2H, H-Bz), 7.62 – 7.56 (m, 1H, H-Bz), 7.45 (dd, J = 10.8, 4.8 Hz, 2H, H-Bz), 4.44 – 4.37 (qd, J = 11.7, 4.6 Hz, 2H,CH_2-OCO), 4.19 – 4.13 (m, 1H,

CH-OH), 3.49 (qd, J = 12.6, 5.4 Hz, 2H, CH_2-N_3), 2.70 (br, 1H, OH); ^{13}C NMR (151 MHz, $CDCl_3$) δ 166.69, 133.41, 129.82, 129.70, 129.41, 128.49, 69.23, 66.15, 53.56; IR (neat, cm^{-1}) ν 3465, 2951, 2104, 1721, 1274, 1114, 712; HRMS (ESI): exact mass calculated for $C_{10}H_{11}N_3O_3Na$ [$(M + Na)^+$], 244.0698; found 244.0686.

3-Azido-2-oxopropyl benzoate (SI4).

3-azido-2-hydroxypropyl benzoate (3.122 g, 14.11 mmol), $NaHCO_3$ (3.320 g, 39.52 mmol, 2.8 equiv), NaBr (0.144 g, 1.41 mmol, 0.1 equiv) and TEMPO (0.044 g, 0.28 mmol, 0.02 equiv) were dissolved in CH_2Cl_2 (45 mL). The mixture was cooled to 0°C, and cold 0.83 M NaOCl (36.08 mL, 70.57 mmol, 5.0 equiv) buffered with $NaHCO_3$ (3.320 g, 39.52 mmol, 2.8 equiv) was added slowly. The reaction turned from red to orange and produced a white-yellow precipitate in the organic layer over 30 min, of which TLC analysis (CH_2Cl_2) showed reaction completion. The organic layer was separated and the aqueous layer was extracted with CH_2Cl_2 (2 X 25 mL). The organic extracts were combined, dried with Na_2SO_4 and concentrated to yield 2.274 g of a clear oil, which was filtered through a silica pad to yield a white solid (Bischofberger, 1988).

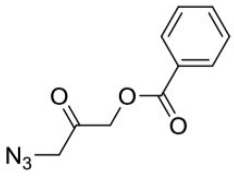

Yield: 74%; M.P.: 58-61 °C (solidified from CH_2Cl_2), [lit.[19] 61 °C (recrystallized from $CHCl_3$/cyclohexane, 1:1)]; TLC(CH_2Cl_2:MeOH, 95:5 v/v, UV): R_f = 0.32; ^{1}H NMR (600 MHz, $CDCl_3$) δ 8.12 – 8.07 (m, 2H, H-Bz), 7.61 (t, J = 7.5 Hz, 1H, H-Bz), 7.48 (t, J = 7.8 Hz, 2H, H-Bz), 5.15 (s, 2H, CH_2-Bz), 4.02 (s, 2H, CH_2-N_3); ^{13}C NMR (151 MHz, $CDCl_3$) δ 195.88, 165.78, 133.68, 129.95, 128.82, 128.57, 66.51, 30.50; IR (neat, cm^{-1}) ν 3000, 2098,1721,1277, 1131, 704; HRMS (ESI): exact mass calculated for $C_{10}H_{10}N_3O_3$ [$(M + H)^+$], 220.0722; found 220.0716; DSC: Endothermic transition at 61.6 °C, exothermic transition at 155.8 °C (onset at 138.4 °C);

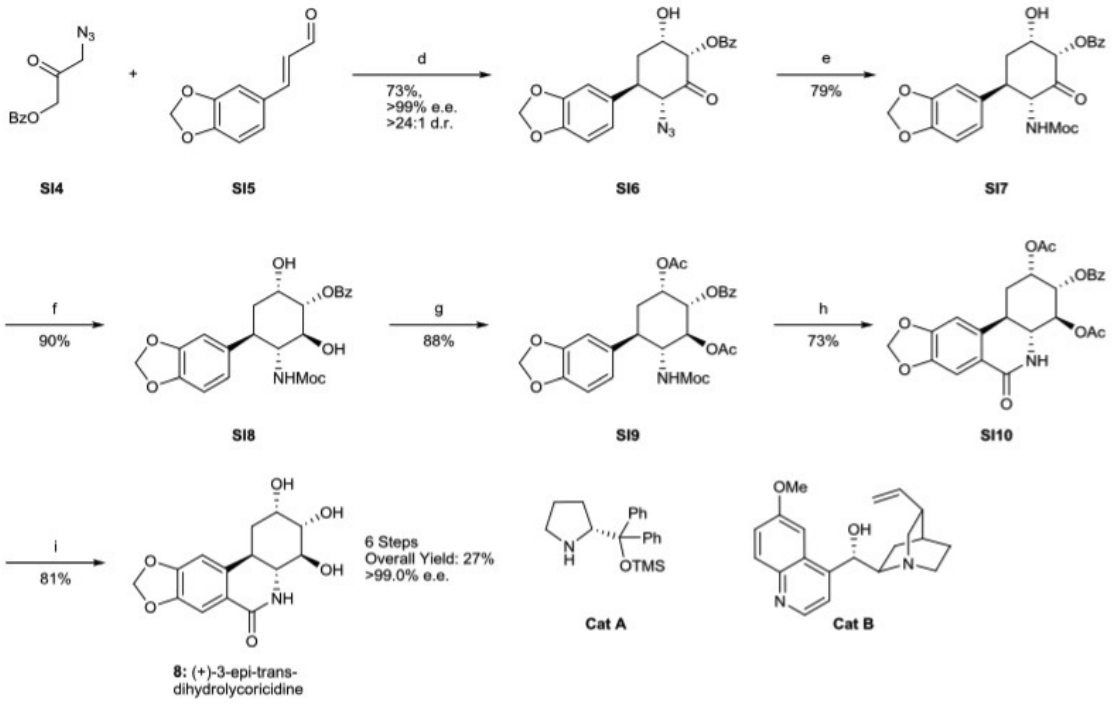

Figure 62. Supplementary Scheme 2

Reagents and conditions: Yields of isolated products (%) are indicated. d) SI5 (1.05 equiv), Cat A (10 mol%), Cat B (10 mol%), CH_2Cl_2, -10 °C →RT, 73%. e) DMDC (3.0 equiv), H_2, 10 % Pd/C (0.075 equiv), EtOAc, 50 psi, RT, 79%. f) $Me_4NHB(OAc)_3$ (4.0 equiv), AcOH (10.0 equiv), MeCN, RT, 90%. g) AcCl (100 equiv). h) Tf_2O (5.0 equiv), DMAP (3.0 equiv), CH_2Cl_2, 0 °C → RT, 73%. i) K_2CO_3 (0.10 equiv), H_2O/MeOH 9:1, RT, 81%. DMDC = Dimethyl dicarbonate, Tf = Triflic, DMAP = 4-Dimethylaminopyridine, Moc = Methyloxycarbonyl.

(1S,3R,4R,6S)-3-azido-4-(1,3-benzodioxol-5-yl)-6-hydroxy-2-oxocyclo hexyl benzoate (SI6).

A solution of (2E)-3-(1,3-benzodioxol-5-yl)-2-propenal (SI5; McNulty et al., 2013) (0.4246 g, 2.410 mmol, 1.05 equiv) and (R)-(+)-α,α-Diphenyl-2- pyrrolidinemethanol trimethylsilyl ether (Cat A, 0.0747 g, 0.230 mmol, 0.10 equiv) in dichloromethane (5.0 mL) was stirred for 10 min, after which it was cooled to -10 °C. 3-Azido-2-oxopropyl benzoate (0.5032 g, 2.296 mmol) was added dropwise over 5 min. The yellow solution was stirred for 20 min at room temperature and quinidine (Cat B, 0.0745 g, 0.230 mmol, 0.10 equiv) was added in one

portion. The reaction was stirred at room temperature for 16 h, after which HPLC analysis showed full conversion, the d.r. was determined at this stage (96:4). The product precipitated out of solution while most of the impurities remained in solution. The dichloromethane was carefully evaporated (30 °C, 32 mbar) yielding a yellow solid within a brown oil that was purified by filtration using MeOH (3 X 5.0 mL) giving the title product as a white solid (0.427 g).

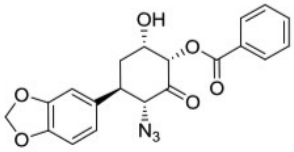

Yield: 73%; M.P.: 189-190 °C (material crystalized from acetone); TLC(CH_2Cl_2:MeOH, 98:2 v/v, UV): R_f = 0.62; $[\alpha]^{23}_D$ = +75.4 (c = 0.11, Acetone, l = 1 dm); ^{1}H NMR (600 MHz, Acetone) δ 8.18 (dd, J = 8.3, 1.2 Hz, 2H, H-Ph), 7.70 – 7.65 (m, 1H, H-Ph), 7.54 (t, J = 7.8 Hz, 2H, H-Ph), 7.08 (d, J = 1.7 Hz, 1H, H-Ar), 6.92 (dd, J = 7.9, 1.7 Hz, 1H, H-Ar), 6.85 (d, J = 7.9 Hz, 1H, H-Ar), 6.02 (s, 2H, OCH_2O), 5.81 (dd, J = 3.0, 0.9 Hz, 1H, CH-OBz), 4.72 (d, J = 12.1 Hz, 1H, CH-N_3), 4.70 (br, 1H, CH-OH), 3.44 (td, J = 12.5, 4.0 Hz, 1H, CH-Ar), 2.58 (dd, J = 14.5, 1.9 Hz, 1H, CH_2), 2.23 (dt, J = 14.4, 4.0 Hz, 1H, CH_2); ^{13}C NMR (151 MHz, Acetone) δ 198.76, 165.80, 149.06, 147.78, 136.16, 134.28, 130.73, 130.65, 129.38, 122.00, 109.10, 108.39, 102.10, 80.05, 70.76, 70.60, 45.18, 37.73; IR (neat, cm^{-1}) ν 3475, 2907, 2101, 1709, 1505, 1494, 1444, 1328, 1248, 1128, 1100, 1040, 935, 821; HRMS (ESI): exact mass calculated for $C_{20}H_{17}N_3NaO_6$ [$(M + Na)^+$], 418.1015; found 418.1015; e.e.: was determined after the filtration. τ_{major} = 12.8 min, τ_{minor} = 8.7 min (>99% e.e.), Daicel Chiralpak AS-RH column (150 x 4.6 mm, 5μ), Water/ACN (60:40) as a mobile phase; flow rate 0.75 mL/min, column temperature 20 °C, λ236; d.r.: 96:4 (HPLC).

(1R,3S,4S,6R)-3-azido-4-(1,3-benzodioxol-5-yl)-6-hydroxy-2-oxocyclo hexyl benzoate (ent-SI6)

The title compound was isolated by filtration, as a white solid.

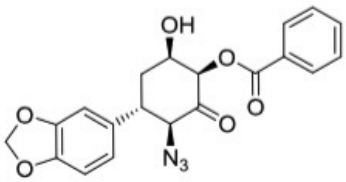

Yield: 70%; M.P.: 179-180 °C (material solidified from acetone); $[\alpha]^{24}_{D}$ = -67 (c = 0.46, Acetone, l = 1 dm); e.e.: τ_{major} = 8.7 min, τ_{minor} = 12.8 min (>99% e.e.), Daicel Chiralpak AS-RH column (150 x 4.6 mm, 5µ), Water/ACN (60:40) as a mobile phase; flow rate 0.75 mL/min, column temperature 20 °C, λ236; d.r.: 96:4 (HPLC).

N-[(1R,3R,4R,6R)-6-(1,3-benzodioxol-5-yl)-3-benzoyloxy-4-hydroxy-2-oxocyclohexyl]-carbamic acid methyl ester (SI7). Into a stainless steel hydrogenation vessel SI6 (0.1950 g, 0.493 mmol), dimethyl dicarbonate (0.1984 g, 1.480 mmol, 3.0 equiv) and 10 % Pd/C (0.0394 g, 0.037 mmol, 0.075 equiv) were suspended in EtOAc (8.0 mL). The vessel was sealed and subjected to 50 psi of hydrogen gas with vigorous stirring for 36 hr after which TLC (CH_2Cl_2/MeOH 95:5) showed full conversion. The suspension was filtered through a Celite® pad and carefully evaporated (20 °C, 0.1 mbar). The translucent grey oil was purified by flash chromatography (eluent CH_2Cl_2/MeOH 100:0 to 97:3) giving the product as a white semi-solid (0.1665 g).

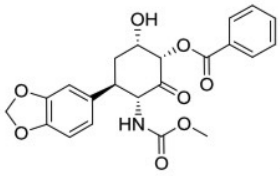

Yield: 79%; M.P.: 196-197 °C (material solidified from Acetone); TLC(CH_2Cl_2:MeOH, 98:2 v/v, UV): R_f = 0.17; $[\alpha]^{23}_{D}$ = +58 (c = 2.17, Acetone, l = 1 dm); ^{1}H NMR (600 MHz, Acetone) δ 8.17 (d, J = 7.1 Hz, 2H, H-Ph), 7.66 (t, J = 7.4 Hz, 1H, H-Ph), 7.52 (t, J = 7.8 Hz, 2H, H-Ph), 7.06 (s, 1H, H-Ar), 6.89 (d, J = 7.9 Hz, 1H, H-Ar), 6.78 (d, J = 7.9 Hz, 1H, H-Ar), 6.25 (d, J = 9.3 Hz, 1H, NH), 5.98 (d, J = 3.1 Hz, 2H, OCH_2O), 5.86 (d, J = 2.6 Hz, 1H, CH-OBz), 4.81 (dd, J = 11.9, 9.7 Hz, 1H, CH-NH), 4.69 (s, 1H, CH- OH), 3.44 (td, J = 12.5, 4.0 Hz, 1H, CH-Ar), 3.44 (s, 3H, CH_3O), 2.65 (dd, J = 13.6, 1.9 Hz, 1H, CH_2), 2.20 (dt, J = 14.3, 4.0 Hz, 1H, CH_2); ^{13}C NMR (151 MHz, Acetone) δ 200.19, 165.75, 157.51, 148.70, 147.36,

136.87, 134.10, 130.91, 130.69, 129.31, 122.18, 108.77, 101.90, 80.39, 70.82, 63.57, 51.87, 44.77, 38.22; IR (neat, cm^{-1}) ν 3373, 2922, 1705, 1531, 1505 1489, 1449, 1248, 1126, 1066, 1038 935, 712; HRMS (ESI): exact mass calculated for $C_{22}H_{22}NO_8$ [$(M + H)^+$], 428.1345; found 428.1346.

(1S,2S,3S,4R,5R)-2-Benzoyloxy-1,3-dihydroxy-4-(methoxycarbonyl amino)-5-(3,4-methylenedioxyphenyl)cyclohexane (SI8). To a solution of tetramethylammonium triacetoxyborohydride (0.2509 g, 0.954 mmol, 4.0 equiv) and acetic acid (0.136 mL 2.384 mmol, 10.0 equiv) in acetonitrile (5.0 mL) was added a solution of N-[6-(1,3- benzodioxol-5-yl)-3-benzoyloxy-4-hydroxy-2-oxocyclohexyl]-carbamic acid methyl ester (0.1019 g, 0.238 mmol) in 0.5 mL of acetonitrile. The reaction mixture was stirred at room temperature for 12 h before it was quenched with 1.5 mL of saturated aqueous ammonium chloride solution. After effervescence had ceased, the solution was treated with 1.5 mL of 1.0 M aqueous sodium/potassium tartrate solution and stirred for 30 min. The aqueous solution was extracted with CH_2Cl_2 (10 X 2 mL). The combined organic extracts were washed with 1.0 mL of saturated aqueous sodium chloride solution, dried over anhydrous Na_2SO_4, filtered, and concentrated in vacuo. The yellow product was purified by flash column chromatography (CH_2Cl_2 / MeOH; 100:0 to 98:2) to afford 0.0921 g of a white solid.

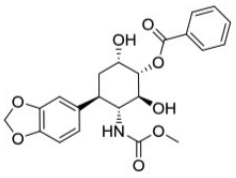

Yield: 90%; M.P.: 198-210 °C (material solidified from CH_2Cl_2); TLC(CH_2Cl_2:MeOH, 98:2 v/v; UV): R_f = 0.13; $[\alpha]^{22}_D$ = +50 (c = 1.69, MeOH, l = 1 dm); ^1H NMR (700 MHz, Acetone) δ 8.11 (dd, J = 8.2, 1.1 Hz, 2H, H-Ph), 7.62 (t, J = 7.4 Hz, 1H, H-Ph), 7.50 (t, J = 7.8 Hz, 2H, H-Ph), 6.91 (d, J = 1.4 Hz, 1H, H-Ar), 6.78 (dd, J = 7.9, 1.6 Hz, 1H, H-Ar), 6.73 (d, J = 7.9 Hz, 1H, H-Ar), 6.11 (d, J = 8.7 Hz, 1H, NH), 5.94 (dd, J = 8.1, 1.1 Hz, 2H, OCH_2O), 5.11 (dd, J = 9.8, 2.8 Hz, 1H, CH-OBz), 4.47 (br, 1H, CH_2-CH- OH), 4.33 (s, 1H, CH_2-CH-OH), 4.25 (t, J = 8.2 Hz, 1H, CH-OH), 4.17 (br, 1H, OH), 3.83 (q, J = 9.9 Hz, 1H, CH-NH),

3.40 (s, 3H, OCH_3), 3.30 (td, J = 10.8, 3.4 Hz, 1H, CH-Ar), 2.02 (t, J = 13.1 Hz, 1H, CH_2), 1.95 (dt, J = 14.0, 3.8 Hz, 1H, CH_2); ^{13}C NMR (176 MHz, Acetone) δ 166.56, 157.86, 148.41, 146.88, 137.84, 133.63, 131.80, 130.55, 129.11, 122.14, 108.99, 108.56, 101.65, 79.87, 72.06, 67.60, 60.12, 51.61, 41.93, 38.81; IR (neat, cm^{-1}) ν 3407, 3062, 2947, 2899, 1714, 1540, 1504, 1489, 1315, 1248, 1039, 930, 734, 713; HRMS (ESI): exact mass calculated for $C_{22}H_{24}NO_8$ [$(M + H)^+$], 430.1502; found 430.1495.

(1S,2S,3S,4R,5R)-2-Benzoyloxy-1,3-diacetoxy-4-(methoxycarbonyl amino)-5-(3,4-methylenedioxyphenyl)cyclohexane (SI9).

2-Benzoyloxy-1,3-dihydroxy-4-(methoxycarbonylamino)-5-(3,4-methyl enedioxyphenyl) cyclohexane (0.0161 g, 0.037 mmol) and acetyl chloride (0.265 mL, 3.73 mmol, 100 equiv) were stirred for 16 h. After that the suspension was poured into a cooled, saturated aq. $NaHCO_3$ solution and extracted with CH_2Cl_2 (2 mL) dried with anhydrous Na_2SO_4 and concentrated. The yellow product was purified by flash column chromatography (CH_2Cl_2 / MeOH; 100:0 to 98:2) to afford 0.0169 g of a yellow oil.

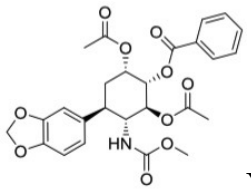

Yield: 88%; TLC(CH_2Cl_2:MeOH, 98:2 v/v; UV): R_f = 0.33; $[\alpha]^{22}_D$ = + 71 (c = 0.73, MeOH, l = 1 dm); ^1H NMR (600 MHz, $CDCl_3$) δ 7.95 (d, J = 7.1 Hz, 2H, H-Ph), 7.56 (t, J = 7.4 Hz, 1H, H-Ph), 7.43 (t, J = 7.8 Hz, 2H, H-Ph), 6.75 (d, J = 7.9 Hz, 1H, H-Ar), 6.71 (s, 1H, H-Ar), 6.67 (d, J = 7.8 Hz, 1H, H-Ar), 5.94 (dd, J = 4.2, 1.4 Hz, 2H, OCH_2O), 5.62 (dd, J = 5.6, 3.1 Hz, 1H, CH_2-CH-OAc), 5.53 (t, J = 10.3 Hz, 1H, CH-OAc), 5.29 (dd, J = 10.3, 3.2 Hz, 1H, CH-OBz), 4.52 (d, J = 8.9 Hz, 1H, NH), 4.01 (d, J = 8.4 Hz, 1H, CH-NH), 3.50 (s, 3H, CH_3O), 3.01 (t, J = 10.9 Hz 1H, CH-Ar), 2.13 (s, 3H, CH_3CO), 2.11 (dt, J = 14.8, 3.7 Hz, 1H, CH_2), 1.95 (m, 1H, CH_2), 1.95 (s, 3H, CH_3O); ^{13}C NMR (151 MHz, $CDCl_3$) δ 170.99, 169.73, 165.40, 156.39, 147.90, 146.73, 133.57, 133.35, 129.63, 129.30, 128.52, 120.92, 108.38, 107.79, 101.05, 72.96, 72.01, 68.56, 56.85, 52.21, 42.63, 35.21, 21.00, 20.67; IR (neat, cm^{-1}) ν 3363, 2950, 1732, 1522, 1506, 1490, 1276, 1242, 1093, 1039, 931, 714; HRMS (ESI): exact mass calculated for $C_{26}H_{28}NO_{10}$ [$(M + H)^+$], 514.1713; found 514.1704.

(2S,3S,4S,4aR,10bR)-3-Benzoyloxy-2,4-diacetoxy-8,9-methylenedioxy- 1,2,3,4,4a,5-hexahydrophenanthridin-6(10bH)-one (SI10).

2-Benzoyloxy-1,3-diacetoxy-4-(methoxycarbonylamino)-5-(3,4-methyl enedioxyphenyl)cyclohexane (0.0169 mg, 0.033 mmol) and DMAP (0.0121 mg, 0.099 mmol, 3.0 equiv) were dissolved in CH_2Cl_2 (1 mL) at 0 °C. 1.0 M solution of Tf_2O in CH_2Cl_2 (0.164 mL, 0.164 mmol, 5.0 equiv) was added drop-wise over a period of 10 min. The reaction was stirred for 16 h at RT. The solvent was evaporated and the residue treated with a mixture of THF (1 mL) and 1 N HCl (0.25 mL). After stirring for 1 h at RT, the mixture was partitioned between a saturated aqueous solution of $NaHCO_3$ (0.5 mL) and CH_2Cl_2 (2 mL). The organic phases were combined, dried with anhydrous Na_2SO_4 and concentrated. The brown product was purified by flash column chromatography (CH_2Cl_2 / MeOH; 100:0 to 98:2) to afford 0.0115 g of a white oil.

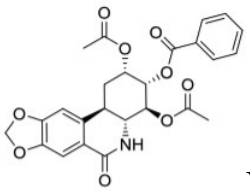

Yield: 73%; TLC (CH_2Cl_2:MeOH, 98:2 v/v; UV): R_f = 0.17; $[\alpha]^{22}_D$ = +91 (c = 1.2, MeOH, l = 1 dm); ^{1}H NMR (600 MHz, $CDCl_3$) δ 7.96 (dd, J = 8.3, 1.3 Hz, 2H, H-Ph), 7.60 – 7.54 (m, 1H, H-Ph), 7.52 (s, 1H, H-Ar), 7.44 (t, J = 7.8 Hz, 2H, H-Ph), 7.08 (br, 1H, NH), 6.69 (d, J = 0.7 Hz, 1H, H-Ar), 6.02 (dd, J = 5.1, 1.3 Hz, 2H, OCH_2O), 5.72 (d, J = 2.7 Hz, 1H, CH_2-CH-OAc), 5.71 (t, J = 10.1 Hz, 2H, CH-OAc), 5.15 (dd, J = 10.1, 3.2 Hz, 1H, CH-OBz), 3.60 (dd, J = 12.7, 10.2 Hz, 1H, CH-NH), 3.31 (td, J = 12.6, 3.9 Hz, 1H, CH-Ar), 2.61 (dt, J = 14.5, 3.8 Hz, 1H, CH_2), 2.11 (s, 3H, CH_3O), 2.05 (s, 3H, CH_3O), 1.86 – 1.79 (m, 1H, CH_2); ^{13}C NMR (151 MHz, $CDCl_3$) δ 170.73, 169.80, 165.60, 165.51, 151.49, 147.04, 135.18, 133.49, 129.68, 128.98, 128.55, 122.99, 108.34, 103.98, 101.79, 72.94, 71.10, 68.25, 56.97, 34.63, 29.03, 20.98, 20.92; IR (neat, cm^{-1}) ν 3344, 2916, 1727, 1666, 1505, 1488, 1450, 1274, 1227, 1038, 932, 714; HRMS (ESI): exact mass calculated for $C_{25}H_{24}NO_9$ $[(M + H)^+]$, 482.1451; found 482.1454.

(+)-trans-3-Epidihydrolycoricidine (8). 3-Benzoyloxy-2,4-diacetoxy-8,9-methylenedioxy-1,2,3,4,4a,5-hexahydrophenanthridin-6(10bH)-one 0.0011 g (0.024 mmol) and

potassium carbonate (0.0003 g, 0.002 mmol, 0.10 equiv) were dissolved in MeOH (0.022 mL) and water (0.198 mL) and stirred at room temperature until a white solid precipitate formed; TLC analysis showed full conversion after 16 hr. The mixture was concentrated under a flow of N_2. The white product was dissolved in 9:1 CH_2Cl_2 / MeOH and filtered through a path of silica. The white solid was recrystallized from methanol to afford 0.0058 g of fine white needles.

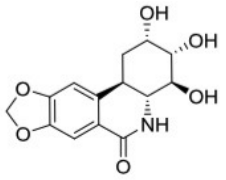

Yield: 81%; M.P.: 298-299 °C (material solidified from MeOH); TLC (CH_2Cl_2:MeOH, 9:1 v/v; UV): R_f = 0.09; $[\alpha]^{22}_D$ = +38 (c = 0.14, DMSO, l = 1 dm); ^{1}H NMR (600 MHz, DMSO) δ 7.30 (s, 1H, H-Ar), 7.04 (br, 1H, NH), 6.93 (s, 1H, H-Ar), 6.07 (d, J = 1.4 Hz, 2H, OCH_2O), 5.09 (br, 1H, CH_2-CH-OH), 4.69 (br, 2H, OH, OH), 3.95 (d, J = 2.0 Hz, 1H, CH_2-CH-OH), 3.59 (t, J = 8.9 Hz, 1H, CH(OH)-CHN), 3.25 (dd, J = 9.2, 2.7 Hz, 1H, CHO-CH(OH)CHO), 3.01 – 2.91 (m, 2H, CH-NH, CH-Ar), 2.38 (dt, J = 13.6, 3.1 Hz, 1H, CH_{2eq}), 1.47 – 1.39 (m, 1H, CH_{2ax}); ^{1}H NMR (600 MHz, DMSO, D_2O) δ 7.26 (s, 1H, H-Ar), 6.85 (s, 1H, H-Ar), 6.00 (d, J = 2.9 Hz, 2H, OCH_2O), 3.99 (d, J = 2.4 Hz, 1H, CH_2-CH-OD), 3.58 (t, J = 9.4 Hz, 1H, CH(OD)-CHN), 3.28 (dd, J = 9.4, 3.0 Hz, 1H, CHO-CH(OD)CHO), 2.99 (dd, J = 12.8, 9.3 Hz, 1H, CH-ND), 2.93 (td, J = 12.3, 3.4 Hz, 1H, CH-Ar), 2.33 (dt, J = 13.7, 3.5 Hz, 1H, CH_{2eq}), 1.45 (t, J = 12.9 Hz, 1H, CH_{2ax}); ^{13}C NMR (151 MHz, DMSO) δ 164.13, 150.65, 145.98, 137.63, 123.10, 106.89, 104.54, 101.57, 73.78, 71.47, 68.14, 59.06, 33.70, 31.18; IR (neat, cm^{-1}) ν 3464, 3261, 2895, 1642, 1608, 1472, 1355, 1270, 1067, 934, 778; HRMS (ESI): exact mass calculated for $C_{14}H_{16}NO_6$ [$(M + H)^+$], 294.0978; found 294.0963.

Synthesis of (+)-3-deoxydihydrolycoricidine

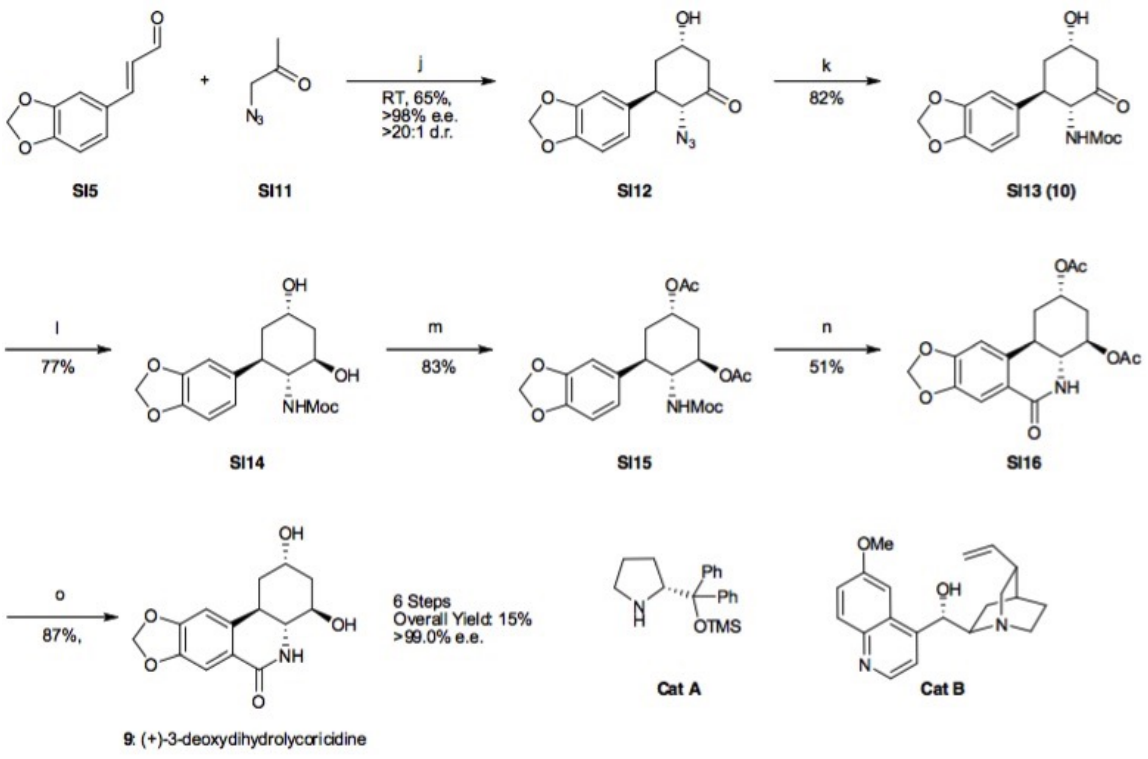

Figure 63. Supplementary Scheme 3.

Reagents and conditions: Yields of isolated products (%) are indicated. j) SI5 (1.5 equiv), Cat A (10 mol%) and Cat B (10 mol%), CH_2Cl_2, RT, 65%. k) DMDC (3.0 equiv), H_2, 10% Pd/C (0.075 equiv), 50 psi, MeOH, RT, 82%. l) $Me_4NHB(OAc)_3$ (4.0 equiv), ACN/AcOH 96:4, RT, 77%. m) Ac_2O (6.0 equiv), py (6.0 equiv), RT, 83%. n) Tf_2O (5.0 equiv), DMAP (3.0 equiv), CH_2Cl_2, 0 °C → RT, 51% o) K_2CO_3 (0.10 equiv), MeOH /H_2O 9:1, RT, 87%. DMDC = Dimethyl dicarbonate, ACN = acetonitrile, py = pyridine, Tf = Triflic, DMAP = 4-Dimethylaminopyridine, Moc = Methyloxycarbonyl.

N-[(1R,2R,4S,6R)-2,4-Dihydroxy-6-(1,3-benzodioxol-5-yl)-cyclohexyl] carbamic acid methyl ester (SI14).

The title compound was prepared from SI5 and SI11 as shown above following the procedure described by McNulty et. al., 2013.

(1S,3R,4R,5R)-5-(1,3-Benzodioxol-5-yl)-4-(methoxycarbonylamino)- cyclohexane-1,3-

diyldiacetate (SI15). To a solution of SI14 (0.0820 g, 0.259 mmol) in pyridine (0.125 mL, 1.56 mmol, 6.0 equiv) was added acetic anhydride (0.146 mL, 1.55 mmol, 6.0 equiv). The reaction mixture was stirred at room temperature for 16 h. After that the pyridine was removed in vacuo (0.1 mbar). The residue was dissolved in CH_2Cl_2 (5 mL) and washed with saturated $NaHCO_3$ (2 x 10 mL) and water (5.0 mL). The solvent was removed in vacuo (35 °C, 0.1 mbar) and the product purified by flash column chromatography (CH_2Cl_2 / MeOH; 100:0 to 98:2) to afford 15 (0.0843 g) as a clear yellow oil.

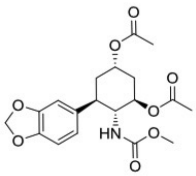

Yield: 83%; TLC(CH_2Cl_2:MeOH, 98:2 v/v; UV): R_f = 0.47; $[\alpha]^{21}_D$ = +35 (c = 5.10, MeOH, l = 1 dm); ^{1}H NMR (600 MHz, $CDCl_3$) δ 6.70 (d, J = 7.9 Hz, 1H, H-Ar,), 6.68 (s, 1H, H-Ar,), 6.63 (d, J = 7.9 Hz, 1H, H-Ar,), 5.90 (dd, J = 3.9, 1.3 Hz, 2H, OCH_2O), 5.21 (q, J = 2.73 Hz, 1H, CH_2CHCH_2), 5.13-5.09 (m, 1H, CH(O)CHN), 4.50 (d, J = 9.9 Hz, 1H, NH), 3.84 (d, J = 7.7 Hz, 1H, CH-NH), 3.46 (s, 3H, OCH_3), 2.87 (t, J = 10.8 Hz, 1H, CH-Ar), 2.24 (d, J = 13.7 Hz, 1H, $COCH_{2ax}CO$), 2.09 (s, 3H, $COCH_3$), 2.03 (dq, J = 14.8, 3.1 Hz, 1H, $CH_{2eq}CHAr$), 2.01 (s, 3H, $COCH_3$), 1.81 (d, J = 12.3 Hz, 1H, $COCH_{2eq}CO$), 1.79 – 1.72 (m, 1H, $CH_{2ax}CHAr$); ^{13}C NMR (151 MHz, $CDCl_3$) δ 170.87, 170.05, 156.57, 147.69, 146.38, 134.50, 120.80, 108.18, 107.77, 100.87, 71.15, 68.54, 57.85, 51.98, 43.41, 37.88, 34.90, 21.22, 20.90; IR (neat, cm^{-1}) ν 3353, 2952, 1733, 1533, 1505, 1490, 1444, 1372, 1247, 1038, 933; HRMS (ESI): exact mass calculated for $C_{19}H_{24}NO_8$ [$(M + H)^+$], 394.1502; found 394.1485.

(+)-2,4-Diacetoxy-3-deoxydihydrolycoricidin (SI16).

5-(1,3-Benzodioxol-5-yl)-4-(methoxycarbonylamino)- cyclohexane-1,3- diyldiacetate SI15 (0.1442 mg, 0.319 mmol) and DMAP (0.1171 mg, 0.958 mmol, 3.0 equiv) were dissolved in CH_2Cl_2 (8.0 mL) at 0 °C. 1.0 M solution of Tf_2O in CH_2Cl_2 (1.597 mL, 1.60 mmol, 5.0 equiv) was added dropwise over a period of 10 min. The reaction was stirred for 16 h at RT. The

solvent was evaporated and the residue treated with a mixture of THF (5 mL) and 1 N HCl (1.0 mL). After stirring for 1 h at RT, the mixture was partitioned between a saturated aqueous solution of $NaHCO_3$ (1.0 mL) and CH_2Cl_2 (20 mL). The organic phases were combined, dried with anhydrous Na_2SO_4 and concentrated. The brown product was purified by flash column chromatography (CH_2Cl_2 / MeOH; 100:0 to 98:2) to afford 0.0398 g of a yellow oil.

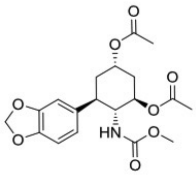

Yield: 51%; TLC(CH_2Cl_2:MeOH, 98:2 v/v; UV): R_f = 0.15; $[\alpha]^{21}_D$ = +24 (c = 1.17, MeOH, l = 1 dm); ^{1}H NMR (600 MHz, $CDCl_3$) δ 7.54 (s, 1H, CH-Ar), 6.69 (s, 1H CH-Ar), 6.54 (s, 1H, NH), 6.01 (d, J = 2.2 Hz, 2H, OCH_2O), 5.37 – 5.34 (m, 1H, CH_2CHCH_2), 5.15 (td, J = 11.0, 4.6 Hz, 1H, CH(O)CHN), 3.44 (dd, J = 12.5, 10.1 Hz, 1H, CH-NH), 3.18 (td, J = 12.5, 3.8 Hz, 1H, CH-Ar), 2.53 (d, J = 14.0 Hz, 1H, CH_{2eq}CHAr), 2.44 (ddd, J = 6.6, 5.1, 3.2 Hz, 1H, $COCH_{2ax}CO$), 2.14 (d, J = 3.9 Hz, 3H, $COCH_3$), 2.09 (d, J = 6.2 Hz, 3H, $COCH_3$), 1.64 – 1.56 (m, 2H, $COCH_{2eq}CO$, CH_{2ax}CHAr); ^{13}C NMR (151 MHz, $CDCl_3$) δ 170.55, 170.13, 165.28, 151.46, 146.91, 135.95, 123.00, 108.31, 103.97, 101.74, 71.39, 67.99, 58.17, 34.99, 33.63, 30.65, 21.24, 21.16; IR (neat, cm^{-1}) ν 3197, 2923, 1737, 1667, 1464, 1382, 1364, 1246, 1040, 931; HRMS (ESI): exact mass calculated for $C_{18}H_{20}NO_7$ [$(M + H)^+$], 362.1240; found 362.1241.

(+)-3-Deoxydihydrolycoricidine (9). 2,4-diacetoxy-3-deoxydihydrolycoricidin SI16 (0.0085 g, 0.024 mmol) and potassium carbonate (0.0003 g, 0.001 mmol, 0.10 equiv) were dissolved in CH_3OH (0.153 mL) and water (0.017 mL) and stirred at room temperature until a white solid precipitate, TLC analysis showed full conversion after 16 h. The mixture was concentrated under a flow of N_2. The white product was dissolved in 9:1 CH_2Cl_2 / MeOH and filtered through a path of silica. The white solid was recrystallized from methanol to afford 0.0057 g of fine white needles.

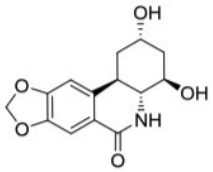

Yield: 87%; M.P.: 255-257 °C (recrystallized from MeOH); TLC(CH_2Cl_2:MeOH, 95:5 v/v; UV): R_f = 0.08; $[\alpha]^{21}_D$ = +32 (c = 0.527, MeOH, l = 1 dm); ^{1}H NMR (600 MHz, MeOD) δ 7.39 (s, 1H, CH-Ar), 6.86 (s, 1H, CH-Ar), 6.03 (dd, J = 7.5, 0.9 Hz, 2H, OCH_2O), 4.33 – 4.27 (m, 1H, CH_2CHCH_2), 3.96 (ddd, J = 11.5, 9.1, 4.5 Hz, 1H, CH(O)CHN), 3.11 (dd, J = 11.8, 3.5 Hz, 1H, CH-Ar), 3.09 (d, J = 9.0 Hz, 1H, CH-NH), 2.42 (ddd, J = 13.7, 5.5, 3.1 Hz, 1H, CH_2CHAr), 2.21 – 2.13 (m, 1H, $COCH_2CO$), 1.56 (ddt, J = 14.0, 11.6, 2.5 Hz, 2H, CH_2, CH_2); ^{13}C NMR (151 MHz, MeOD) δ 167.64, 153.20, 148.13, 139.52, 123.79, 108.43, 105.32, 103.28, 68.94, 66.65, 62.63, 40.59, 35.50, 34.52; IR (KBr, cm^{-1}) ν 3243, 3080, 2919, 1732, 1675, 1487, 1457, 1355, 1240, 1040, 934; HRMS (ESI): exact mass calculated for $C_{14}H_{16}NO_5$ [$(M + H)^+$], 278.1028; found 278.1028.

APPENDIX E: INDIVIDUAL CONTRIBUTION

My personal contributions to the work described in this thesis are outlined below, by section.

In the additional methods section: I cultured Vero cells, CV-28 cells, fibroblasts, iPSCs, NSC/eNPCs, and iPSC-neurons and performed viral propagation and quantitation of HSV-1 (strains KOS, HSV-1 from Dr. Kinchington, and HSV-1 from Dr. Homa) on their respective cell types. I performed viral plaque assays on Vero cells. I performed HSV-1 infections in iPSC-neurons for lytic infection, inducing quiescent infections, and viral reactivation, as well as lytic infections in Vero cells. In addition to the FISH studies listed below, I also performed FISH in suspension and RNA FISH. I performed PCR *in situ,* reverse transcriptase quantitative PCR, and DNA sequencing. I performed the lytic infections in Vero and the quiescent HSV-1 infections in iPSC-neurons using Dr. Homa's HSV-1 replication defective virus.

Manuscript 1: I contributed to cell culture work, immunocytochemistry of the neurosphere-like objects (NLSs), microscopy, and preparation of the manuscript.

Manuscript 2: I contributed to and analyzed viral infections, plaque assays on Vero cells, the pathway analysis for the microarray data by using Ingenuity Pathway Analysis program, and preparation of the manuscript.

Additional virological assays: I contributed to the design of the project and analyzed the viral copy number (Experiment 1). I also performed the 2D and 3D FISH studies (Experiment

2), the Co-ICC/FISH experiments (Experiment 3), and the CHART-PCR experiments (Experiment 4).

Manuscript 3: I contributed to the design of the project and analysis of drug testing on Vero and iPSC-neurons, plaque assays on Vero cells, viral copy number assays, flow cytometry analysis, FISH on iPSC-neurons, immunocytochemistry, viral attachment/entry assays, statistical analyses for IC50 and CC50 calculations, testing for VZV efficacy and toxicity, and preparation of the manuscript.

Manuscript 4: I contributed to the analysis of HSV-1 viral infections, flow cytometry analysis, viral copy number assays, statistical analyses for IC50 and CC50 calculations, and preparation of the manuscript. I also contributed to the design and analysis of antiviral activity of selected compounds on VZV infections.

Groundwork for moderate throughput drug screening. I contributed to the design of the experiments, and performed cell culture, viral infections (lytic, quiescent, and viral reactivation), NSC purifications, immunocytochemistry, and preparation of the cells for microscopy at the Drug Discovery Institute at the University of Pittsburgh.

BIBLIOGRAPHY

Aasen, T., Raya, A., Barrero, M. J., Garreta, E., Consiglio, A., Gonzalez, F., et al. (2008). Efficient and rapid generation of induced pluripotent stem cells from human keratinocytes. *Nat Biotechnol, 26*(11), 1276-1284.

Acquaah-Harrison, G., Zhou, S., Hines, J. V. & Bergmeier, S. C. Library of 1,4-Disubstituted 1,2,3-Triazole Analogues of Oxazolidinone RNA-Binding Agents. J. Comb. Chem. 12, 491–496 (2010).

Agut, H., Bonnafous, P., & Gautheret-Dejean, A. (2015). Laboratory and clinical aspects of human herpesvirus 6 infections. *Clin Microbiol Rev, 28*(2), 313-335.

Aiello, A. E., Haan, M. N., Pierce, C. M., Simanek, A. M., & Liang, J. (2008). Persistent infection, inflammation, and functional impairment in older Latinos. *J Gerontol A Biol Sci Med Sci, 63*(6), 610-618.

Al-Dujaili LJ, Clerkin PP, Clement C, McFerrin HE, Bhattacharjee PS, Varnell ED, Kaufman HE, Hill JM. (2011). Ocular herpes simplex virus: how are latency, reactivation, recurrent disease and therapy interrelated? *Future Microbiol*. Aug;6(8):877-907.

Amelio, A. L., McAnany, P. K., & Bloom, D. C. (2006). A chromatin insulator-like element in the herpes simplex virus type 1 latency-associated transcript region binds CCCTC-binding factor and displays enhancer-blocking and silencing activities. *J Virol, 80*(5), 2358-2368.

Antoine, T. E., Park, P. J., & Shukla, D. (2013). Glycoprotein targeted therapeutics: a new era of anti-herpes simplex virus-1 therapeutics. *Rev Med Virol, 23*(3), 194-208.

Anuradha, K., Singh, H. M., Gopal, K. V., Rama Rao, G. R., Ramani, T. V., & Padmaja, J. (2008). Herpes simplex virus 2 infection: a risk factor for HIV infection in heterosexuals. *Indian J Dermatol Venereol Leprol, 74*(3), 230-233.

Asahi, T., Tsutsui, M., Wakasugi, M., Tange, D., Takahashi, C., Tokui, K., et al. (2009). Valacyclovir neurotoxicity: clinical experience and review of the literature. *Eur J Neurol, 16*(4), 457-460.

Aslani, A., Olsson, M., & Elias, P. (2002). ATP-dependent unwinding of a minimal origin of DNA replication by the origin-binding protein and the single-strand DNA-binding protein ICP8 from herpes simplex virus type I. *J Biol Chem, 277*(43), 41204-41212.

Avilion, A. A., Nicolis, S. K., Pevny, L. H., Perez, L., Vivian, N., & Lovell-Badge, R. (2003). Multipotent cell lineages in early mouse development depend on SOX2 function. *Genes Dev, 17*(1), 126-140.

Azari H, Sharififar S, Darioosh RP, Fortin JM, Rahman M, et al. (2014) Purifying Immature Neurons from Differentiating Neural Stem Cell Progeny Using a Simple Shaking Method. J Stem Cell Res Ther 4:178. doi: 10.4172/2157-7633.1000178

Bagasra, O. (2007). Protocols for the in situ PCR-amplification and detection of mRNA and DNA sequences. *Nat Protoc, 2*(11), 2782-2795.

Baharvand, H., Mehrjardi, N. Z., Hatami, M., Kiani, S., Rao, M., & Haghighi, M. M. (2007). Neural differentiation from human embryonic stem cells in a defined adherent culture condition. *Int J Dev Biol, 51*(5), 371-378.

Baines, J. D., Jacob, R. J., Simmerman, L., & Roizman, B. (1995). The herpes simplex virus 1 UL11 proteins are associated with cytoplasmic and nuclear membranes and with nuclear bodies of infected cells. *J Virol, 69*(2), 825-833.

Baringer, J. R., & Pisani, P. (1994). Herpes simplex virus genomes in human nervous system tissue analyzed by polymerase chain reaction. *Ann Neurol, 36*(6), 823-829.

Baringer, J. R., & Swoveland, P. (1973). Recovery of herpes-simplex virus from human trigeminal ganglions. *N Engl J Med, 288*(13), 648-650.

Barker, K. R., Sarafino-Wani, R., Khanom, A., Griffiths, P. D., Jacobs, M. G., & Webster, D. P. (2014). Encephalitis in an immunocompetent man. *J Clin Virol, 59*(1), 1-3.

Barnett, E. M., Evans, G. D., Sun, N., Perlman, S., & Cassell, M. D. (1995). Anterograde tracing of trigeminal afferent pathways from the murine tooth pulp to cortex using herpes simplex virus type 1. *J Neurosci, 15*(4), 2972-2984.

Bastian, F. O., Rabson, A. S., Yee, C. L., & Tralka, T. S. (1972). Herpesvirus hominis: isolation from human trigeminal ganglion. *Science, 178*(4058), 306-307.

Bates, P. A., & DeLuca, N. A. (1998). The polyserine tract of herpes simplex virus ICP4 is required for normal viral gene expression and growth in murine trigeminal ganglia. *J Virol, 72*(9), 7115-7124.

Batterson, W., Furlong, D., & Roizman, B. (1983). Molecular genetics of herpes simplex virus. VIII. further characterization of a temperature-sensitive mutant defective in release of viral DNA and in other stages of the viral reproductive cycle. *J Virol, 45*(1), 397-407.

Bauer, D. W., Huffman, J. B., Homa, F. L., & Evilevitch, A. (2013). Herpes virus genome, the pressure is on. *J Am Chem Soc, 135*(30), 11216-11221.

Bauwens, C. L., Peerani, R., Niebruegge, S., Woodhouse, K. A., Kumacheva, E., Husain, M., et al. (2008). Control of human embryonic stem cell colony and aggregate size heterogeneity influences differentiation trajectories. *Stem Cells, 26*(9), 2300-2310.

Bayer, A., Delorme-Axford, E., Sleigher, C., Frey, T. K., Trobaugh, D. W., Klimstra, W. B., et al. (2015). Human trophoblasts confer resistance to viruses implicated in perinatal infection. *Am J Obstet Gynecol, 212*(1), 71.e71-78.

Becker, Y. (1995). HSV-1 brain infection by the olfactory nerve route and virus latency and reactivation may cause learning and behavioral deficiencies and violence in children and adults: a point of view. *Virus Genes, 10*(3), 217-226.

Beevers, J. E., Caffrey, T. M., & Wade-Martins, R. (2013). Induced pluripotent stem cell (iPSC)-derived dopaminergic models of Parkinson's disease. *Biochem Soc Trans, 41*(6), 1503-1508.

Bermek, O., Willcox, S., & Griffith, J. D. (2015). DNA replication catalyzed by herpes simplex virus type 1 proteins reveals trombone loops at the fork. *J Biol Chem, 290*(5), 2539-2545.

Besecker, M. I., Furness, C. L., Coen, D. M., & Griffiths, A. (2007). Expression of extremely low levels of thymidine kinase from an acyclovir-resistant herpes simplex virus mutant supports reactivation from latently infected mouse trigeminal ganglia. *J Virol, 81*(15), 8356-8360.

Bi Y, Sun L, Gao D, Ding C, Li Z, Li Y, Cun W, Li Q. (2014). High-efficiency targeted editing of large viral genomes by RNA-guided nucleases. *PLoS Pathog*. May 1;10(5):e1004090.

Biedler, J. L., Roffler-Tarlov, S., Schachner, M., & Freedman, L. S. (1978). Multiple neurotransmitter synthesis by human neuroblastoma cell lines and clones. *Cancer Res, 38*(11 Pt 1), 3751-3757.

Biron, K. K. (2006). Antiviral drugs for cytomegalovirus diseases. *Antiviral Res, 71*(2-3), 154-163.

Biron, K. K., Harvey, R. J., Chamberlain, S. C., Good, S. S., Smith, A. A., Davis, M. G., et al. (2002). Potent and selective inhibition of human cytomegalovirus replication by 1263W94, a benzimidazole L-riboside with a unique mode of action. *Antimicrob Agents Chemother, 46*(8), 2365-2372.

Bischofberger, N. et al. Synthesis of analogues of 1, 3-dihydroxyacetone phosphate and glyceraldehyde 3-phosphate for use in studies of fructose-1, 6-diphosphate aldolase. J. Org. Chem. 53, 3457–3465 (1988).

Biswas, S., Swift, M., & Field, H. J. (2007). High frequency of spontaneous helicase-primase inhibitor (BAY 57-1293) drug-resistant variants in certain laboratory isolates of HSV-1. *Antivir Chem Chemother, 18*(1), 13-23.

Blaho, J. A., Mitchell, C., & Roizman, B. (1993). Guanylylation and adenylylation of the alpha regulatory proteins of herpes simplex virus require a viral beta or gamma function. *J Virol, 67*(7), 3891-3900.

Blaho, J. A., Morton, E. R., & Yedowitz, J. C. (2005). Herpes simplex virus: propagation, quantification, and storage. *Curr Protoc Microbiol, Chapter 14*, Unit 14E.11.

Block, T., Barney, S., Masonis, J., Maggioncalda, J., Valyi-Nagy, T., & Fraser, N. W. (1994). Long term herpes simplex virus type 1 infection of nerve growth factor-treated PC12 cells. *J Gen Virol, 75 (Pt 9)*, 2481-2487.

Block, T. M., Spivack, J. G., Steiner, I., Deshmane, S., McIntosh, M. T., Lirette, R. P., et al. (1990). A herpes simplex virus type 1 latency-associated transcript mutant reactivates with normal kinetics from latent infection. *J Virol, 64*(7), 3417-3426.

Bloom, D. C., Devi-Rao, G. B., Hill, J. M., Stevens, J. G., & Wagner, E. K. (1994). Molecular analysis of herpes simplex virus type 1 during epinephrine-induced reactivation of latently infected rabbits in vivo. *J Virol, 68*(3), 1283-1292.

Bloom, D. C., Giordani, N. V., & Kwiatkowski, D. L. (2010). Epigenetic regulation of latent HSV-1 gene expression. *Biochim Biophys Acta, 1799*(3-4), 246-256.

Bogner, E. (2002). Human cytomegalovirus terminase as a target for antiviral chemotherapy. *Rev Med Virol, 12*(2), 115-127.

Bogner, E., Radsak, K., & Stinski, M. F. (1998). The gene product of human cytomegalovirus open reading frame UL56 binds the pac motif and has specific nuclease activity. *J Virol, 72*(3), 2259-2264.

Boissart, C., Poulet, A., Georges, P., Darville, H., Julita, E., Delorme, R., et al. (2013). Differentiation from human pluripotent stem cells of cortical neurons of the superficial layers amenable to psychiatric disease modeling and high-throughput drug screening. *Transl Psychiatry, 3*, e294.

Boshoff, C., & Weiss, R. A. (1998). Kaposi's sarcoma-associated herpesvirus. *Adv Cancer Res, 75*, 57-86.

Brennand, K. J., Simone, A., Jou, J., Gelboin-Burkhart, C., Tran, N., Sangar, S., et al. (2011). Modelling schizophrenia using human induced pluripotent stem cells. *Nature, 473*(7346), 221-225.

Brown, J. C. (2007). High G+C Content of Herpes Simplex Virus DNA: Proposed Role in Protection Against Retrotransposon Insertion. *Open Biochem J, 1*, 33-42.

Brown, Z. A., Selke, S., Zeh, J., Kopelman, J., Maslow, A., Ashley, R. L., et al. (1997). The acquisition of herpes simplex virus during pregnancy. *N Engl J Med, 337*(8), 509-515.

Brown, Z. A., Wald, A., Morrow, R. A., Selke, S., Zeh, J., & Corey, L. (2003). Effect of serologic status and cesarean delivery on transmission rates of herpes simplex virus from mother to infant. *JAMA, 289*(2), 203-209.

Burgos, J. S., Ramirez, C., Sastre, I., Bullido, M. J., & Valdivieso, F. (2002). Involvement of apolipoprotein E in the hematogenous route of herpes simplex virus type 1 to the central nervous system. *J Virol, 76*(23), 12394-12398.

Burrel, S., Aime, C., Hermet, L., Ait-Arkoub, Z., Agut, H., & Boutolleau, D. (2013). Surveillance of herpes simplex virus resistance to antivirals: a 4-year survey. [Research Support, Non-U.S. Gov't]. *Antiviral Res, 100*(2), 365-372.

Camarena, V., Kobayashi, M., Kim, J. Y., Roehm, P., Perez, R., Gardner, J., et al. (2010). Nature and duration of growth factor signaling through receptor tyrosine kinases regulates HSV-1 latency in neurons. *Cell Host Microbe, 8*(4), 320-330.

Cannon, M. J., Schmid, D. S., & Hyde, T. B. (2010). Review of cytomegalovirus seroprevalence and demographic characteristics associated with infection. *Rev Med Virol, 20*(4), 202-213.

Canzio, D., Chang, E. Y., Shankar, S., Kuchenbecker, K. M., Simon, M. D., Madhani, H. D., et al. (2011). Chromodomain-mediated oligomerization of HP1 suggests a nucleosome-bridging mechanism for heterochromatin assembly. *Mol Cell, 41*(1), 67-81.

Carter, C. S., Perlstein, W., Ganguli, R., Brar, J., Mintun, M., & Cohen, J. D. (1998). Functional hypofrontality and working memory dysfunction in schizophrenia. *Am J Psychiatry, 155*(9), 1285-1287.

Cartwright, P., McLean, C., Sheppard, A., Rivett, D., Jones, K., & Dalton, S. (2005). LIF/STAT3 controls ES cell self-renewal and pluripotency by a Myc-dependent mechanism. *Development, 132*(5), 885-896.

Casrouge, A., Zhang, S. Y., Eidenschenk, C., Jouanguy, E., Puel, A., Yang, K., et al. (2006). Herpes simplex virus encephalitis in human UNC-93B deficiency. *Science, 314*(5797), 308-312.

Catez, F., Picard, C., Held, K., Gross, S., Rousseau, A., Theil, D., et al. (2012). HSV-1 genome subnuclear positioning and associations with host-cell PML-NBs and centromeres regulate LAT locus transcription during latency in neurons. *PLoS Pathog, 8*(8), e1002852.

Catez F, Rousseau A, Labetoulle M, Lomonte P. (2014). Detection of the genome and transcripts of a persistent DNA virus in neuronal tissues by fluorescent in situ hybridization combined with immunostaining. *J Vis Exp.* Jan 23;(83):e51091.

Centers for Disease Control (CDC). (February 8, 2011). Blindness and Vision Impairment. from http://www.cdc.gov/healthcommunication/ToolsTemplates/EntertainmentEd/Tips/Blindness.html.

Cereghini, S., & Yaniv, M. (1984). Assembly of transfected DNA into chromatin: structural changes in the origin-promoter-enhancer region upon replication. *EMBO J, 3*(6), 1243-1253.

Charbord, J., Poydenot, P., Bonnefond, C., Feyeux, M., Casagrande, F., Brinon, B., et al. (2013). High throughput screening for inhibitors of REST in neural derivatives of human embryonic stem cells reveals a chemical compound that promotes expression of neuronal genes. *Stem Cells, 31*(9), 1816-1828.

Chattopadhyay S, Chen Y, Weller SK. (2006). The two helicases of herpes simplex virus type 1 (HSV-1). *Front Biosci*. Sep 1;11:2213-23.

Chemaly, R. F., Ullmann, A. J., Stoelben, S., Richard, M. P., Bornhäuser, M., Groth, C., et al. (2014). Letermovir for cytomegalovirus prophylaxis in hematopoietic-cell transplantation. *N Engl J Med, 370*(19), 1781-1789.

Chen X, Schmidt MC, Goins WF, Glorioso JC. (1995). Two herpes simplex virus type 1 latency-active promoters differ in their contributions to latency-associated transcript expression during lytic and latent infections. *J Virol.* Dec;69(12):7899-908.

Chisholm, C., & Lopez, L. (2011). Cutaneous infections caused by Herpesviridae: a review. *Arch Pathol Lab Med, 135*(10), 1357-1362.

Cho, M. S., Hwang, D. Y., & Kim, D. W. (2008). Efficient derivation of functional dopaminergic neurons from human embryonic stem cells on a large scale. *Nat Protoc, 3*(12), 1888-1894.

Choudhary, M., Kumar, A., Tripathi, M., Bhatia, T., Shivakumar, V., Beniwal, R. P., et al. (2015). F-18 fluorodeoxyglucose positron emission tomography study of impaired emotion processing in first episode schizophrenia. Schizophr Res, 162(1-3), 103-107.

Cisneros, J. A. et al. Structure−Activity Relationship of a Series of Inhibitors of Monoacylglycerol Hydrolysis Comparison with Effects upon Fatty Acid Amide Hydrolase. J. Med. Chem. 50, 5012–5023 (2007).

Cleary, M. A., Stern, S., Tanaka, M., & Herr, W. (1993). Differential positive control by Oct-1 and Oct-2: activation of a transcriptionally silent motif through Oct-1 and VP16 corecruitment. *Genes Dev, 7*(1), 72-83.

Cliffe, A. R., Garber, D. A., & Knipe, D. M. (2009). Transcription of the herpes simplex virus latency-associated transcript promotes the formation of facultative heterochromatin on lytic promoters. *J Virol, 83*(16), 8182-8190.

Cocchi, F., Fusco, D., Menotti, L., Gianni, T., Eisenberg, R. J., Cohen, G. H., et al. (2004). The soluble ectodomain of herpes simplex virus gD contains a membrane-proximal pro-fusion domain and suffices to mediate virus entry. *Proc Natl Acad Sci U S A, 101*(19), 7445-7450.

Cocchi, F., Menotti, L., Mirandola, P., Lopez, M., & Campadelli-Fiume, G. (1998). The ectodomain of a novel member of the immunoglobulin subfamily related to the poliovirus receptor has the attributes of a bona fide receptor for herpes simplex virus types 1 and 2 in human cells. *J Virol, 72*(12), 9992-10002.

Coen, D. M. (1994). Acyclovir-resistant, pathogenic herpesviruses. *Trends Microbiol, 2*(12), 481-485.

Cohen, G. H., Ponce de Leon, M., Diggelmann, H., Lawrence, W. C., Vernon, S. K., & Eisenberg, R. J. (1980). Structural analysis of the capsid polypeptides of herpes simplex virus types 1 and 2. *J Virol, 34*(2), 521-531.

Cohrs, R. J., Randall, J., Smith, J., Gilden, D. H., Dabrowski, C., van Der Keyl, H., et al. (2000). Analysis of individual human trigeminal ganglia for latent herpes simplex virus type 1 and varicella-zoster virus nucleic acids using real-time PCR. *J Virol, 74*(24), 11464-11471.

Colapinto, M., Mila, S., Giraudo, S., Stefanazzi, P., Molteni, M., Rossetti, C., et al. (2006). alpha-Synuclein protects SH-SY5Y cells from dopamine toxicity. *Biochem Biophys Res Commun, 349*(4), 1294-1300.

Conn, K. L., & Schang, L. M. (2013). Chromatin dynamics during lytic infection with herpes simplex virus 1. *Viruses, 5*(7), 1758-1786.

Creech, C. C., & Neumann, D. M. (2010). Changes to euchromatin on LAT and ICP4 following reactivation are more prevalent in an efficiently reactivating strain of HSV-1. *PLoS One, 5*(11), e15416.

Cremer, M., Müller, S., Köhler, D., Brero, A., & Solovei, I. (2007). Cell Preparation and Multicolor FISH in 3D Preserved Cultured Mammalian Cells. *CSH Protoc, 2007*, pdb.prot4723.

Cruickshank, M., Fenwick, E., Abraham, L. J., & Ulgiati, D. (2008). Quantitative differences in chromatin accessibility across regulatory regions can be directly compared in distinct cell-types. *Biochem Biophys Res Commun, 367*(2), 349-355.

Cundy, K. C., Bidgood, A. M., Lynch, G., Shaw, J. P., Griffin, L., & Lee, W. A. (1996). Pharmacokinetics, bioavailability, metabolism, and tissue distribution of cidofovir (HPMPC) and cyclic HPMPC in rats. *Drug Metab Dispos, 24*(7), 745-752.

Curanović D, Ch'ng TH, Szpara M, Enquist L. (2009). Compartmented neuron cultures for directional infection by alpha herpesviruses. *Curr Protoc Cell Biol*. Jun;Chapter 26:Unit 26.4.

D'Aiuto, L., Antonacci, R., Marzella, R., Archidiacono, N., & Rocchi, M. (1993). Cloning and comparative mapping of a human chromosome 4-specific alpha satellite DNA sequence. *Genomics, 18*(2), 230-235.

D'Aiuto, L., Di Maio, R., Heath, B., Raimondi, G., Milosevic, J., Watson, A. M., et al. (2012). Human induced pluripotent stem cell-derived models to investigate human cytomegalovirus infection in neural cells. *PLoS One, 7*(11), e49700.

D'Aiuto, L., Prasad, K. M., Upton, C. H., Viggiano, L., Milosevic, J., Raimondi, G., et al. (2014). Persistent Infection by HSV-1 Is Associated With Changes in Functional Architecture of iPSC-Derived Neurons and Brain Activation Patterns Underlying Working Memory Performance. *Schizophr Bull*.

D'Aiuto, L., Robison, C. S., Gigante, M., Nwanegbo, E., Shaffer, B., Sukhwani, M., et al. (2008). Human IL-12 p40 as a reporter gene for high-throughput screening of engineered mouse embryonic stem cells. *BMC Biotechnol, 8*, 52.

D'Aiuto, L., Zhi, Y., Kumar Das, D., Wilcox, M. R., Johnson, J. W., McClain, L., et al. (2014). Large-scale generation of human iPSC-derived neural stem cells/early neural progenitor cells and their neuronal differentiation. *Organogenesis, 10*(4), 365-377.

Damato, E. G., & Winnen, C. W. (2002). Cytomegalovirus infection: perinatal implications. *J Obstet Gynecol Neonatal Nurs, 31*(1), 86-92.

Danaher, R. J., Cook, R. K., Wang, C., Triezenberg, S. J., Jacob, R. J., & Miller, C. S. (2013). C-terminal trans-activation sub-region of VP16 is uniquely required for forskolin-induced herpes simplex virus type 1 reactivation from quiescently infected-PC12 cells but not for replication in neuronally differentiated-PC12 cells. *J Neurovirol, 19*(1), 32-41.

Danaher, R. J., Jacob, R. J., Steiner, M. R., Allen, W. R., Hill, J. M., & Miller, C. S. (2005). Histone deacetylase inhibitors induce reactivation of herpes simplex virus type 1 in a latency-associated transcript-independent manner in neuronal cells. *J Neurovirol, 11*(3), 306-317.

Davie, J. R. (2003). Inhibition of histone deacetylase activity by butyrate. *J Nutr, 133*(7 Suppl), 2485S-2493S.

De Clercq E. (2013). Highlights in antiviral drug research: antivirals at the horizon. *Med Res Rev.* Nov;33(6):1215-48.

De Clercq, E. (2005). (E)-5-(2-bromovinyl)-2'-deoxyuridine (BVDU). *Med Res Rev, 25*(1), 1-20.

De Clercq, E., Naesens, L., De Bolle, L., Schols, D., Zhang, Y., & Neyts, J. (2001). Antiviral agents active against human herpesviruses HHV-6, HHV-7 and HHV-8. *Rev Med Virol, 11*(6), 381-395.

Deaton, A. M., & Bird, A. (2011). CpG islands and the regulation of transcription. *Genes Dev, 25*(10), 1010-1022.

Debiasi, R. L., & Tyler, K. L. (2004). Molecular methods for diagnosis of viral encephalitis. *Clin Microbiol Rev, 17*(4), 903-925, table of contents.

Decman, V., Freeman, M. L., Kinchington, P. R., & Hendricks, R. L. (2005). Immune control of HSV-1 latency. *Viral Immunol, 18*(3), 466-473.

Deisboeck, T. S., Wakimoto, H., Nestler, U., Louis, D. N., Sehgal, P. K., Simon, M., et al. (2003). Development of a novel non-human primate model for preclinical gene vector safety studies. Determining the effects of intracerebral HSV-1 inoculation in the common marmoset: a comparative study. *Gene Ther, 10*(15), 1225-1233.

Deniaud, E., & Bickmore, W. A. (2009). Transcription and the nuclear periphery: edge of darkness? *Curr Opin Genet Dev, 19*(2), 187-191.

Deo, A. J., Goldszer, I. M., Li, S., DiBitetto, J. V., Henteleff, R., Sampson, A., et al. (2013). PAK1 protein expression in the auditory cortex of schizophrenia subjects. *PLoS One, 8*(4), e59458.

Deshmane, S. L., & Fraser, N. W. (1989). During latency, herpes simplex virus type 1 DNA is associated with nucleosomes in a chromatin structure. *J Virol, 63*(2), 943-947.

Dhara, S. K., & Stice, S. L. (2008). Neural differentiation of human embryonic stem cells. *J Cell Biochem, 105*(3), 633-640.

Dickerson, F., Stallings, C., Origoni, A., Vaughan, C., Khushalani, S., & Yolken, R. (2012). Additive effects of elevated C-reactive protein and exposure to Herpes Simplex Virus type 1 on cognitive impairment in individuals with schizophrenia. *Schizophr Res, 134*(1), 83-88.

Dickerson, F., Stallings, C., Sullens, A., Origoni, A., Leister, F., Krivogorsky, B., et al. (2008). Association between cognitive functioning, exposure to Herpes Simplex Virus type 1, and the COMT Val158Met genetic polymorphism in adults without a psychiatric disorder. *Brain Behav Immun, 22*(7), 1103-1107.

Dickerson, F. B., Boronow, J. J., Stallings, C., Origoni, A. E., Cole, S., Krivogorsky, B., et al. (2004). Infection with herpes simplex virus type 1 is associated with cognitive deficits in bipolar disorder. *Biol Psychiatry, 55*(6), 588-593.

Dickerson, F. B., Boronow, J. J., Stallings, C., Origoni, A. E., Ruslanova, I., & Yolken, R. H. (2003). Association of serum antibodies to herpes simplex virus 1 with cognitive deficits in individuals with schizophrenia. *Arch Gen Psychiatry, 60*(5), 466-472.

Diefenbach, R. J., Miranda-Saksena, M., Diefenbach, E., Holland, D. J., Boadle, R. A., Armati, P. J., et al. (2002). Herpes simplex virus tegument protein US11 interacts with conventional kinesin heavy chain. *J Virol, 76*(7), 3282-3291.

Dolan, A., Jamieson, F. E., Cunningham, C., Barnett, B. C., & McGeoch, D. J. (1998). The genome sequence of herpes simplex virus type 2. *J Virol, 72*(3), 2010-2021.

Dorsky, D. I., & Crumpacker, C. S. (1988). Expression of herpes simplex virus type 1 DNA polymerase gene by in vitro translation and effects of gene deletions on activity. *J Virol, 62*(9), 3224-3232.

Doyle, S., Vaidya, S., O'Connell, R., Dadgostar, H., Dempsey, P., Wu, T., et al. (2002). IRF3 mediates a TLR3/TLR4-specific antiviral gene program. *Immunity, 17*(3), 251-263.

Dressler, G. R., Rock, D. L., & Fraser, N. W. (1987). Latent herpes simplex virus type 1 DNA is not extensively methylated in vivo. *J Gen Virol, 68 (Pt 6)*, 1761-1765.

Dropulic, L. K., & Cohen, J. I. (2010). Update on new antivirals under development for the treatment of double-stranded DNA virus infections. *Clin Pharmacol Ther, 88*(5), 610-619.

Duan, R., de Vries, R. D., Osterhaus, A. D., Remeijer, L., & Verjans, G. M. (2008). Acyclovir-resistant corneal HSV-1 isolates from patients with herpetic keratitis. *J Infect Dis, 198*(5), 659-663.

Dukhovny, A., Sloutskin, A., Markus, A., Yee, M. B., Kinchington, P. R., & Goldstein, R. S. (2012). Varicella-zoster virus infects human embryonic stem cell-derived neurons and neurospheres but not pluripotent embryonic stem cells or early progenitors. *J Virol, 86*(6), 3211-3218.

Dyson, H., Shimeld, C., Hill, T. J., Blyth, W. A., & Easty, D. L. (1987). Spread of herpes simplex virus within ocular nerves of the mouse: demonstration of viral antigen in whole mounts of eye tissue. *J Gen Virol, 68 (Pt 12)*, 2989-2995.

Döhner, K., Wolfstein, A., Prank, U., Echeverri, C., Dujardin, D., Vallee, R., et al. (2002). Function of dynein and dynactin in herpes simplex virus capsid transport. *Mol Biol Cell, 13*(8), 2795-2809.

Efstathiou, S., Minson, A. C., Field, H. J., Anderson, J. R., & Wildy, P. (1986). Detection of herpes simplex virus-specific DNA sequences in latently infected mice and in humans. *J Virol, 57*(2), 446-455.

Efthymiou, A., Shaltouki, A., Steiner, J. P., Jha, B., Heman-Ackah, S. M., Swistowski, A., et al. (2014). Functional screening assays with neurons generated from pluripotent stem cell-derived neural stem cells. *J Biomol Screen, 19*(1), 32-43.

Eigentler, A., Boesch, S., Schneider, R., Dechant, G., & Nat, R. (2013). Induced pluripotent stem cells from friedreich ataxia patients fail to upregulate frataxin during in vitro differentiation to peripheral sensory neurons. *Stem Cells Dev, 22*(24), 3271-3282.

Elbadawy HM, Gailledrat M, Desseaux C, Salvalaio G, Di Iorio E, Ferrari B, Bertolin M, Barbaro V, Parekh M, Gayon R, Munegato D, Franchin E, Calistri A, Palù G, Parolin C, Ponzin D, Ferrari S. (2014). Gene transfer of integration defective anti-HSV-1 meganuclease to human corneas ex vivo. *Gene Ther*. Mar;21(3):272-81.

Elkabetz, Y., & Studer, L. (2008). Human ESC-derived neural rosettes and neural stem cell progression. *Cold Spring Harb Symp Quant Biol, 73*, 377-387.

Emeny JM, Morgan MJ. (1979). Regulation of the interferon system: evidence that Vero cells have a genetic defect in interferon production. *J Gen Virol.* Apr;43(1):247-52.

Evidente, A., Kireev, A. S., Jenkins, A. R., Romero, A. E., Steelant, W. F., Van Slambrouck, S., et al. (2009). Biological evaluation of structurally diverse amaryllidaceae alkaloids and their synthetic derivatives: discovery of novel leads for anticancer drug design. *Planta Med, 75*(5), 501-507.

Farooq, A. V., & Shukla, D. (2012). Herpes simplex epithelial and stromal keratitis: an epidemiologic update. *Surv Ophthalmol, 57*(5), 448-462.

Farrell, M. J., Dobson, A. T., & Feldman, L. T. (1991). Herpes simplex virus latency-associated transcript is a stable intron. *Proc Natl Acad Sci U S A, 88*(3), 790-794.

Feldman LT, Ellison AR, Voytek CC, Yang L, Krause P, Margolis TP. (2002). Spontaneous molecular reactivation of herpes simplex virus type 1 latency in mice. *Proc Natl Acad Sci U S A.* Jan 22;99(2):978-83.

Fenwick, M. L., & Everett, R. D. (1990). Inactivation of the shutoff gene (UL41) of herpes simplex virus types 1 and 2. *J Gen Virol, 71 (Pt 12)*, 2961-2967.

Ferenczy, M. W., & DeLuca, N. A. (2009). Epigenetic modulation of gene expression from quiescent herpes simplex virus genomes. *J Virol, 83*(17), 8514-8524.

Field, H. J., Huang, M. L., Lay, E. M., Mickleburgh, I., Zimmermann, H., & Birkmann, A. (2013). Baseline sensitivity of HSV-1 and HSV-2 clinical isolates and defined acyclovir-resistant strains to the helicase-primase inhibitor pritelivir. *Antiviral Res, 100*(2), 297-299.

Field, H. J., & Thackray, A. M. (2000). Early therapy with valaciclovir or famciclovir reduces but does not abrogate herpes simplex virus neuronal latency. *Nucleosides Nucleotides Nucleic Acids, 19*(1-2), 461-470.

First, M. B., Spitzer, R. L., Gibbon, M., & Williams, J. B. W. (1995). *Structured Clinical Interview for DSM-IV Axis I Disorders- Patient Edition*. New York: New York State Psychiatric Institute.

Flagg, E. W., & Weinstock, H. (2011). Incidence of neonatal herpes simplex virus infections in the United States, 2006. *Pediatrics, 127*(1), e1-8.

Frank, K. B., Chiou, J. F., & Cheng, Y. C. (1984). Interaction of herpes simplex virus-induced DNA polymerase with 9-(1,3-dihydroxy-2-propoxymethyl)guanine triphosphate. *J Biol Chem, 259*(3), 1566-1569.

Freeman, E. E., Weiss, H. A., Glynn, J. R., Cross, P. L., Whitworth, J. A., & Hayes, R. J. (2006). Herpes simplex virus 2 infection increases HIV acquisition in men and women: systematic review and meta-analysis of longitudinal studies. *AIDS, 20*(1), 73-83.

Friedman, H. R., & Goldman-Rakic, P. S. (1994). Coactivation of prefrontal cortex and inferior parietal cortex in working memory tasks revealed by 2DG functional mapping in the rhesus monkey. *J Neurosci, 14*(5 Pt 1), 2775-2788.

Fruchter, E., Goldberg, S., Fenchel, D., Grotto, I., Ginat, K., & Weiser, M. (2015). The impact of Herpes simplex virus type 1 on cognitive impairments in young, healthy individuals - A historical prospective study. *Schizophr Res, 168*(1-2), 292-296.

Fukayama, M. (2010). Epstein-Barr virus and gastric carcinoma. *Pathol Int, 60*(5), 337-350.

Furukawa, H., Singh, S. K., Mancusso, R., & Gouaux, E. (2005). Subunit arrangement and function in NMDA receptors. *Nature, 438*(7065), 185-192.

Fusaki, N., Ban, H., Nishiyama, A., Saeki, K., & Hasegawa, M. (2009). Efficient induction of transgene-free human pluripotent stem cells using a vector based on Sendai virus, an RNA virus that does not integrate into the host genome. *Proc Jpn Acad Ser B Phys Biol Sci, 85*(8), 348-362.

Gabrielsen, B., Monath, T. P., Huggins, J. W., Kefauver, D. F., Pettit, G. R., Groszek, G., et al. (1992). Antiviral (RNA) activity of selected Amaryllidaceae isoquinoline constituents and synthesis of related substances. *J Nat Prod, 55*(11), 1569-1581.

Gao, Z., Ure, K., Ables, J. L., Lagace, D. C., Nave, K. A., Goebbels, S., et al. (2009). Neurod1 is essential for the survival and maturation of adult-born neurons. *Nat Neurosci, 12*(9), 1090-1092.

Geraghty, R. J., Krummenacher, C., Cohen, G. H., Eisenberg, R. J., & Spear, P. G. (1998). Entry of alphaherpesviruses mediated by poliovirus receptor-related protein 1 and poliovirus receptor. *Science, 280*(5369), 1618-1620.

Gilden, D., Nagel, M. A., Mahalingam, R., Mueller, N. H., Brazeau, E. A., Pugazhenthi, S., et al. (2009). Clinical and molecular aspects of varicella zoster virus infection. *Future Neurol, 4*(1), 103-117.

Giordani, N. V., Neumann, D. M., Kwiatkowski, D. L., Bhattacharjee, P. S., McAnany, P. K., Hill, J. M., et al. (2008). During herpes simplex virus type 1 infection of rabbits, the ability to express the latency-associated transcript increases latent-phase transcription of lytic genes. *J Virol, 82*(12), 6056-6060.

Gnann, J. W. (2002). Varicella-zoster virus: atypical presentations and unusual complications. *J Infect Dis, 186 Suppl 1*, S91-98.

Gonzalez-Perez, O. (2012). Neural stem cells in the adult human brain. *Biol Biomed Rep, 2*(1), 59-69.

Gordon, Y. J., Yates, K. A., Mah, F. S., & Romanowski, E. G. (2003). The effects of Xalatan on the recovery of ocular herpes simplex virus type 1 (HSV-1) in the induced reactivation and spontaneous shedding rabbit models. *J Ocul Pharmacol Ther, 19*(3), 233-245.

Green, M. T., Rosborough, J. P., & Dunkel, E. C. (1981). In vivo reactivation of herpes simplex virus in rabbit trigeminal ganglia: electrode model. *Infect Immun, 34*(1), 69-74.

Greene, L. A., & Tischler, A. S. (1976). Establishment of a noradrenergic clonal line of rat adrenal pheochromocytoma cells which respond to nerve growth factor. *Proc Natl Acad Sci U S A, 73*(7), 2424-2428.

Guo H, Omoto S, Harris PA, Finger JN, Bertin J, Gough PJ, Kaiser WJ, Mocarski ES (2015). Herpes simplex virus suppression of necroptosis in human cells. *Cell Host Microbe* 17:243–251.

Gupta, R., Warren, T., & Wald, A. (2007). Genital herpes. *Lancet, 370*(9605), 2127-2137.

Gussow, A. M., Giordani, N. V., Tran, R. K., Imai, Y., Kwiatkowski, D. L., Rall, G. F., et al. (2006). Tissue-specific splicing of the herpes simplex virus type 1 latency-associated transcript (LAT) intron in LAT transgenic mice. *J Virol, 80*(19), 9414-9423.

Hadinoto, V., Shapiro, M., Sun, C. C., & Thorley-Lawson, D. A. (2009). The dynamics of EBV shedding implicate a central role for epithelial cells in amplifying viral output. *PLoS Pathog, 5*(7), e1000496.

Hafezi, W., Lorentzen, E. U., Eing, B. R., Müller, M., King, N. J., Klupp, B., et al. (2012). Entry of herpes simplex virus type 1 (HSV-1) into the distal axons of trigeminal neurons favors the onset of nonproductive, silent infection. *PLoS Pathog, 8*(5), e1002679.

Halford, W. P., Balliet, J. W., & Gebhardt, B. M. (2004). Re-evaluating natural resistance to herpes simplex virus type 1. *J Virol, 78*(18), 10086-10095.

Halford, W. P., Gebhardt, B. M., & Carr, D. J. (1996). Persistent cytokine expression in trigeminal ganglion latently infected with herpes simplex virus type 1. *J Immunol, 157*(8), 3542-3549.

Halford WP, Kemp CD, Isler JA, Davido DJ, Schaffer PA. (2001). ICP0, ICP4, or VP16 expressed from adenovirus vectors induces reactivation of latent herpes simplex virus type 1 in primary cultures of latently infected trigeminal ganglion cells. *J Virol.* Jul;75(13):6143-53.

Hall, C. B., Long, C. E., Schnabel, K. C., Caserta, M. T., McIntyre, K. M., Costanzo, M. A., et al. (1994). Human herpesvirus-6 infection in children. A prospective study of complications and reactivation. *N Engl J Med, 331*(7), 432-438.

Hambleton, S., Steinberg, S. P., Larussa, P. S., Shapiro, E. D., & Gershon, A. A. (2008). Risk of herpes zoster in adults immunized with varicella vaccine. *J Infect Dis, 197 Suppl 2*, S196-199.

Harada, A., Teng, J., Takei, Y., Oguchi, K., & Hirokawa, N. (2002). MAP2 is required for dendrite elongation, PKA anchoring in dendrites, and proper PKA signal transduction. *J Cell Biol, 158*(3), 541-549.

Hardy, I., Gershon, A. A., Steinberg, S. P., & LaRussa, P. (1991). The incidence of zoster after immunization with live attenuated varicella vaccine. A study in children with leukemia. Varicella Vaccine Collaborative Study Group. *N Engl J Med, 325*(22), 1545-1550.

Harkness, J. M., Kader, M., & DeLuca, N. A. (2014). Transcription of the herpes simplex virus 1 genome during productive and quiescent infection of neuronal and nonneuronal cells. *J Virol, 88*(12), 6847-6861.

Harley, C. A., Dasgupta, A., & Wilson, D. W. (2001). Characterization of herpes simplex virus-containing organelles by subcellular fractionation: role for organelle acidification in assembly of infectious particles. *J Virol, 75*(3), 1236-1251.

Haruta, Y., Rootman, D. S., Xie, L. X., Kiritoshi, A., & Hill, J. M. (1989). Recurrent HSV-1 corneal lesions in rabbits induced by cyclophosphamide and dexamethasone. *Invest Ophthalmol Vis Sci, 30*(3), 371-376.

Hayes, T. L., & Lewis, D. A. (1992). Nonphosphorylated neurofilament protein and calbindin immunoreactivity in layer III pyramidal neurons of human neocortex. *Cereb Cortex, 2*(1), 56-67.

He, J., Qi, W. B., Wang, L., Tian, J., Jiao, P. R., Liu, G. Q., et al. (2013). Amaryllidaceae alkaloids inhibit nuclear-to-cytoplasmic export of ribonucleoprotein (RNP) complex of highly pathogenic avian influenza virus H5N1. *Influenza Other Respir Viruses, 7*(6), 922-931.

He, R., Sandford, G., Hayward, G. S., Burns, W. H., Posner, G. H., Forman, M., et al. (2011). Recombinant luciferase-expressing human cytomegalovirus (CMV) for evaluation of CMV inhibitors. *Virol J, 8*, 40.

Herman, M. A., Ackermann, F., Trimbuch, T., & Rosenmund, C. (2014). Vesicular glutamate transporter expression level affects synaptic vesicle release probability at hippocampal synapses in culture. *J Neurosci, 34*(35), 11781-11791.

Herpetic Eye Disease Study Group. Acyclovir for the prevention of recurrent herpes simplex virus eye disease. N Engl J Med. 1998 Jul 30;339(5):300-6.

Higaki, S., Watanabe, K., Itahashi, M., & Shimomura, Y. (2009). Cyclooxygenase (COX)-inhibiting drug reduces HSV-1 reactivation in the mouse eye model. *Curr Eye Res, 34*(3), 171-176.

Higashi, M., Kolla, V., Iyer, R., Naraparaju, K., Zhuang, T., Kolla, S., et al. (2015). Retinoic acid-induced CHD5 upregulation and neuronal differentiation of neuroblastoma. *Mol Cancer, 14*, 150.

Hill, G. M., Ku, E. S., & Dwarakanathan, S. (2014). Herpes simplex keratitis. *Dis Mon, 60*(6), 239-246.

Hill, J. M., Nolan, N. M., McFerrin, H. E., Clement, C., Foster, T. P., Halford, W. P., et al. (2012). HSV-1 latent rabbits shed viral DNA into their saliva. *Virol J, 9*, 221.

Hill JM, Quenelle DC, Cardin RD, Vogel JL, Clement C, Bravo FJ, Foster TP, Bosch-Marce M, Raja P, Lee JS, Bernstein DI, Krause PR, Knipe DM, Kristie TM. (2014). Inhibition of LSD1 reduces herpesvirus infection, shedding, and recurrence by promoting epigenetic suppression of viral genomes. *Sci Transl Med*. Dec 3;6(265):265ra169.

Hill, J. M., Sedarati, F., Javier, R. T., Wagner, E. K., & Stevens, J. G. (1990). Herpes simplex virus latent phase transcription facilitates in vivo reactivation. *Virology, 174*(1), 117-125.

Hill, J. M., Shimomura, Y., Kwon, B. S., & Gangarosa, L. P. (1985). Iontophoresis of epinephrine isomers to rabbit eyes induced HSV-1 ocular shedding. *Invest Ophthalmol Vis Sci, 26*(9), 1299-1303.

Hislop, A. D. (2015). Early virological and immunological events in Epstein-Barr virus infection. *Curr Opin Virol, 15*, 75-79.

Hogk, I., Kaufmann, M., Finkelmeier, D., Rupp, S., & Burger-Kentischer, A. (2013). An In Vitro HSV-1 Reactivation Model Containing Quiescently Infected PC12 Cells. *Biores Open Access, 2*(4), 250-257.

Hokkanen, L., & Launes, J. (2000). Cognitive outcome in acute sporadic encephalitis. *Neuropsychol Rev, 10*(3), 151-167.

Hollingshead, A. B. (1975). *Four-factor index of social status*. New Haven, CT: Yale University Press.

Holmberg, S. D., Stewart, J. A., Gerber, A. R., Byers, R. H., Lee, F. K., O'Malley, P. M., et al. (1988). Prior herpes simplex virus type 2 infection as a risk factor for HIV infection. *JAMA, 259*(7), 1048-1050.

Honess, R. W., & Roizman, B. (1974). Regulation of herpesvirus macromolecular synthesis. I. Cascade regulation of the synthesis of three groups of viral proteins. *J Virol, 14*(1), 8-19.

Honess, R. W., & Roizman, B. (1975). Regulation of herpesvirus macromolecular synthesis: sequential transition of polypeptide synthesis requires functional viral polypeptides. *Proc Natl Acad Sci U S A, 72*(4), 1276-1280.

Horien, C., & Grose, C. (2012). Neurovirulence of varicella and the live attenuated varicella vaccine virus. *Semin Pediatr Neurol, 19*(3), 124-129.

Huang, L. M., Lee, C. Y., Liu, M. Y., & Lee, P. I. (1997). Primary infections of human herpesvirus-7 and herpesvirus-6: a comparative, longitudinal study up to 6 years of age. *Acta Paediatr, 86*(6), 604-608.

Huang Z, Wu S-Q, Liang Y, Zhou X, Chen W, Li L, Wu J, Zhuang Q, Chen C, Li J, Zhong C, Xia W, Zhou R, Zheng C, Han J (2015). Targeting HSV-1 protein ICP6 by RIP1 and RIP3 initiates necroptosis to restrict HSV-1 propagation in mice. *Cell Host Microbe* 17:229–242.

Hwang, Y. C., Chu, J. J., Yang, P. L., Chen, W., & Yates, M. V. (2008). Rapid identification of inhibitors that interfere with poliovirus replication using a cell-based assay. *Antiviral Res, 77*(3), 232-236.

Ieven, M., Vlietinck, A. J., Vanden Berghe, D. A., Totte, J., Dommisse, R., Esmans, E., et al. (1982). Plant antiviral agents. III. Isolation of alkaloids from Clivia miniata Regel (Amaryllidaceae). *J Nat Prod, 45*(5), 564-573.

Ivashkiv, L. B., & Donlin, L. T. (2014). Regulation of type I interferon responses. *Nat Rev Immunol, 14*(1), 36-49.

Iwayama, S., Ono, N., Ohmura, Y., Suzuki, K., Aoki, M., Nakazawa, H., et al. (1998). Antiherpesvirus activities of (1'S,2'R)-9-[[1',2'-bis(hydroxymethyl)cycloprop-1'-yl]methyl]guanine (A-5021) in cell culture. *Antimicrob Agents Chemother, 42*(7), 1666-1670.

Izzedine, H., Launay-Vacher, V., & Deray, G. (2005). Antiviral drug-induced nephrotoxicity. *Am J Kidney Dis, 45*(5), 804-817.

Jabs, D. A., Enger, C., Dunn, J. P., & Forman, M. (1998). Cytomegalovirus retinitis and viral resistance: ganciclovir resistance. CMV Retinitis and Viral Resistance Study Group. *J Infect Dis, 177*(3), 770-773.

Jackson, S. A., & DeLuca, N. A. (2003). Relationship of herpes simplex virus genome configuration to productive and persistent infections. *Proc Natl Acad Sci U S A, 100*(13), 7871-7876.

Jacobs, B. L., & Langland, J. O. (1996). When two strands are better than one: the mediators and modulators of the cellular responses to double-stranded RNA. *Virology, 219*(2), 339-349.

Jacobs, S. A., Taverna, S. D., Zhang, Y., Briggs, S. D., Li, J., Eissenberg, J. C., et al. (2001). Specificity of the HP1 chromo domain for the methylated N-terminus of histone H3. *EMBO J, 20*(18), 5232-5241.

Javier, R. T., Stevens, J. G., Dissette, V. B., & Wagner, E. K. (1988). A herpes simplex virus transcript abundant in latently infected neurons is dispensable for establishment of the latent state. *Virology, 166*(1), 254-257.

Jin, Z. (2013). Amaryllidaceae and Sceletium alkaloids. *Nat Prod Rep, 30*(6), 849-868.

Johnson, D. C., & Baines, J. D. (2011). Herpesviruses remodel host membranes for virus egress. *Nat Rev Microbiol, 9*(5), 382-394.

Johnson, D. C., Webb, M., Wisner, T. W., & Brunetti, C. (2001). Herpes simplex virus gE/gI sorts nascent virions to epithelial cell junctions, promoting virus spread. *J Virol, 75*(2), 821-833.

Joubert, P. E., Meiffren, G., Grégoire, I. P., Pontini, G., Richetta, C., Flacher, M., et al. (2009). Autophagy induction by the pathogen receptor CD46. *Cell Host Microbe, 6*(4), 354-366.

Kang, W., Mukerjee, R., & Fraser, N. W. (2003). Establishment and maintenance of HSV latent infection is mediated through correct splicing of the LAT primary transcript. *Virology, 312*(1), 233-244.

Kapur, N., Barker, S., Burrows, E. H., Ellison, D., Brice, J., Illis, L. S., et al. (1994). Herpes simplex encephalitis: long term magnetic resonance imaging and neuropsychological profile. *J Neurol Neurosurg Psychiatry, 57*(11), 1334-1342.

Karatas, H., Gurer, G., Pinar, A., Soylemezoglu, F., Tezel, G. G., Hascelik, G., et al. (2008). Investigation of HSV-1, HSV-2, CMV, HHV-6 and HHV-8 DNA by real-time PCR in surgical resection materials of epilepsy patients with mesial temporal lobe sclerosis. *J Neurol Sci, 264*(1-2), 151-156.

Kastrukoff, L., Hamada, T., Schumacher, U., Long, C., Doherty, P. C., & Koprowski, H. (1982). Central nervous system infection and immune response in mice inoculated into the lip with herpes simplex virus type 1. *J Neuroimmunol, 2*(3-4), 295-305.

Kastrukoff, L. F., Lau, A. S., Takei, F., Smyth, M. J., Jones, C. M., Clarke, S. R., et al. (2010). Redundancy in the immune system restricts the spread of HSV-1 in the central nervous system (CNS) of C57BL/6 mice. *Virology, 400*(2), 248-258.

Kastrukoff, L. F., Lau, A. S., & Thomas, E. E. (2012). The effect of mouse strain on herpes simplex virus type 1 (HSV-1) infection of the central nervous system (CNS). *Herpesviridae, 3*, 4.

Kaufman, H. E., Azcuy, A. M., Varnell, E. D., Sloop, G. D., Thompson, H. W., & Hill, J. M. (2005). HSV-1 DNA in tears and saliva of normal adults. *Invest Ophthalmol Vis Sci, 46*(1), 241-247.

Kaye, J. A., & Finkbeiner, S. (2013). Modeling Huntington's disease with induced pluripotent stem cells. *Mol Cell Neurosci, 56*, 50-64.

Kennedy EM, Cullen BR. (2015). Bacterial CRISPR/Cas DNA endonucleases: A revolutionary technology that could dramatically impact viral research and treatment. *Virology*. May;479-480:213-20.

Kent, J. R., Kang, W., Miller, C. G., & Fraser, N. W. (2003). Herpes simplex virus latency-associated transcript gene function. *J Neurovirol, 9*(3), 285-290.

Kent, J. R., Zeng, P. Y., Atanasiu, D., Gardner, J., Fraser, N. W., & Berger, S. L. (2004). During lytic infection herpes simplex virus type 1 is associated with histones bearing modifications that correlate with active transcription. *J Virol, 78*(18), 10178-10186.

Kim, D. S., Lee, D. R., Kim, H. S., Yoo, J. E., Jung, S. J., Lim, B. Y., et al. (2012). Highly pure and expandable PSA-NCAM-positive neural precursors from human ESC and iPSC-derived neural rosettes. *PLoS One, 7*(7), e39715.

Kim, J. Y., Mandarino, A., Chao, M. V., Mohr, I., & Wilson, A. C. (2012). Transient reversal of episome silencing precedes VP16-dependent transcription during reactivation of latent HSV-1 in neurons. *PLoS Pathog, 8*(2), e1002540.

Kimberlin, D., & Whitley, R. (2007). Antiviral therapy of HSV-1 and -2. In Arvin A, Campadelli-Fiume G, Mocarski E, Moore PS, Roizman B, Whitley R & Y. K (Eds.), *Human Herpesviruses: Biology, Therapy, and Immunoprophylaxis*: Cambridge University Press

Kimberlin, D. W. (2004). Neonatal herpes simplex infection. *Clin Microbiol Rev, 17*(1), 1-13.

Kinchington, P. R., Leger, A. J., Guedon, J. M., & Hendricks, R. L. (2012). Herpes simplex virus and varicella zoster virus, the house guests who never leave. *Herpesviridae, 3*(1), 5.

Kirkeby, A., Nelander, J., & Parmar, M. (2012). Generating regionalized neuronal cells from pluripotency, a step-by-step protocol. *Front Cell Neurosci, 6*, 64.

Kleymann, G., Fischer, R., Betz, U. A., Hendrix, M., Bender, W., Schneider, U., et al. (2002). New helicase-primase inhibitors as drug candidates for the treatment of herpes simplex disease. *Nat Med, 8*(4), 392-398.

Knipe, D. M., & Cliffe, A. (2008). Chromatin control of herpes simplex virus lytic and latent infection. *Nat Rev Microbiol, 6*(3), 211-221.

Kobayashi, M., Kim, J. Y., Camarena, V., Roehm, P. C., Chao, M. V., Wilson, A. C., et al. (2012). A primary neuron culture system for the study of herpes simplex virus latency and reactivation. *J Vis Exp*(62).

Kosz-Vnenchak, M., Coen, D. M., & Knipe, D. M. (1990). Restricted expression of herpes simplex virus lytic genes during establishment of latent infection by thymidine kinase-negative mutant viruses. *J Virol, 64*(11), 5396-5402.

Kramer, M. F., Cook, W. J., Roth, F. P., Zhu, J., Holman, H., Knipe, D. M., et al. (2003). Latent herpes simplex virus infection of sensory neurons alters neuronal gene expression. *J Virol, 77*(17), 9533-9541.

Kramer, M. F., Jurak, I., Pesola, J. M., Boissel, S., Knipe, D. M., & Coen, D. M. (2011). Herpes simplex virus 1 microRNAs expressed abundantly during latent infection are not essential for latency in mouse trigeminal ganglia. *Virology, 417*(2), 239-247.

Krepstakies, M., Lucifora, J., Nagel, C. H., Zeisel, M. B., Holstermann, B., Hohenberg, H., et al. (2012). A new class of synthetic peptide inhibitors blocks attachment and entry of human pathogenic viruses. *J Infect Dis, 205*(11), 1654-1664.

Kristie, T. M., & Roizman, B. (1987). Host cell proteins bind to the cis-acting site required for virion-mediated induction of herpes simplex virus 1 alpha genes. *Proc Natl Acad Sci U S A, 84*(1), 71-75.

Kristie TM. (2015). Dynamic modulation of HSV chromatin drives initiation of infection and provides targets for epigenetic therapies. *Virology*. May;479-480:555-61.

Kubat, N. J., Tran, R. K., McAnany, P., & Bloom, D. C. (2004). Specific histone tail modification and not DNA methylation is a determinant of herpes simplex virus type 1 latent gene expression. *J Virol, 78*(3), 1139-1149.

Kudelova, M., Rajcani, J., Pogady, J., & Sramka, M. (1988). Herpes simplex virus DNA in the brain of psychotic patients. *Acta Virol, 32*(5), 455-460.

Kumar, M., Hill, J. M., Clement, C., Varnell, E. D., Thompson, H. W., & Kaufman, H. E. (2009). A double-blind placebo-controlled study to evaluate valacyclovir alone and with aspirin for asymptomatic HSV-1 DNA shedding in human tears and saliva. *Invest Ophthalmol Vis Sci, 50*(12), 5601-5608.

Kuo, T., Wang, C., Badakhshan, T., Chilukuri, S., & BenMohamed, L. (2014). The challenges and opportunities for the development of a T-cell epitope-based herpes simplex vaccine. *Vaccine, 32*(50), 6733-6745.

Kurosawa, H. (2007). Methods for inducing embryoid body formation: in vitro differentiation system of embryonic stem cells. *J Biosci Bioeng, 103*(5), 389-398.

Kwiatkowski, D. L., Thompson, H. W., & Bloom, D. C. (2009). The polycomb group protein Bmi1 binds to the herpes simplex virus 1 latent genome and maintains repressive histone marks during latency. *J Virol, 83*(16), 8173-8181.

Kwon, B. S., Gangarosa, L. P., Burch, K. D., deBack, J., & Hill, J. M. (1981). Induction of ocular herpes simplex virus shedding by iontophoresis of epinephrine into rabbit cornea. *Invest Ophthalmol Vis Sci, 21*(3), 442-449.

Labetoulle, M., Kucera, P., Ugolini, G., Lafay, F., Frau, E., Offret, H., et al. (2000). Neuronal propagation of HSV1 from the oral mucosa to the eye. *Invest Ophthalmol Vis Sci, 41*(9), 2600-2606.

Laboratories, R. (2016). Valcyte.

Lafaille, F. G., Pessach, I. M., Zhang, S. Y., Ciancanelli, M. J., Herman, M., Abhyankar, A., et al. (2012). Impaired intrinsic immunity to HSV-1 in human iPSC-derived TLR3-deficient CNS cells. *Nature, 491*(7426), 769-773.

Lalezari, J. P., Aberg, J. A., Wang, L. H., Wire, M. B., Miner, R., Snowden, W., et al. (2002). Phase I dose escalation trial evaluating the pharmacokinetics, anti-human cytomegalovirus (HCMV) activity, and safety of 1263W94 in human immunodeficiency virus-infected men with asymptomatic HCMV shedding. *Antimicrob Agents Chemother, 46*(9), 2969-2976.

Lazarov NE. (2002). Comparative analysis of the chemical neuroanatomy of the mammalian trigeminal ganglion and mesencephalic trigeminal nucleus. *Prog Neurobiol*. Jan;66(1):19-59.

Lemaster, S., & Roizman, B. (1980). Herpes simplex virus phosphoproteins. II. Characterization of the virion protein kinase and of the polypeptides phosphorylated in the virion. *J Virol, 35*(3), 798-811.

Li, J., Hu, S., Zhou, L., Ye, L., Wang, X., Ho, J., et al. (2011). Interferon lambda inhibits herpes simplex virus type I infection of human astrocytes and neurons. *Glia, 59*(1), 58-67.

Li, S. Y., Chen, C., Zhang, H. Q., Guo, H. Y., Wang, H., Wang, L., et al. (2005). Identification of natural compounds with antiviral activities against SARS-associated coronavirus. *Antiviral Res, 67*(1), 18-23.

Li, Y., McClintick, J., Zhong, L., Edenberg, H. J., Yoder, M. C., & Chan, R. J. (2005). Murine embryonic stem cell differentiation is promoted by SOCS-3 and inhibited by the zinc finger transcription factor Klf4. *Blood, 105*(2), 635-637.

Liang Y, Quenelle D, Vogel JL, Mascaro C, Ortega A, Kristie TM. (2013). A novel selective LSD1/KDM1A inhibitor epigenetically blocks herpes simplex virus lytic replication and reactivation from latency. *MBio*. Feb 5;4(1):e00558-12.

Lim, H. K., Seppänen, M., Hautala, T., Ciancanelli, M. J., Itan, Y., Lafaille, F. G., et al. (2014). TLR3 deficiency in herpes simplex encephalitis: high allelic heterogeneity and recurrence risk. *Neurology, 83*(21), 1888-1897.

Limaye, A. P. (2002). Ganciclovir-resistant cytomegalovirus in organ transplant recipients. *Clin Infect Dis, 35*(7), 866-872.

Lista, A., Arbilla, S., & Langer, S. Z. (1988). Modulation of the electrically evoked release of 5-[3H]hydroxytryptamine from rat cerebral cortex: effects of alpidem, CL 218872, and diazepam. *J Neurochem, 51*(5), 1414-1421.

Liu, A.L. et al. Comparative analysis of selected innate immune-related genes following infection of immortal DF-1 cells with highly pathogenic (H5N1) and low pathogenic (H9N2) avian influenza viruses. Virus Genes (2015).

Liu, G. H., Qu, J., Suzuki, K., Nivet, E., Li, M., Montserrat, N., et al. (2012). Progressive degeneration of human neural stem cells caused by pathogenic LRRK2. *Nature, 491*(7425), 603-607.

Liu, T., Khanna, K. M., Chen, X., Fink, D. J., & Hendricks, R. L. (2000). CD8(+) T cells can block herpes simplex virus type 1 (HSV-1) reactivation from latency in sensory neurons. *J Exp Med, 191*(9), 1459-1466.

Livak, K.J. Allelic discrimination using fluorogenic probes and the 5' nuclease assay. Genet Anal 14, 143-9 (1999).

Lo KW, Chung GT, To KF. (2012). Deciphering the molecular genetic basis of NPC through molecular, cytogenetic, and epigenetic approaches. *Semin Cancer Biol.* Apr;22(2):79-86

Lorette G, Crochard A, Mimaud V, et al. (2006) A survey on the prevalence of orofacial herpes in France: the INSTANT Study. *J Am Acad Dermatol*.; 55:225–32.

Lowe DM, Alderton WK, Ellis MR, Parmar V, Miller WH, Roberts GB, Fyfe JA, Gaillard R, Ertl P, Snowden W, et al. (1995). Mode of action of (R)-9-[4-hydroxy-2-(hydroxymethyl)butyl]guanine against herpesviruses. *Antimicrob Agents Chemother*. Aug;39(8):1802-8.

Lycke, E., Hamark, B., Johansson, M., Krotochwil, A., Lycke, J., & Svennerholm, B. (1988). Herpes simplex virus infection of the human sensory neuron. An electron microscopy study. *Arch Virol, 101*(1-2), 87-104.

Ma, J. Z., Russell, T. A., Spelman, T., Carbone, F. R., & Tscharke, D. C. (2014). Lytic gene expression is frequent in HSV-1 latent infection and correlates with the engagement of a cell-intrinsic transcriptional response. *PLoS Pathog, 10*(7), e1004237.

MacDonald, M. L., Ciccimaro, E., Prakash, A., Banerjee, A., Seeholzer, S. H., Blair, I. A., et al. (2012). Biochemical fractionation and stable isotope dilution liquid chromatography-mass spectrometry for targeted and microdomain-specific protein quantification in human postmortem brain tissue. *Mol Cell Proteomics, 11*(12), 1670-1681.

Maldjian, J. A., Laurienti, P. J., Kraft, R. A., & Burdette, J. H. (2003). An automated method for neuroanatomic and cytoarchitectonic atlas-based interrogation of fMRI data sets. *Neuroimage, 19*(3), 1233-1239.

Malvy, D., Treilhaud, M., Bouée, S., Crochard, A., Vallée, D., El Hasnaoui, A., et al. (2005). A retrospective, case-control study of acyclovir resistance in herpes simplex virus. *Clin Infect Dis, 41*(3), 320-326.

Margolis, T. P., Elfman, F. L., Leib, D., Pakpour, N., Apakupakul, K., Imai, Y., et al. (2007). Spontaneous reactivation of herpes simplex virus type 1 in latently infected murine sensory ganglia. *J Virol, 81*(20), 11069-11074.

Marschall, M., Stamminger, T., Urban, A., Wildum, S., Ruebsamen-Schaeff, H., Zimmermann, H., et al. (2012). In vitro evaluation of the activities of the novel anticytomegalovirus compound AIC246 (letermovir) against herpesviruses and other human pathogenic viruses. *Antimicrob Agents Chemother, 56*(2), 1135-1137.

Martin, J. N. (2011). Kaposi sarcoma-associated herpesvirus/human herpesvirus 8 and Kaposi sarcoma. *Adv Dent Res, 23*(1), 76-78.

Martinez, R., Sarisky, R. T., Weber, P. C., & Weller, S. K. (1996). Herpes simplex virus type 1 alkaline nuclease is required for efficient processing of viral DNA replication intermediates. *J Virol, 70*(4), 2075-2085.

Matthews, J. T., Terry, B. J., & Field, A. K. (1993). The structure and function of the HSV DNA replication proteins: defining novel antiviral targets. *Antiviral Res, 20*(2), 89-114.

McClain, L., Zhi, Y., Cheng, H., Ghosh, A., Piazza, P., Yee, M. B., et al. (2015). Broad-spectrum non-nucleoside inhibitors of human herpesviruses. *Antiviral Res, 121*, 16-23.

McGrath, N., Anderson, N. E., Croxson, M. C., & Powell, K. F. (1997). Herpes simplex encephalitis treated with acyclovir: diagnosis and long term outcome. *J Neurol Neurosurg Psychiatry, 63*(3), 321-326.

McKendall, R. R. (1980). Comparative neurovirulence and latency of HSV1 and HSV2 following footpad inoculation in mice. *J Med Virol, 5*(1), 25-32.

McMahon, R., & Walsh, D. (2008). Efficient quiescent infection of normal human diploid fibroblasts with wild-type herpes simplex virus type 1. *J Virol, 82*(20), 10218-10230.

McNulty, J., D'Aiuto, L., Zhi, Y., McClain, L., Zepeda-Velázquez, C., Ler, S., et al. (2016). iPSC Neuronal Assay Identifies Amaryllidaceae Pharmacophore with Multiple Effects against Herpesvirus Infections. *ACS Med Chem Lett, 7*(1), 46-50.

McNulty, J., Zepeda-Velázquez, C. & McLeod, D. Development of a robust reagent for the two-carbon homologation of aldehydes to (E)-α,β-unsaturated aldehydes in water. Green Chem. 15, 3146-3149 (2013).

McNulty, J., & Zepeda-Velázquez, C. (2014). Enantioselective organocatalytic Michael/aldol sequence: anticancer natural product (+)-trans-dihydrolycoricidine. Angew Chem Int Ed Engl, 53(32), 8450-8454.

McNulty, J. & Zepeda-Velázquez, C. Enantioselective Organocatalytic Michael/Aldol

Sequence: Anticancer Natural Product (+)-trans-Dihydrolycoricidine. Angew. Chem. Int. Ed. 53, 8450–8454 (2014) and Angew. Chem. 126, 8590–8594 (2014).

Mehta, A., Maggioncalda, J., Bagasra, O., Thikkavarapu, S., Saikumari, P., Valyi-Nagy, T., et al. (1995). In situ DNA PCR and RNA hybridization detection of herpes simplex virus sequences in trigeminal ganglia of latently infected mice. Virology, 206(1), 633-640.

Mellerick, D. M., & Fraser, N. W. (1987). Physical state of the latent herpes simplex virus genome in a mouse model system: evidence suggesting an episomal state. *Virology, 158*(2), 265-275.

Meyding-Lamadé, U. K., Oberlinner, C., Rau, P. R., Seyfer, S., Heiland, S., Sellner, J., et al. (2003). Experimental herpes simplex virus encephalitis: a combination therapy of acyclovir and glucocorticoids reduces long-term magnetic resonance imaging abnormalities. *J Neurovirol, 9*(1), 118-125.

Millhouse, S., Wang, X., Fraser, N. W., Faber, L., & Block, T. M. (2012). Direct evidence that HSV DNA damaged by ultraviolet (UV) irradiation can be repaired in a cell type-dependent manner. *J Neurovirol, 18*(3), 231-243.

Mohan RP, Verma S, Singh U, Agarwal N. Acute primary herpetic gingivostomatitis. (2013). *BMJ Case Rep.* Jul 8;2013.

Montgomery, R. I., Warner, M. S., Lum, B. J., & Spear, P. G. (1996). Herpes simplex virus-1 entry into cells mediated by a novel member of the TNF/NGF receptor family. *Cell, 87*(3), 427-436.

Muratore, C. R., Srikanth, P., Callahan, D. G., & Young-Pearse, T. L. (2014). Comparison and optimization of hiPSC forebrain cortical differentiation protocols. *PLoS One, 9*(8), e105807.

Muylaert, I., Tang, K. W., & Elias, P. (2011). Replication and recombination of herpes simplex virus DNA. *J Biol Chem, 286*(18), 15619-15624.

Myles, M. E., Azcuy, A. M., Nguyen, N. T., Reisch, E. R., Barker, S. A., Thompson, H. W., et al. (2004). Bupropion (Zyban, Wellbutrin) inhibits nicotine-induced viral reactivation in herpes simplex virus type 1 latent rabbits. *J Pharmacol Exp Ther, 311*(2), 640-644.

Nagel, M. A., & Gilden, D. (2014). Neurological complications of varicella zoster virus reactivation. *Curr Opin Neurol, 27*(3), 356-360.

Naldinho-Souto, R., Browne, H., & Minson, T. (2006). Herpes simplex virus tegument protein VP16 is a component of primary enveloped virions. *J Virol, 80*(5), 2582-2584.

Narayanan A, Ruyechan WT, Kristie TM. (2007). The coactivator host cell factor-1 mediates Set1 and MLL1 H3K4 trimethylation at herpesvirus immediate early promoters for initiation of infection. *Proc Natl Acad Sci U S A.* Jun 26; 104(26):10835-40.

Nesburn, A. B., Burke, R. L., Ghiasi, H., Slanina, S. M., & Wechsler, S. L. (1998). Therapeutic periocular vaccination with a subunit vaccine induces higher levels of herpes simplex virus-specific tear secretory immunoglobulin A than systemic vaccination and provides protection against recurrent spontaneous ocular shedding of virus in latently infected rabbits. *Virology, 252*(1), 200-209.

Nesburn, A. B., Cook, M. L., & Stevens, J. G. (1972). Latent herpes simplex virus. Isolation from rabbit trigeminal ganglia between episodes of recurrent ocular infection. *Arch Ophthalmol, 88*(4), 412-417.

Nesburn, A. B., Green, M. T., Radnoti, M., & Walker, B. (1977). Reliable in vivo model for latent herpes simplex virus reactivation with peripheral virus shedding. *Infect Immun, 15*(3), 772-775.

Neumann, D. M., Bhattacharjee, P. S., Giordani, N. V., Bloom, D. C., & Hill, J. M. (2007). In vivo changes in the patterns of chromatin structure associated with the latent herpes simplex virus type 1 genome in mouse trigeminal ganglia can be detected at early times after butyrate treatment. *J Virol, 81*(23), 13248-13253.

Neumann, D. M., Bhattacharjee, P. S., & Hill, J. M. (2007). Sodium butyrate: a chemical inducer of in vivo reactivation of herpes simplex virus type 1 in the ocular mouse model. *J Virol, 81*(11), 6106-6110.

National health and nutrition examination survey. The national center for health statistics; http://www.cdc.gov/nchs/nhanes.htm); data accessed Feb 2016.

Nichols, J., Zevnik, B., Anastassiadis, K., Niwa, H., Klewe-Nebenius, D., Chambers, I., et al. (1998). Formation of pluripotent stem cells in the mammalian embryo depends on the POU transcription factor Oct4. *Cell, 95*(3), 379-391.

Nicola, A. V., Hou, J., Major, E. O., & Straus, S. E. (2005). Herpes simplex virus type 1 enters human epidermal keratinocytes, but not neurons, via a pH-dependent endocytic pathway. *J Virol, 79*(12), 7609-7616.

Nicola, A. V., McEvoy, A. M., & Straus, S. E. (2003). Roles for endocytosis and low pH in herpes simplex virus entry into HeLa and Chinese hamster ovary cells. *J Virol, 77*(9), 5324-5332.

Nicoll, M. P., Proença, J. T., & Efstathiou, S. (2012). The molecular basis of herpes simplex virus latency. *FEMS Microbiol Rev, 36*(3), 684-705.

Nieland, T. J., Feng, Y., Brown, J. X., Chuang, T. D., Buckett, P. D., Wang, J., et al. (2004). Chemical genetic screening identifies sulfonamides that raise organellar pH and interfere with membrane traffic. *Traffic, 5*(7), 478-492.

Nguyen, T. D., Widera, D., Greiner, J., Mueller, J., Martin, I., Slotta C., et al. (2013). Prolonged cultivation of hippocampal neural precursor cells shifts their differentiation potential and selects for aneuploid cells. *Biol Chem*, 394:1623-36.

Nsabimana, J. M., Moutschen, M., Thiry, E., & Meurens, F. (2008). [Human infection with simian herpes B virus in Africa]. *Sante, 18*(1), 3-8.

O'Hare, P. (1993). The virion transactivator of herpes simplex virus (Vol. 4, pp. 145-155). Semin Virol: Elsevier.

Oh, J., & Fraser, N. W. (2008). Temporal association of the herpes simplex virus genome with histone proteins during a lytic infection. *J Virol, 82*(7), 3530-3537.

Ojala, P. M., Sodeik, B., Ebersold, M. W., Kutay, U., & Helenius, A. (2000). Herpes simplex virus type 1 entry into host cells: reconstitution of capsid binding and uncoating at the nuclear pore complex in vitro. *Mol Cell Biol, 20*(13), 4922-4931.

Painter, W., Robertson, A., Trost, L. C., Godkin, S., Lampert, B., & Painter, G. (2012). First pharmacokinetic and safety study in humans of the novel lipid antiviral conjugate CMX001, a broad-spectrum oral drug active against double-stranded DNA viruses. *Antimicrob Agents Chemother, 56*(5), 2726-2734.

Park, P. J., Antoine, T. E., Farooq, A. V., Valyi-Nagy, T., & Shukla, D. (2013). An investigative peptide-acyclovir combination to control herpes simplex virus type 1 ocular infection. *Invest Ophthalmol Vis Sci, 54*(9), 6373-6381.

Parkin, D. M. (2006). The global health burden of infection-associated cancers in the year 2002. *Int J Cancer, 118*(12), 3030-3044.

Patel, P., Bush, T., Mayer, K. H., Desai, S., Henry, K., Overton, E. T., et al. (2012). Prevalence and risk factors associated with herpes simplex virus-2 infection in a contemporary cohort of HIV-infected persons in the United States. *Sex Transm Dis, 39*(2), 154-160.

Pellett, P. E., McKnight, J. L., Jenkins, F. J., & Roizman, B. (1985). Nucleotide sequence and predicted amino acid sequence of a protein encoded in a small herpes simplex virus DNA fragment capable of trans-inducing alpha genes. *Proc Natl Acad Sci U S A, 82*(17), 5870-5874.

Pereira FT, Oliveira LJ, Barreto Rda S, Mess A, Perecin F, Bressan FF, Mesquita LG, Miglino MA, Pimentel JR, Fantinato Neto P, Meirelles FV. (2013). Fetal-maternal interactions in the synepitheliochorial placenta using the eGFP cloned cattle model. *PLoS One.* May 28;8(5):e64399.

Perng, G. C., Esmaili, D., Slanina, S. M., Yukht, A., Ghiasi, H., Osorio, N., et al. (2001). Three herpes simplex virus type 1 latency-associated transcript mutants with distinct and asymmetric effects on virulence in mice compared with rabbits. *J Virol, 75*(19), 9018-9028.

Perng, G. C., Osorio, N., Jiang, X., Geertsema, R., Hsiang, C., Brown, D., et al. (2015). Large Amounts of Reactivated Virus in Tears Precedes Recurrent Herpes Stromal Keratitis in Stressed Rabbits Latently Infected with Herpes Simplex Virus. *Curr Eye Res*, 1-8.

Perng, G. C., Slanina, S. M., Yukht, A., Ghiasi, H., Nesburn, A. B., & Wechsler, S. L. (2000). The latency-associated transcript gene enhances establishment of herpes simplex virus type 1 latency in rabbits. *J Virol, 74*(4), 1885-1891.

Pescovitz, M. D., Rabkin, J., Merion, R. M., Paya, C. V., Pirsch, J., Freeman, R. B., et al. (2000). Valganciclovir results in improved oral absorption of ganciclovir in liver transplant recipients. *Antimicrob Agents Chemother, 44*(10), 2811-2815.

Petit, I., Kesner, N. S., Karry, R., Robicsek, O., Aberdam, E., Müller, F. J., et al. (2012). Induced pluripotent stem cells from hair follicles as a cellular model for neurodevelopmental disorders. *Stem Cell Res, 8*(1), 134-140.

Pettit, G. R. et al. Isolation and Structural Modification of 7-Deoxynarciclasine and 7-Deoxy- trans-Dihydronarciclasine. J. Nat. Prod. 69, 7–13 (2006).

Pierce, A. T., DeSalvo, J., Foster, T. P., Kosinski, A., Weller, S. K., & Halford, W. P. (2005). Beta interferon and gamma interferon synergize to block viral DNA and virion synthesis in herpes simplex virus-infected cells. *J Gen Virol, 86*(Pt 9), 2421-2432.

Pignatti, P. F., & Cassai, E. (1980). Analysis of herpes simplex virus nucleoprotein complexes extracted from infected cells. *J Virol, 36*(3), 816-828.

Piret, J., & Boivin, G. (2014). Antiviral drug resistance in herpesviruses other than cytomegalovirus. *Rev Med Virol, 24*(3), 186-218.

Poe, S. L. & Morken, J. P. A Boron-Based Synthesis of the Natural Product (+)-trans-Dihydrolycoricidine. Angew. Chem. Int. Ed. 50, 4189–4192 (2011) and Angew. Chem. 123, 4275–4278 (2011).

Polcicova, K., Biswas, P. S., Banerjee, K., Wisner, T. W., Rouse, B. T., & Johnson, D. C. (2005). Herpes keratitis in the absence of anterograde transport of virus from sensory ganglia to the cornea. *Proc Natl Acad Sci U S A, 102*(32), 11462-11467.

Ponti, R., Bergallo, M., Costa, C., Quaglino, P., Fierro, M. T., Comessatti, A., et al. (2008). Human herpesvirus 7 detection by quantitative real time polymerase chain reaction in primary cutaneous T-cell lymphomas and healthy subjects: lack of a pathogenic role. *Br J Dermatol, 159*(5), 1131-1137.

Prasad, K. M., Eack, S. M., Goradia, D., Pancholi, K. M., Keshavan, M. S., Yolken, R. H., et al. (2011). Progressive gray matter loss and changes in cognitive functioning associated with exposure to herpes simplex virus 1 in schizophrenia: a longitudinal study. *Am J Psychiatry, 168*(8), 822-830.

Prasad, K. M., Eack, S. M., Keshavan, M. S., Yolken, R. H., Iyengar, S., & Nimgaonkar, V. L. (2012). Antiherpes Virus-Specific Treatment and Cognition in Schizophrenia: A Test-of-Concept Randomized Double-Blind Placebo-Controlled Trial. *Schizophr Bull*.

Prasad, K. M., Shirts, B. H., Yolken, R. H., Keshavan, M. S., & Nimgaonkar, V. L. (2007). Brain morphological changes associated with exposure to HSV1 in first-episode schizophrenia. *Mol Psychiatry, 12*(1), 105-113, 101.

Prasad, K. M., Watson, A. M., Dickerson, F. B., Yolken, R. H., & Nimgaonkar, V. L. (2012). Exposure to herpes simplex virus type 1 and cognitive impairments in individuals with schizophrenia. *Schizophr Bull, 38*(6), 1137-1148.

Prieto, P., Moore, G., & Shaw, P. (2007). Fluorescence in situ hybridization on vibratome sections of plant tissues. *Nat Protoc, 2*(7), 1831-1838.

Pérez de Diego, R., Sancho-Shimizu, V., Lorenzo, L., Puel, A., Plancoulaine, S., Picard, C., et al. (2010). Human TRAF3 adaptor molecule deficiency leads to impaired Toll-like receptor 3 response and susceptibility to herpes simplex encephalitis. *Immunity, 33*(3), 400-411.

Qian, A. Q., Antonov, S. M., & Johnson, J. W. (2002). Modulation by permeant ions of Mg2+ inhibition of NMDA-activated whole-cell currents in rat cortical neurons. *Journal of Physiology-London, 538*(1), 65-77.

Quina, A. S., Buschbeck, M., & Di Croce, L. (2006). Chromatin structure and epigenetics. *Biochem Pharmacol, 72*(11), 1563-1569.

Radtke, K., Kieneke, D., Wolfstein, A., Michael, K., Steffen, W., Scholz, T., et al. (2010). Plus- and minus-end directed microtubule motors bind simultaneously to herpes simplex virus capsids using different inner tegument structures. *PLoS Pathog, 6*(7), e1000991.

Ramachandran, S., Knickelbein, J. E., Ferko, C., Hendricks, R. L., & Kinchington, P. R. (2008). Development and pathogenic evaluation of recombinant herpes simplex virus type 1 expressing two fluorescent reporter genes from different lytic promoters. *Virology, 378*(2), 254-264.

Rao, S., Procko, E., & Shannon, M. F. (2001). Chromatin remodeling, measured by a novel real-time polymerase chain reaction assay, across the proximal promoter region of the IL-2 gene. *J Immunol, 167*(8), 4494-4503.

Read, G. S., & Patterson, M. (2007). Packaging of the virion host shutoff (Vhs) protein of herpes simplex virus: two forms of the Vhs polypeptide are associated with intranuclear B and C capsids, but only one is associated with enveloped virions. *J Virol, 81*(3), 1148-1161.

Regnell, C. E., Hildrestrand, G. A., Sejersted, Y., Medin, T., Moldestad, O., Rolseth, V., et al. (2012). Hippocampal adult neurogenesis is maintained by Neil3-dependent repair of oxidative DNA lesions in neural progenitor cells. *Cell Rep, 2*(3), 503-510.

Renard-Nozaki, J., Kim, T., Imakura, Y., Kihara, M., & Kobayashi, S. (1989). Effect of alkaloids isolated from Amaryllidaceae on herpes simplex virus. *Res Virol, 140*(2), 115-128.

Reynolds, A. E., Wills, E. G., Roller, R. J., Ryckman, B. J., & Baines, J. D. (2002). Ultrastructural localization of the herpes simplex virus type 1 UL31, UL34, and US3 proteins suggests specific roles in primary envelopment and egress of nucleocapsids. *J Virol, 76*(17), 8939-8952.

Reynolds, M. A., Kruszon-Moran, D., Jumaan, A., Schmid, D. S., & McQuillan, G. M. (2010). Varicella seroprevalence in the U.S.: data from the National Health and Nutrition Examination Survey, 1999-2004. *Public Health Rep, 125*(6), 860-869.

Rivera, L., Beuerman, R. W., & Hill, J. M. (1988). Corneal nerves contain intra-axonal HSV-1 after virus reactivation by epinephrine iontophoresis. *Curr Eye Res, 7*(10), 1001-1008.

Rock, D. L., & Fraser, N. W. (1983). Detection of HSV-1 genome in central nervous system of latently infected mice. *Nature, 302*(5908), 523-525.

Rodahl E., Stevens J. (1992) Differential accumulation of herpes simplex virus type 1 latency-associated transcripts in sensory and autonomic ganglia. *Virology* 189:385–388.

Roehm PC, Camarena V, Nayak S, Gardner JB, Wilson A, Mohr I, Chao MV. (2011). Cultured vestibular ganglion neurons demonstrate latent HSV1 reactivation. *Laryngoscope*. Oct;121(10):2268-75.

Roizman, B. (1979). The structure and isomerization of herpes simplex virus genomes. *Cell, 16*(3), 481-494.

Ross, R. A., Spengler, B. A., & Biedler, J. L. (1983). Coordinate morphological and biochemical interconversion of human neuroblastoma cells. *J Natl Cancer Inst, 71*(4), 741-747.

Russell, J., & Preston, C. M. (1986). An in vitro latency system for herpes simplex virus type 2. *J Gen Virol, 67 (Pt 2)*, 397-403.

Sae-Ueng, U., Li, D., Zuo, X., Huffman, J. B., Homa, F. L., Rau, D., et al. (2014). Solid-to-fluid DNA transition inside HSV-1 capsid close to the temperature of infection. *Nat Chem Biol, 10*(10), 861-867.

Safrin, S., Cherrington, J., & Jaffe, H. S. (1997). Clinical uses of cidofovir. *Rev Med Virol, 7*(3), 145-156.

Salinas-Jazmín N, Estrada-Parra S, Becerril-García MA, Limón-Flores AY, Vázquez-Leyva S, Medina-Rivero E, Pavón L, Velasco-Velázquez MA, Pérez-Tapia SM. (2015). Herpes murine model as a biological assay to test dialyzable leukocyte extracts activity. *J Immunol Res.*146305.

Samaniego, L. A., Neiderhiser, L., & DeLuca, N. A. (1998). Persistence and expression of the herpes simplex virus genome in the absence of immediate-early proteins. *J Virol, 72*(4), 3307-3320.

Sancho-Shimizu, V., Pérez de Diego, R., Lorenzo, L., Halwani, R., Alangari, A., Israelsson, E., et al. (2011). Herpes simplex encephalitis in children with autosomal recessive and dominant TRIF deficiency. *J Clin Invest, 121*(12), 4889-4902.

Sawtell, N. M., Poon, D. K., Tansky, C. S., & Thompson, R. L. (1998). The latent herpes simplex virus type 1 genome copy number in individual neurons is virus strain specific and correlates with reactivation. *J Virol, 72*(7), 5343-5350.

Sawtell, N. M., & Thompson, R. L. (1992). Herpes simplex virus type 1 latency-associated transcription unit promotes anatomical site-dependent establishment and reactivation from latency. *J Virol, 66*(4), 2157-2169.

Schang, L. M., Bantly, A., & Schaffer, P. A. (2002). Explant-induced reactivation of herpes simplex virus occurs in neurons expressing nuclear cdk2 and cdk4. *J Virol, 76*(15), 7724-7735.

Schmittgen, T. D., & Livak, K. J. (2008). Analyzing real-time PCR data by the comparative C(T) method. *Nat Protoc, 3*(6), 1101-1108.

Schmutzhard, E. (2001). Viral infections of the CNS with special emphasis on herpes simplex infections. *J Neurol, 248*(6), 469-477.

Schretlen, D. J., Vannorsdall, T. D., Winicki, J. M., Mushtaq, Y., Hikida, T., Sawa, A., et al. (2010). Neuroanatomic and cognitive abnormalities related to herpes simplex virus type 1 in schizophrenia. *Schizophr Res, 118*(1-3), 224-231.

Sherma, J. & Fried, B. Handbook of Thin-layer Chromatography. (Marcel Dekker, 2003).

Shimeld, C., Hill, T. J., Blyth, W. A., & Easty, D. L. (1990). Reactivation of latent infection and induction of recurrent herpetic eye disease in mice. *J Gen Virol, 71 (Pt 2)*, 397-404.

Shirts, B. H., Prasad, K. M., Pogue-Geile, M. F., Dickerson, F., Yolken, R. H., & Nimgaonkar, V. L. (2008). Antibodies to cytomegalovirus and Herpes Simplex Virus 1 associated with cognitive function in schizophrenia. *Schizophr Res, 106*(2-3), 268-274.

Shukla, D., Liu, J., Blaiklock, P., Shworak, N. W., Bai, X., Esko, J. D., et al. (1999). A novel role for 3-O-sulfated heparan sulfate in herpes simplex virus 1 entry. *Cell, 99*(1), 13-22.

Silva, L., Cliffe, A., Chang, L., & Knipe, D. M. (2008). Role for A-type lamins in herpesviral DNA targeting and heterochromatin modulation. *PLoS Pathog, 4*(5), e1000071.

Skaliter, R., Makhov, A. M., Griffith, J. D., & Lehman, I. R. (1996). Rolling circle DNA replication by extracts of herpes simplex virus type 1-infected human cells. *J Virol, 70*(2), 1132-1136.

Smith, G. (2012). Herpesvirus transport to the nervous system and back again. *Annu Rev Microbiol, 66*, 153-176.

Smith JR, Thackray AM, Bujdoso R. (2001). Reduced herpes simplex virus type 1 latency in Flt-3 ligand-treated mice is associated with enhanced numbers of natural killer and dendritic cells. *Immunology*. Mar;102(3):352-8.

Smith, J. S., & Robinson, N. J. (2002). Age-specific prevalence of infection with herpes simplex virus types 2 and 1: a global review. *J Infect Dis, 186*(Suppl 1), S3-28.

Smith, M. C., Boutell, C., & Davido, D. J. (2011). HSV-1 ICP0: paving the way for viral replication. *Future Virol, 6*(4), 421-429.

Sodeik, B., Ebersold, M. W., & Helenius, A. (1997). Microtubule-mediated transport of incoming herpes simplex virus 1 capsids to the nucleus. *J Cell Biol, 136*(5), 1007-1021.

Spivack, J. G., & Fraser, N. W. (1987). Detection of herpes simplex virus type 1 transcripts during latent infection in mice. *J Virol, 61*(12), 3841-3847.

Spivack J., Fraser N. (1988) Expression of herpes simplex virus type 1 latency-associated transcripts in trigeminal ganglia of mice during acute infection and reactivation of latent infection. *J. Virol.* 62:1479–1485.

Spruance SL. (1985). Pathogenesis of herpes simplex labialis: experimental induction of lesions with UV light. *J Clin Microbiol.* Sep;22(3):366-8.

Spruance SL, Kriesel JD, Evans TG, McKeough MB. (1995). Susceptibility to herpes labialis following multiple experimental exposures to ultraviolet radiation. *Antiviral Res.* Sep;28(1):57-67.

Steiner, I., Kennedy, P. G., & Pachner, A. R. (2007). The neurotropic herpes viruses: herpes simplex and varicella-zoster. *Lancet Neurol, 6*(11), 1015-1028.

Steiner, I., Spivack, J. G., Deshmane, S. L., Ace, C. I., Preston, C. M., & Fraser, N. W. (1990). A herpes simplex virus type 1 mutant containing a nontransinducing Vmw65 protein establishes latent infection in vivo in the absence of viral replication and reactivates efficiently from explanted trigeminal ganglia. *J Virol, 64*(4), 1630-1638.

Steiner, I., Spivack, J. G., Lirette, R. P., Brown, S. M., MacLean, A. R., Subak-Sharpe, J. H., et al. (1989). Herpes simplex virus type 1 latency-associated transcripts are evidently not essential for latent infection. *EMBO J, 8*(2), 505-511.

Stern, S., Tanaka, M., & Herr, W. (1989). The Oct-1 homoeodomain directs formation of a multiprotein-DNA complex with the HSV transactivator VP16. *Nature, 341*(6243), 624-630.

Stevens, J. G., Wagner, E. K., Devi-Rao, G. B., Cook, M. L., & Feldman, L. T. (1987). RNA complementary to a herpesvirus alpha gene mRNA is prominent in latently infected neurons. *Science, 235*(4792), 1056-1059.

Still, W. C., Kahn, M. & Mitra, A. Rapid chromatographic technique for preparative separations with moderate resolution. J. Org. Chem. 43, 2923–2925 (1978).

Stock C, Guillén-Grima F, de Mendoza JH, Marin-Fernandez B, Aguinaga-Ontoso I, Krämer A. (2001). Risk factors of herpes simplex type 1 (HSV-1) infection and lifestyle factors associated with HSV-1 manifestations. *Eur J Epidemiol.*;17(9):885-90.

Stoelben, S., Arns, W., Renders, L., Hummel, J., Mühlfeld, A., Stangl, M., et al. (2014). Preemptive treatment of Cytomegalovirus infection in kidney transplant recipients with letermovir: results of a Phase 2a study. *Transpl Int, 27*(1), 77-86.

Stolz, E., Pancholi, K. M., Goradia, D. D., Paul, S., Keshavan, M. S., Nimgaonkar, V. L., et al. (2012). Brain activation patterns during visual episodic memory processing among first-degree relatives of schizophrenia subjects. *Neuroimage, 63*(3), 1154-1161.

Strang, B. L., & Stow, N. D. (2005). Circularization of the herpes simplex virus type 1 genome upon lytic infection. *J Virol, 79*(19), 12487-12494.

Strasfeld, L., & Chou, S. (2010). Antiviral drug resistance: mechanisms and clinical implications. *Infect Dis Clin North Am, 24*(3), 809-833.

Stránská, R., Schuurman, R., Nienhuis, E., Goedegebuure, I. W., Polman, M., Weel, J. F., et al. (2005). Survey of acyclovir-resistant herpes simplex virus in the Netherlands: prevalence and characterization. *J Clin Virol, 32*(1), 7-18.

Sugii, S., Kida, Y., Kawamura, T., Suzuki, J., Vassena, R., Yin, Y. Q., et al. (2010). Human and mouse adipose-derived cells support feeder-independent induction of pluripotent stem cells. *Proc Natl Acad Sci U S A, 107*(8), 3558-3563.

Sugimoto, K., Uema, M., Sagara, H., Tanaka, M., Sata, T., Hashimoto, Y., et al. (2008). Simultaneous tracking of capsid, tegument, and envelope protein localization in living cells infected with triply fluorescent herpes simplex virus 1. *J Virol, 82*(11), 5198-5211.

Sukla, S., Biswas, S., Birkmann, A., Lischka, P., Zimmermann, H., & Field, H. J. (2010). Mismatch primer-based PCR reveals that helicase-primase inhibitor resistance mutations pre-exist in herpes simplex virus type 1 clinical isolates and are not induced during incubation with the inhibitor. *J Antimicrob Chemother, 65*(7), 1347-1352.

Sun Z, Yang H, Shi Y, Wei M, Xian J, Hu W. (2010). Establishment of a cell model system of herpes simplex virus type II latent infection and reactivation in SH-SY5Y cells. *Wei Sheng Wu Xue Bao.* Jan;50(1):98-106.

Suter, D. M., Tirefort, D., Julien, S., & Krause, K. H. (2009). A Sox1 to Pax6 switch drives neuroectoderm to radial glia progression during differentiation of mouse embryonic stem cells. *Stem Cells, 27*(1), 49-58.

Taapken, S. M., Nisler, B. S., Newton, M. A., Sampsell-Barron, T. L., Leonhard, K. A., McIntire, E. M., et al. (2011). Karotypic abnormalities in human induced pluripotent stem cells and embryonic stem cells. *Nat Biotechnol, 29*(4), 313-314.

Takahashi, K., & Yamanaka, S. (2006). Induction of pluripotent stem cells from mouse embryonic and adult fibroblast cultures by defined factors. *Cell, 126*(4), 663-676.

Takahashi, K., & Yamanaka, S. (2013). Induced pluripotent stem cells in medicine and biology. *Development, 140*(12), 2457-2461.

Talkowski, M. E., McCann, K. L., Chen, M., McClain, L., Bamne, M., Wood, J., et al. (2010). Fine-mapping reveals novel alternative splicing of the dopamine transporter. *Am J Med Genet B Neuropsychiatr Genet, 153B*(8), 1434-1447.

Tan CS, Frederico B, Stevenson PG. (2014). Herpesvirus delivery to the murine respiratory tract. *J Virol Methods.* Sep;206:105-14. doi: 10.1016/j.jviromet.2014.06.003.

Tengelsen, L. A., Pederson, N. E., Shaver, P. R., Wathen, M. W., & Homa, F. L. (1993). Herpes simplex virus type 1 DNA cleavage and encapsidation require the product of the UL28 gene: isolation and characterization of two UL28 deletion mutants. *J Virol, 67*(6), 3470-3480.

Thomas, P., Bhatia, T., Gauba, D., Wood, J., Long, C., Prasad, K., et al. (2013). Exposure to herpes simplex virus, type 1 and reduced cognitive function. *J Psychiatr Res*.

Thompson, R. L., & Sawtell, N. M. (1997). The herpes simplex virus type 1 latency-associated transcript gene regulates the establishment of latency. *J Virol, 71*(7), 5432-5440.

Thompson, R. L., & Sawtell, N. M. (2001). Herpes simplex virus type 1 latency-associated transcript gene promotes neuronal survival. *J Virol, 75*(14), 6660-6675.

Tischler, A. S., Perlman, R. L., Morse, G. M., & Sheard, B. E. (1983). Glucocorticoids increase catecholamine synthesis and storage in PC12 pheochromocytoma cell cultures. *J Neurochem, 40*(2), 364-370.

Trousdale, M. D., Steiner, I., Spivack, J. G., Deshmane, S. L., Brown, S. M., MacLean, A. R., et al. (1991). In vivo and in vitro reactivation impairment of a herpes simplex virus type 1 latency-associated transcript variant in a rabbit eye model. *J Virol, 65*(12), 6989-6993.

Turcotte, S., Letellier, J., & Lippé, R. (2005). Herpes simplex virus type 1 capsids transit by the trans-Golgi network, where viral glycoproteins accumulate independently of capsid egress. *J Virol, 79*(14), 8847-8860.

Turner, A., Bruun, B., Minson, T., & Browne, H. (1998). Glycoproteins gB, gD, and gHgL of herpes simplex virus type 1 are necessary and sufficient to mediate membrane fusion in a Cos cell transfection system. *J Virol, 72*(1), 873-875.

Umbach, J. L., Kramer, M. F., Jurak, I., Karnowski, H. W., Coen, D. M., & Cullen, B. R. (2008). MicroRNAs expressed by herpes simplex virus 1 during latent infection regulate viral mRNAs. *Nature, 454*(7205), 780-783.

Umbach, J. L., Nagel, M. A., Cohrs, R. J., Gilden, D. H., & Cullen, B. R. (2009). Analysis of human alphaherpesvirus microRNA expression in latently infected human trigeminal ganglia. *J Virol, 83*(20), 10677-10683.

van Bijsterveld, O. P., Meurs, P. J., de Clercq, E., & Maudgal, P. C. (1989). Bromovinyldeoxyuridine and interferon treatment in ulcerative herpetic keratitis: a double masked study. *Br J Ophthalmol, 73*(8), 604-607.

van Velzen, M., van Loenen, F. B., Meesters, R. J., de Graaf, M., Remeijer, L., Luider, T. M., et al. (2012). Latent acyclovir-resistant herpes simplex virus type 1 in trigeminal ganglia of immunocompetent individuals. *J Infect Dis, 205*(10), 1539-1543.

Velasco, I., Salazar, P., Giorgetti, A., Ramos-Mejía, V., Castaño, J., Romero-Moya, D., et al. (2014). Concise review: generation of neurons from somatic cells of healthy individuals and neurological patients through induced pluripotency or direct conversion. *Stem Cells, 32*(11), 2811-2817.

Venere, M., Han, Y. G., Bell, R., Song, J. S., Alvarez-Buylla, A., & Blelloch, R. (2012). Sox1 marks an activated neural stem/progenitor cell in the hippocampus. *Development, 139*(21), 3938-3949.

Vere Hodge, R. A., & Field, H. J. (2013). Antiviral agents for herpes simplex virus. *Adv Pharmacol, 67*, 1-38.

Vierbuchen, T., Ostermeier, A., Pang, Z. P., Kokubu, Y., Sudhof, T. C., & Wernig, M. (2010, Feb 25). Direct conversion of fibroblasts to functional neurons by defined factors. *Nature*, pp. 1035-1041.

von Bohlen Und Halbach, O. (2007). Immunohistological markers for staging neurogenesis in adult hippocampus. *Cell Tissue Res, 329*(3), 409-420.

Vrijsen, R., Vanden Berghe, D. A., Vlietinck, A. J., & Boeyé, A. (1986). Lycorine: a eukaryotic termination inhibitor? *J Biol Chem, 261*(2), 505-507.

Wald, A., & Link, K. (2002). Risk of human immunodeficiency virus infection in herpes simplex virus type 2-seropositive persons: a meta-analysis. *J Infect Dis, 185*(1), 45-52.

Wang J, Quake SR. (2014). RNA-guided endonuclease provides a therapeutic strategy to cure latent herpesviridae infection. *Proc Natl Acad Sci U S A.* Sep 9;111(36):13157-62.

Wang QY, Zhou C, Johnson KE, Colgrove RC, Coen DM, Knipe DM (2005). Herpesviral latency-associated transcript gene promotes assembly of heterochromatin on viral lytic-gene promoters in latent infection. *Proc Natl Acad Sci U S A.* Nov 1; 102(44):16055-9.
defense. *Proc Natl Acad Sci USA* 111:15438–15443.

Wang, Y.-H. et al. Benzylphenethylamine Alkaloids from Hosta plantaginea with Inhibitory Activity against Tobacco Mosaic Virus and Acetylcholinesterase. J. Nat. Prod. 70, 1458–1461 (2007).

Ward B. D., Simultaneous Inference for fMRI Data. Milwaukee, WI: University of Wisconsin; 2000.

Ward, K. N. (2005). The natural history and laboratory diagnosis of human herpesviruses-6 and -7 infections in the immunocompetent. *J Clin Virol, 32*(3), 183-193.

Warren, K. G., Brown, S. M., Wroblewska, Z., Gilden, D., Koprowski, H., & Subak-Sharpe, J. (1978). Isolation of latent herpes simplex virus from the superior cervical and vagus ganglions of human beings. *N Engl J Med, 298*(19), 1068-1069.

Watson, A. M., Prasad, K. M., Klei, L., Wood, J. A., Yolken, R. H., Gur, R. C., et al. (2013). Persistent infection with neurotropic herpes viruses and cognitive impairment. *Psychol Med, 43*(5), 1023-1031.

Webre, J. M., Hill, J. M., Nolan, N. M., Clement, C., McFerrin, H. E., Bhattacharjee, P. S., et al. (2012). Rabbit and mouse models of HSV-1 latency, reactivation, and recurrent eye diseases. *J Biomed Biotechnol, 2012*, 612316.

Weir, J. P. (2001). Regulation of herpes simplex virus gene expression. *Gene, 271*(2), 117-130.

Weller, S. K., & Coen, D. M. (2012). Herpes simplex viruses: mechanisms of DNA replication. *Cold Spring Harb Perspect Biol, 4*(9), a013011.

Weller, S. K., & Sawitzke, J. A. (2014). Recombination promoted by DNA viruses: phage λ to herpes simplex virus. *Annu Rev Microbiol, 68*, 237-258.

Whitley, R. J. (1996). Herpes Simplex Viruses *Fields Virology* (3 ed., Vol. 2, pp. 2297-2342). Philadelphia, PA: Lippincott-Raven Publishers.

Whitley, R. J., Nahmias, A. J., Visintine, A. M., Fleming, C. L., & Alford, C. A. (1980). The natural history of herpes simplex virus infection of mother and newborn. *Pediatrics, 66*(4), 489-494.

Wigdahl, B., Scheck, A. C., Ziegler, R. J., De Clercq, E., & Rapp, F. (1984). Analysis of the herpes simplex virus genome during in vitro latency in human diploid fibroblasts and rat sensory neurons. *J Virol, 49*(1), 205-213.

Wigdahl, B., Smith, C. A., Traglia, H. M., & Rapp, F. (1984). Herpes simplex virus latency in isolated human neurons. *Proc Natl Acad Sci U S A, 81*(19), 6217-6221.

Wigdahl, B. L., Scheck, A. C., De Clercq, E., & Rapp, F. (1982). High efficiency latency and activation of herpes simplex virus in human cells. *Science, 217*(4565), 1145-1146.

Wilcox, C. L., & Johnson, E. M. (1987). Nerve growth factor deprivation results in the reactivation of latent herpes simplex virus in vitro. *J Virol, 61*(7), 2311-2315.

Wilcox, C. L., & Johnson, E. M. (1988). Characterization of nerve growth factor-dependent herpes simplex virus latency in neurons in vitro. *J Virol, 62*(2), 393-399.

Wilkinson, D. E., & Weller, S. K. (2003). The role of DNA recombination in herpes simplex virus DNA replication. *IUBMB Life, 55*(8), 451-458.

Willey, D. E., Trousdale, M. D., & Nesburn, A. B. (1984). Reactivation of murine latent HSV infection by epinephrine iontophoresis. *Invest Ophthalmol Vis Sci, 25*(8), 945-950.

Williams, S. L., Hartline, C. B., Kushner, N. L., Harden, E. A., Bidanset, D. J., Drach, J. C., et al. (2003). In vitro activities of benzimidazole D- and L-ribonucleosides against herpesviruses. *Antimicrob Agents Chemother, 47*(7), 2186-2192.

Wisner, T. W., & Johnson, D. C. (2004). Redistribution of cellular and herpes simplex virus proteins from the trans-golgi network to cell junctions without enveloped capsids. *J Virol, 78*(21), 11519-11535.

Wozniak, M. A., Mee, A. P., & Itzhaki, R. F. (2009). Herpes simplex virus type 1 DNA is located within Alzheimer's disease amyloid plaques. *J Pathol, 217*(1), 131-138.

Xie, H. R., Hu, L. S., & Li, G. Y. (2010). SH-SY5Y human neuroblastoma cell line: in vitro cell model of dopaminergic neurons in Parkinson's disease. *Chin Med J (Engl), 123*(8), 1086-1092.

Xu, F., Sternberg, M. R., Kottiri, B. J., McQuillan, G. M., Lee, F. K., Nahmias, A. J., et al. (2006). Trends in herpes simplex virus type 1 and type 2 seroprevalence in the United States. *JAMA, 296*(8), 964-973.

Xu, K., Liu, X. N., Zhang, H. B., An, N., Wang, Y., Zhang, Z. C., et al. (2014). Replication-defective HSV-1 effectively targets trigeminal ganglion and inhibits viral pathopoiesis by mediating interferon gamma expression in SH-SY5Y cells. *J Mol Neurosci, 53*(1), 78-86.

Yang, H. K., Sundholm-Peters, N. L., Goings, G. E., Walker, A. S., Hyland, K., & Szele, F. G. (2004). Distribution of doublecortin expressing cells near the lateral ventricles in the adult mouse brain. *J Neurosci Res, 76*(3), 282-295.

Yang, L., Voytek, C. C., & Margolis, T. P. (2000). Immunohistochemical analysis of primary sensory neurons latently infected with herpes simplex virus type 1. *J Virol, 74*(1), 209-217.

The University of Rhode Island Genomics and Sequencing Center calculator; (http://cels.uri.edu/gsc/cndna.html).date accessed Feb 2016

Yolken, R. H., Torrey, E. F., Lieberman, J. A., Yang, S., & Dickerson, F. B. (2011). Serological evidence of exposure to Herpes Simplex Virus type 1 is associated with cognitive deficits in the CATIE schizophrenia sample. *Schizophr Res, 128*(1-3), 61-65.

Yu, D., & Weller, S. K. (1998). Herpes simplex virus type 1 cleavage and packaging proteins UL15 and UL28 are associated with B but not C capsids during packaging. *J Virol, 72*(9), 7428-7439.

Zambrano, A., Solis, L., Salvadores, N., Cortés, M., Lerchundi, R., & Otth, C. (2008). Neuronal cytoskeletal dynamic modification and neurodegeneration induced by infection with herpes simplex virus type 1. *J Alzheimers Dis, 14*(3), 259-269.

Zhang, D., Pekkanen-Mattila, M., Shahsavani, M., Falk, A., Teixeira, A. I., & Herland, A. (2014). A 3D Alzheimer's disease culture model and the induction of P21-activated kinase mediated sensing in iPSC derived neurons. *Biomaterials, 35*(5), 1420-1428.

Zhang, S. Y., Herman, M., Ciancanelli, M. J., Pérez de Diego, R., Sancho-Shimizu, V., Abel, L., et al. (2013). TLR3 immunity to infection in mice and humans. *Curr Opin Immunol, 25*(1), 19-33.

Zhang, S. Y., Jouanguy, E., Ugolini, S., Smahi, A., Elain, G., Romero, P., et al. (2007). TLR3 deficiency in patients with herpes simplex encephalitis. *Science, 317*(5844), 1522-1527.

Zhang, Y., & McKnight, J. L. (1993). Herpes simplex virus type 1 UL46 and UL47 deletion mutants lack VP11 and VP12 or VP13 and VP14, respectively, and exhibit altered viral thymidine kinase expression. *J Virol, 67*(3), 1482-1492.

Zhao, W. N., Cheng, C., Theriault, K. M., Sheridan, S. D., Tsai, L. H., & Haggarty, S. J. (2012). A high-throughput screen for Wnt/β-catenin signaling pathway modulators in human iPSC-derived neural progenitors. *J Biomol Screen, 17*(9), 1252-1263.

Zheng, X. (2002). Reactivation and donor-host transmission of herpes simplex virus after corneal transplantation. *Cornea, 21*(7 Suppl), S90-93.

Zhu, X. X., Chen, J. X., Young, C. S., & Silverstein, S. (1990). Reactivation of latent herpes simplex virus by adenovirus recombinants encoding mutant IE-0 gene products. *J Virol, 64*(9), 4489-4498.

Zou, G., Puig-Basagoiti, F., Zhang, B., Qing, M., Chen, L., Pankiewicz, K. W., et al. (2009). A single-amino acid substitution in West Nile virus 2K peptide between NS4A and NS4B confers resistance to lycorine, a flavivirus inhibitor. *Virology, 384*(1), 242-252.

Zwaagstra, J. C., Ghiasi, H., Slanina, S. M., Nesburn, A. B., Wheatley, S. C., Lillycrop, K., et al. (1990). Activity of herpes simplex virus type 1 latency-associated transcript (LAT) promoter in neuron-derived cells: evidence for neuron specificity and for a large LAT transcript. *J Virol, 64*(10), 5019-5028.